NASA CR-168,245

NASA CR-168245 R82AEB437

ENERGY EFFICIENT ENGINE

HIGH PRESSURE COMPRESSOR COMPONENT PERFORMANCE REPORT

by

S.J. Cline
W. Fesler
H.S. Liu
R.C. Lovell
S.J. Shaffer

LIBRARY COPY

1983

LANGLEY RESEARCH CENTER
LIBRARY, NASA
HAMPTON, VIRGINIA

GENERAL ELECTRIC COMPANY

Prepared for

National Aeronautics and Space Administration

(NASA-CR-168245) HIGH PRESSURE COMPRESSOR COMPONENT PERFORMANCE REPORT (General Electric Co.) 170 p HC A08/MF A01 CSCL 21E

N85-34138

Unclas

G3/07 16669

SEP 1985
RECEIVED
NASA STI FACILITY
ACCESS DEPT.

NASA Lewis Research Center
Contract NAS3-20643

1. Report No.	2. Government Accession No.	3. Recipient's Catalog No.
NASA CR-168245		

4. Title and Subtitle	5. Report Date
High Pressure Compressor Component Performance Report	September 1983
	6. Performing Organization Code
7. Author(s)	8. Performing Organization Report No.
S.J. Cline, W. Fesler, H.S. Liu, R.C. Lovell and S.J. Shaffer	R82AEB437
	10. Work Unit No.
9. Performing Organization Name and Address	
General Electric Company Aircraft Engine Business Group Cincinnati, Ohio 45215	11. Contract or Grant No. NAS3-20643
	13. Type of Report and Period Covered
12. Sponsoring Agency Name and Address	Topical Report
National Aeronautics and Space Administration Washington, D.C. 20546	14. Sponsoring Agency Code

15. Supplementary Notes

NASA Project Manager: C.C. Ciepluch GE Project Manager: R.W. Bucy
NASA Project Engineer: R.D. Hager

16. Abstract

A compressor optimization study defined a 10-stage configuration with a 22.6:1 pressure ratio, an adiabatic efficiency goal of 86.1%, and a polytropic efficiency of 90.6%; the corrected airflow is 53.5 kg/s. Subsequent component testing included three full-scale tests: a six-stage rig test, a 10-stage rig test, and another 10-stage rig test completed in the second quarter of 1982. Information from these tests is being used to select the configuration for a core engine test scheduled for August 1982 and an integrated core/low spool test slated for the second quarter of 1983. The test results will also provide data base for the flight propulsion system. This report presents the results of the test series with both aerodynamic and mechanical performance of each compressor build. The second 10-stage compressor adiabatic efficiency was 0.848 at a cruise operating point versus a test goal of 0.846.

17. Key Words (Suggested by Author(s))	18. Distribution Statement
High Efficiency Energy Efficient Engine 10-Stage Compressor Rig Test Perofmrance High Pressure Ratio	[redacted]

19. Security Classif. (of this report)	20. Security Classif. (of this page)	21. No. of Pages	22. Price*
Unclassified	Unclassified		

[redacted]

NASA-C-168 (Rev. 10-75)

Foreword

This report presents the results of the high pressure compressor performance verification test series performed by the General Electric Company for the National Aeronautics and Space Administration, Lewis Research Center, under Contract NAS3-20643. This work was performed as part of the Aircraft Energy Efficiency (ACEE) Program, Energy Efficient Engine (E^3) Project. Mr. C. C. Ciepluch is the NASA Project Manager, and Mr. P. G. Batterton is the NASA Assistant Project Manager. Mr. R. D. Hager is the NASA Project Engineer responsible for managing the effort associated with the high pressure compressor performance test series presented in this report. Mr. R. W. Bucy is the Manager of the Energy Efficient Engine Project for the General Electric Company. This report was prepared by Messrs. S. J. Cline, W. Fesler, H. S. Liu, R. C. Lovell, and S. J. Shaffer of the General Electric Company, Evendale, Ohio.

PRECEDING PAGE BLANK NOT FILMED

TABLE OF CONTENTS

Section		Page
1.0	INTRODUCTION AND SUMMARY	1
2.0	OVERALL TEST OBJECTIVES	3
3.0	TEST COMPONENT DESCRIPTION	5
	3.1 Six-Stage Compressor Vehicle	5
	3.1.1 Description of Test Vehicle Configuration	5
	3.1.1.1 Rotor System	5
	3.1.1.2 Stator System	7
	3.1.1.3 Forward Frame System	7
	3.1.1.4 Aft Frame System	7
	3.1.2 Description of Test Facility and Vehicle Installation	8
	3.1.2.1 Full-Scale Compressor Test Facility	8
	3.1.2.2 Inlet System	8
	3.1.2.3 Lube System	11
	3.1.2.4 Air Systems	11
	3.1.2.5 Bleed Systems	12
	3.1.2.6 Hydraulic System	13
	3.1.3 Description of Test Vehicle Instrumentation	13
	3.1.3.1 Aerodynamic Instrumentation	13
	3.1.3.2 Operational Instrumentation	15
	3.2 Ten-Stage Compressor Vehicle, First Build	19
	3.2.1 Description of Test Vehicle Configuration	19
	3.2.1.1 Rotor System	19
	3.2.1.2 Stator System	21
	3.2.1.3 Forward Frame System	22
	3.2.1.4 Aft Frame System	22
	3.2.2 Description of Test Facility and Vehicle Installation	22
	3.2.2.1 Full Scale Compressor Test Facility	22
	3.2.2.2 Vehicle Inlet System	25
	3.2.2.3 Bleed Systems	26
	3.2.3 Description of Test Vehicle Instrumentation	27
	3.2.3.1 Aerodynamic Instrumentation	27
	3.2.3.2 Operational Instrumentation	29
	3.3 Ten-Stage Compressor Vehicle, Second Build	34

PAGE iv INTENTIONALLY BLANK

PRECEDING PAGE BLANK NOT FILMED

TABLE OF CONTENTS (Concluded)

Section		Page
	3.3.1 Description of Test Vehicle Configuration	34
	3.3.1.1 Rotor System	34
	3.3.1.2 Stator System	35
	3.3.1.3 Forward Frame System	35
	3.3.1.4 Aft Frame System	35
	3.3.2 Description of Test Facility and Vehicle Installation	35
	3.3.2.1 Full-Scale Compressor Test Facility	35
	3.3.2.2 Vehicle Inlet System	36
	3.3.2.3 Lube System	36
	3.3.2.4 Air Systems	36
	3.3.2.5 Bleed Systems	36
	3.3.2.6 Hydraulic System	36
	3.3.3 Description of Test Vehicle Instrumentation	36
	3.3.3.1 Aerodynamic Instrumentation	36
	3.3.3.2 Operational Instrumentation	37
4.0	AERODYNAMIC PERFORMANCE SUMMARY	39
	4.1 Six-Stage Compressor Test Results	39
	4.2 Ten-Stage Compressor Test Results, First Build	46
	4.3 Ten-Stage Compressor Test Results, Second Build	57
	4.4 Summary	73
5.0	SYSTEM DYNAMICS SUMMARY	77
	5.1 Six-Stage Compressor Test Results	77
	5.2 Ten-Stage Compressor Test Results, First Build	77
	5.3 Ten-Stage Compressor Test Results, Second Build	87
6.0	MECHANICAL/AEROMECHANICAL SUMMARY	90
	6.1 Six-Stage Compressor Test	90
	6.1.1 Mechanical Results	90
	6.1.2 Aeromechanical Results	90
	6.2 Ten-Stage Compressor Test, First Build	91
	6.2.1 Rotor Mechanical Results	91
	6.2.2 Rotor Aeromechanical Results	109
	6.2.3 Stator Mechanical Results	124
	6.2.4 Stator Aeromechanical Results	127
	6.3 Ten-Stage Compressor Test, Second Build	127
	6.3.1 Rotor Mechanical Results	139
	6.3.2 Rotor Aeromechanical Results	141
	6.3.3 Stator Mechanical Results	153
	6.3.4 Stator Aeromechanical Results	153
	6.4 Summary	155
APPENDIX - COMPRESSOR PERFORMANCE SUMMARY OF THE SECOND TEN-STAGE TEST		157

LIST OF ILLUSTRATIONS

Figure		Page
1.	High Pressure Compressor Cross Section.	4
2.	Six-Stage Compressor Vehicle.	6
3.	Lynn Full Scale Compressor Test Facility.	9
4.	Lynn Full Scale Compressor Test Facility Diagram.	10
5.	First 10-Stage Compressor Test Vehicle.	20
6.	FSCT Inlet Refrigeration Schematic.	23
7.	Schematic of Inlet Duct for 10-Stage Compressor Vehicle.	24
8.	Ten-Stage Compressor Cooling Air and Bleed Air Systems.	28
9.	Six-Stage Compressor Performance Map.	41
10.	Compressor Six-Stage Test Stator Schedule.	42
11.	Six-Stage Compressor Radial Total Pressure Distribution.	45
12.	Performance Map for the First 10-Stage Compressor Test.	49
13.	Final Stator Schedule for the First 10-Stage Compressor Test.	51
14.	Performance Map of Stages 7 through 10.	54
15.	Performance Map for Stages 1 through 6.	55
16.	First 10-Stage Compressor Radial Total Pressure Distribution.	56
17.	Second 10-Stage Compressor Performance Map.	60
18.	Second 10-Stage Compressor Test Stator Schedule.	61
19.	Second 10-Stage Compressor Test, Front Six-Stage Map.	65
20.	Second 10-Stage Compressor Test, Rear Block Map.	67
21.	Second 10-Stage Compressor Test, Traverse Data.	68
22.	Second 10-Stage Compressor Test, Traverse Data.	69

LIST OF ILLUSTRATIONS (Continued)

Figure		Page
23.	Second 10-Stage Compressor Absolute Air Angle Distribution.	70
24.	Second 10-Stage Compressor Test, Inlet Distortion Patterns.	72
25.	10B Compressor Circumferential Distortion Sensitivity.	74
26.	10B Compressor Radial Distortion Sensitivity.	75
27.	Six-Stage Compressor Test Vehicle Modal Deflection for Critical Speed at 11,997 RPM.	78
28.	Six-Stage Compressor Test Bellmouth Vertical Accelerometer Response at 10,410 RPM.	79
29.	Six-Stage Compressor.	80
30.	Hard-Mounted, 10-Stage Compressor Rotor Modal Deflection for Critical Speed at 6621 RPM.	82
31.	Ten-Stage Compressor Rig, Build 1, Soft-Mounted Rotor Modal Deflection for Critical Speed at 6606 RPM.	83
32.	First 10-Stage Compressor Rig Squeeze Film Damper Design Subsystems and Connecting Elements.	84
33.	First 10-Stage Compressor Forward Bearing Damper Housing Synchronous Response Comparison.	86
34.	Ten-Stage Compressor, Build 2, Frequency Response at Forward Damper Housing.	88
35.	Compressor Rotor Stage 1 Blade Campbell Diagram.	92
36.	Compressor Rotor Stage 2 Blade Campbell Diagram.	93
37.	Compressor Rotor Stage 3 Blade Campbell Diagram.	94
38.	Compressor Rotor Stage 4 Blade Campbell Diagram.	95
39.	Compressor Rotor Stage 5 Blade Campbell Diagram.	96
40.	Compressor Rotor Stage 6 Blade Campbell Diagram.	97

LIST OF ILLUSTRATIONS (Continued)

Figure		Page
41.	Compressor Stator IGV Campbell Diagram.	98
42.	Compressor Stator 1 Campbell Diagram.	99
43.	Compressor Stator 2 Campbell Diagram.	100
44.	Compressor Stator 3 Campbell Diagram.	101
45.	Compressor Stator 4 Campbell Diagram.	102
46.	Compressor Stator 5 Campbell Diagram.	103
47.	Compressor Stator 6 Campbell Diagram.	104
48.	10A Compressor Rotor Temperature Comparison.	106
49.	First 10-Stage Compressor Bore Cooling Flow Effects.	107
50.	Wear on a Single Tooth Discourager Seal.	110
51.	Campbell Diagram Stage 5 Blade Root Gages.	112
52.	Campbell Diagram Stage 6 Blade Root Gages.	113
53.	Ten-Stage Compressor Rotor Stage 1 Blade Campbell Diagram.	114
54.	Ten-Stage Compressor Rotor Stage 2 Blade Campbell Diagram.	115
55.	Ten-Stage Compressor Rotor Stage 3 Blade Campbell Diagram.	116
56.	Ten-Stage Compressor Rotor Stage 4 Blade Campbell Diagram.	117
57.	Ten-Stage Compressor Rotor Stage 5 Blade Campbell Diagram.	118
58.	Ten-Stage Compressor Rotor Stage 6 Blade Campbell Diagram.	119
59.	Ten-Stage Compressor Rotor Stage 7 Blade Campbell Diagram.	120
60.	Ten-Stage Compressor Rotor Stage 8 Blade Campbell Diagram.	121
61.	Ten-Stage Compressor Rotor Stage 9 Blade Campbell Diagram.	122
62.	Ten-Stage Compressor Rotor Stage 10 Blade Campbell Diagram.	123
63.	Stage 6 Stator Vanes, Ten-Stage Compressor.	126

LIST OF ILLUSTRATIONS (Concluded)

Figure		Page
64.	Ten-Stage Compressor IGV Campbell Diagram.	128
65.	Ten-Stage Compressor Stator 1 Campbell Diagram.	129
66.	Ten-Stage Compressor Stator 2 Campbell Diagram.	130
67.	Ten-Stage Compressor Stator 3 Campbell Diagram.	131
68.	Ten-Stage Compressor Stator 4 Campbell Diagram.	132
69.	Ten-Stage Compressor Stator 5 Campbell Diagram.	133
70.	Ten-Stage Compressor Stator 6 Campbell Diagram.	134
71.	Ten-Stage Compressor Stator 7 Campbell Diagram.	135
72.	Ten-Stage Compressor Stator 8 Campbell Diagram.	136
73.	Ten-Stage Compressor Stator 9 Campbell Diagram.	137
74.	Ten-Stage Compressor Stator OGV Campbell Diagram.	138
75.	10B Compressor Temperature Comparison.	140
76.	10B Compressor Stage 6 Campbell Diagram.	142
77.	10B Compressor Stage 7 Campbell Diagram.	143
78.	10B Compressor Rotor Stage 3 Blade Campbell Diagram.	144
79.	10B Compressor Rotor Stage 4 Blade Campbell Diagram.	145
80.	10B Compressor Rotor Stage 5 Blade Campbell Diagram.	146
81.	10B Compressor Rotor Stage 6 Blade Campbell Diagram.	147
82.	10B Compressor Rotor Stage 7 Blade Campbell Diagram.	148
83.	10B Compressor Rotor Stage 8 Blade Campbell Diagram.	149
84.	10B Compressor Rotor Stage 9 Blade Campbell Diagram.	150
85.	10B Compressor Rotor Stage 10 Blade Campbell Diagram.	151
86.	10B Compressor Casing Temperature Comparison.	154

LIST OF TABLES

Table		Page
I.	Comparison of Efficiencies.	43
II.	High Speed Efficiency Summary.	52
III.	Maximum Cruise Efficiency Versus Goals.	63
IV.	Ten-Stage Compressor Squeeze Film Damper Parameters.	85

1.0 INTRODUCTION AND SUMMARY

On January 25, 1980, the first in a series of three scheduled E^3 compressor development tests was initiated in the Full Scale Compressor Test Facility (FSCT) at General Electric's Lynn, Massachusetts plant. The object of this first development test was to determine the efficiency and pumping characteristics of the variable geometry, six-stage front block of the 10-stage compressor. The test was successfully completed on February 29, 1980, with 428 data points being taken during 117 hours of running. All test objectives were met, however; analysis of the test data indicated a weakness in the hub performance. Corrective changes to the front block blading were defined and incorporated prior to assembly of the full, 10-stage compressor.

Testing of the first 10-stage compressor rig was first initiated on March 20, 1981, in the FSCT facility. Test goals achieved were (1) evaluate the effect of the front stage modifications on hub performance, (2) measure high speed performance and stall margin, (3) optimize the stator schedule, (4) investigate the subidle start region, and (5) measure the effects of compressor bleeds on performance. Termination of testing due to R1 blade foreign object damage (FOD) precluded the planned radial traverse and distortion tests. The test was terminated on April 10, 1981, after 200 data points were taken during 80 hours of running.

Analysis of the data showed that front hub performance improvements were realized with the blading changes that were made. To further enhance performance and improve stall margin, additional blading changes were incorporated into the second build of the 10-stage compressor. Testing was initiated on December 18, 1981, and continued until April 10, 1982, during 514 data points were taken. The following test objectives were successfully accomplished: improved high speed stall margin, finalized the stator schedule, evaluated the effects of Stage 5 and 7 bleeds, measured active clearance control capabilities, evaluated Reynolds number effects, performed the radial traverse and distortion tests, and determined the effects of fixing Stator 5.

This test concluded The E^3 Compressor Development Program. This program proved to be highly successful, producing an efficient, rugged compressor for the subsequent core and turbofan engine tests. Detailed descriptions of each compressor vehicle assembly, test objectives, and test results are presented in the following text.

2.0 OVERALL TEST OBJECTIVES

The primary objective of the E^3 core compressor development effort was to evolve a 10-stage, high performance, high stage loading design (Figure 1) capable of achieving a pressure ratio of 23:1 at the engine's maximum climb design point. The primary aerodynamic design challenge was to provide adequate levels of stall margin at part-speed operation while achieving the high efficiency levels required by the E^3 engine cycle. The FPS compressor efficiency goal was established as 0.861 at a Mach 10.8, 10.67 km (35,000 ft), standard day maximum cruise power setting.

The mechanical design requirements included the development of an active clearance control system for the rear block of compressor stages to achieve tip clearances at cruise compatible with the efficiency and stall margin goals and to enhance performance retention. The compressor has fewer, longer chord airfoils (low aspect ratio) to increase blade life and general ruggedness and to reduce performance deterioration and operational costs. The compressor is short and stiff and, in conjunction with the short combustor and high pressure turbine, permits the use of only two bearings to support the core rotor.

A sequential arrangement of the component tests allowed refinements to the design to be introduced throughout the compressor development test program. The Core Compressor Development program will culminate with the integrated core-low spool (ICLS) system test in 1983.

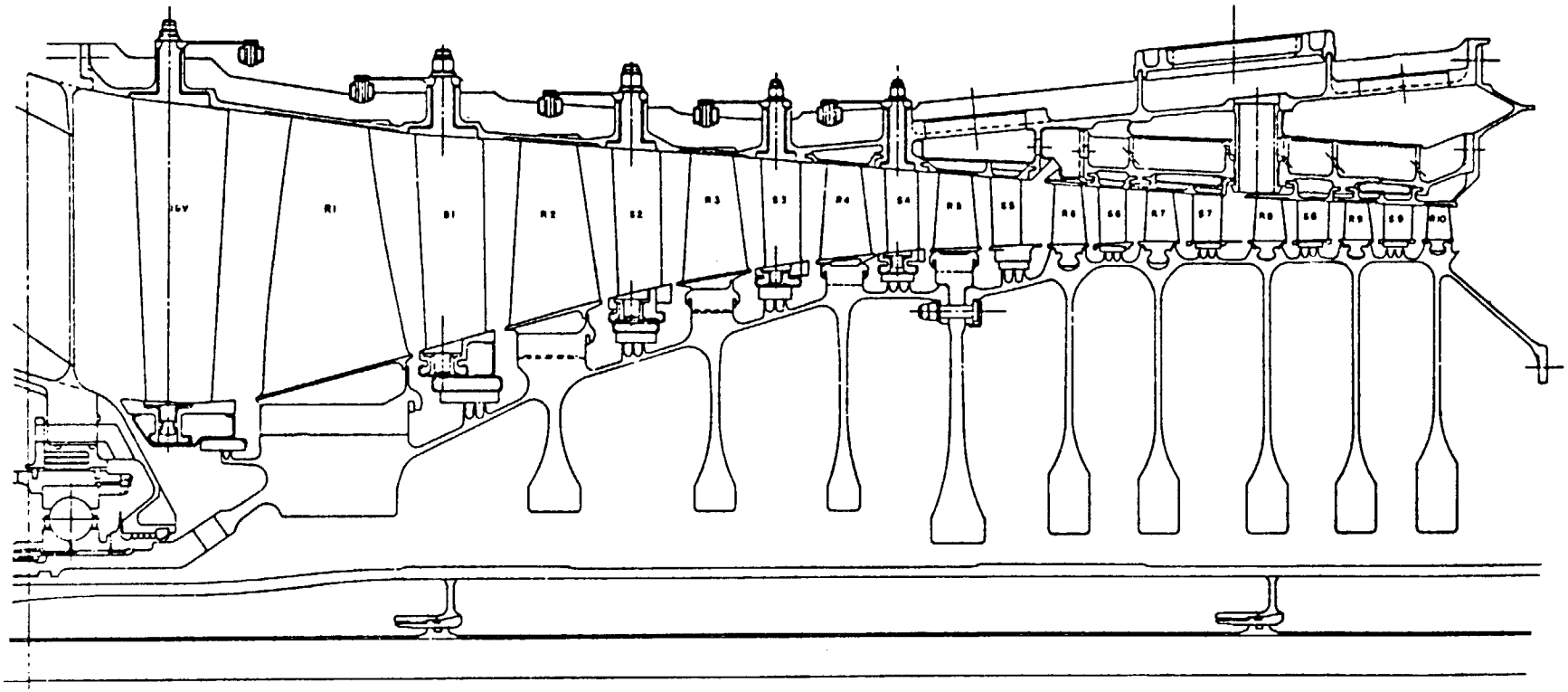

- Efficiency - MXCR - 86.1%
- 10 Stage, 23:1 PR-MXCL
- Low Aspect Ratio, Rugged Blades
- Steel Casing
- Inertial Welded Spools
- Ti 17 Forward, R95 Aft Spool
- Digital Control of Variable Stators
- Active Clearance Control Stages 6-10
- Adequate Stall Margin

Figure 1. High Pressure Compressor Cross Section.

3.0 TEST COMPONENT DESCRIPTION

3.1 SIX-STAGE COMPRESSOR VEHICLE

3.1.1 Description of Test Vehicle Configuration

The E^3 six-stage compressor vehicle was designed to test the flowpath hardware of the variable geometry front block of the E^3 10-stage high pressure compressor. The six-stage compressor vehicle assembly is shown in Figure 2.

The six-stage compressor vehicle was a two-bearing design incorporating a ball thrust bearing housed in the forward frame and a roller bearing housed in the slave aft frame. The compressor rotor system was driven from the aft end with a crowned spline adapter coupling it to the test facility drive system. Drive power was provided by the test facility's 33,000 horsepower steam turbine.

3.1.1.1 Rotor System

The compressor rotor assembly consisted of six stages of low aspect ratio blades. The rotor blades of Stages 1 through 4 were made of titanium 6-4, and were installed in a titanium 6-4 forward spool which had axial-type dovetails. The Stage 5 rotor blades were made of Inconel 718 and were installed in a separate, titanium 6-4 disk which had axial-type dovetails. The Stage 6 rotor blades were made of Inconel 718 and were installed in a slave Inconel 718 disk which had circumferential-type dovetails. This slave six-stage disk was fabricated for this test rig only and was not used in either of the 10-stage compressor rigs. A single bolt joint attached the forward spool, Stage 5 disk, and Stage 6 disk.

The aft section of the compressor rotor system was made up of slave hardware consisting of a CDP seal, drive spool, thrust balance disk, and an aft stub shaft. The thrust balance disk was utilized to reduce the compressor forward thrust loads to prevent overloading of the ball thrust bearing in the

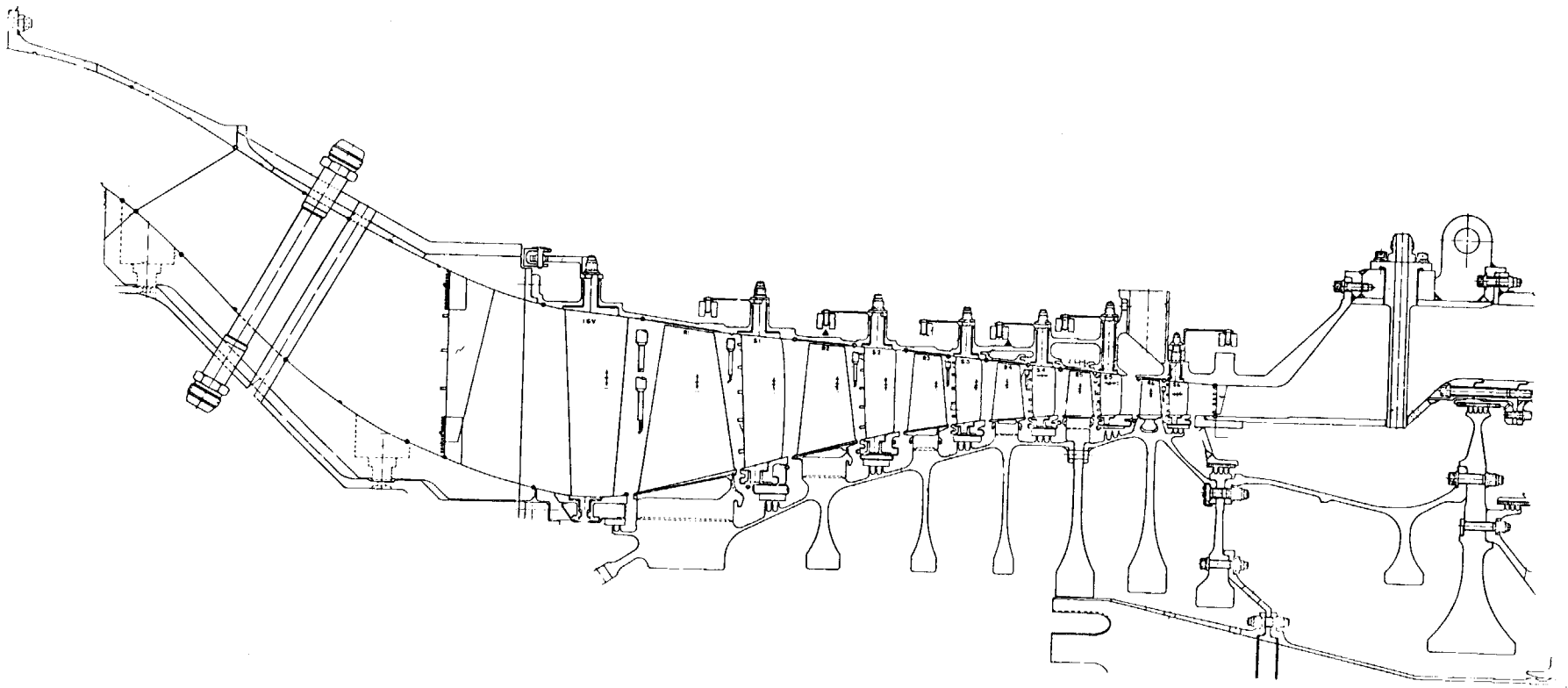

Figure 2. Six-Stage Compressor Vehicle.

forward frame. This slave hardware also contained instrumentation leadout tubes through which all compressor rotor instrumentation leads were routed to the externally mounted test facility slipring.

3.1.1.2 Stator System

The compressor stator system consisted of horizontally-split forward and aft cases made of M152 and 1010 steel, respectively. The forward case contained inlet guide vanes (IGV) through Stage 5 vanes and the aft case contained Stage 6 vanes, all variable. All stator vanes were made of A286. Each of the seven variable vane rows had an inner shroud and seal. Removable segmented liners were installed in the forward stator case over Rotors 4 and 5. Provisions were made in the aft stator case for the extraction of bleed air ahead of the Stage 6 rotor.

3.1.1.3 Forward Frame System

The forward frame was a slave-type design and provided support for the ball thrust bearing. The slave frame contained eight struts which had drilled passages to provide lube and air services to the forward frame sump. The inner flowpath segments between frame struts were removable wood panels. The ball thrust bearing was a split inner race design which utilized underrace lubrication for cooling. A shop-air pressurized carbon seal was located on the aft side of the sump housing to provide a dam against lube oil entering the compressor air stream. Rotor cooling air was piped through the forward frame struts and entered the rotor at its forward centerline. Outer and inner transition ducts were attached to the forward flanges of the frame to mate with the inlet bellmouth and bulletnose. The outer transition duct also contained provisions for supporting the forward end of the vehicle in the test facility.

3.1.1.4 Aft Frame System

The aft frame was a slave-type design that supported the aft roller bearing. The frame contained the necessary provisions for supplying lube and air services to the aft bearing sump. The aft frame also contained passages for the extraction of rotor cooling air and thrust balance seal leakage air.

3.1.2 Description of Test Facility and Vehicle Installation

3.1.2.1 Full Scale Compressor Test (FSCT) Facility

The six-stage compressor vehicles was tested in the FSCT facility. This facility was designed for the testing of full scale compressors and fans in single- or dual-rotor configurations. The FSCT facility is shown in Figures 3 and 4. The facility consists of a 3.098 m (10-ft) diameter by 12.19 m (40-ft) long test chamber in which vehicles can be tested with airflows up to 226.8 kg/s (500 lb/s). Steam turbines drive the compressor or fan rotors through speed increasing gears. Compressors are driven by a 33,000 horsepower turbine downstream of the chamber which has the capability of providing drive speeds up to 15,000 rpm.

The FSCT facility has the capability of being operated in either close-cycle or open-cycle mode. In the close-cycle mode, the compressor air is discharged through a valve into an ASME flow-measuring section, through a water-cooled heat exchanger, and is then returned to the inlet of the test chamber. The desired tank pressure level at the face of the compressor is controlled by a steam ejector system. In open-cycle operation, outside air enters the test chamber through an inlet control valve. This valve is used to set the desired pressure level at the face of the compressor. The compressor exit air is discharged to the atmosphere through a throttle valve and metered by ASME flow-nozzles. The six-stage compressor was tested in a open-cycle mode.

Controls are highly automated. An electrohydraulic system holds speeds within 10 rpm at 15,000 rpm and regulates speed changes at rates from 1 to 1000 rpm per second. An electropneumatic control maintains inlet pressure within 0.02 in. Hg and controls the rate of prescribed changes between 2 and 45 in. Hg absolute. An electrohydraulic system positions variable stator vanes in accordance with preprogrammed schedules. Another feature is automatic opening of the main discharge valve within 0.02 second after a stall is detected.

3.1.2.2 Inlet System

As part of the installation of the vehicles in the test facility, an aluminum bellmouth and bulletnose were attached to the forward ends of the transition ducts. The bellmouth contained pads for the installation of four

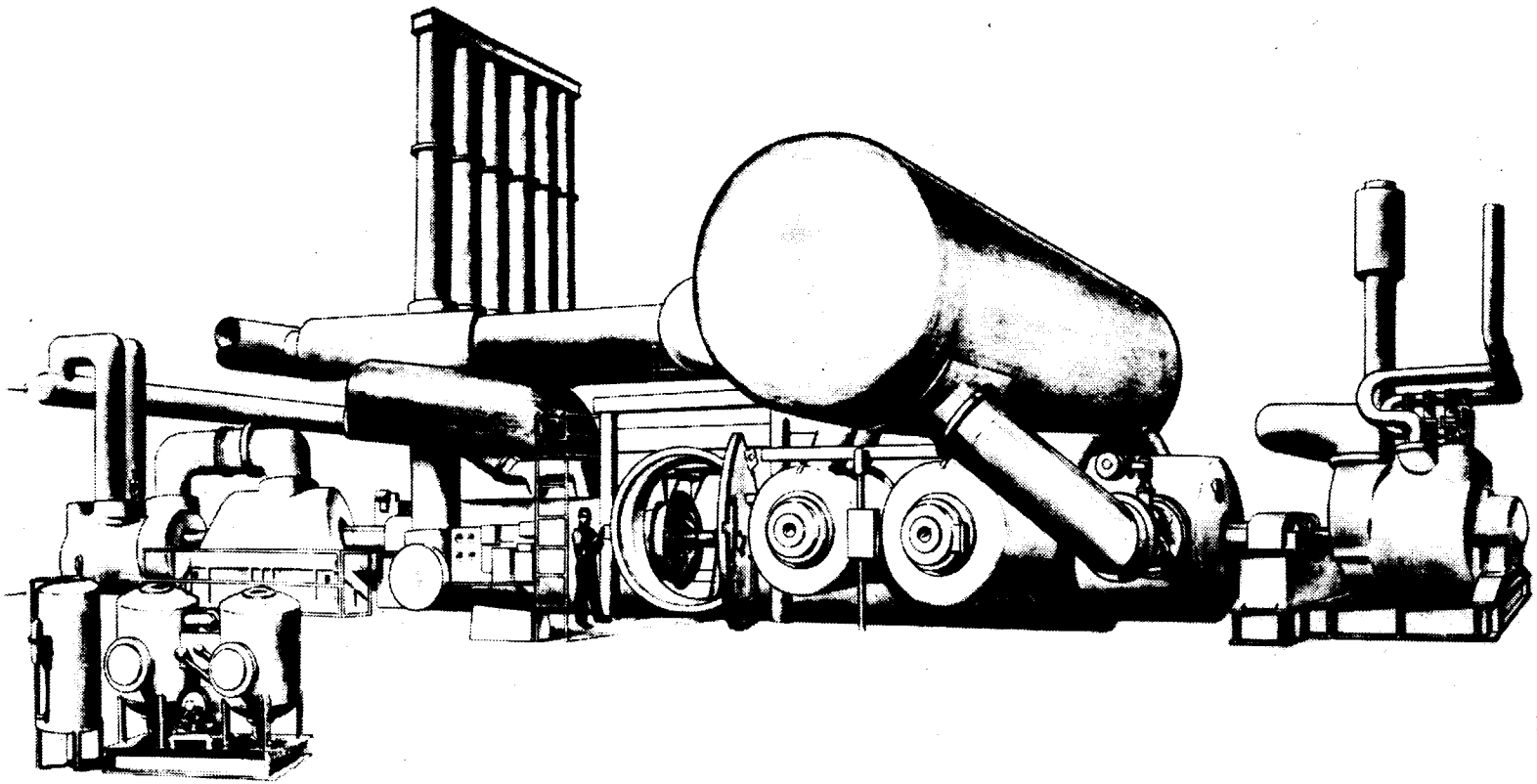

Figure 3. Lynn Full Scale Compressor Test Facility.

ORIGINAL PAGE IS
OF POOR QUALITY

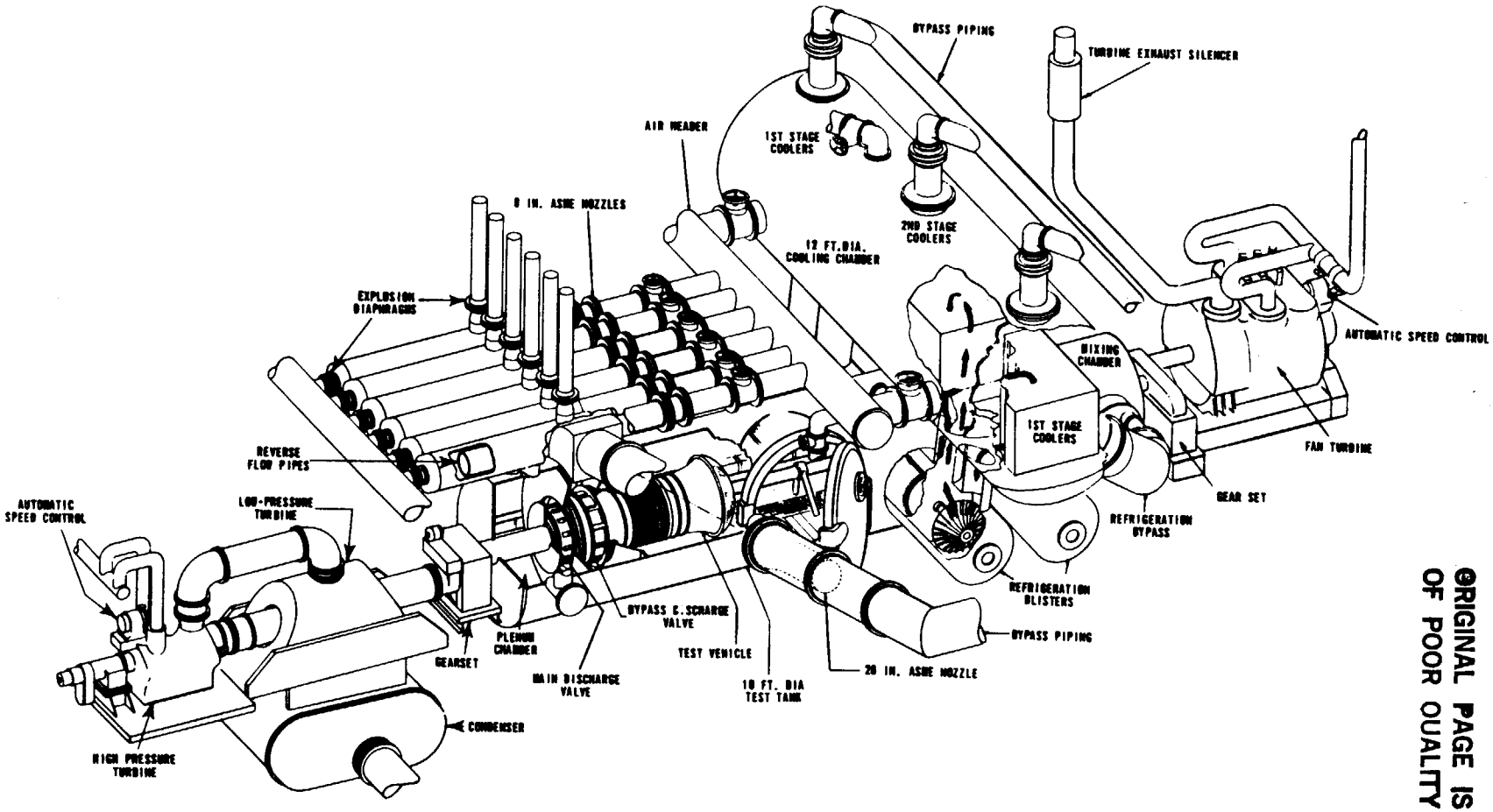

Figure 4. Lynn Full Scale Compressor Test Facility Diagram.

ORIGINAL PAGE IS OF POOR QUALITY

pitot static rakes, which were utilized for the calculation of bellmouth airflow. Four wall static pressure taps were located on each of the bellmouth and bulletnose in the same axial plane as the pitot static rakes. A separately supported inlet screen was located just ahead of the bellmouth lip to prevent foreign objects from entering the compressor inlet. Twenty-four thermocouples were attached to the inlet screen for measurement of the compressor inlet air temperature. An aluminum shroud was installed between the bellmouth outer diameter and the test facility tank wall to prevent warm air around the aft end of the vehicle from entering the inlet.

3.1.2.3 Lube System

The Lynn test facility had a central lube supply system which provided oil to the test facility and the test vehicle. The normal supply temperature of the oil was 311 K (100° F).

Lube oil supplied to the ball thrust bearing in the forward sump through lines installed in the forward frame. These lines connected to two lube nozzles which directed lube oil into a cavity beneath the thrust bearing inner race. A lube oil flow rate of 0.013 m^3/m (3.5 gpm) was required for this bearing. Scavenge lines were also provided in the forward frame to return this lube oil to the main supply system.

Lube oil was supplied to the roller bearing in the aft sump through lines installed in the aft frame. These lines were connected to two lube nozzles which directed lube oil on the bearing rollers. These same jets were also used to supply a small amount of lube oil to the carbon seal race and the drive spline. A lube oil flow rate of 0.011 m^3/m (3.0 gpm) was required for this bearing. The aft sump lube oil was scavenged through the test facility drive scavenge system.

The test facility air-scavenge system utilized a steam ejector which reduced vehicle sump pressures below atmospheric.

3.1.2.4 Air Systems

The Lynn test facility had external air supplies which were used for vehicle cooling air and for seal and cavity pressurization.

External air was supplied to the forward and aft frames as follows:

Forward Frame

Shop air was supplied to the carbon seal in order to maintain a seal pressure higher than the sump pressure. This was to prevent lube oil from entering the compressor air stream ahead of the first stage rotor.

Cooling air was supplied to the inside of the compressor rotor. The test facility system which provided this cooling air contained provisions for filtering the air, remotely controlling the flow, and for airflow measurement. The cooling air entered the forward end of the compressor rotor, passed through the bore of the rotor, and exited through the aft frame struts where it was exhausted to the atmosphere.

Aft Frame

Shop air was supplied to the carbon seal in order to maintain a seal pressure higher than the sump pressure.

Shop air was supplied to two cavities for cavity pressurization.

3.1.2.5 Bleed Systems

Bleed air was extracted from the compressor between the Stage 5 stator and the Stage 6 rotor. The bleed air exited the compressor stator through six ports on the casing. Test facility piping collected the bleed air from these six ports and conducted it through a flow measurement system and a remote control valve system prior to exhausting it to the atmosphere.

Thrust Balance Bleed

Bleed lines were provided in the aft frame for the extraction of the air which leaked past the seal teeth on the balance piston disk. Test facility piping collected the bleed air from the aft frame lines and conducted it through a flow measurement system and a remote control valve system prior to exhausting it to the atmosphere.

3.1.2.6 Hydraulic System

In order to optimize the compressor stator vane angles and investigate off-design performance, each compressor stator row had the capability of being independently varied. Seven hydraulic actuators, one for each vane row drove a rocker arm linkage that connected to each actuation ring. Separate servovalves controlled the movement of each hydraulic actuator. Two rotary vane angle readouts were mounted to each stator row to provide angle feedback to the vane position system. Each compressor stator row could be moved manually on an individual basis or could be programmed to move automatically as a function of compressor corrected speed.

3.1.3 Description of Test Vehicle Instrumentation

3.1.3.1 Aerodynamic Instrumentation

Facility-Provided Instrumentation

Primary flow was measured by calibrated facility flow nozzles at the discharge valve exit and at each bleed exit. Total inlet flow was calculated from the sum of all exit flows.

Twenty-four thermocouples were mounted on the bellmouth inlet screen to monitor test vehicle inlet temperature.

Compressor speed was measured from a 1/rev signal on a slipring located on the main facility drive shaft.

Overall Performance Instrumentation

The compressor inlet measurement plane (Plane 25), located immediately forward of the inlet guide vane, contained static pressure taps on the outer and inner walls which were used to measure circumferential uniformity of airflow as well as inlet static pressure levels. Four 5-element, total pressure and total temperature radial rakes located in the same plane as the static taps measured core inlet total conditions. These rakes were also used to verify circumferential and radial uniformity of pressure and temperature.

Plane 257 was the discharge plane for the six-stage compressor test and was located immediately aft of Stage 6 stator vane row. Five 5-element, total pressure and total temperature radial rakes measured overall pressure rise and temperature rise as well as indicating circumferential and radial distributions. Discharge static pressure was measured from outer and inner wall manifolded static taps.

Interstage Instrumentation

Manifolded static taps were mounted in the outer wall at all rotor inlet and rotor exit planes to measure the interstage static pressure distribution. Individual static taps on the forward and aft side of the stator shrouds below the flowpath measured the hub shroud seal pressure difference for detecting seal leakage. They were also used to give an approximate indication of the tip-to-hub radial pressure distribution.

Rotor exit plane total pressures and total temperatures, used for stage characteristics, were measured by vane leading-edge-mounted sensors at five radial immersions.

Over the Stage 1 rotor, 10 axially spaced static taps and 10 Kulite dynamic pressure transducers were installed in the casing to map the tip flow field.

Traverse Probes

Radially traversable cobra probes were provided in each rotor exit plane. Detailed radial profiles of total pressure, total temperature, and yaw angle measured by these probes were used in conjunction with vane-mounted sensor data to evaluate blade element performance.

Bleed System Instrumentation

Bleed port flow properties were measured using one static pressure tap and one thermocouple in the Stage 5 bleed manifold. Bleed flow was metered by facility orifices.

Inlet Duct Instrumentation

The transition duct inlet measuring station (Plane 23) was immediately downstream of the bellmouth and forward of the front frame. Mounted at this station were four 4-element radial rakes equipped with sensors which measured free stream static pressure and total pressures. These pressures, combined with outer wall and inner wall static pressures, were used to measure flow independently of the test facility flowmeters.

Outer wall and inner wall static taps were provided at selected axial stations from the bellmouth through the front frame and transition duct to the core inlet.

Outer wall and inner wall boundary layer rakes, located at the same Plane 25 station as the inlet static taps and radial rakes, provided total-pressure measurements close to the walls. These rakes complemented the radial profile measurements near the end wall region in the inlet and were used to determine duct wall losses.

At the Stage 1 rotor inlet plane, a radially and circumferentially traversable cobra probe was provided to investigate the rotor inlet conditions and to measure guide vane and inlet duct strut losses. A radially traversable wedge probe in this same plane was used to measure radial static pressure distributions.

3.1.3.2 Operational Instrumentation

Pressures

The following operational pressures were monitored on gages located in the FSCT control room. Log sheet readings were taken every 30 minutes or as directed by the Evaluation Engineer.

Item No.	Location	Limits
281	Forward carbon seal	Min. 5 psi greater than sump pressure
282	Forward sump	Max. scavenge pressure
283	Forward sump	Max. scavenge pressure
292	Rotor cooling air inlet	Max. cooling air supply pressure
754	Dual seal cavity	Equal to aft thrust disk cavity pressure
755	Aft sump - fwd	Max. scavenge pressure
756	Aft sump - fwd	Max. scavenge pressure

Item No.	Location	Limits
757	Aft sump - aft	Max. scavenge pressure
758	Aft sump - aft	Max. scavenge pressure
762	Single seal cavity	Equal to rotor cool disch cavity
763	Single seal cavity	Equal to rotor cool disch cavity
767	Fwd thrust disk cavity	Monitor
770	Aft thrust disk cavity	Monitor
772	Rotor cool disch cavity	Monitor
773	Rotor cool disch cavity	Monitor
775	Aft carbon seal	Min. 5 psi greater than sump pressure
783	CDP seal cavity	Monitor
784	CDP seal cavity	Monitor

Temperatures

The following operational temperatures were monitored on a Metrascope in the FSCT control room. The Metrascope automatic alarm was set at the indicated limits. A paper tape printout of these temperatures was taken at each data point or as directed by the Evaluation Engineer.

Item No.	Location	Limit K (° F)
276	No. 1 bearing outer race	478 (400)
277	No. 1 bearing oil in	339 (150)
278	No. 1 bearing oil in	339 (150)
284	No. 1 bearing oil out	450 (350)
285	No. 1 bearing oil out	450 (350)
289	No. 1 bearing inner race	478 (400)
350	Stage 1 disk bore air	339 (150)
351	Stage 1 disk bore air	339 (150)
411	Stage 2 disk bore skin	347 (165)
412	Stage 2 disk bore skin	347 (165)
524	Stage 4 disk bore skin	375 (215)
525	Stage 4 disk bore skin	375 (215)
643	Stage 6 disk bore air	439 (330)
644	Stage 6 disk bore skin	450 (350)
645	Stage 6 disk bore skin	450 (350)
342	Stator case - Stage 1	367 (200)
343	Stator case - Stage 1	367 (200)
403	Stator case - Stage 2	422 (300)
404	Stator case - Stage 2	422 (300)
462	Stator case - Stage 3	478 (400)
463	Stator case - Stage 3	478 (400)
526	Stator case - Stage 4	533 (500)
527	Stator case - Stage 4	533 (500)

Item No.	Location	Limit K (° F)
575	Stator case - Stage 5	589 (600)
576	Stator case - Stage 5	589 (600)
640	Stator case - Stage 6	630 (675)
641	Stator case - Stage 6	630 (675)
293	Rotor cool air in	339 (150)
752	No. 2 bearing outer race	395 (250)
753	No. 2 bearing outer race	395 (250)
760	Aft sump skin	408 (275)
761	Aft sump skin	408 (275)
764	Single seal cavity air	422 (300)
765	Single seal cavity air	422 (300)
768	Fwd thrust disk cavity air	700 (800)
771	Aft thrust disk cavity air	700 (800)
774	Rotor cool disch cavity air	533 (500)
776	CDP seal fwd cavity air	700 (800)
777	CDP seal fwd cavity air	700 (800)
778	CDP seal fwd cavity air	700 (800)
779	No. 2 bearing oil in	339 (150)
800	Stage 3 clearanceometer (360°)	395 (250)
801	Stage 5 clearanceometer (51°)	395 (250)
802	Stage 5 clearanceometer (315°)	395 (250)
805	Dual seal cavity air	422 (300)

Strain Gages

Rotor - A total of 36 strain gages were applied to the blades (six gages per stage). For the initial monitoring setup, 24 rotor gages were monitored on scopes with 23 of these being recorded on magnetic tape.

Stator - A total of 44 strain gages were applied to the stator vanes. For the initial monitoring setup, 22 stator gages were monitored on scopes and recorded on magnetic tape.

Rakes - A total of 18 strain gages were applied to the compressor inlet rakes. For the initial monitoring setup, 12 gages were monitored on scopes and recorded on magnetic tape.

Vibrations

A total of 11 accelerometers were installed on the compressor vehicle, 5 internal and 6 external, as listed below. Each pickup was monitored on a scope and recorded on magnetic tape. Two X-Y plotters were available for plotting selected pickup readings versus compressor rpm.

Item No.	Location	Limits
125	Bellmouth vertical	(See figure in Appendix)
126	Bellmouth horizontal	(See figure in Appendix)
273	No. 1 bearing vertical	(See figure in Appendix)
274	No. 1 bearing horizontal	(See figure in Appendix)
291	No. 1 bearing axial	(See figure in Appendix)
286	Front frame vertical	(See figure in Appendix)
287	Front frame horizontal	(See figure in Appendix)
747	Aft frame vertical	(See figure in Appendix)
748	Aft frame horizontal	(See figure in Appendix)
749	No. 2 bearing vertical	(See figure in Appendix)
750	No. 2 bearing horizontal	(See figure in Appendix)

Sanborn Recorders

Two 8-channel Sanborn recorders continuously recorded selected vehicle operational parameters. The initial setup on the two recorders was as follows:

Sanborn No. 1

Channel	Parameter	Item No.	Range
1	Speed	810	0-15,000 rpm
2	No. 1 bearing T/C	275	0-533 K (500° F)
3	No. 1 bearing T/C	288	0-533 K (500° F)
4	No. 2 bearing T/C	751	0-395 K (250° F)
5	Inlet Ps	182	0-172 kPa (25 psia)
6	Fwd thrust disk cavity pres	766	0-1724 kPa (250 psia)
7	Aft thrust disk cavity pres	769	0-345 kPa (50 psia)
8	Stage 6 bore air T/C	642	0-533 K (500° F)

Sanborn No. 2

Channel	Parameter	Item No.	Range
1	Speed	810	0-15,000 rpm
2	IGV cylinder ΔP	300	±17,237 kPa (2500 psi)
3	Stage 1 cylinder ΔP	383	±34,475 kPa (5000 psi)
4	Stage 2 cylinder ΔP	450	±1,737 kPa (2500 psi)
5	Stage 3 cylinder ΔP	514	±1,737 kPa (2500 psi)
6	Stage 4 cylinder ΔP	565	±1,737 kPa (2500 psi)
7	Stage 5 cylinder ΔP	627	±1,737 kPa (2500 psi)
8	Stage 6 cylinder ΔP	676	±1,737 kPa (2500 psi)

Clearanceometers and Touch Probes

A total of three clearanceometers were installed in the six-stage compressor stator case. One was installed over the Stage 3 rotor and two were installed over the Stage 5 rotor. The signals from the three clearanceometers were recorded on magnetic tape in the Data Recording Center and were also displayed on a calibrated scope for on-line determination of rotor tip clearances during the compressor test. Cooling air and water were supplied to each clearanceometer to maintain a temperature level below 395 K (250° F).

Two touch probes were installed in the compressor stator case; one over Stage 3 rotor and one over Stage 5 rotor. These touch probes measured the radial clearance between the highest rotor blade and the compressor stator case on each of the two stages. The touch probe readout was located in the Data Recording Center and was manually recorded on log sheets.

3.2 TEN-STAGE COMPRESSOR VEHICLE, FIRST BUILD

3.2.1 Description of Test Vehicle Configuration

The E^3 10-stage compressor vehicle was assembled for the initial test of the high pressure compressor system of the core module of the E^3 turbofan engine. The 10-stage compressor vehicle assembly is shown in Figure 5.

The 10-stage compressor vehicle was a two-bearing design incorporating a ball thrust bearing housed in the forward frame and a roller bearing housed in the slave aft frame. The compressor rotor system was driven from the aft end with a crowned spline adapter coupling it to the test facility drive system. Drive power was provided by the 33,000 horsepower facility steam turbine.

3.2.1.1 Rotor System

The compressor rotor consisted of 10 stages of low aspect ratio blades. Stage 1 through 4 rotor blades were made of titanium 6-4, had axial-type dovetails, and were installed in a titanium 6-4 forward spool. The Stage 5 rotor blades were made from Inconel 718, had axial-type dovetails, and were installed in a separate, titanium 6-4 disk. The Stage 6 through 10 rotor blades were

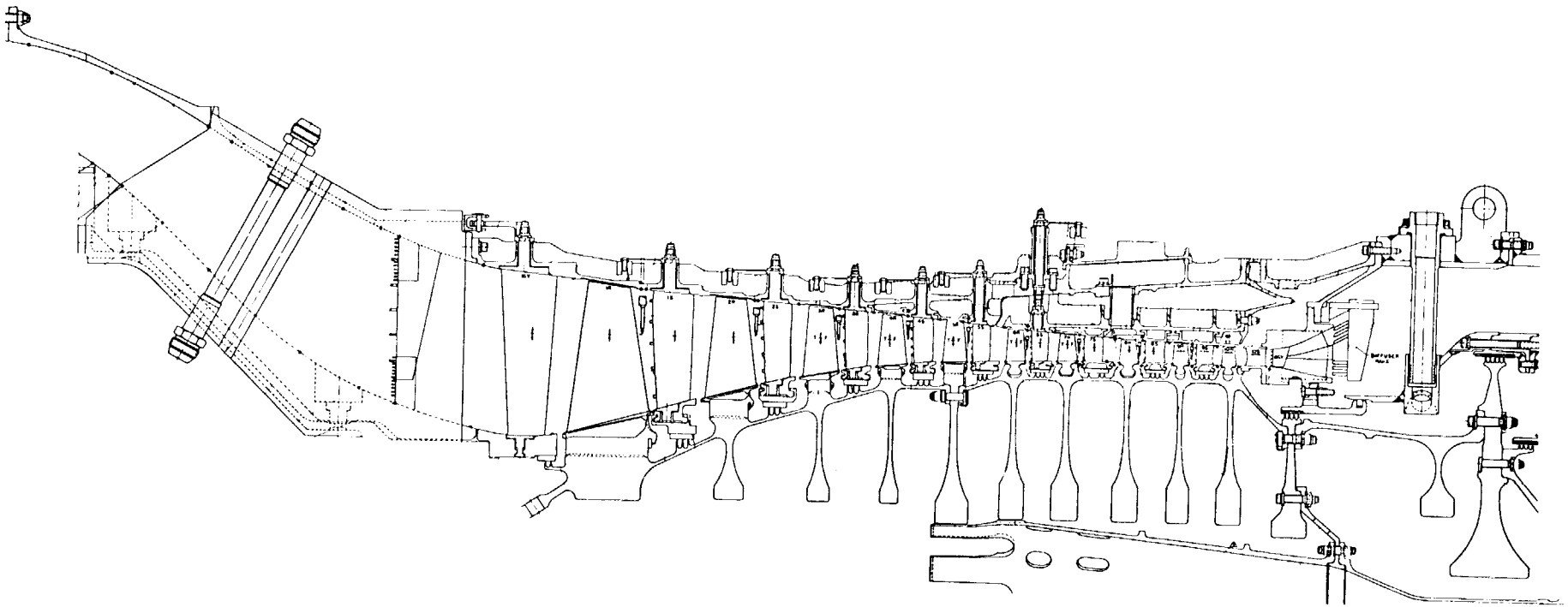

Figure 5. First 10-Stage Compressor Test Vehicle.

ORIGINAL PAGE IS
OF POOR QUALITY

made from Inconel 718, had circumferential-type dovetails, and were installed in a powder René 95 spool. A single-bolt circle joined the forward spool and the aft spool to the Stage 5 disk. The Stage 2 through 6 blades, the forward spool, and the Stage 5 disk were the same hardware previously used in the six-stage compressor vehicle. The Stage 1 blades were also from the six-stage compressor but were modified for the 10-stage compressor. The aft spool and the Stage 7 through 10 blades were new for the 10-stage compressor.

The aft section of the compressor rotor system was made up of slave hardware consisting of a CDP seal, drive spool, thrust balance disk, and an aft stub shaft. The thrust balance disk regulated the compressor forward thrust loads to prevent overloading of the ball thrust bearing in the forward frame. This slave hardware also contained instrumentation leadout tubes through which all compressor rotor instrumentation leads were routed aft to the externally mounted test facility slipring.

3.2.1.2 Stator System

The compressor stator system consisted of horizontally split forward and aft cases made from M152 material. The forward case provided mounting of the IGV through Stage 5 variable vanes while the aft case provided mounting of the Stage 6 variable vanes and the Stage 7 through 9 fixed vanes. The IGV through Stage 6 variable vanes were made from A 286 while the fixed Stage 7 through 9 vanes were made from cast Inconel 718. All of the stator vane stages had inner shrouds and honeycomb seals. Removable, segmented liners were installed in the forward case over rotor Stages 4 and 5. The liners for rotor Stages 7, 8, 9, and 10 are integral with the Stage 7, 8, and 9 fixed stator vane segments. Provisions were made in the forward and aft cases for the extraction of bleed air aft of both the Stage 5 and Stage 7 stators. The variable Stage 6 vanes located in the aft case were actuated by hardware which was mounted to and penetrated the forward case. All bleed extraction pads were located on the forward case.

The aft case was supported inside the forward case by an Inconel 718 wishbone. The Stage 10 vanes were attached to the diffuser frame. The diffuser frame also supported the stationary CDP seal.

3.2.1.3 Forward Frame System

The 10-stage vehicle utilized the slave forward frame from the six-stage vehicle. The frame had provisions for similar bearing and seal service lines, instrumentation leadout, and rotor cooling air as on the previous vehicle. The inner and outer flowpaths remained unchanged, as did the inlet and compressor mounting flanges.

3.2.1.4 Aft Frame System

The aft frame was a slave-type design that served as the support for the aft roller bearing. The frame contained the necessary provisions for supplying lube and air services to the aft bearing sump. The aft frame also contained passages for the extraction of rotor cooling air and balance piston seal leakage air.

3.2.2 Description of Test Facility and Vehicle Installation

3.2.2.1 Full-Scale Compressor Test Facility

High discharge temperatures generated by the E^3 10-stage compressor at SLS inlet conditions would have exceeded the 417 K (750° F) limit of the test facility discharge flow system. An inlet refrigeration system was designed and constructed that assured the compressor discharge temperature remained at an acceptable level. The refrigeration system was able to provide 18.1 kg/s (40 lb/s) airflow at a temperature of 220 K (-65° F). This system is shown schematically in Figure 6. High pressure air from the Lynn plant air supply system, supplemented with additional air from the Combustor Air Supply Lynn (CASL), was used to drive three AD-10 refrigeration units each consisting of a compressor, cooler, and expansion turbine. Prior to entering each AD-10 unit, the high pressure supply air passed through dryers which were designed to eliminate moisture from the air. The air left the AD-10 units as dry, refrigerated air and was piped to the inlet of the FSCT facility tank.

Ducting located inside the FSCT facility tank channeled the refrigerated air from its entering point to the compressor vehicle inlet bellmouth. A schematic of the ducting is shown in Figure 7. An inlet FOD screen with 0.635 cm (0.25 in.) square mesh was located upstream of the vehicle bellmouth.

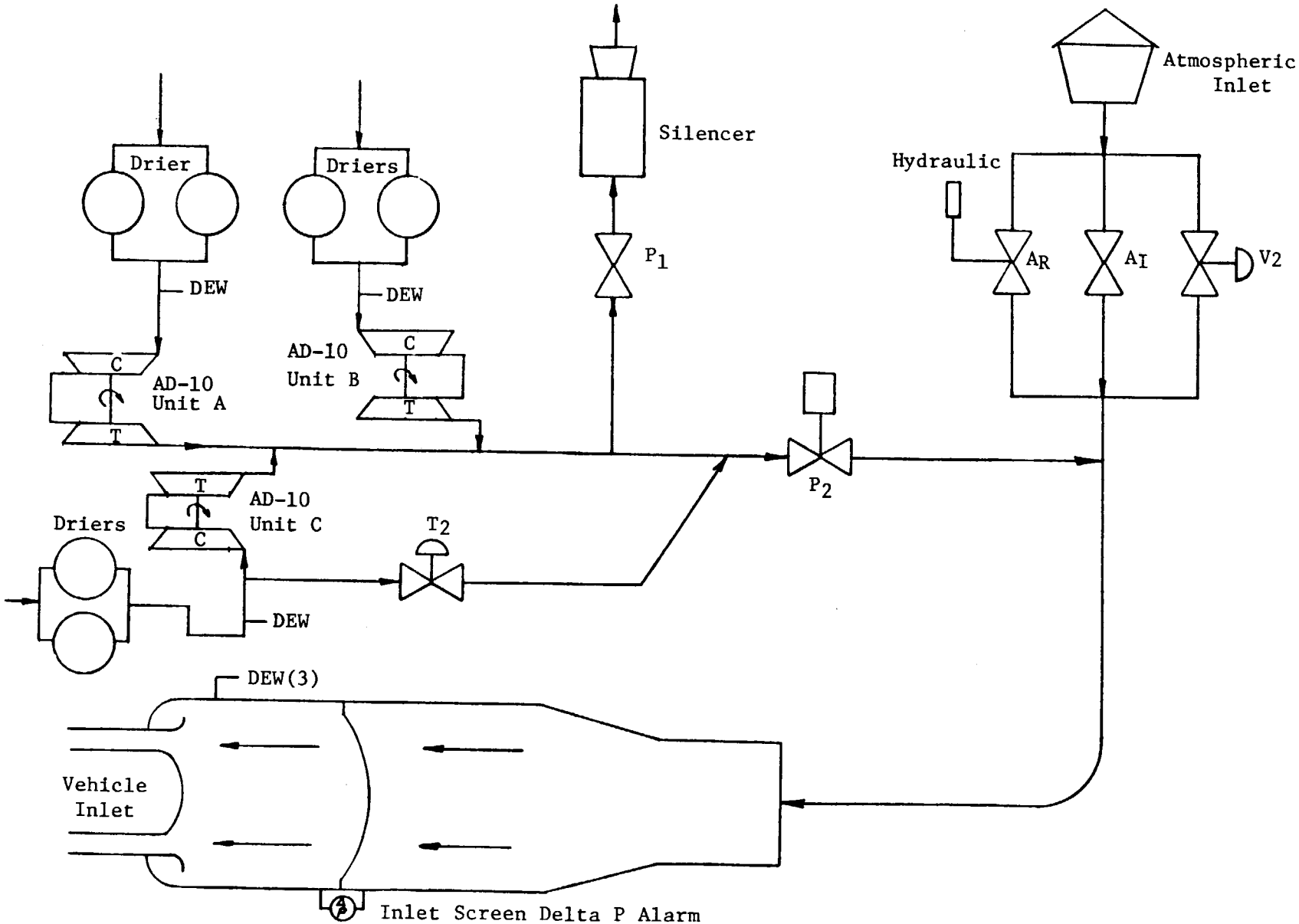

Figure 6. FSCT Inlet Refrigeration Schematic.

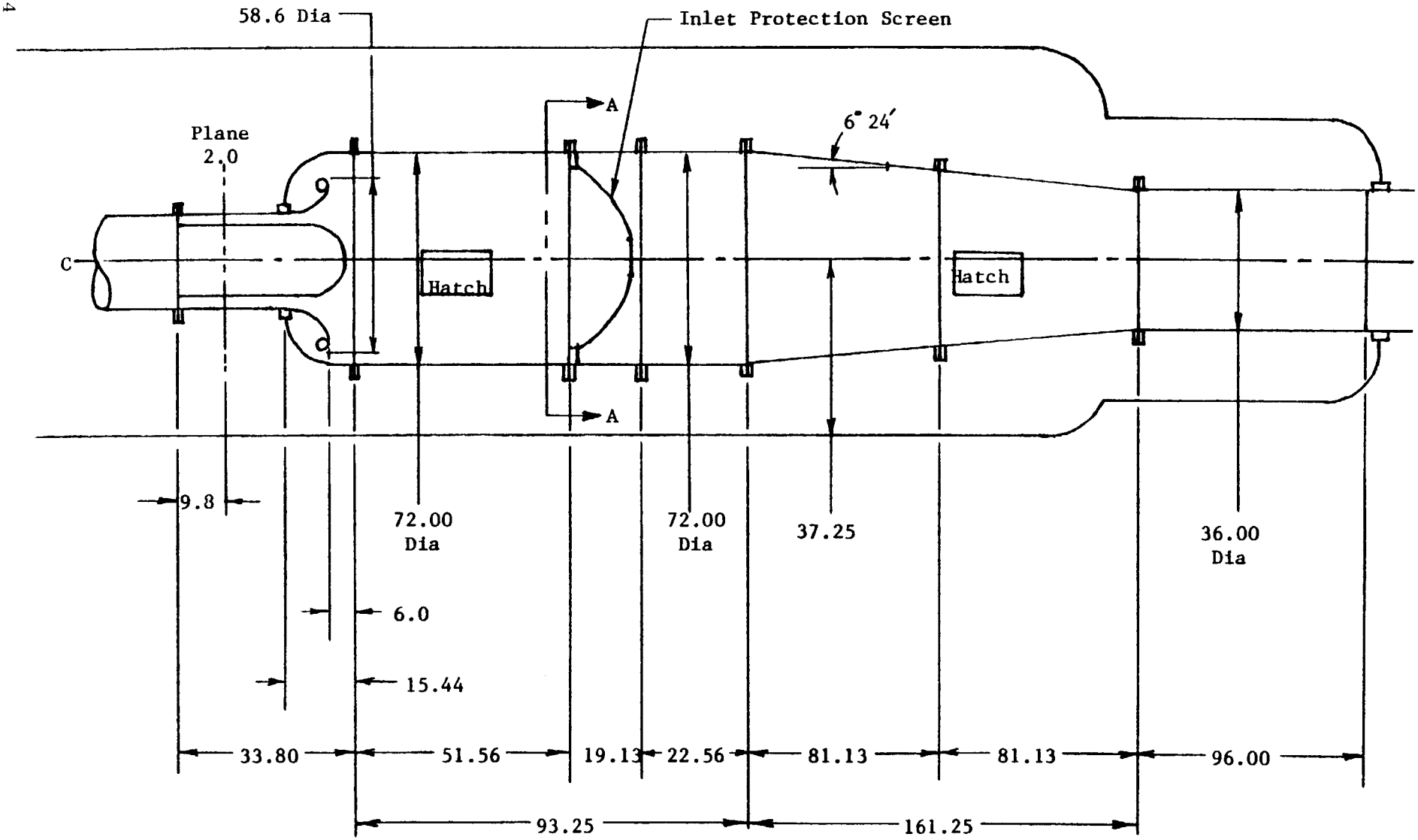

Figure 7. Schematic of Inlet Duct for 10-Stage Compressor Vehicle.

One of the major considerations during the design of the refrigeration system was the possibility of inlet icing. In order to detect the development of moisture in the supply air, dew point sensors were installed in the piping between the exit of the dryers and the refrigeration unit inlets. Three dew point sensors were also installed in the ducting just upstream of the bell-mouth inlet to detect any increase in the moisture content of the refrigerated inlet air. It was assumed that the first indication of ice formation in the inlet would occur on the 0.635 cm (0.25 in.) square mesh inlet FOD screen. In order to detect this possible ice formation, a differential pressure system was incorporated in the inlet ducting to monitor the pressure drop across the screen and to give an alarm should the pressure differential exceed 2.54 cm (1.0 in.) of water.

The incorporation of the new refrigeration system was the only change made to the FSCT facility after the six-stage compressor test was completed. The basic test facility description remains as described in Section 3.1.2.1.

3.2.2.2 Vehicle Inlet System

The aluminum bellmouth and bulletnose, which were utilized on the six-stage compressor, were moved forward approximately 50.8 cm (20 in.) in order to provide axial space for the distortion screen assembly. The bellmouth contained pads for the installation of four pitot static rakes utilized in the calculation of bellmouth airflow. Four wall static pressure taps were located on each of the bellmouth and bulletnose walls in the same axial plane as the pitot static rakes. The distortion screen support frame and gear drive for rotating the screen had been used previously. The weight of the screen assembly was supported by spring hangers from the overhead facility rail. Axial loads were reacted through side links into knee braces anchored to the facility floor. The outer shell of the distortion screen and the bellmouth were coupled to the vehicle front frame with a rubber seal slip joint. The center spool of the distortion screen and bulletnose were rigidly bolted to the front frame hub.

3.2.2.3 Bleed Systems

Stage 5 Compressor Bleed

In the engine, Stage 5 air, extracted from the outer flowpath between Stator 5 and Rotor 6, is intended to be used for customer bleed and to provide active clearance control (ACC) of the aft stator case. The customer bleed is extracted through the compressor case aft of Stator 5. The ACC air passes over the aft stator case and is extracted through the forward case in the plane of Rotor 10. On the vehicle, the two bleeds were collected by separate piping systems which conducted the bleeds through measuring sections and control valves prior to exhausting it to the atmosphere.

Stage 7 Compressor Bleed

Stage 7 compressor bleed air, designed to provide additional starting capability, was extracted from the compressor stator outer wall flowpath between Stage 7 stator and Stage 8 rotor. The bleed air was directed through the wall of the forward case into a manifold. Bleed air exited the bleed manifold through four ports on the manifold case. Four additional ports were available if they were needed for more bleed flow. Test facility piping collected the Stage 7 bleed air and conducted it through a flow measuring system and a remote control valve prior to exhausting it to the atmosphere.

Thrust Balance Bleed

Compressor discharge air was allowed to bleed into the cavity between the CDP seal and the rotor balance piston disk. This air was used to pressurize the forward side of the rotor balance piston disk to provide aft thrust on the rotor system. This aft thrust was used to regulate the amount of forward thrust in order to maintain safe thrust loads on the forward ball bearing. Bleed lines were provided in the aft frame for the extraction of the air which leaked past the seal teeth on the rotor balance piston disk. Test facility piping collected this seal leakage air as it exited through the six aft frame struts and conducted it through a flow measuring system and a remote control valve prior to exhausting to the atmosphere.

A schematic of the 10-stage compressor cooling air and bleed air systems is shown in Figure 8.

3.2.3 Description of Test Vehicle Instrumentation

3.2.3.1 Aerodynamic Instrumentation

Facility-provided instrumentation and inlet duct instrumentation remained unchanged from the six-stage compressor test.

Overall Performance Instrumentation

The core inlet measuring section (Plane 25), located immediately forward of the inlet guide vanes, contained static pressure taps on the outer wall and inner wall which were used to measure circumferential uniformity of airflow as well as inlet static-pressure levels. Four 5-element, total-pressure and total-temperature radial rakes located in the same plane as the static taps measured core inlet conditions. These rakes were also used to verify circumferential and radial uniformity of pressure and temperature during the clean inlet testing and were used to measure the level of inlet distortion as well as the face-average total pressure and total temperature during the distortion testing.

Plane 3 was the discharge measuring plane for the 10-stage compressor test and was located immediately aft of Stage 10 (OGV) stator vane row. Five 5-element, total pressure and five 5-element total-temperature radial rakes provided overall pressure rise and temperature rise measurements as well as indicating circumferential and radial distributions. Discharge static pressure was measured by five outer and five inner-wall static taps.

One 6-element, total-pressure and total-temperature rake was located at the diffuser exit (Plane 31). Three elements were located at the outer flowpath exit, and three elements were located at the inner flowpath exit. These measurements were to be used for comparison with engine test performance data.

Interstage Instrumentation

Manifolded static taps were mounted in the outer wall at all rotor inlet and rotor exit planes to measure the interstage static pressure distribution.

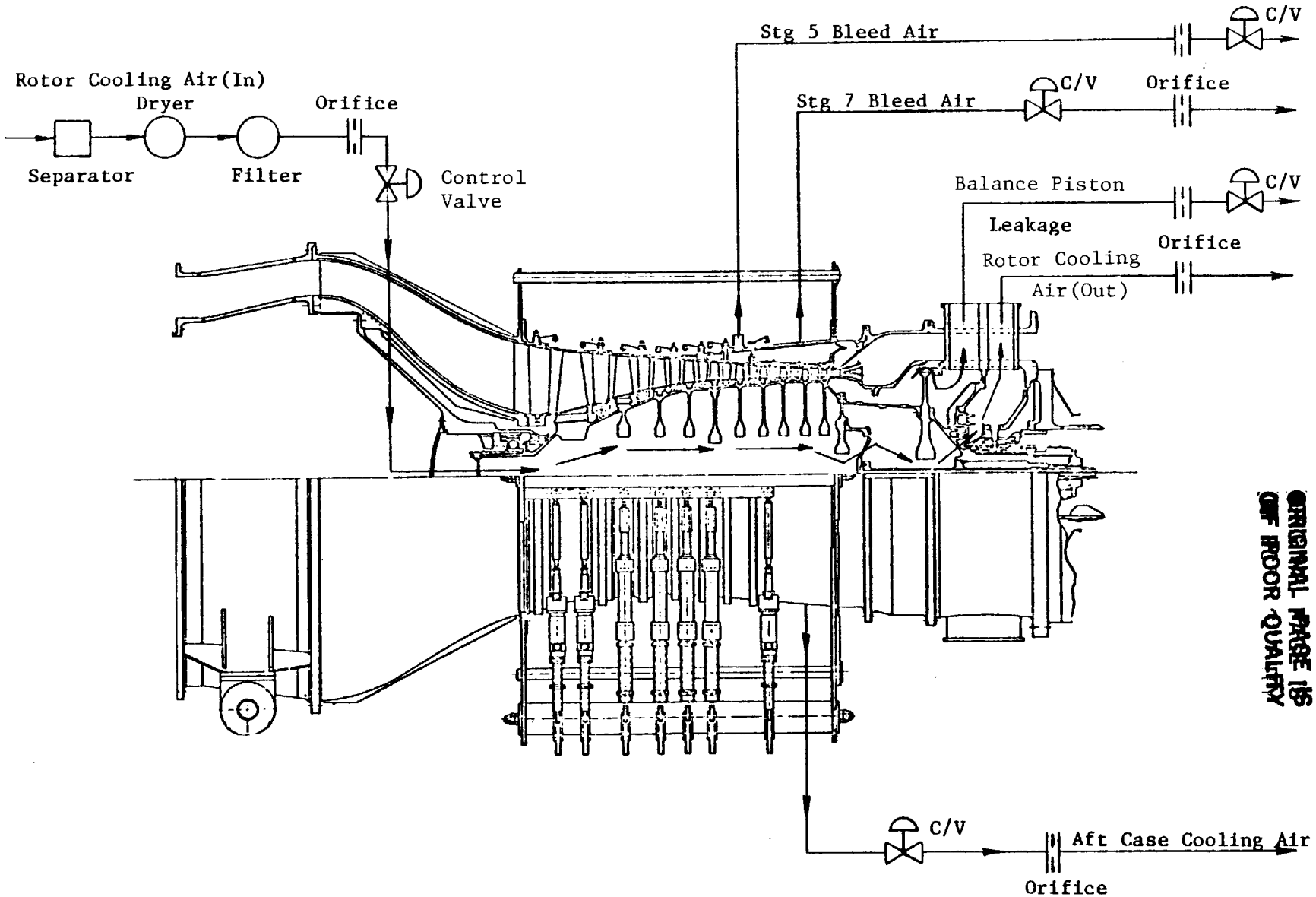

ORIGINAL PAGE IS
OF POOR QUALITY

Figure 8. Ten-Stage Compressor Cooling Air and Bleed Air Systems.

Individual static taps on the forward and aft side of the stator shrouds below the flowpath measured the hub shroud seal pressure difference which determined the seal leakage flow. They were also used to give an approximate indication of the tip-to-hub radial pressure distribution.

Rotor exit plane total pressures and total temperatures, used to calculate stage characteristics, were measured by vane leading-edge-mounted sensors at various radial immersions.

Traverse Probes

Radially traversable cobra probes were provided in each rotor exit plane. Detailed radial profiles of total pressure, total temperature, and yaw angle measured by these probes were used in conjunction with vane-mounted sensor data to evaluate blade element performance.

Bleed System Instrumentation

Bleed port air properties were monitored using two total pressure and two total temperature probes in the Stage 5 and 7 bleed manifolds. Bleed flow was metered by the facility.

3.2.3.2 Operational Instrumentation

Pressures

The following vehicle operational pressures were monitored on pressure gages in the FSCT control room and on the operating engineer's console in the DRC. Log sheet readings were taken every 30 minutes or as often as directed by the Evendale Evaluation Engineer.

Item No.	Parameter	Operating Requirements kPa (psig) Normal	Max.	Min.
282	Forward sump cavity	---	---	---
281-283	Carbon seal/fwd sump delta pressure	+68.95 (10)	+103.4 (15)	+34.5 (5)
943	Dual seal cavity	0	+13.8 (2)	---
939-943	Aft thrust disk/dual seal delta pressure	0	+6.9 (1)	-6.9 (1)
939	Aft thrust disk cavity	0	+3.8 (2)	---
294	Rotor cooling air supply	---	+1034 (150)	0
951	Aft sump cavity	0	+13.8 (2)	---
950-952	Carbon seal/aft sump delta pressure	+68.95 (10)	+103.4 (15)	+34.5 (5)
961	Rotor cooling air disch. cav.	0	+13.8 (2)	0
947	Single seal cavity	0	+27.6 (4)	0
947-961	Single seal/rotor cool delta pressure	0	+13.8 (2)	0
953	Aft sump cavity	0	+13.8 (2)	---
954	Aft sump cavity	0	+13.8 (2)	---
919	Forward CDP seal cavity	---	---	---
935	Aft CDP seal cavity	---	---	---
279	No. 1 bearing damper oil supply	---	+620 (90)	0
280	No. 1 bearing damper oil supply	---	+620 (90)	0
968	No. 2 bearing damper oil supply	---	+620 (90)	0

Temperatures

The following vehicle operational temperatures were monitored on Metrascopes in the FSCT control room and the steam turbine control room. Metrascope automatic alarms were set at the indicated temperature limits and were not changed unless approved by the Evendale Evaluation Engineer. During initial testing, paper tape printouts of these temperatures were taken at every steady-state data point reading or as requested by the Evendale Evaluation Engineer.

Item No.	Parameter	Limit K (° F)
275	No. 1 bearing outer race (360°)	478 (400)
276	No. 1 bearing outer race (90°)	478 (400)
277	No. 1 bearing oil in (internal)	333 (140)
278	No. 1 bearing oil in (external)	333 (140)
284	No. 1 bearing oil out (internal)	450 (350)
285	No. 1 bearing oil out (external)	450 (350)
921	Forward CDP seal cavity	700 (800)
937	Aft CDP seal cavity	700 (800)
941	Aft thrust disk cavity	700 (800)
945	Dual seal cavity	533 (500)
949	Single seal cavity	422 (300)
956	No. 2 bearing housing skin	408 (275)
957	No. 2 bearing outer race (22.5°)	395 (250)
958	No. 2 bearing outer race (142.5°)	395 (250)
959	No. 2 bearing outer race (262.5°)	395 (250)
963	Rotor cooling air discharge cavity	533 (500)
969	No. 2 bearing oil in	333 (140)

Strain Gages

Rotor

A total of 44 dynamic strain gages were applied to the blade airfoils on the 10-stage rotor. The distribution of strain gages is as follows: (Note TF denotes thin film gages)

Stage	Blades Instrumented	Gages Per Blade	Total Gages
1	2	2	4
2	4	1	4
3	4	1	4 (TF)
4	4	1	4 (TF)
5	4	1	4 (TF)
6	4	1	4 (TF)
7	5	1	5 (TF)
8	5	1	5
9	5	1	5
10	5	1	5

The signals from 24 rotor strain gages were monitored on scopes, 23 of which were simultaneously recorded on magnetic tape.

Stator

A total of 68 dynamic strain gages were applied to the stator vane airfoils. The distribution of strain gages is as follows:

Stage	Vanes Instrumented	Gages Per Vane	Total Gages
IGV	3	2	6
1	3	2	6
2	4	2	8
3	3	2	6
4	6	1	6
5	6	1	6
6	6	1	6
7	3	2	6
8	3	2	6
9	3	2	6
OGV	6	1	6

The signals from 36 stator strain gages were monitored on scopes and simultaneously recorded on magnetic tape.

Inlet Rakes

A total of 16 dynamic strain gages were applied to the compressor inlet pitot static and Plane 25 rakes. The signals from 12 rake strain gages were monitored on scopes and simultaneously recorded on magnetic tape.

Vibrations

A total of 15 accelerometers were mounted on the compressor vehicle and were located as follows:

Item No.	Vehicle Location	Vibration Direction	Accelerometer Part No.	Serial No.
125	Bellmouth	Vertical		
126	Bellmouth	Horizontal		
977	Inlet duct flange	Vertical	7701-100*	AT63
978	Inlet duct flange	Horizontal	7701-100*	AT69
273	No. 1 brg sump plate	Vertical	A6222M34*	2403
274	No. 1 brg sump plate	Horizontal	A6222M34*	2402
291	No. 1 brg sump plate	Axial	A6222M48*	2402
286	Front frame	Vertical	7701-100*	AT70
287	Front frame	Horizontal	7701-100*	AT74
295	No. 1 brg damper housing	Vertical	MDL 606-3	236

Item No.	Vehicle Location	Vibration Direction	Accelerometer Part No.	Serial No.
296	No. 1 brg damper housing	Horizontal	MDL 606-3	227
964	No. 2 brg service housing	Vertical	A6222M48*	2401
965	No. 2 brg service housing	Horizontal	A6222M48*	2404
966	Rear frame	Vertical	CA900-41	3178
967	Rear frame	Horizontal	CA900-41	3142

*Denotes Endevco models.

Of the above 15 accelerometers, 12 were monitored on scopes and simultaneously recorded on magnetic tape. Two X-Y plotters were used to plot the signals from selected pickups against vehicle rpm.

Sanborn Recorder

One 8-channel Sanborn strip chart recorder was used to monitor and continuously record line pressure differences of the IGV through Stage 6 variable stator vane actuators. The setup on the recorder was as follows:

Channel	Parameter	Item No.	Range
1	Vehicle speed	---	0 - 15,000 rpm
2	IGV actuator ΔP	300	0 ± 17,237 kPa (2500 psi)
3	Stage 1 actuator ΔP	383	0 ± 17,237 kPa (2500 psi)
4	Stage 2 actuator ΔP	452	0 ± 17,237 kPa (2500 psi)
5	Stage 3 actuator ΔP	514	0 ± 17,237 kPa (2500 psi)
6	Stage 4 actuator ΔP	565	0 ± 17,237 kPa (2500 psi)
7	Stage 5 actuator ΔP	620	0 ± 17,237 kPa (2500 psi)
8	Stage 6 actuator ΔP	676	0 ± 17,237 kPa (2500 psi)

Clearanceometers and Touch Probes

A total of seven clearanceometers were installed on the 10-stage compressor stator case. The location of these clearanceometers are as follows:

Item No.	Axial Location	Angular Location, degrees	Temperature Sensor Item No.	Limit, K (° F)
464	Stage 3	0	970	395 (250)
465	Stage 3	130	971	395 (250)

577	Stage 5	50	972	395 (250)
578	Stage 5	315	973	395 (250)
817	Stage 10	110.6	974	395 (250)
818	Stage 10	230.6	975	395 (250)
819	Stage 10	350.6	976	395 (250)

The signals from the seven clearanceometers were recorded on magnetic tape in the Data Recording Center and were also displayed on calibrated scopes for on-line determination of rotor tip clearances during the compressor test. Cooling air and water were supplied to each clearanceometer to prevent the operating temperature from reaching the 395 K (250° F) limit. Type E thermocouples attached to each clearanceometer were monitored on a Metrascope located in the turbine operator control room.

Three radially actuated touch probes were installed on the compressor stator case. These were located over Stage 3, 5, and 10 rotors. Each touch probe measured the radial clearance between the high rotor blade of the stage and the compressor stationary flowpath. The touch probe readout was located in the Data Recording Center and was manually recorded on log sheets.

3.3 TEN-STAGE COMPRESSOR VEHICLE, SECOND BUILD

3.3.1 Description of Test Vehicle Configuration

The second build of the 10-stage compressor vehicle (10B) was basically the same as the first build (10A). Rotor and stator hardware changes made to this build of the vehicle are defined in the following sections.

3.3.1.1 Rotor System

The Stage 1 and 2 blades, forward spool, Stage 5 disk, and aft spool remain unchanged from the 10A compressor vehicle. New rotor blades were installed in Stages 3 through 10. The blades in Stages 3 through 7 were a new design with increased hub camber. The blades in Stages 8, 9, and 10 were the original design airfoils which replaced the alternate higher camber airfoils used in the 10A compressor vehicle.

The aft section of the compressor rotor system was made up of slave hardware consisting of a CDP seal, drive spool, thrust balance disk, and an aft stub shaft. All of the slave rotor hardware was the same as that used on the 10A compressor rotor system.

3.3.1.2 Stator System

After the 10A compressor test, the stator vanes in Stages 2, 3, 4, and 5 were recambered back to their original airfoil configuration as used in the six-stage compressor vehicle. All other stator hardware remained unchanged.

3.3.1.3 Forward Frame System

All forward frame system hardware was the same as the 10A compressor vehicle except for the installation of a new ball thrust bearing.

3.3.1.4 Aft Frame System

All aft frame hardware was the same as the 10A compressor vehicle except for the installation of a new aft roller bearing.

3.3.2 Description of Test Facility and Vehicle Installation

3.3.2.1 Full Scale Compressor Test Facility

The basic FSCT facility is described in Section 3.1.2.1. For the 10B compressor vehicle test, an emergency stall recovery control was installed to minimize the time in compressor stall at high corrected speed conditions. In the event of a high speed compressor stall, a single button was depressed which opened the discharge throttle valve, moved the variable compressor stator vanes to the closed position, and decelled the compressor vehicle to 6000 rpm.

After use of the new inlet refrigeration system on the 10A compressor vehicle test, the following system changes were made in an effort to minimize the possibilities of inlet icing during the 10B compressor test:

- The flow direction through the drying towers was reversed to avoid packing of the tower desiccant and the resulting excessive drying tower pressure drop.

- The pretest recycling temperature of the drying towers was increased to improve the moisture absorbing capacity of the desiccant.
- The CASL air supply system was repaired to eliminate the vibration problems experienced during its use on the 10A compressor vehicle test.
- The FSCT facility ejector valve was replaced to allow further reduction of the FSCT facility tank pressure.
- A pressure check of the inlet ducting was made to identify and eliminate inflow leakage of moist ambient air.
- Improved techniques for the physical handling and interpretation of data from the dew point sensors were devised.

3.3.2.2 Vehicle Inlet System

This system remained the same as that described for the 10A compressor vehicle.

3.3.2.3 Lube System

This system remained the same as that described for the 10A compressor vehicle.

3.3.2.4 Air Systems

This system remained the same as that described for the 10A compressor vehicle.

3.3.2.5 Bleed Systems

This system remained the same as that described for the 10A compressor vehicle.

3.3.2.6 Hydraulic System

This system remained the same as described for the 10A compressor vehicle.

3.3.3 Description of Test Vehicle Instrumentation

3.3.3.1 Aerodynamic Instrumentation

The aerodynamic instrumentation of the 10B compressor vehicle was the same as that described in Section 3.2.3.1 for the 10A compressor vehicle except for the following:

- An additional 6-element, total pressure and total temperature rake was installed at the diffuser exit (Plane 31).

- Three static pressure tubes were installed on the outer wall of the exit plenum.

3.3.3.2 Operational Instrumentation

The operational instrumentation of the 10B compressor vehicle was the same as that described in Section 3.2.3.2 for the 10A compressor vehicle except for the following:

Strain Gages

Rotor

A total of 32 dynamic strain gages were applied to the blade airfoils on the 10B rotor. The distribution of strain gages is as follows: (Note: TF denotes thin film gages)

Stage	Blades Instrumented	Gages Per Blade	Total Gages
1	2	2	4
2	4	1	4
3	3	1	3 (TF)
4	3	1	3 (TF)
5	3	1	3 (TF)
6	3	1	3 (TF)
7	3	1	3 (TF)
8	3	1	3 (TF)
9	3	1	3 (TF)
10	3	1	3 (TF)

Stator

A total of 34 dynamic strain gages were applied to the stator vane airfoils. The distribution of strain gages is as follows:

Stage	Vanes Instrumented	Gages Per Vane	Total Gages
IGV	3	2	6
1	3	2	6
2	0	0	0

Stage	Vanes Instrumented	Gages Per Vane	Total Gages
3	0	0	0
4	0	0	0
5	0	0	0
6	0	0	0
7	3	2	6
8	3	2	6
9	3	2	6
OGV	4	1	4

4.0 AERODYNAMIC PERFORMANCE SUMMARY

4.1 SIX-STAGE COMPRESSOR TEST RESULTS

The test of the front six stages was the first in a series of development tests on the E^3 core compressor. These stages constituted the front variable geometry block of the compressor to which the fixed geometry rear stages were to be matched. The primary goal of the six-stage test was to determine the efficiency and pumping characteristics of the critical front stages of the compressor. Since interstage data in multistage compressors were rarely complete enough (and often not accurate enough) to obtain reliable efficiency values, knowledge of front block overall efficiency aided in directing development to those stages where performance improvements were needed most. In addition, the six-stage front block could be operated over a much wider range of back pressures than would have been possible if the fixed rear stages were present, so a much better understanding of each stage's full pumping characteristic from choke to stall was obtained.

The E^3 Six-Stage Compressor Test Plan called for a 120-hour test program divided among eight phases and 10 to 15 test runs. The program called for mechanical checkout, determination of the stall line and brief mapping with a preselected stator schedule, stator schedule optimization, mapping and stall line determination with the final selected stator schedule, and traverse and rotor tip Kulite data accumulation. Tests were initiated on January 25, 1980, and were completed on February 29, 1980. All of the above test objectives were accomplished. Over 117 hours of testing were performed during 14 test runs. A total of 428 data points were recorded of which 111 were traverse readings. Data were recorded at corrected speeds ranging from 40% to 105% of design, at inlet pressures between one quarter and one full atmosphere. Test vehicle and test facility operations were very good throughout the test; and as a result, the test was successful in demonstrating the front block performance and in producing sufficient data to guide further development efforts.

Compressor overall aerodynamic performance data were computed based upon inlet data from the four 5-element combination total-pressure, total-temperature rakes at Plane 25, which was located immediately ahead of the inlet guide vanes. The rakes were placed circumferentially halfway between the front frame struts in the core inlet transition duct. Discharge total temperatures and total pressures were measured by five 5-element combination total-pressure, total-temperature rakes immediately downstream of Stator 6. The exit radial rakes were indexed circumferentially to sample the flow at 0%, 20%, 40%, 60%, and 80% of a stator passage width. Elements on both the inlet and exit rakes were located radially at centers of equal annulus area. Arithmetic averages of the temperatures and pressures were used in calculating performance quantities. Because of the spacing of the rake elements, this was the equivalent of calculating an area-weighted average. This data averaging method was fully consistent with General Electric engine testing practice, and was to be used on the subsequent component and engine tests so that the data would be comparable. Overall performance was computed using the real gas properties of air including the effects of humidity.

The performance map for the optimized stator schedule is shown in Figure 9, and the stator schedule is shown in Figure 10. In Figure 9, the aero design point total pressure ratio of 9.83 at a corrected flow of 54.4 kg/s (120 lbm/s) is shown by the target symbol. The objective stall line for the front block of six-stages is shown by the solid line, while the estimated operating line is shown by the dashed line. Note that the operating line pressure ratio at design flow is 9.6, somewhat below the 9.83 design value. This reflects the fact that overall compressor design pressure ratio was 25 compared to an engine operating line value of 23. The efficiencies shown are the unadjusted measured data.

The test results shown in the performance map indicate that the airflow and as-tested efficiency goals were met, but the stall line generally was low. Since it was determined that efficiency held up well at overspeed conditions, a stator schedule was selected that kept the IGV and first stator a few degrees closed at design speed and above in order to improve stall margin. As a result of using this schedule, the design flow was reached at 102% speed.

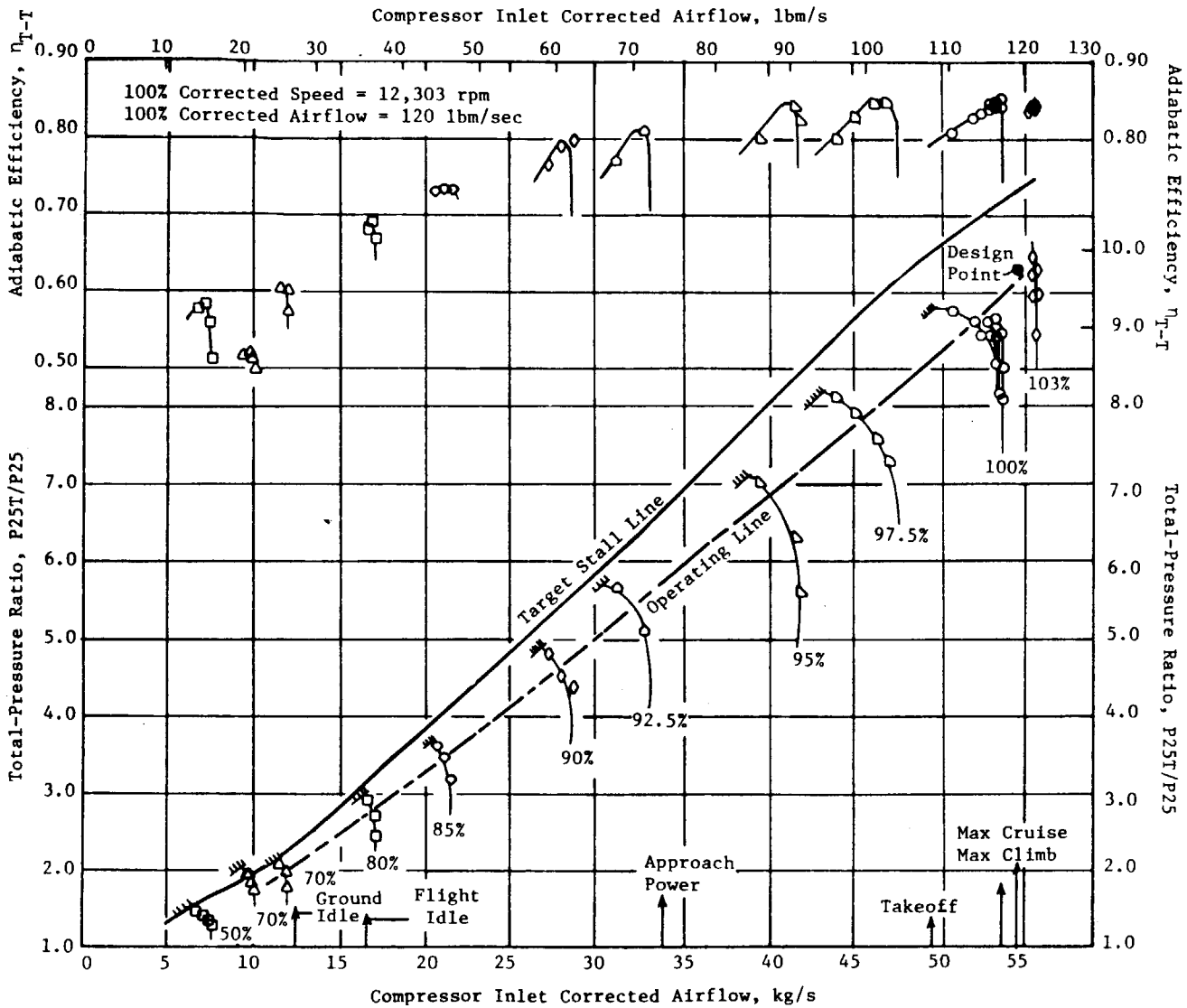

Figure 9. Six-Stage Compressor Performance Map.

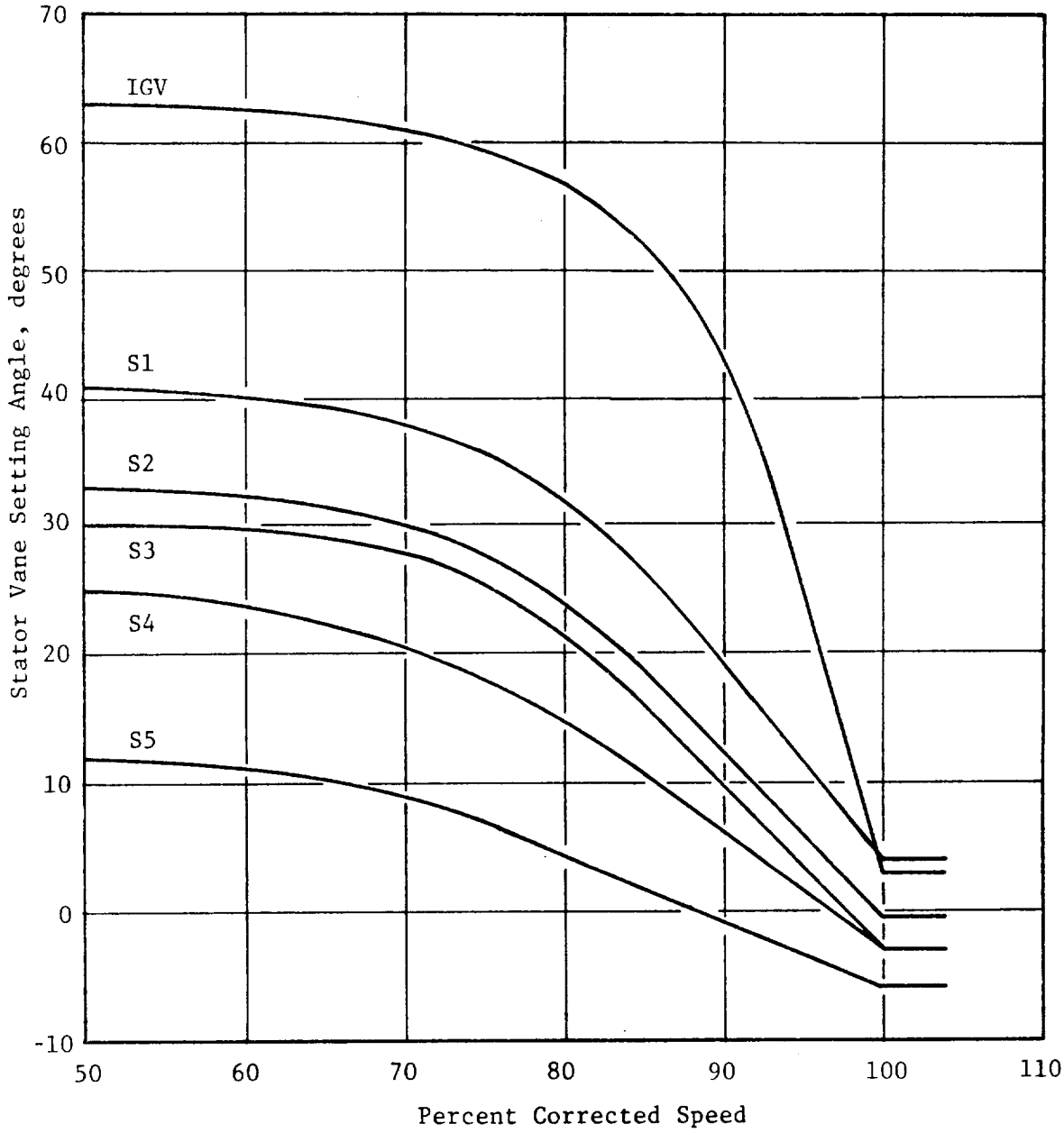

Figure 10. Compressor Six-Stage Test Stator Schedule.

Measured efficiencies at this condition did meet the test goal, so this schedule was acceptable for interim development. A test efficiency of 84.7% was measured at 104% of design speed (102% design flow) on an operating line 6% below the objective operating line. The best efficiency measured was 85.6% at 100% speed on a somewhat lower operating line. Front block test efficiencies agreed with pretest predictions within 1 point over the whole speed range when measured on an operating line 8% below the objective.

An adjustment to the measured efficiency, required to correct the data upward to conditions expected during engine operation, amounted to 2.1 points. This adjustment consisted of the following effects:

- Transition duct and front frame strut pressure losses undetected by the Plane 25 rakes - 0.80 point
- Losses due to inlet rakes and airfoil-mounted instrumentation - 1.04 points
- Losses resulting from hardware variance - 0.76 point
- A bookkeeping adjustment due to instrumentation location variances - -0.5 point.

No adjustments were made for rotor tip clearance or Reynolds number effects, since they were comparable to the actual engine values. Comparisons of peak test efficiency data and the performance goals near two primary E^3 engine operating condition are given in Table I.

Table I. Comparison of Efficiencies.

	Max. Cruise	Max. Climb
Corrected airflow kg/s, (lbm/s)	53.5 (118)	55.6 (122.5)
Corrected speed, %	100	103
Measured peak efficiency	0.856	0.847
adjustments	+0.021	+0.021
Adjusted test efficiency	0.877	0.868
Test efficiency goal	0.855	0.851*
ICLS efficiency goal	0.869	0.865*
FPS efficiency goal	0.878	0.874*°

*@54.4 kg/s (120 lbm/s)

As indicated by the data in Table I, the adjusted peak test efficiencies appeared to be exceeding the ICLS objectives in the high speed operating region. However, in this region, peak efficiencies occurred below the objective operating line whereas efficiencies on the operating line were several tenths of a point lower than those listed above. At ground idle airflow and below, the objective stall line was met with the efficiency level being close to the objective. However, at airflows above ground idle, the stall line gradually dropped below the objective. At flight idle, it was 4.5% low, and the difference grew to about 7.5% low at 100% speed (91% airflow), the highest speed at which a stall was recorded with a reasonably well balanced stator schedule. The fact that the stall line in the start region exceeded the target was quite encouraging because this was the area of greatest concern for the ultimate practicality of this compressor. However, it was clear that further development was required to meet the high speed stall margin requirements.

The flow versus speed relationship for this compressor was very steep, because the front block of a very high pressure ratio spool must run with extremely closed stators at intermediate speeds, as evidenced by Figure 10. Thus 50% airflow was attained at 89% speed and 25% airflow at 74% speed. The rear block of the spool was predicted to operate at its design corrected speed and flow for all front block flows above 40% of the design value. Development of the rear stages was expected to consist primarily of assuring that the design pumping was achieved with sufficient stall margin.

Data obtained from vane-mounted sensor and traverse probes indicated that the flow was weak (low total pressure and low axial velocity) in the hub region at high speeds. Comparisons of the vane-mounted total pressures and the traverse probe data with the predicted pressures at the exit of Rotors 3 and 6 are shown in Figure 11. It appeared that the weak hub profile initiated in Stage 3 and continued to deteriorate through Rotor 6. The low stall margin and the low operating line along which peak efficiency occurred were clearly associated with this.

Design changes intended to improve the hub flow conditions were specified as a result of the front block test. Preferred rotor blading changes could not be implemented in time for the first 10-stage compressor test, so changes to the existing variable stators were specified. The changes were designed to

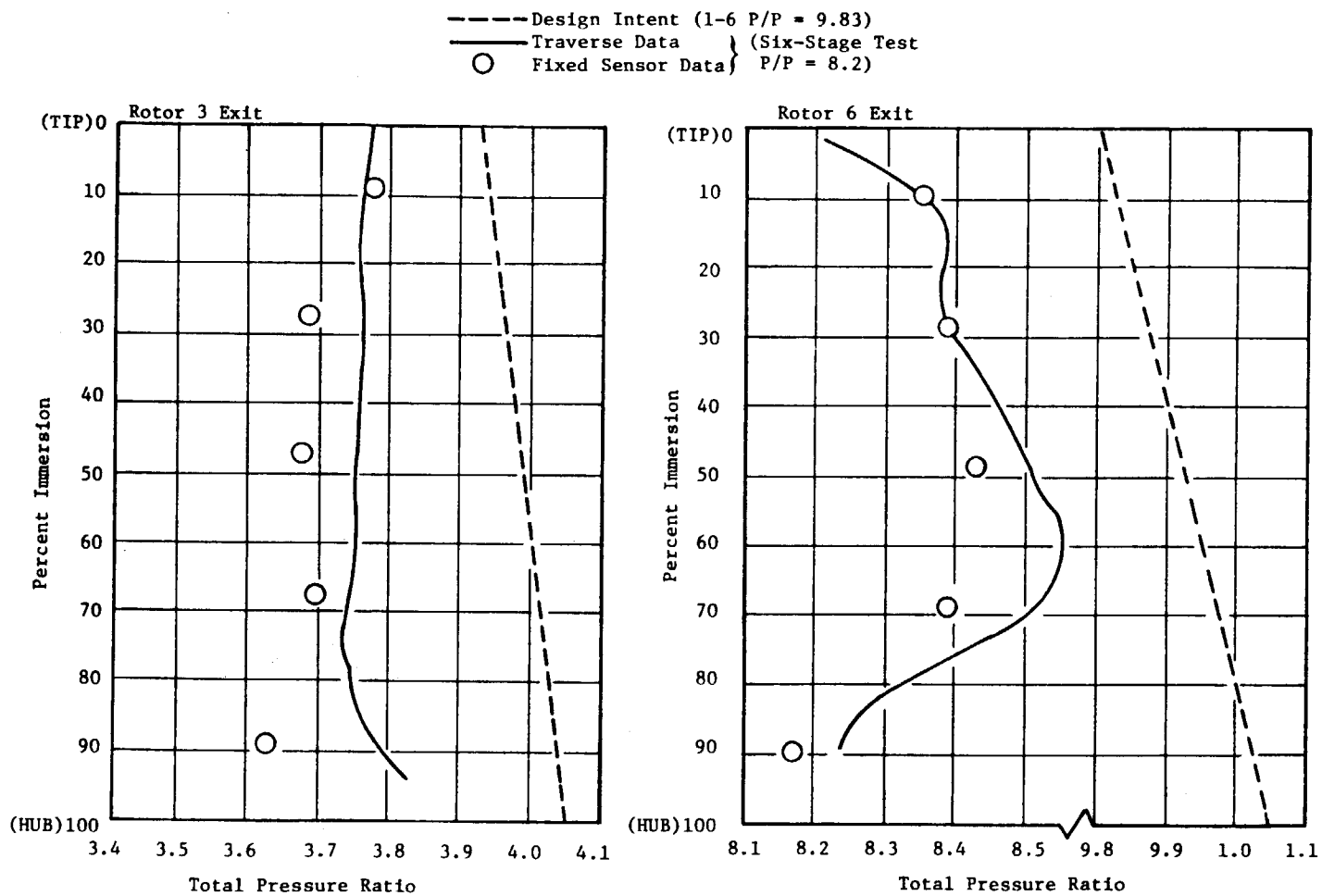

Figure 11. Six-Stage Compressor Radial Total Pressure Distribution.

strengthen the hub flow as much as the preferred rotor changes. However, the full efficiency potential of the compressor was not expected to be realized until all the front rotor modifications were incorporated. A general description of the design changes incorporated into the two 10-stage test vehicles is given in the following two sections.

4.2 TEN-STAGE COMPRESSOR TEST RESULTS, FIRST BUILD

The second of the series of E^3 core compressor component tests was the first build (10A) of the full 10-stage compressor. As a result of the six-stage test, several modifications were incorporated into the first 10-stage test vehicle. Blading changes to the front six stages included twisting the IGV hub open by 4°, twisting the Rotor 1 tip closed by 2.5°, and twisting the hub of Stators 1 through 6 open by 3.5° plus adding more hub camber to their trailing edge, 8° for Stators 1 through 4 and 5° for Stators 5 and 6. In addition, the axial dovetails of the front five rotors were sealed with silicone rubber to reduce recirculations that were predicted, using data from a dovetail leakage test conducted after the six-stage test, to result in significant efficiency penalties. The rear stators for the initial test of the full 10-stage compressor were built per the original design. However, an alternate set of high camber rear rotors (6° more camber at all radii) was used in Stages 8 through 10 in order to favor low speed start region performance. Use of these rotors also gruarded against the possibility that the original design rear rotors might also have insufficient hub camber, as had evidently occurred in the front rotors. The inlet guide vane and first six stators were variable in this test vehicle, and Stage 7 exit start bleed was provided. Customer bleed air and rear case active clearance control air extractions at Stage 5 exit were also incorporated. The compressor was tested with the same simulated core engine inlet transition duct as had been used in the six-stage test in order to provide realistic inlet flow conditions.

The test plan called for a 150-hour test program divided among nine phases and 15 to 18 test runs. The primary goals of the initial 10-stage test were to determine if the front stage modifications would correct the poor hub performance of the original design, and to determine the performance of the rear block of stages. In adddition, high speed efficiency and stall margin goals

were established for this test, and the requirements of the overall engine system in the subidle start region created other goals for this test. Stator schedules were to be refined at all speeds, and the effects of Stage 5 and Stage 7 bleed extraction on start region performance were to be investigated. The effect of Stage 5 customer bleed on high speed performance was to be studied, as was the effect of active clearance control bleed. Rotor exit traverse data were to be obtained, and performance tests with several types of inlet flow distortion were to be conducted.

Tests were initiated on March 20, 1981, and were terminated after Rotor 1 blade foreign object damage was detected following a high speed stall on April 10, 1981. Approximately 80 hours of testing had been performed, and 200 data readings had been obtained. Although traverse and inlet distortion data were not obtained, sufficient data were taken to determine front and rear block performance characteristics and to demonstrate the high and low speed performance potential of the design. The further development of the compressor, accomplished by incorporating the final airfoil design into the second 10-stage component test and into the core engine and ICLS turbofan engine tests, used the data that were obtained from the first 10-stage test described in this section.

Compressor overall aerodynamic performance data for undistorted inlet tests were computed based on inlet data from the four 5-element combination total-pressure, total-temperature rakes at Plane 25, which were located immediately ahead of the IGV's. The rakes were placed circumferentially halfway between front frame struts in the core inlet transition duct. The inlet rakes and their locations were the same as used in the six-stage test. Discharge flow conditions were measured by five 5-element, total pressure and five 5-element, total temperature rakes immediately downstream of Stator 10. The exit radial rakes were indexed circumferentially to sample the flow at 0%, 20%, 40%, 60%, and 80% of a stator passage width. Elements on both the inlet and exit rakes were mounted radially at centers of equal annulus area. Arithmetic average values of the temperatures and pressures were used in calculating performance quantities. Because of the spacing of the rake elements, this was the equivalent of calculating an area-weighted average. This data-averaging method was consistent with General Electric engine testing practice.

A single 6-element, combined total pressure, total temperature rake was located at the diffuser exit in order to duplicate the instrumentation to be used in engine tests. Overall performance was computed by using data from this rake also, to make data from the component test and subsequent core engine and ICLS tests comparable. The real gas properties of air, including the effects of humidity, were used for computing the performance data of the overall compressor as well as that of the front and rear blocks.

Front block (Stages 1 through 6) aerodynamic performance data were calculated from the compressor inlet data measured by the Plane 25 rakes as described above, and from the vane-mounted instrumentation at the leading edge of Stator 6. Total pressure was measured at five immersions corresponding to centers of equal annulus area, and total temperature was measured at the first, third, and fifth immersions. Rear block (Stages 7 through 10) performance data were computed from the Stage 6 leading edge data and from the compressor exit data measured by the OGV exit rakes.

The test results for this initial 10-stage compressor are summarized in the performance map shown in Figure 12, for the final stator schedule shown in Figure 13. All the data points presented were recorded without casing active clearance control bleed and without either Stage 5 or 7 bleed. The vehicle was operated at low speeds in a full open cycle mode, with inlet air at ambient temperature and with the inlet pressure controlled by an inlet throttle valve. At high speeds, above 87% of design speed, test facility discharge temperature limitations required that the inlet air be refrigerated to approximately 200 K (-65° F); limitations on the physical airflow of the refrigeration system required that inlet pressure be reduced to approximately 0.25 atmosphere when operating near design inlet corrected airflow. Thus, for speeds of 87.0% and above, the test compressor was operated at Reynolds numbers lower than the engine cruise operating conditions.

In Figure 12, the engine maximum climb design point, 54.4 kg/s (120 lbm/s) inlet corrected flow and 23:1 total pressure ratio, is shown by the target symbol. The objective stall line is shown by the solid line while the operating line is shown by the dashed line. Peak efficiency points are shown at each speed and are the unadjusted measured data. An adjustment to the measured efficiencies, required to correct the data upward to conditions expected

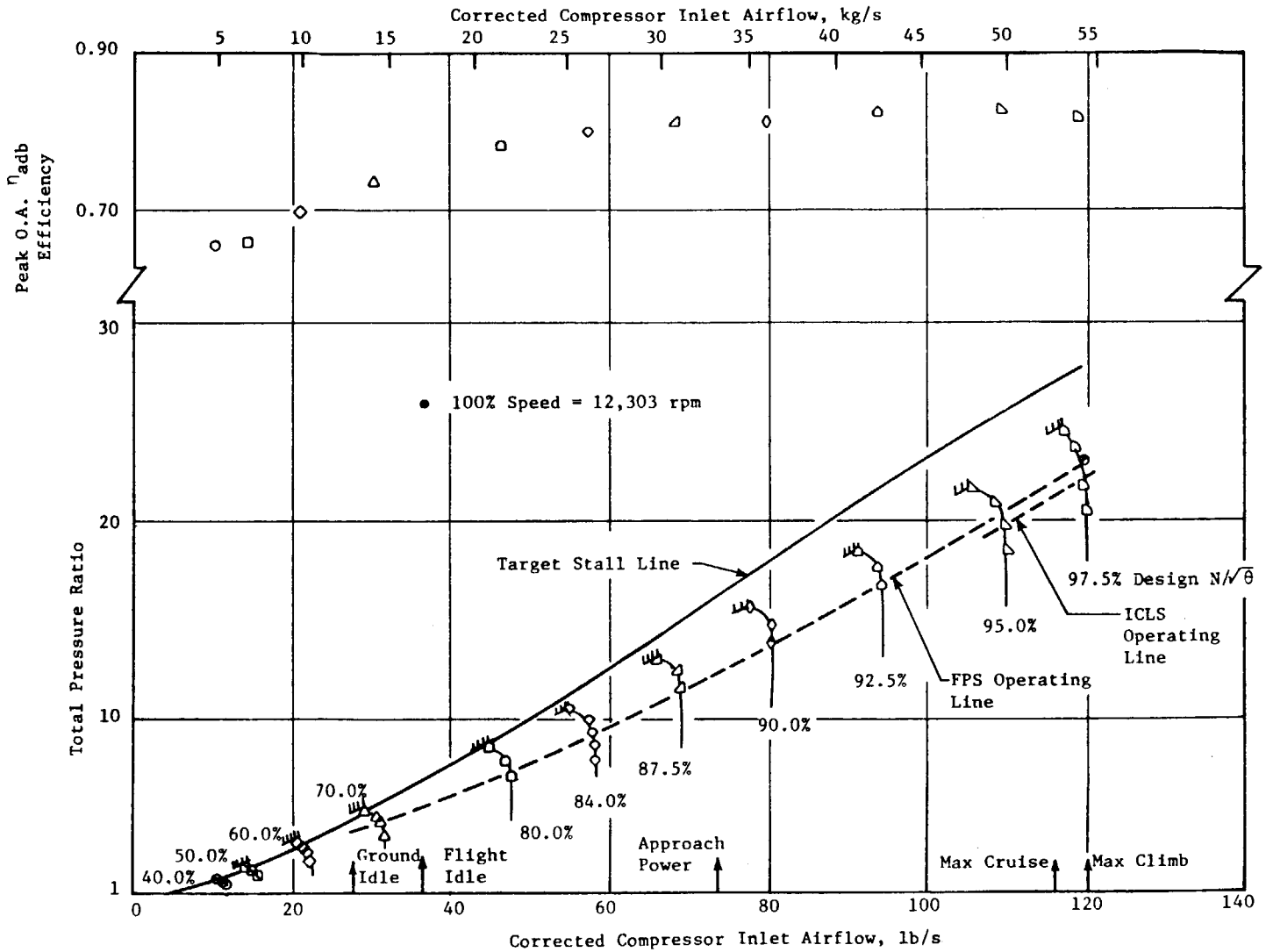

Figure 12. Performance Map For The First 10-Stage Compressor Test.

during engine operation, amounted to 2.1 points. This total adjustment consisted of the following effects:

- The transition duct and the strut pressure losses undetected by the Plane 25 rakes - 0.6 point
- Losses due to the inlet rakes and airfoil-mounted instrumentation - 1.2 points
- Efficiency decrements associated with the Reynolds number being lower than the engine cruise conditions - 0.3 point.

No adjustments were made for hardware quality variations, or for the fact that clearances were somewhat larger than the engine goal since the active clearance control system was not being used.

The design airflow of 54.4 kg/s (120 lbm/s) and the FPS operating line pressure ratio of 23:1 were achieved at 97.5% design speed with the stator schedule shown in Figure 13. A stall margin of 11% was demonstrated relative to this operating condition. After adjustment, the measured peak efficiencies of 0.826 at 95% speed and 0.818 at 97.5% speed exceeded the goals for the first full 10-stage compressor test. A listing of demonstrated high speed efficiencies is given in Table II. A summary of the adjustments added to the measured data is also given in Table II. Peak measured efficiencies for 95% and 97.5% speed are given, and these data points are close to the engine operating line. The efficiency goal for this test was 0.836 at the maximum cruise flow of 118 lbm/s; this goal was exceeded by about 0.5 point, and the goal for the second 10-stage test of 0.846 was nearly achieved. The data points presented in the table were recorded with maximum rotor bore cooling airflow and no rear case active clearance control airflow.

Low speed stall margin and efficiency exceeded goals that had been established based upon engine starting considerations, and this encouraging level of low speed performance was achieved without the use of start bleed or variability in Stator 6. As shown in Figure 12, the low speed stall line, demonstrated without interstage bleed, met or exceeded the objective up to 80% speed. Peak efficiencies measured in this subidle region were a few points higher than the goal. A more extensive analysis of these data indicated that the low speed performance of this compressor, as measured without adjustment or interstage bleed, would allow a 45-second engine start.

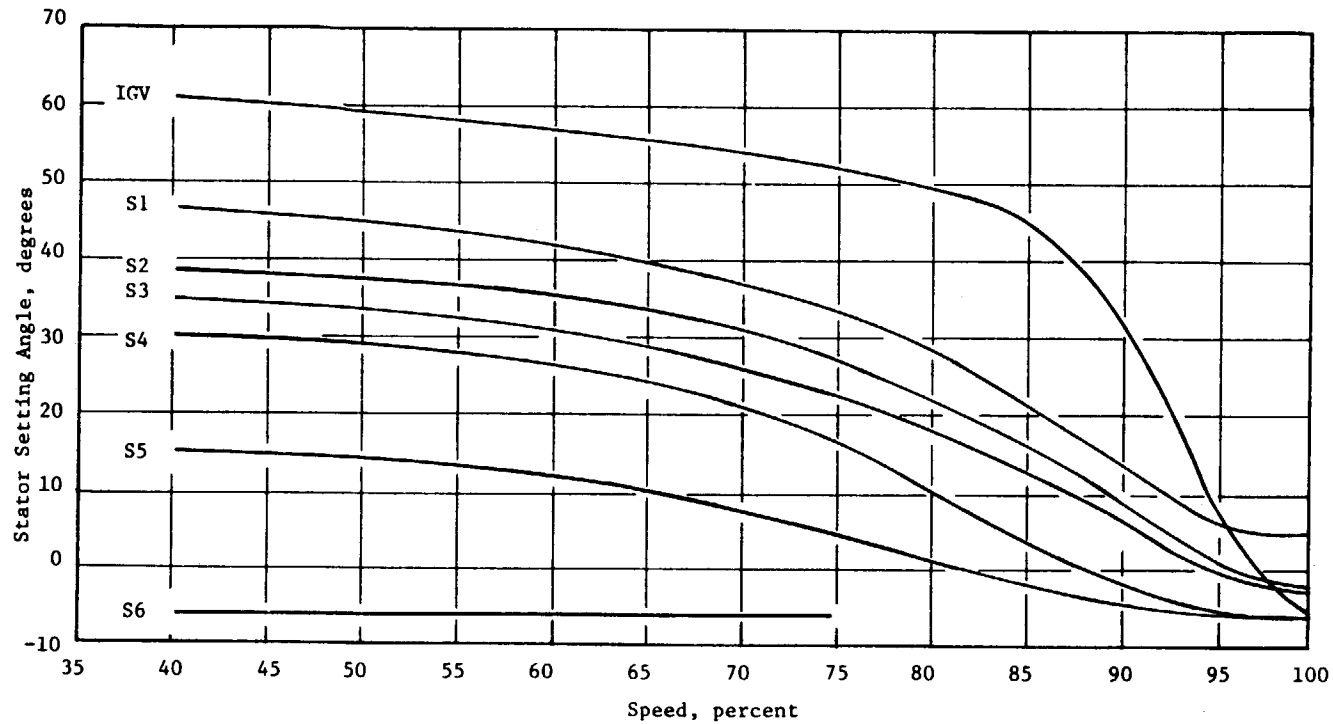

Figure 13. Final Stator Schedule for the First 10-Stage Compressor Test.

Table II. High Speed Efficiency Summary.

	95% Speed 50.0 kg/sm (110 lbm/s flow)	97.5% Speed 54.4 kg/sm (120 lbm/s flow)
Measured efficiency	0.826	0.818
Experimental adjustments:		
Inlet rake interstage instr. losses	0.012	0.012
Inlet duct loss	0.006	0.006
RNI less than FPS at cruise	0.003	0.003
Adjusted efficiency	0.847	0.839
Goal for first test at max cruise 53.5 kg/s (118 lbm/s flow)	0.836	
Goal for second test at max cruise 53.5 kg/s (118 lbm/s flow)	0.846	
ICLS Goal	0.851	
FPS Goal	0.861	

Analysis of the interstage data indicated that using the high camber rear rotors caused the rear group of fixed geometry stages (Stages 7 through 10) to operate at higher than design flow and pressure ratio at the FPS operating line. This is seen in Figure 14 which shows a performance map for Stages 7 through 10. The data points shown were recorded at a constant 97.5% of the full compressor design corrected speed (corrected by the Stage 1 inlet temperature), but the corrected speed of the rear block varied from 98.0% of design to 95.5% as the Stage 7 inlet temperature increased during throttling. The design intent flow and pressure ratio occurred at the intersection of the operating line and the predicted 100% speed line. The rear block pumped approximately 8% more flow than design intent, with correspondingly higher pressure ratio, the speed line was flatter than predicted. These rear stages were the most highly loaded in the machine and were responsible for causing stall at high speed. The peak efficiency of the rear stages occurred slightly below the operating line, but was close to design intent level.

The high pumping of the rear stages also had the effect of reducing the aerodynamic loading of the front stages. Figure 15 presents the performance of the front six stages. The target symbol indicates the design operating point of the front block when the overall compressor pressure ratio was 23:1. The actual operating point for this test is indicated by the dashed operating line, and is seen to be considerably lower than intended. In fact, the front stages could not be throttled much beyond their design point, nor could they be throttled beyond the stall line they demonstrated during the six-stage test. It is believed that the modified front block stall line was higher than in the six-stage test, since the blading modifications and dovetail sealing did result in substantial strengthening of the interstage pressures in the hub region. The mismatch between front and rear block pumping prevented loading up the front stages at high speed, despite use of noticeably opened stator settings for Stators 2 through 6, so the true maximum loading capability of the front block was not determined in this test.

Comparisons of the total pressures measured by the vane-mounted sensors of this test with the six-stage test data and with the design intent at the exit of Rotors 3 and 6 are shown in Figure 16. It is evident that the hub region pressure ratio was significantly improved, and equaled or exceeded the design intent.

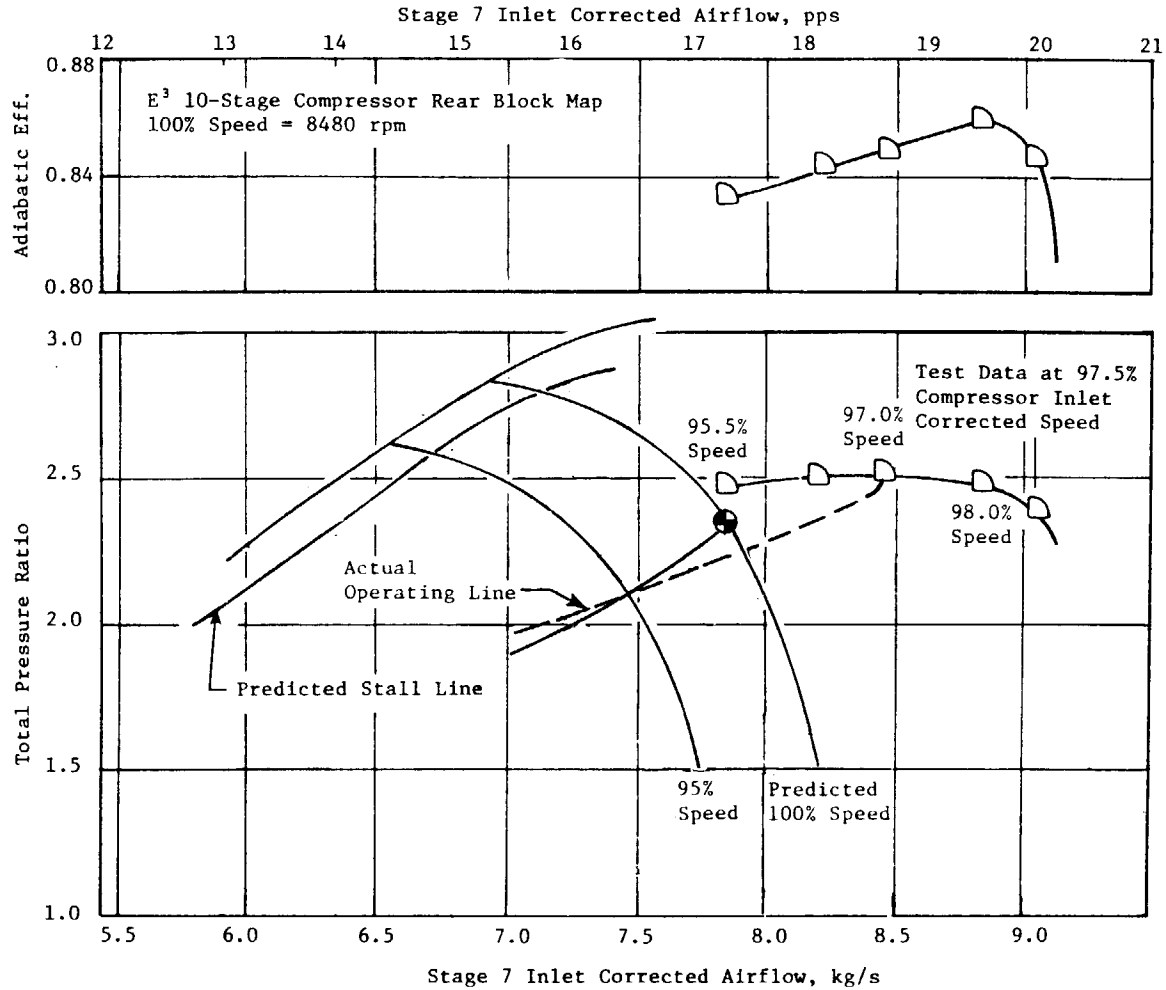

Figure 14. Performance Map of Stages 7 Through 10.

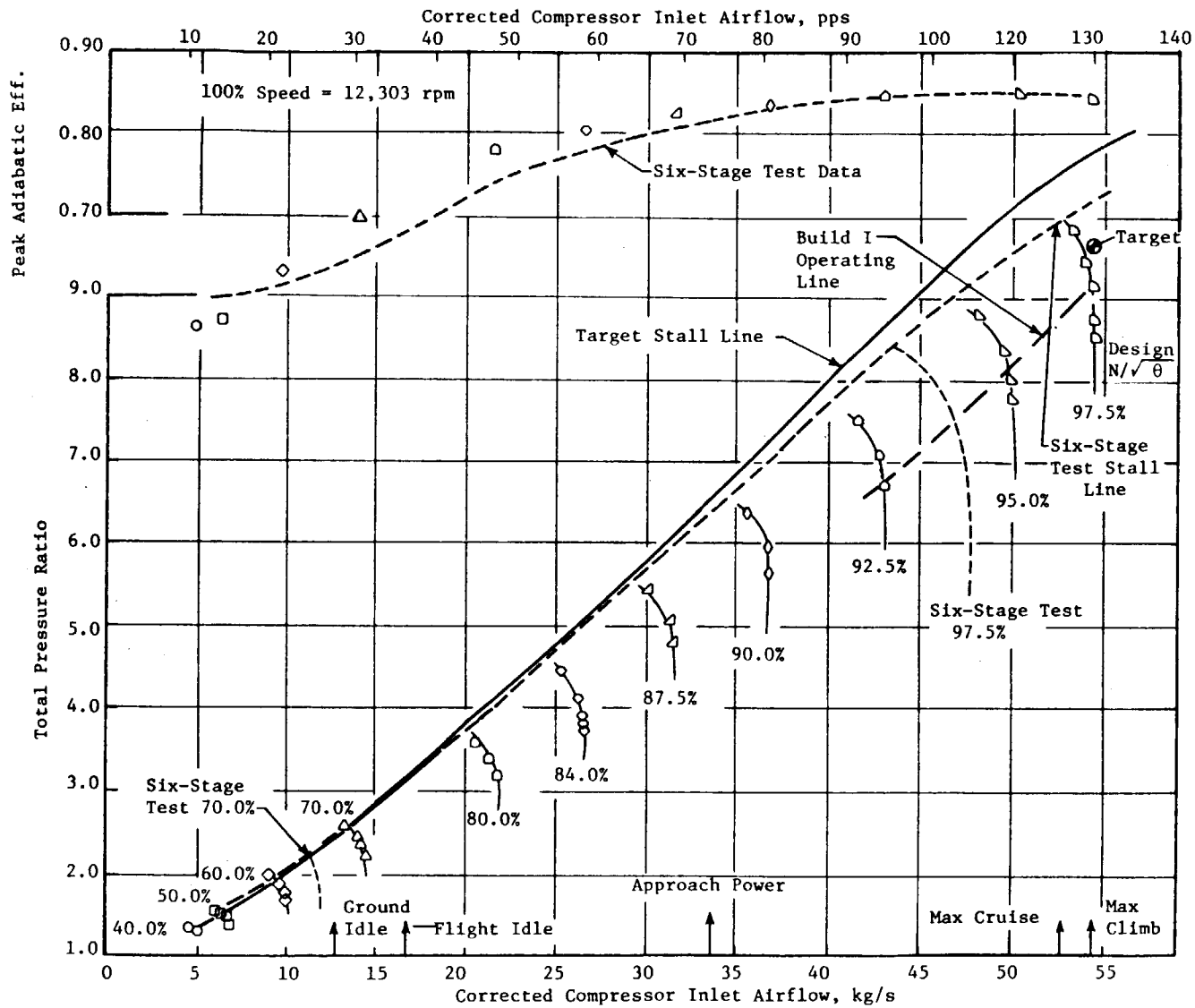

Figure 15. Performance Map for Stages 1 through 6.

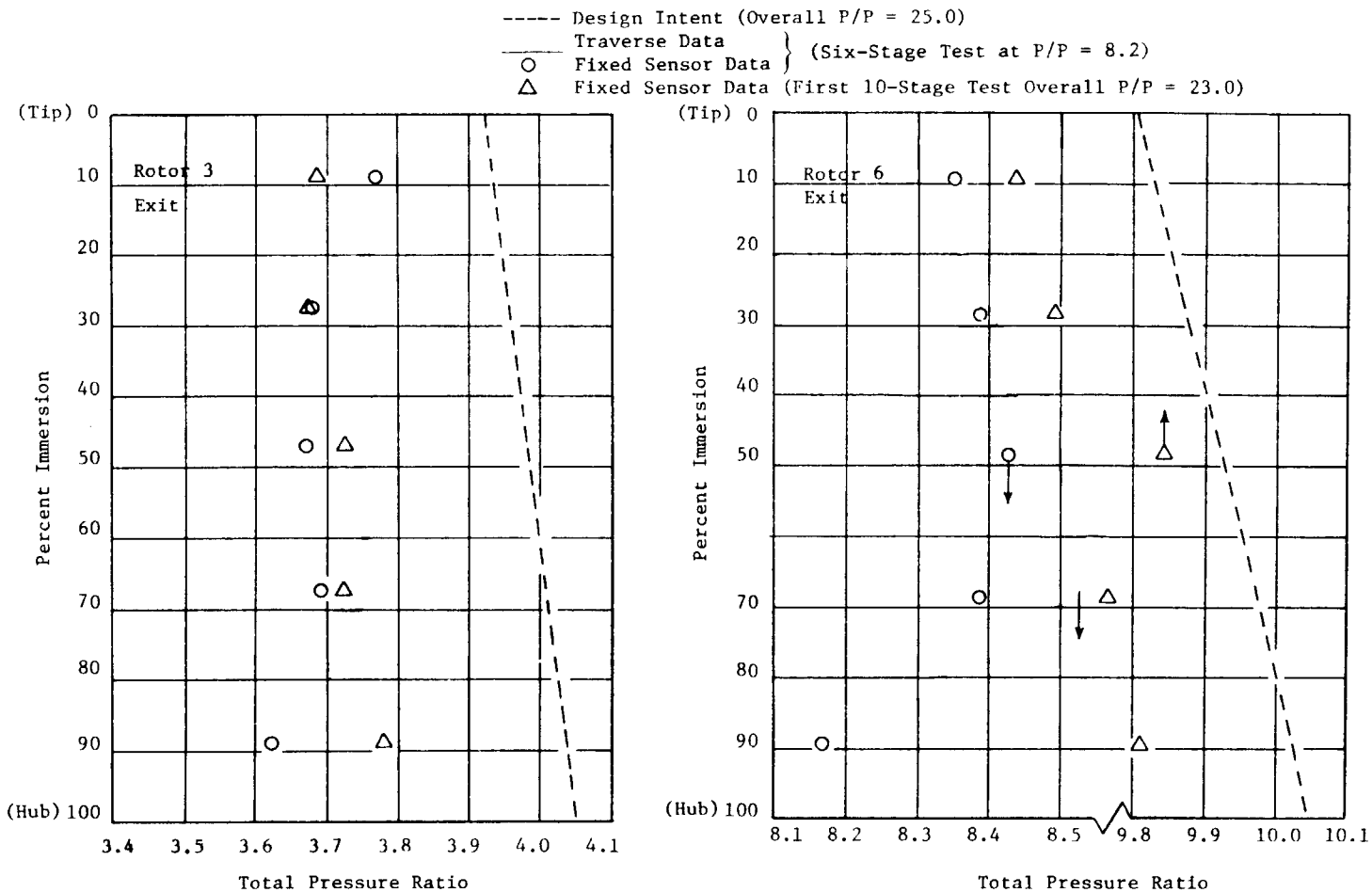

Figure 16. First 10-Stage Compressor Radial Total Pressure Distribution.

The cruise region efficiencies of the front group of stages were not significantly better than demonstrated in the six-stage test despite the large improvement in hub flow quality. Evidently, twisting the stators open at their hubs raised losses due to stator hub incidence and rotor hub Mach number enough to offset any gains due to the reduction in hub diffusion factors and rotor hub incidence angles. In the rear stages the peak efficiencies occurred below the operating line, and there was evidence that the flow was breaking down in the stators as the compressor was throttled. Analysis indicated that use of the redesigned front rotors and rear stators, as planned for future builds of the compressor, would reduce losses in these areas and give improved efficiency.

In summary, the first test of the full 10-Stage E^3 core compressor produced encouraging results. The cruise region efficiency and the subidle performance goals for this test were exceeded. The weak hub flow identified in the six-stage test was corrected. The high speed stall margin needed further improvement, but a reduction in rear block pumping was expected to accomplish this by improving the stage matching.

4.3 TEN-STAGE COMPRESSOR TEST RESULTS - SECOND BUILD

The third and last of the series of E^3 core compressor component tests was the test of the second build (10B) of the full 10-stage compressor. As a result of the six-stage test, airfoil modifications to improve the aerodynamic performance and mechanical integrity of the core compressor were defined. Blading changes from the original design incorporated in the first 10-stage compressor and carried over into the second 10-stage compressor included: twisting open the IGV hub; twisting open and increasing the hub camber of Stators 1 and 6; and twisting closed Rotor 1 tip. Details of these changes are documented in the core compressor detailed design report. Since new Rotors 3 through 7 having 6° additional hub camber were available, the modified Stators 2 through 5 used in the previous build were reworked back to their original design geometry. The original design rear stators used in the first 10-stage build remained unchanged. The high camber Rotors 8 through 10 were replaced by the existing original design blading, with the intention of

bringing the pumping level of the fixed rear block (Stages 7 through 10) down to the original design intent to improve the high speed stall margin. The axial dovetails of the front five stages were again sealed with silicone rubber. In addition, the platform gaps between the rotor blades of the first two stages were sealed with sheet rubber strips.

Since the only hardware changes were in the blading, the following features of the first 10-stage vehicle were retained in the second build:

- Simulated core inlet transition duct
- Variable inlet guide vane and Stators 1 through 6
- Stage 5 customer and active clearance control bleeds
- Rotor bore cooling
- Stage 7 start bleed.

The test plan called for a 150- to 170-hour test program divided among nine phases and 15 to 21 test runs. The primary goals of the 10B test were to improve compressor high speed stall margin without penalizing the low speed stall margin, and also determine the performance improvements that could be realized from employing the final configuration blading in the front block, IGV through Rotor 7.

As in the first 10-stage test, the vehicle was operated with ambient air at low speeds. For speeds above 85% design speed, the compressor inlet air was refrigerated to approximately 200 K (-65° F), and the inlet pressure was reduced to approximately 0.25 atmosphere when operating near design corrected inlet airflow.

Tests were initiated on December 18, 1981, and were successfully completed on April 10, 1982. Five hundred and fourteen steady-state readings and 140 stalls were recorded during 180 hours of testing in 27 runs. A very extensive aero performance evaluation was conducted on this build of the core compressor. Tests included: (1) stator schedule optimization with undistorted inlet flow; (2) 1/rev, tip radial, and hub radial inlet distortions; (3) interstage radial traverses; (4) locked stator decel stalls; (5) Reynolds number effects on flow and efficiency; (6) Stage 5 customer bleed effects on high speed flow and efficiency and on low speed stall margin; (7) Stage 7 start bleed effects on low speed stall margin; and (8) active clearance control effects on high speed performance.

Compressor overall performance data for the undistorted inlet tests were computed based on the inlet Plane 25 and the exit Plane 3 measurements. Front block and rear block performance data were calculated from the Plane 25, the Stator 6 inlet, and the Plane 3 data. The design and locations of aero instruments used in this test were identical to the first 10-stage test and the same procedures as described in the previous section were applied in computing the performance data.

Final aerodynamic performance mapping was accomplished using a variable stator (IGV through S5) schedule that produced the best efficiency and the best stall margin with undistorted inlet flow, and also produced a low sensitivity to inlet distortions. The data readings and stall points recorded with the final stator schedule are shown on the performance map in Figure 17, and are tabulated in the Appendix. The final stator schedule is shown in Figure 18. All of the data points presented were recorded with the rear case active clearance control flow set to two-thirds of the design value and the rotor bore cooling flow set to one-half of its maximum rate. The Stage 5 and 7 cooling bleeds were set to simulate the engine operating requirements.

In Figure 17, the engine maximum climb design point 120 lbm/s inlet corrected airflow and 23:1 total pressure ratio) is shown by the target symbol. The objective stall line is shown by the solid line, while the operating line is shown by the dashed line. Efficiency points shown are the unadjusted measured data. An adjustment to the measured efficiencies, required to correct the data upward to conditions expected during engine operation, amounted to 2.6 points. The total adjustment consisted of the following effects:

- The transition duct and the strut pressure losses undetected by the Plane 25 rakes - 0.6 point
- Losses due to the inlet rakes and airfoil-mounted instrumentation - 1.2 points
- Deterioration resulting from numerous high speed stalls - 0.8 point.

The adjustment for deterioration stated above was for that which occurred after the initial checkout run to high speed but before the final performance data

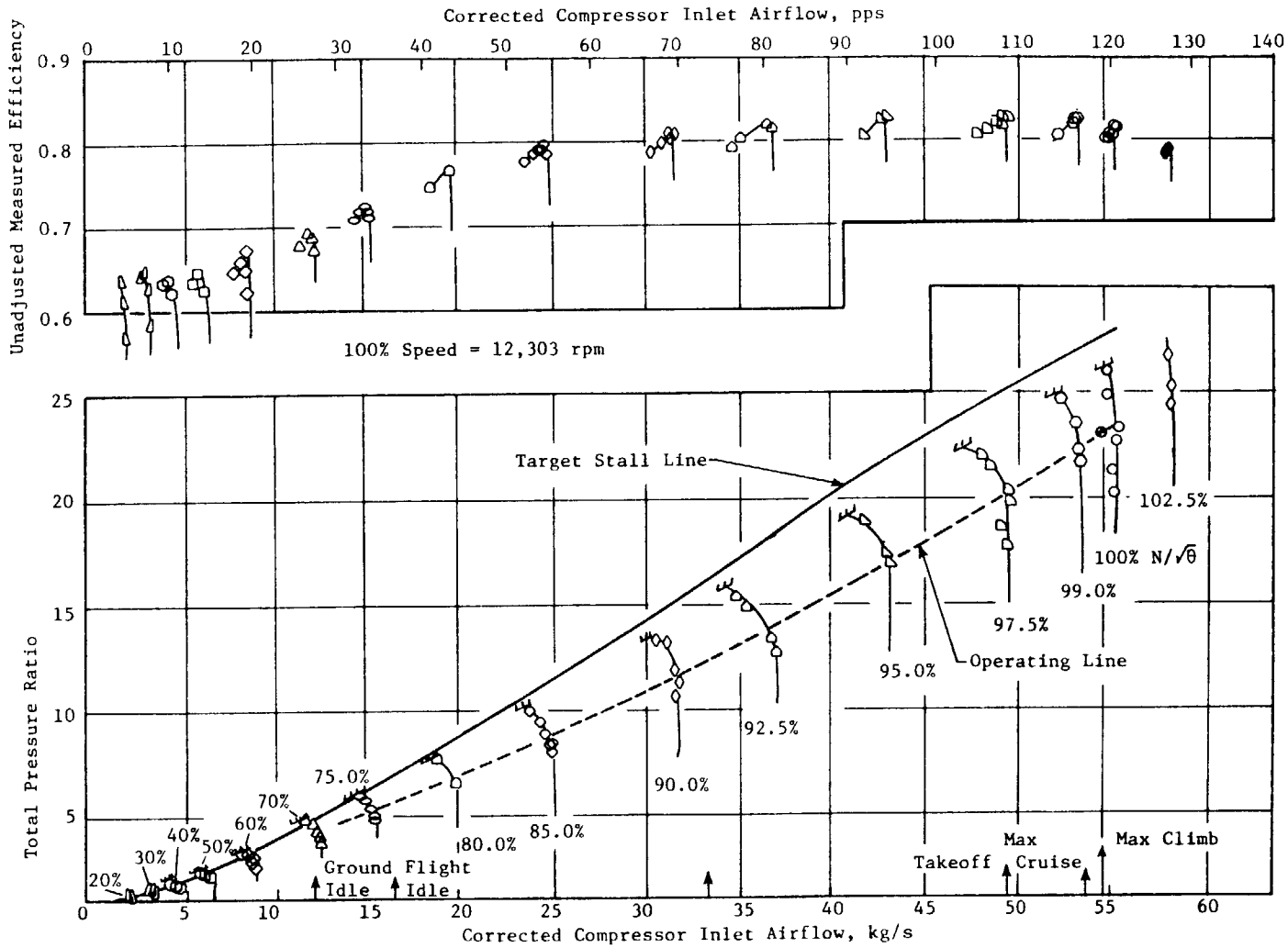

Figure 17. Second 10-Stage Compressor Performance Map.

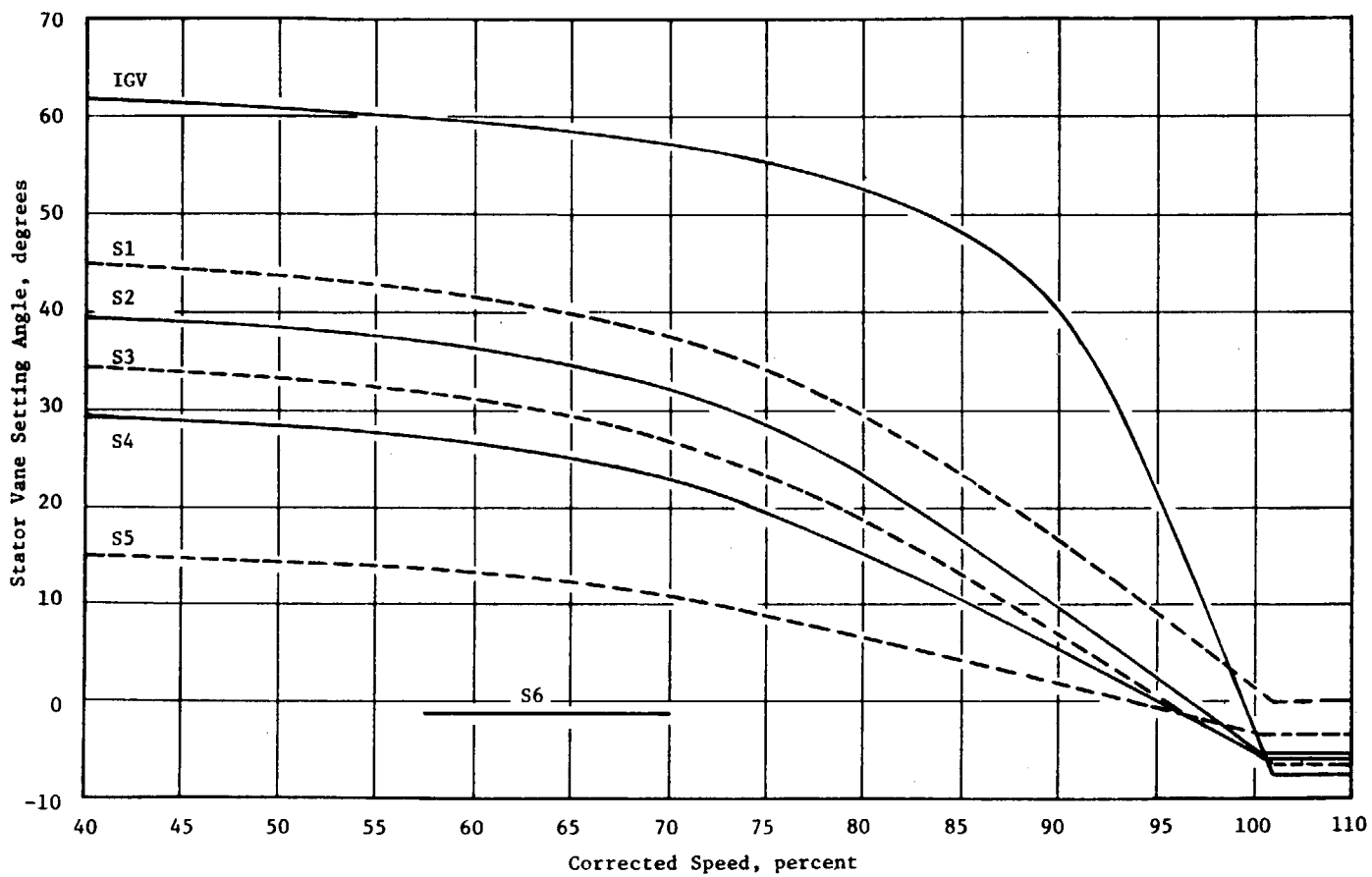

Figure 18. Second 10-Stage Compressor Test Stator Schedule.

were recorded. No further adjustments were made for hardware quality variation or the fact that post checkout run clearances were believed to be larger than the goal. The high speed data were recorded at low inlet pressures and temperatures; the resulting RNI was about 0.5, the maximum cruise value, so no Reynolds number adjustment was applied to the measured efficiencies. A complete assessment of the true efficiency and stall margin potential of this version of the compressor is made difficult, however, by undocumented deterioration that occurred during the initial checkout runs. Several severe stalls occurred at 85% to 90% corrected speed when the electrical stator vane angle position signals failed and the stators moved to their full open position. These runs were being conducted with ambient rather than refrigerated inlet air, so the physical speeds, exit pressures and exit temperatures were all fairly high. Comparable data points near design point before and after these unanticipated stalls were not recorded, so the amount of deterioration could not be determined with any certainty; a loss of 0.5 to 0.8 point would be realistic, however. Because it couldn't be documented, this further adjustment for deterioration was not applied to the measured efficiencies; the true efficiency potential of the design is therefore likely to be some what higher than the values reported here.

As indicated by the data in Figure 17, the design airflow of 54.5 kg/s (120 lbm/s) was exceeded by about 1.5% at design speed; design airflow occurred at 99.6% corrected speed. Data were obtained up to 102.5% speed, at which an operating line pressure ratio of 25 was demonstrated. Extensive mapping of the performance in the subidle region, down to 20% speed, was also accomplished. Peak efficiencies at all of the higher speeds occurred in the region of the FPS operating line, and the efficiency was relatively constant over a fairly wide range of pressure ratio at any given speed. The maximum measured efficiency shown in Figure 17 is 0.824 at 97.5% corrected speed, near the takeoff airflow. At this same speed, an efficiency of 0.832 was recorded early in the test with a slightly different stator schedule before high speed performance deterioration occurred. At maximum cruise airflow, 99% corrected speed, the unadjusted operating line efficiency was 0.822. As shown in Table III, the adjusted efficiency was 0.3 point below the ICLS goal of 0.851, and was 1.3 points below

TABLE III. Maximum Cruise Efficiency Versus Goals.

Test Measured Adiabatic Efficency at Maximum Cruise [(RDG 435 99% Nc SS = 99.2501 WC = 53.1 kg/s (117 lbm/s)]	0.822
Adjustments	
• Instrumentation	0.012
• Transition Duct Loss Bookkeeping	0.006
• Deterioration*	0.008
Total Adjustments	0.026
Rated Max. Cruise Efficiency, Test 10B	0.848
ICLS Max. Cruise Efficiency Goal	0.851
FPS Max. Cruise Efficiency Goal	0.861

* Deterioration measured after initial high speed stalls, but before final performance mapping

the FPS goal. Compared to the first 10-stage test results, the compressor efficiency was improved about 0.8 point.

The high speed stall margin was approximately 17% at takeoff conditions, an improvement of about 4 points compared to the first build of the 10-stage compressor. This was demonstrated with appropriate amounts of interstage turbine cooling bleeds, whereas the first 10-stage vehicles stall line was obtained with zero bleed, a less severe condition. The stall line in the subidle start region was improved somewhat, but start region efficiency was about 2 points lower than that of the previous build. Analysis indicated that the improvement in low speed stall line would more than compensate for the efficiency loss, resulting in a somewhat faster engine start.

The performance map for the front six stages is shown in Figure 19. The front stages were matched so that on the operating line they developed approximately the original design pressure ratio, as shown by the target symbol. The redesigned front block was throttled, in this test, well above the original designs high speed stall line. Since the front stages were not believed to be responsible for stalling the overall compressor at high speed, their actual stall line was thought to be at least equal to the target level shown on the map.

The front block efficiencies of the first and the second 10-stage tests shown in Figure 19 are the unadjusted measured data. It can be seen that the high speed efficiencies of the deteriorated 10B front block were slightly higher than those demonstrated by the undeteriorated 10A front block. Front block efficiencies at low speeds were somewhat lower than in the first 10-stage build, because a more closed stator schedule was used.

The performance map for the rear stages is shown in Figure 20. The speed lines shown on the map are lines of constant overall compressor corrected speed (corrected by Plane 25 inlet temperature). The rear block corrected speed (corrected by Stator 6 leading edge temperature) dropped as the compressor was throttled at a constant speed. A dashed line is shown to indicate the shape of the constant 98% design rear block corrected speed line.

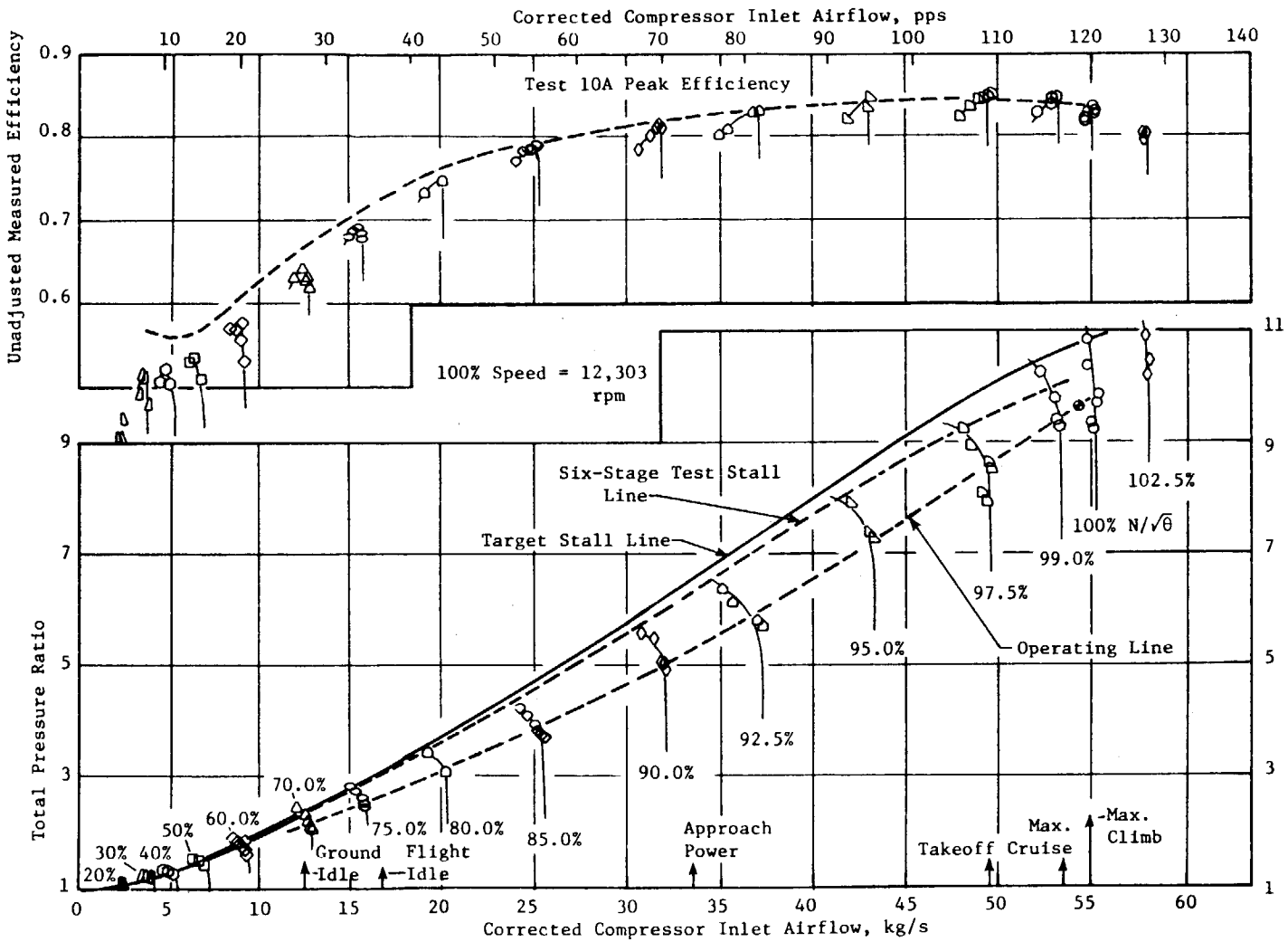

Figure 19. Second 10-Stage Compressor Test, Front Six-Stage Map.

Rear block corrected speed remained virtually constant between 90% and 100% overall compressor corrected speeds, so only the 100% inlet corrected speed line is shown.

High speed data from the first 10-stage test are also shown in Figure 20, and it is evident that the use of lower camber rear rotors reduced the rear block pumping to within 1.4% of the original design intent level shown by the target symbol. This improved the matching with the front stages considerably, and was the main reason for the improved stall line of the 10B compressor. Efficiency of the rear block was essentially the same as measured in the previous test with the higher camber rear rotors.

Radial travere flow surveys were performed with standard four-element cobra probes at the stator leading edges in Stages 1, 3, 5, 6, and 9. Data were recorded at 80%, 87.5%, 92.5%, 97.5%, 100%, and 102.5% of design speed. Total pressure data obtained from the traverse probes at the exit of Rotors 3, 6, and 9 are compared with the vane-mounted sensor data in Figure 21. Comparisons of the corresponding temperature ratio data are shown in Figure 22. Stage 3 and 6 data were recorded at 97.5% of design speed on the operating line, where the inlet corrected flow was 49.4 kg/s (109.0 lbm/s) and the overall pressure was 20.5:1. The operating conditions for the Stage 9 data were 92.5% design speed, 36.7 kg/s (81.0 lbm/s) inlet corrected flow, and 13.2:1 overall pressure ratio. The agreement between the fixed sensor data and the traverse data was good. Comparing the pressure ratio profiles of Stages 3 and 6 with the six-stage test data in Figure 11 and the first 10-stage data in Figure 16 shows that the high hub camber Rotors 3 through 6 produced the same strong hub flow in the front stages as was generated by the twisted open, high hub camber stators of the 10A compressor. The substantial improvement relative to the profiles measured in the orginal six-stage test is also evident. The Stage 9 pressure profile shows no sign of hub weakness.

Flow angle distributions at several conditions obtained from the flow surveys at Stages 6 and 9 are compared with the pretest predictions in Figure 23. The prediction for the Rotor 6 exit at 99.7% speed agreed well with the lower operating line, 97.5% speed data. Good agreement between the predicted and the measured profile at Rotor 9 exit is also seen in Figure 23. This agreement tends to indicate that in most respects the intent of the aero design

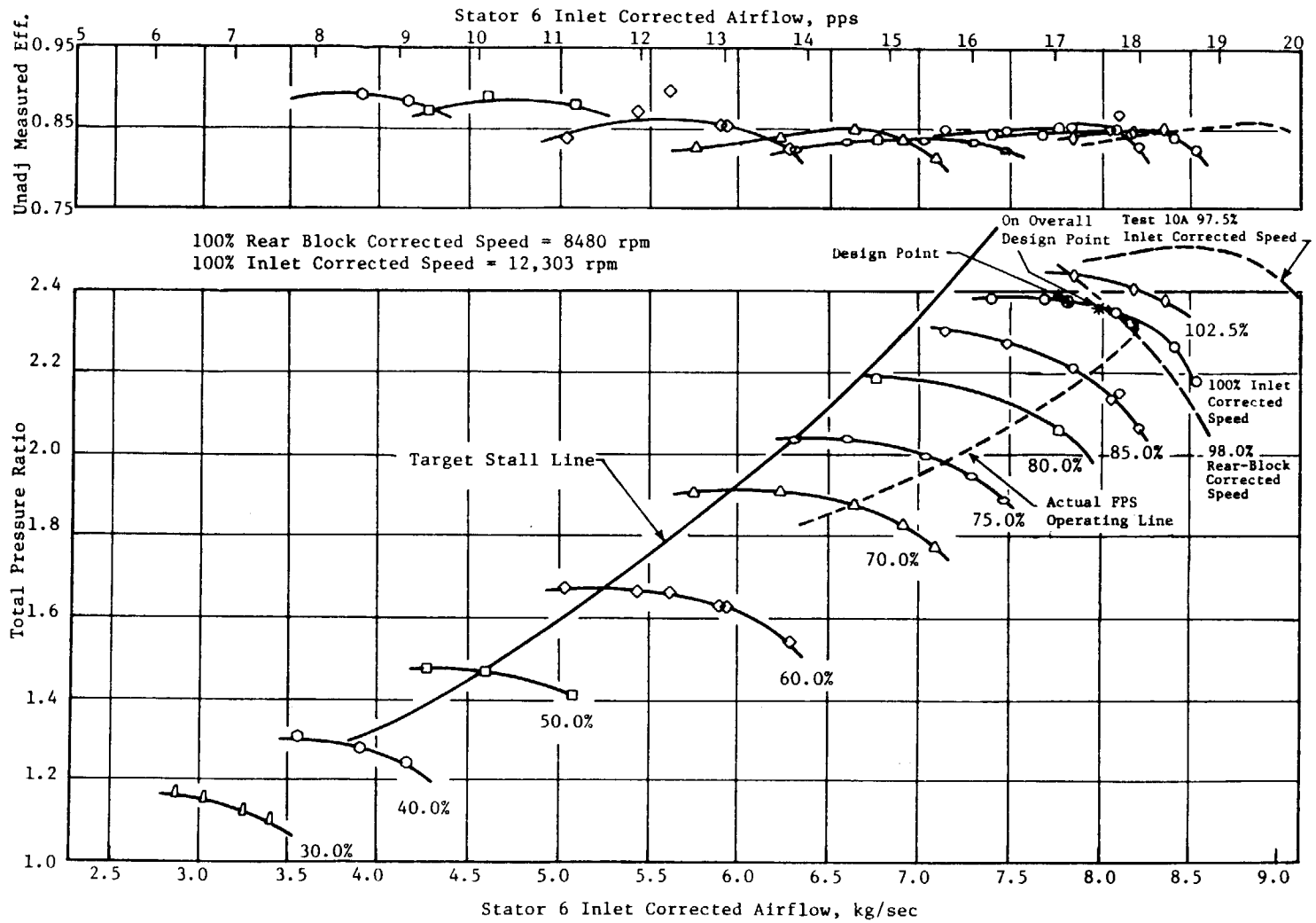

Figure 20. Second 10-Stage Compressor Test, Rear Block Map.

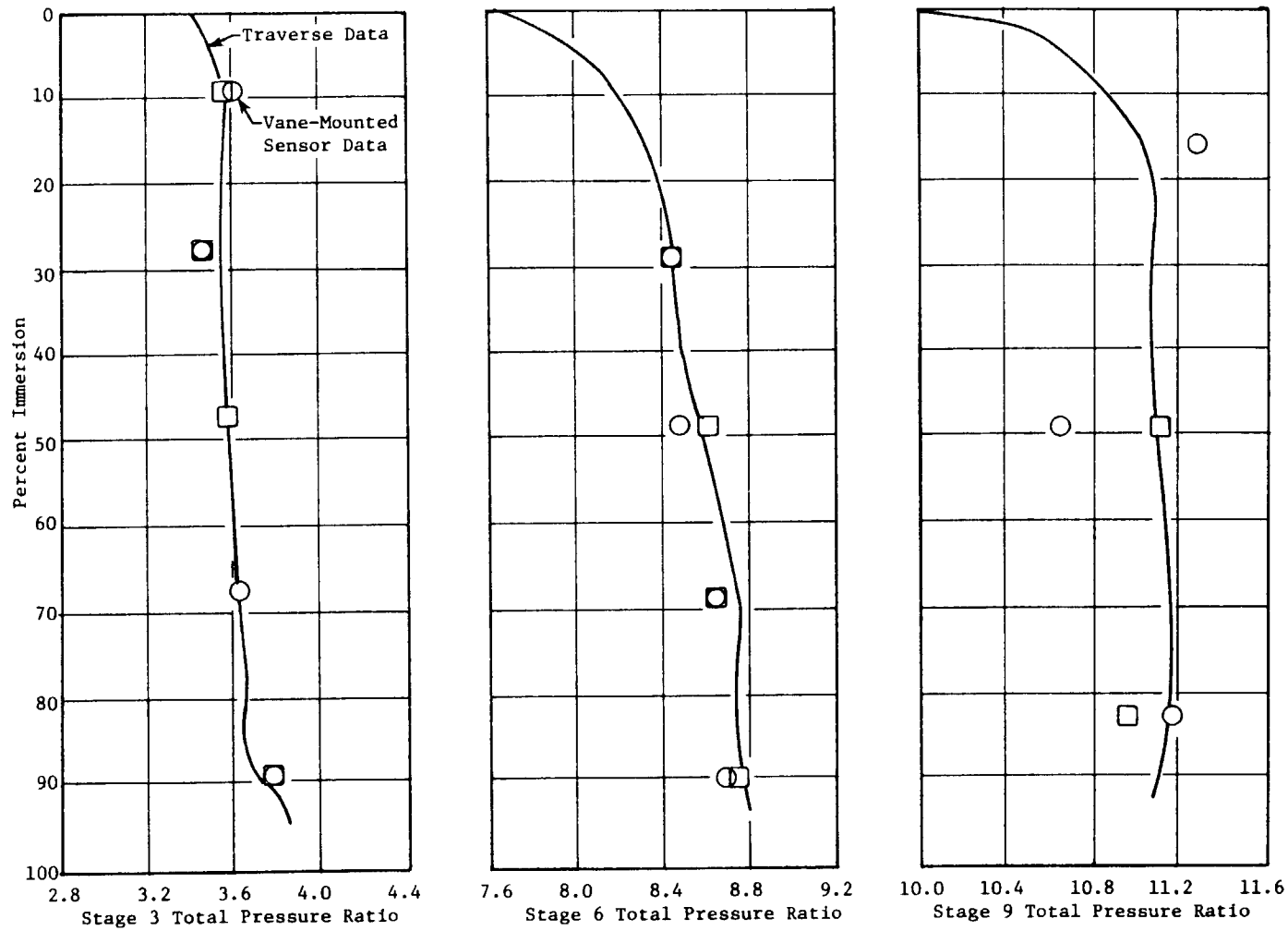

Figure 21. Second 10-Stage Compressor Test, Traverse Data.

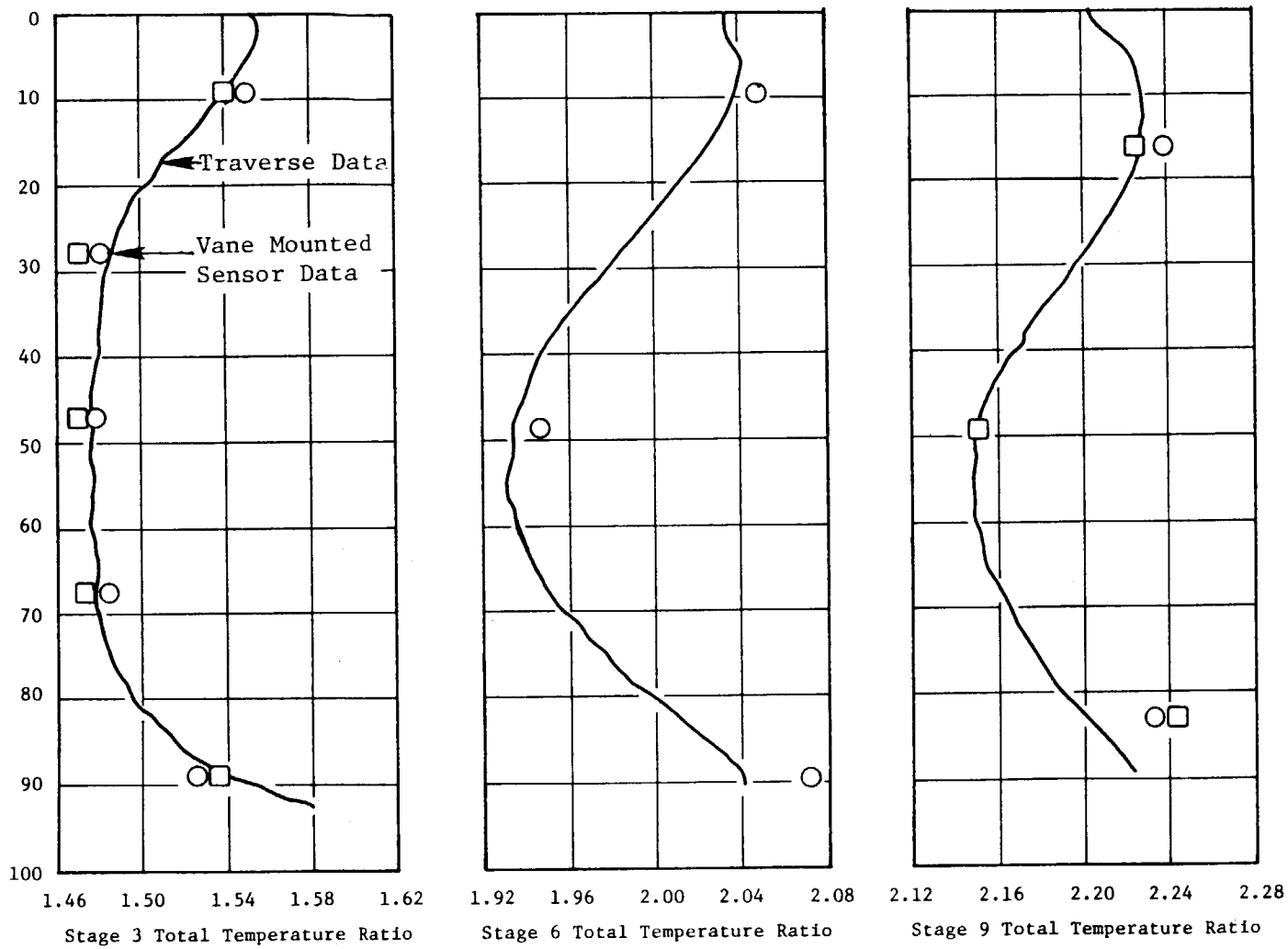

Figure 22. Second 10-Stage Compressor Test, Traverse Data.

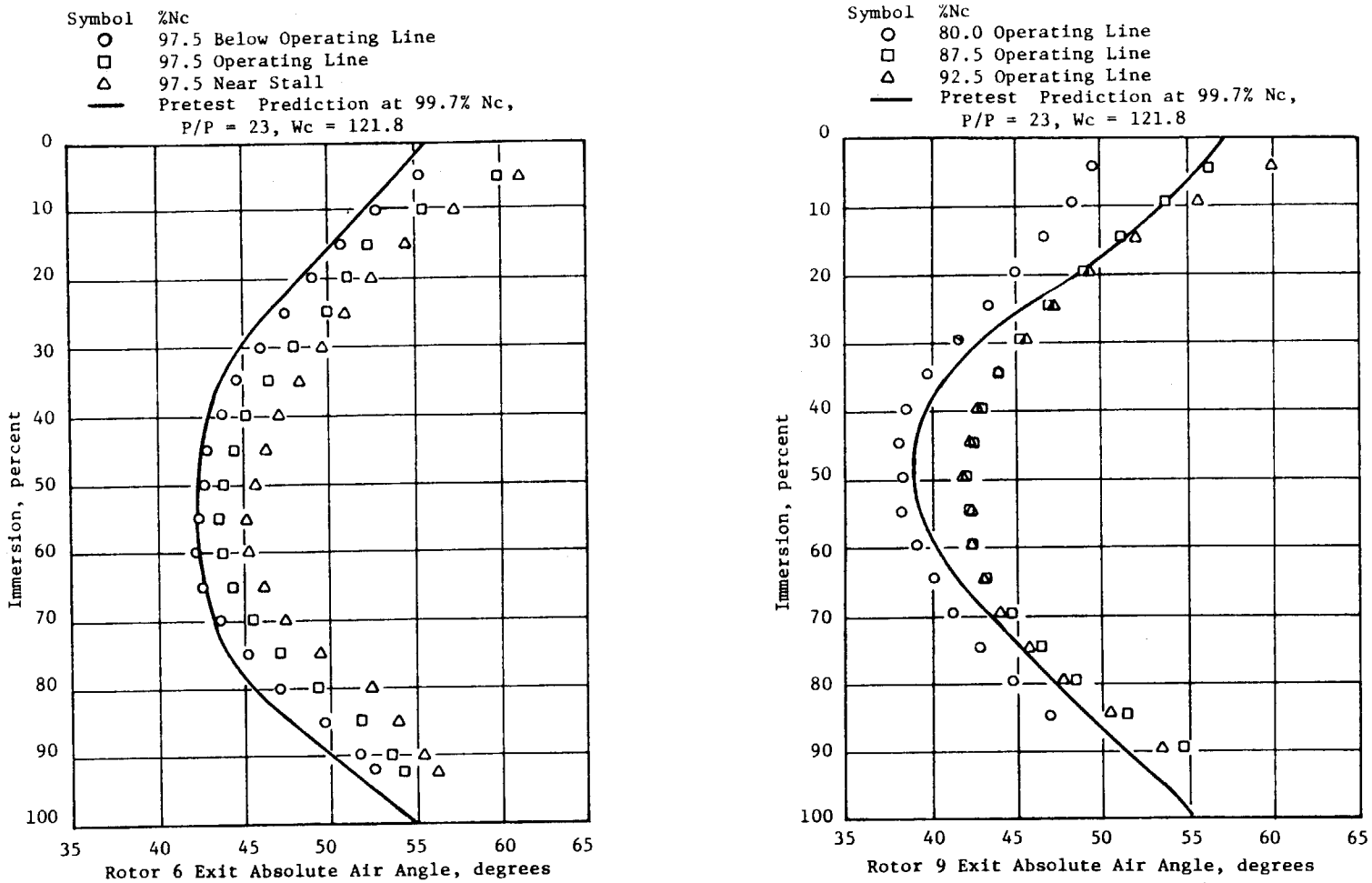

Figure 23. Second 10-Stage Compressor Absolute Air Angle Distribution.

modifications was achieved in the second 10-stage test vehicle. Another observation is that at Rotor 9 exit, the flow angle profiles at 87.5% and 92.5% speeds nearly coincided with each other. This is because the fixed rear block (Stages 7 through 10) operated at a constant corrected speed and corrected flow point for speeds above 87.5%.

Distortion testing was conducted to determine the sensitivity of the com pressor to various inlet distortion patterns. The pattern-generating screens were mounted upstream of the inlet transition duct at an axial distance of approximately 95 cm (37.4 in.) from the IGV leading edge. The inlet distortion flow patterns were measured with the same Plane 25 rakes that were used for compressor overall performance measurements. Three types of classical screen patterns were selected for testing: 180°, one per rev circumferntial; tip radial; and hub radial. A schematic illustration of these screens is shown in Figure 24. The circumferential pattern was a graded screen which consisted of a dense uniform mesh over a 150° sector of the annulus with two lower porosity sectors that extended 15° on either side. The tip radial pattern was graded with a heavier screen covering the outer quarter of tip annulus and a less dense mesh extending radially inward to cover an additional 20% of the annulus. The hub radial pattern had the denser mesh screen covering the inner quarter of the hub annulus and the less dense screen extending radially outward to cover an additional 20% of the annulus.

The distortion methodology developed by General Electric was used to analyze the distortion test data. The method correlates the reduction in stall pressure ratio (ΔPRS) to the calculated distortion indices, which are defined by the flow distortion pattern. As a prelude to calculating the distortion indices, the flow annulus is divided into five equal area rings. To calculate the radial distortion index, the difference between the face-average pressure and the ring-average pressure is divided by the face-average pressure for each of the five rings. The radial distortion index (IDR) is defined as the maximum of these five values. To calculate the circumferential distortion index (IDC), the difference between the ring-average pressure and the minimum ring pressure is divided by the face-average pressure for each of the five rings. These ratios are then averaged for each combination of two adjacent rings and the maximum of these averages is defined as the circumferential distortion index.

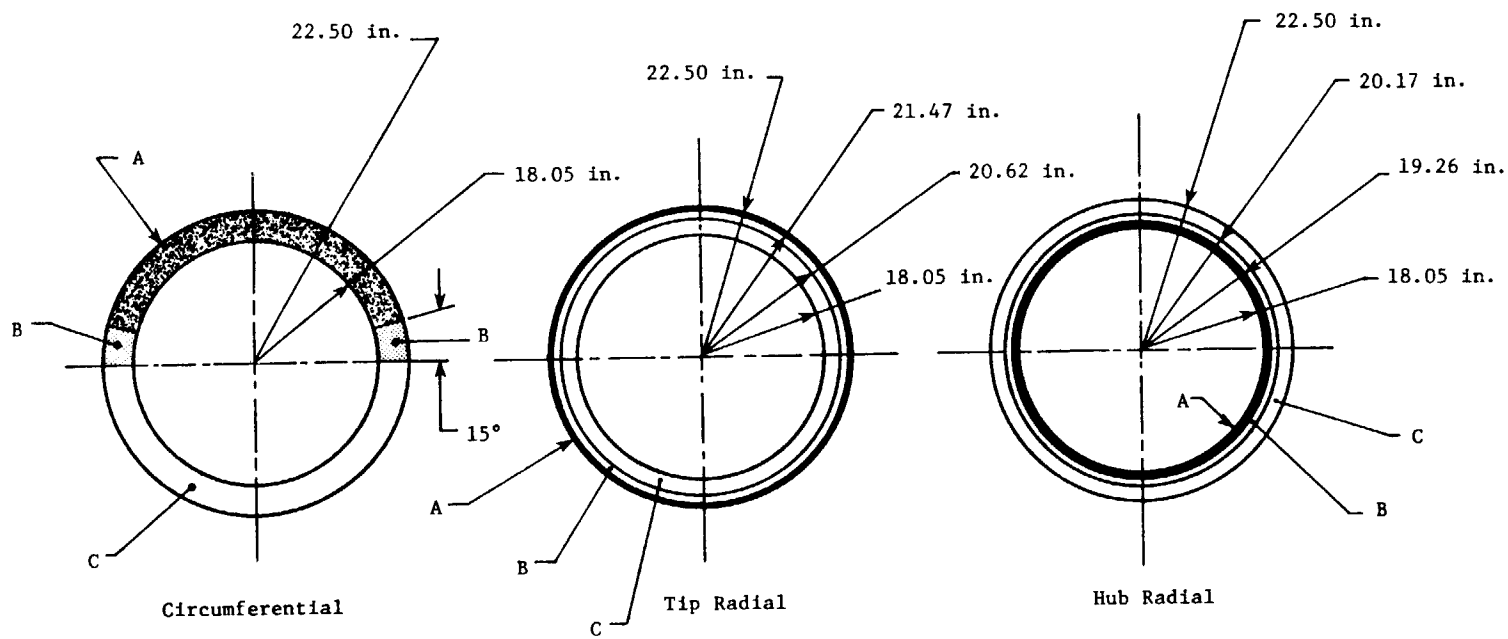

Figure 24. Second 10-Stage Compressor Test, Inlet Distortion Patterns.

Each pattern was tested over a wide range of compressor inlet airflow rates to determine the characteristics of the compressor distortion sensitivity. The circumferential screen was rotated to provide better definition of the distortion pattern. The resulting compressor distortion sensitivities to the circumferential and the radial patterns are shown in Figures 25 and 26, respectively. Since the clean inlet flow of the compressor was inherently distorted in hub radial pattern (i.e., IDRH greater than zero), the change of the hub radial index (ΔIDRH) was used to evaluate the effects of the screen. The circumferential sensitivity (K_c) of the E^3 compressor was slightly lower than similar General Electric high speed, highly loaded compressors near the design speed, and became progressively better at lower speeds. The hub radial distortion sensitvities (K_{R_H}) were low. This indicated a high tolerance of the compressor to distorted hub pressure profiles. The results of tip radial sensitivity (K_{R_T}) showed negative values for flow rates higher than 90 lbm/s. This indicated that tip distortion was favorable to the compressor stall margin, since the compressor stalled at higher pressure ratios with the tip radial distortion screen than with an undistorted inlet.

4.4 SUMMARY

The test of the six-stage front block was a vital first step in the series of compressor component tests. This initial component test demonstrated high speed efficiencies somewhat better than the test goals, and also demonstrated the objective low speed stall margin. High speed stall margin was deficient, however, and the need for design modifications was apparent. Most significantly, the test produced valuable internal performance data to guide the required design refinements.

The first 10-stage test, with interim modified front block blading, demonstrated significantly improved front block internal performance. Stall margin and efficiency exceeded the objectives in the critical subidle start region and the high speed efficiency was above the test goal. The high speed stall margin was below objective because rear block pumping was approximately 9% greater than design intent, indicating the front and rear blocks were improperly matched. The results of these tests allowed selection of the final rear block blading to achieve the proper stage matching.

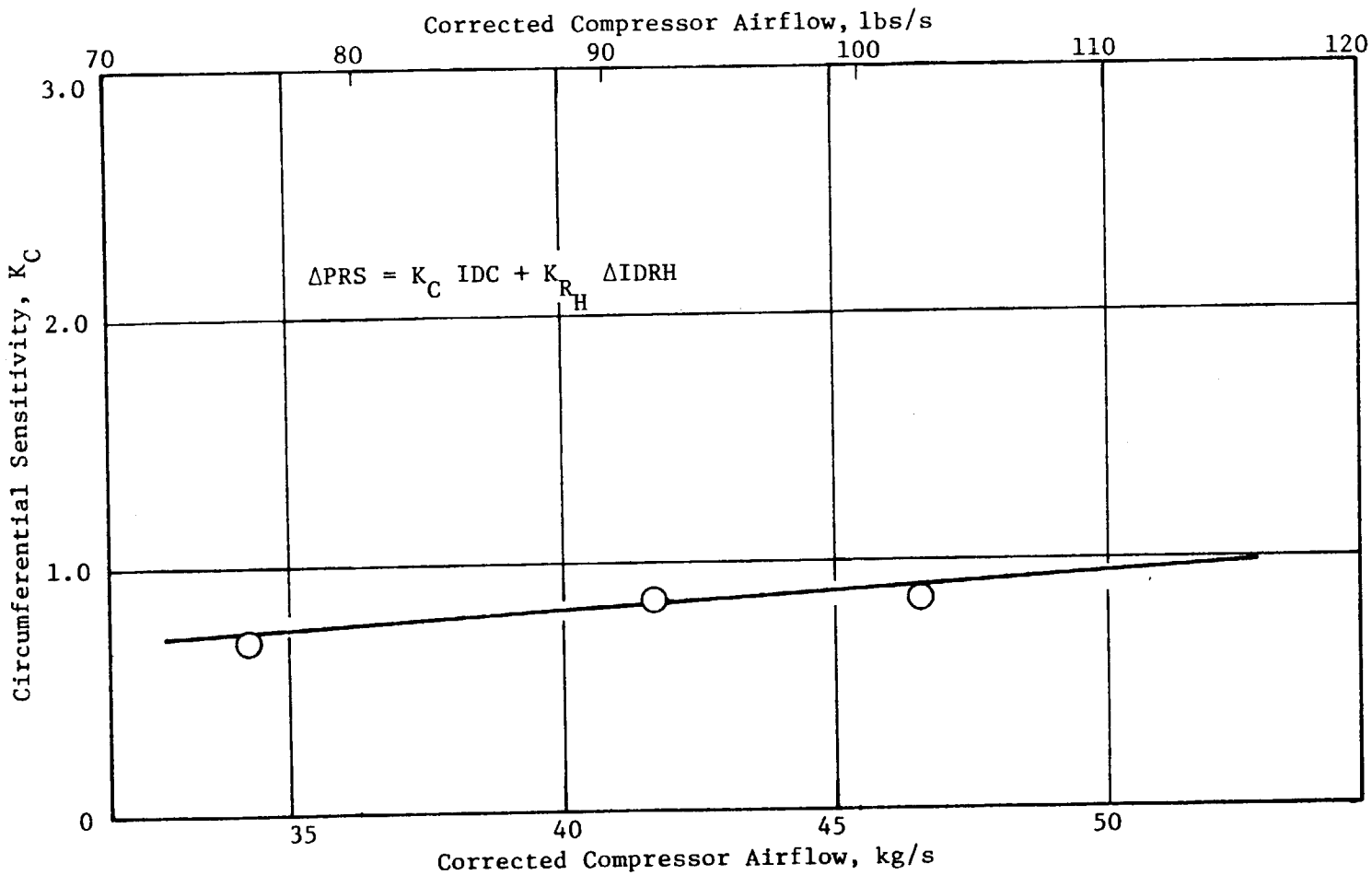

Figure 25. 10B Compressor Circumferential Distortion Sensitivity.

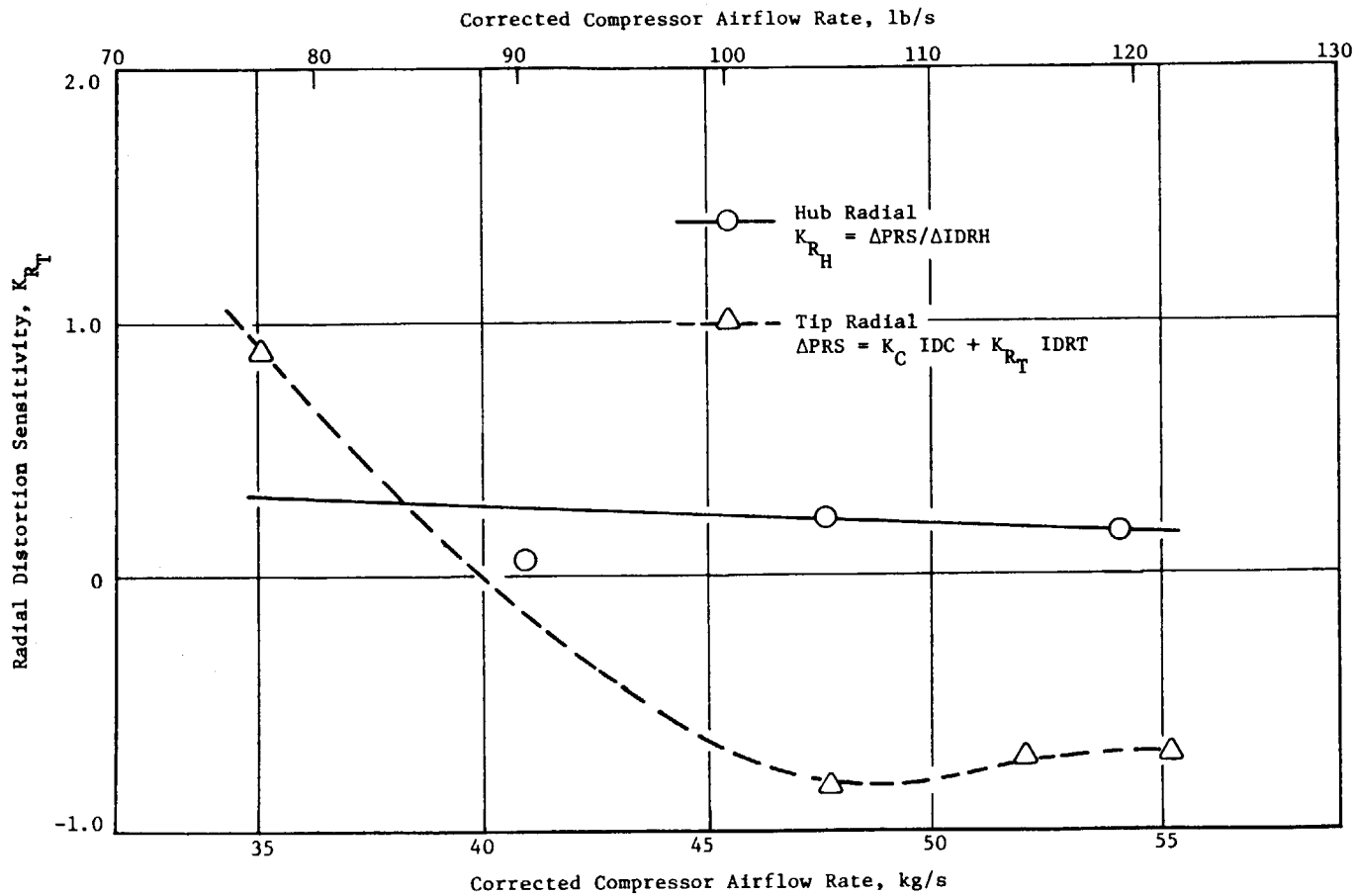

Figure 26. 10B Compressor Radial Distortion Sensitivity.

Results of the second 10-stage test verified the final front block blade modifications and the improved stage matching. The compressor again demonstrated better-than-objective low speed stall margin and efficiency. Relative to the first 10-stage test results, an 0.8 point efficiency improvement and 4 points stall margin increase at the design point were demonstrated. A stator schedule suitable for the engine's ganged actuation system was developed. Most of the performance goals for the overall core compressor development program were either fully demonstrated or closely approached in this final component test.

Overall, the series of compressor component tests provided a systematic approach for developing this high performance, high stage loading core compressor. Steady performance improvements were achieved at each step in the process. The final performance results indicated that the final compressor for the core and the ICLS turbofan engines should meet its performance goals and should have few operability problems.

5.0 SYSTEM DYNAMICS SUMMARY

5.1 SIX-STAGE COMPRESSOR TEST RESULTS

The six-stage compressor test program was completed without encountering any system vibration problems. All synchronous vibration levels were within limits throughout the test program up to and including the maximum physical speed of 12,700 rpm.

Maximum response levels observed during test were recorded on the bellmouth vertical accelerometer at 12,300 rpm. This correlated closely with the analysis. The analysis predicted this critical to occur at 12,000 rpm and that the maximum response would occur on the bellmouth due to the amount of rotor bending in this mode and its sensitivity to rotor imbalance. Figure 27 describes the modal deflection characteristics and energy distribution from the system vibration analysis. Figure 28 compares the combined modes' analytical solution for 50 g-in. of Stage 1 imbalance with the synchronous response recorded during a representative test run.

Early in the test program, an acoustic resonance was detected on several occasions with a dominant frequency of approximately 248 Hz. The phenomenon was easily heard in the control room and was observed on the bellmouth accelerometers as well as stator and rotor strain gages. The resonance occurred between 9000 rpm and 11,000 rpm, and its occurence was dependent on the stator schedule. Figure 29 illustrates the phenomenon using a bellmouth vertical accelerometer spectrum at 10,410 rpm. This acoustic resonance did not restrict the test program, as the stator schedule at which the phenomenon occurred was not aerodynamically desirable. The resonance is thought to be unique to the facility/rig setup and is not expected to occur during core or ICLS engine testing.

5.2 TEN-STAGE COMPRESSOR TEST RESULTS, FIRST BUILD

The first 10-stage compressor test program was completed without encountering any system vibration problems. All synchronous vibration levels were

13% PE - No. 1 Bearing 8% PE in Rotor 1% PE - No. 2 Bearing

——— Undeflected — — — — Deflected Mode Shape

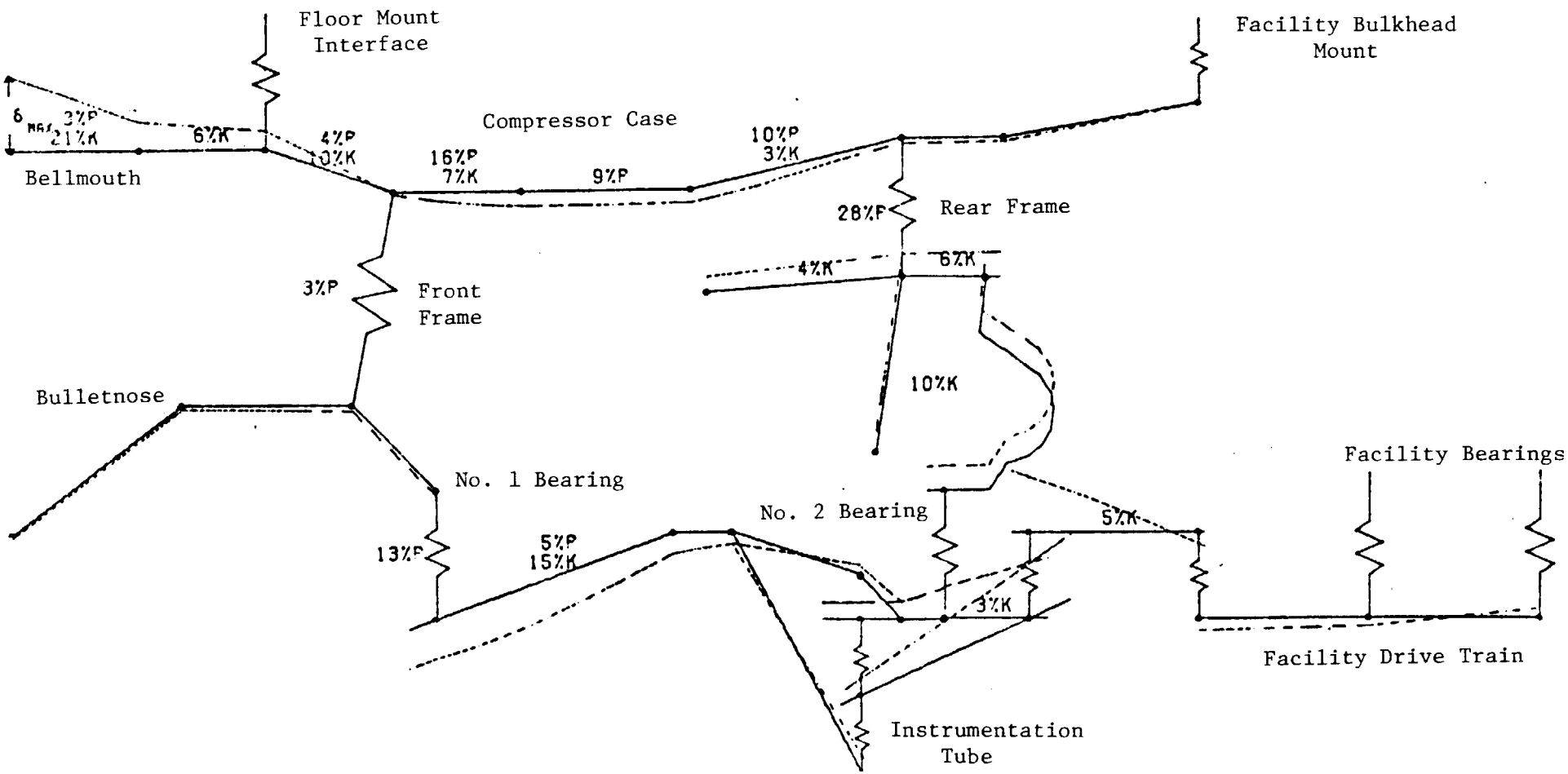

Figure 27. Six-Stage Compressor Test Vehicle Modal Deflection for Critical Speed at 11,997 RPM.

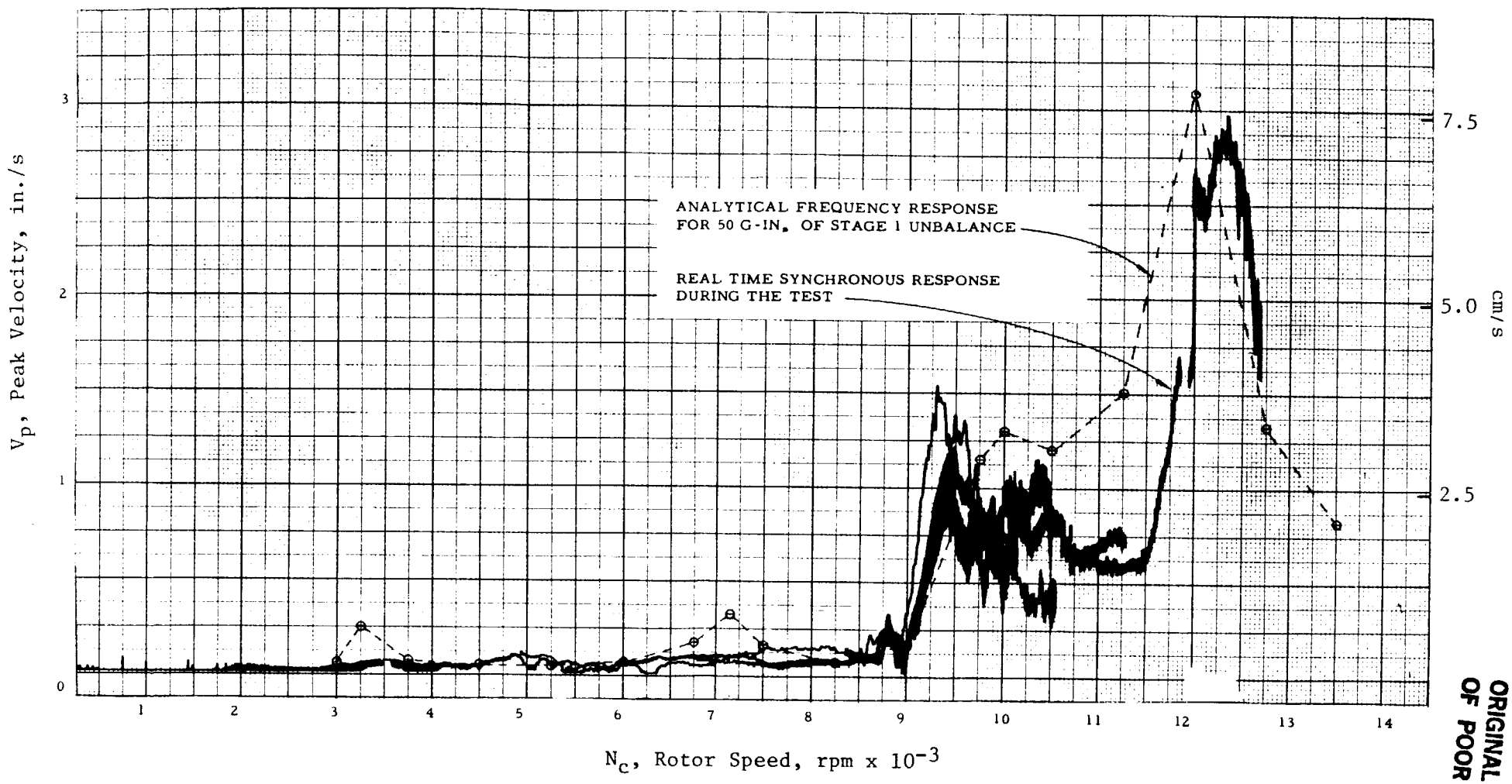

Figure 28. Six-Stage Compressor Test, Bellmouth Vertical Accelerometer Response at 10,410 RPM.

ORIGINAL PAGE IS
OF POOR QUALITY

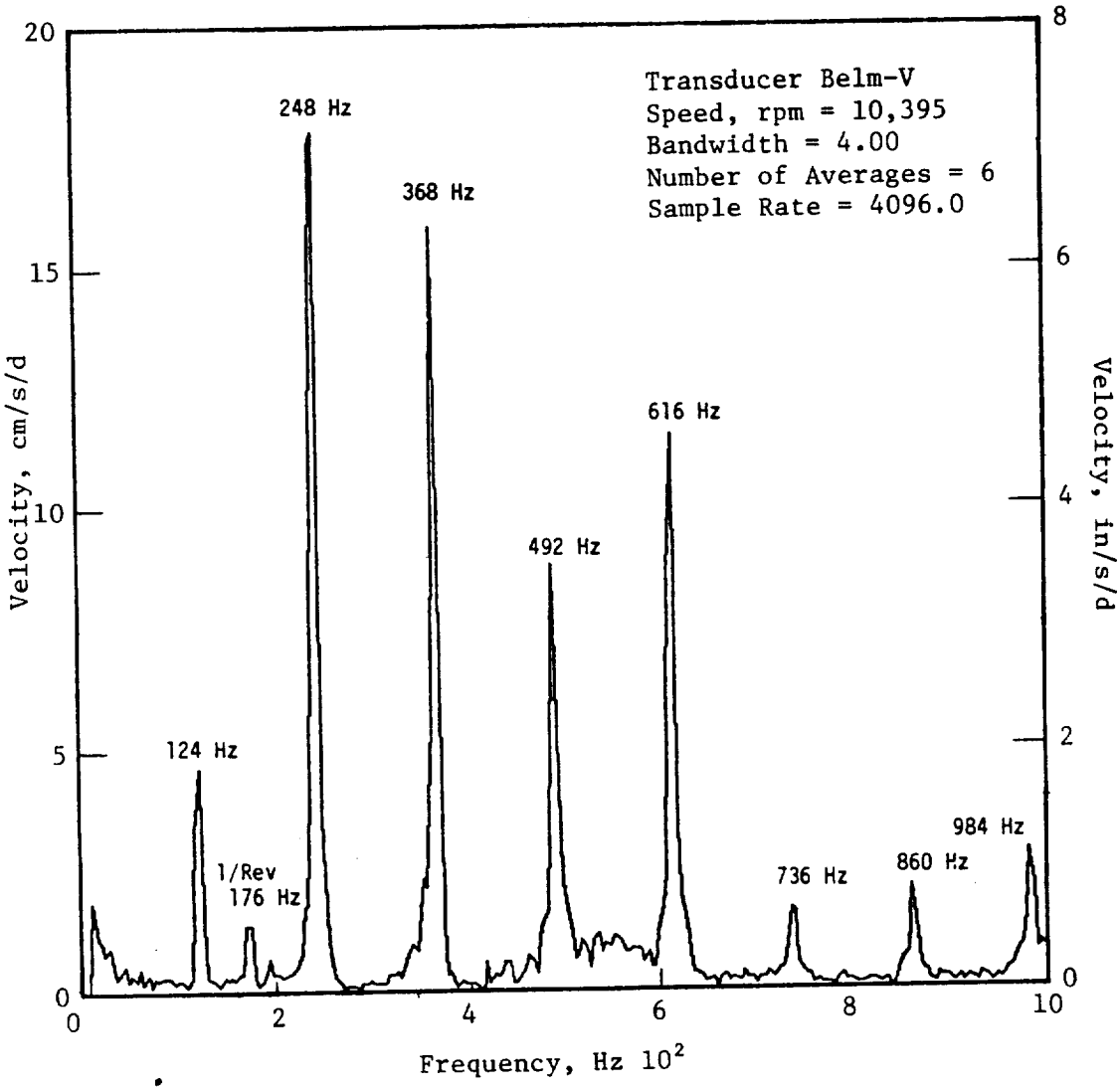

Figure 29. Six-Stage Compressor.

low and within limits throughout the test program up to and including the maximum physical speed of 11,600 rpm.

The 10-stage compressor rig employed a different concept for mounting the rotor and controlling the vibration response than was used for the six-stage compressor rig. A conventional bearing and bearing support arrangement resulting in a hard-mounted rotor was used for the six-stage design. This configuration was acceptable for the six-stage rig with a bearing span of 117.6 cm (46.3 in.) and total rotor weight of 291 kg (642 lb) since no bending modes existed within the operating speed range. However, the 10-stage rig had an overall bearing span of 138.4 cm (54.5 in.) with a total rotor weight of 410 kg (904 lb). This 18% increase in span length coupled with the 41% increase in rotor weight resulted in an unacceptable rotor bending mode within the speed range. Figure 30 illustrates the modal deflection characteristics for this unacceptable rotor bending mode. To eliminate this mode, a soft-mount suspension system was designed to provide for rotor vibration isolation. The soft-mount suspension system consisted of squirrel cage centering springs supporting both ends of the rotor. The system was designed to operate supercritical to the rotor rigid body modes. Squeeze film dampers located at the No. 1 and 2 bearings were designed to dissipate vibration energy associated with the rigid body modes. The soft mounts allowed the rotor to run in a dynamically stiff configuration, i.e., rotor bending did not occur over the operating speed range. The modal deflection characteristics of this rotor rigid body mode are illustrated in Figure 31 along with the energy distribution. As indicated in Figure 31, soft mounting the rotor reduced the strain energy in the rotor to an insignificant 6% thus eliminating rotor bending. The forward squirrel cage spring rate was 437,817 N/cm (250,000 lb/in.), and the aft squirrel cage spring rate was 350,253 N/cm (200,000 lb/in.). Sufficient strain energy was found to exist in both squirrel cages to allow squeeze film dampers to work effectively. A component mode solution was used to design and optimize the damper definition. Figure 32 illustrates the subsystems and connecting elements used in the component mode analysis. Ten modes for the rotor subsystem and 10 modes for the static structure subsystem were used to determine an acceptable solution (satisfactory modal truncation error) with the component mode anlaysis. The forward squeeze film

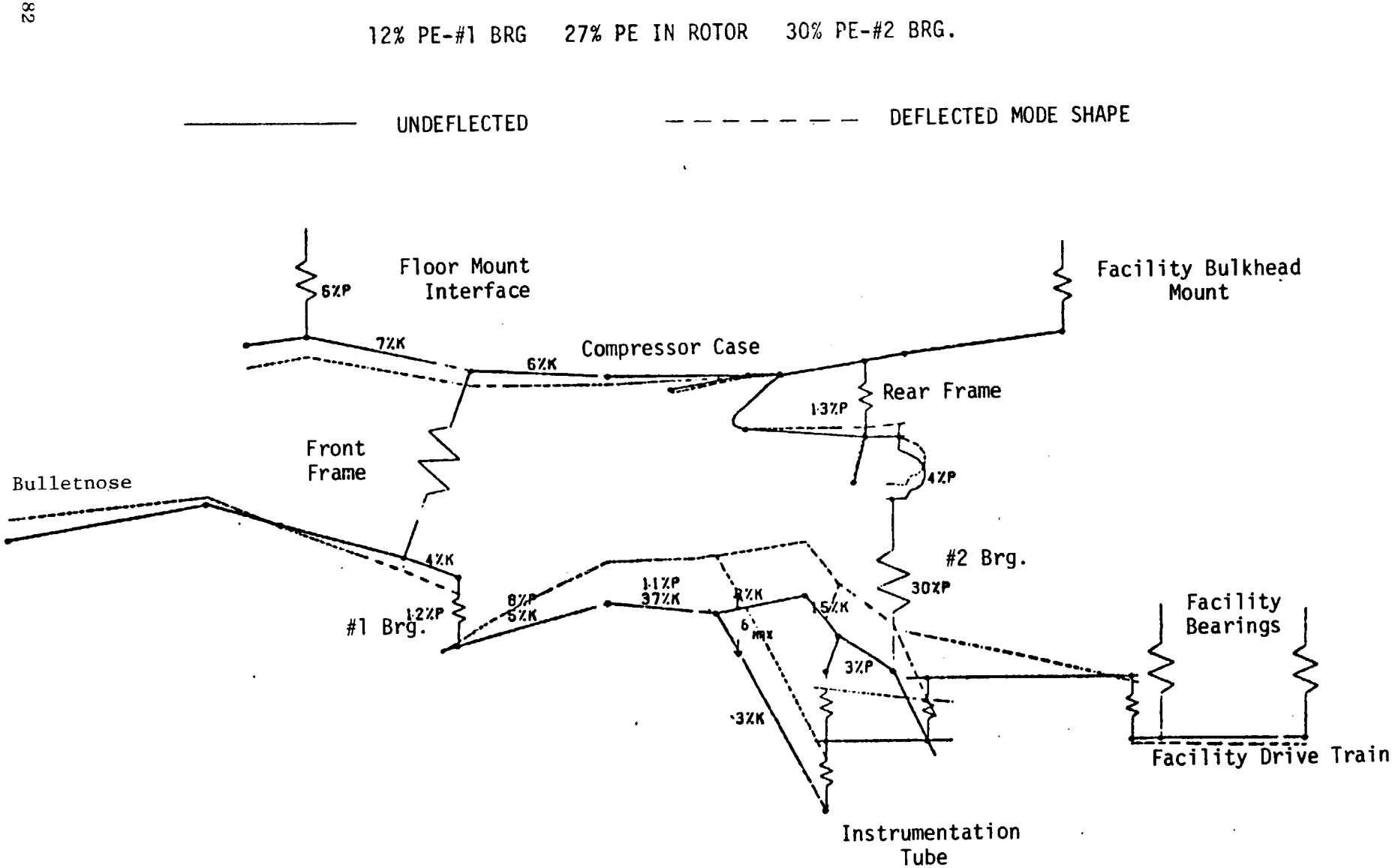

Figure 30. Hard-Mounted, 10-Stage Compressor Rotor Modal Deflection for Critical Speed at 6621 RPM.

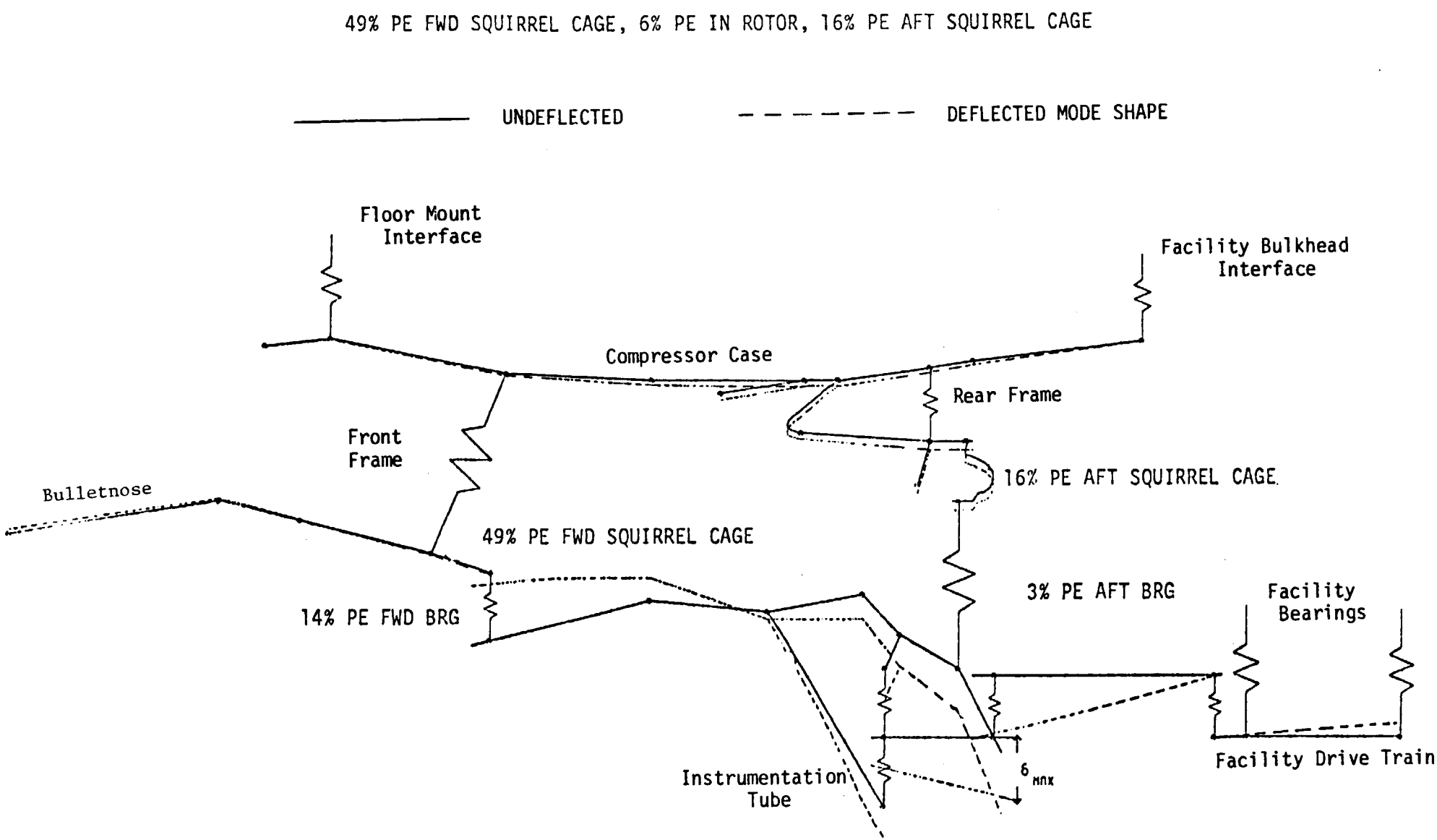

Figure 31. Ten-Stage Compressor Rig, Build 1, Soft-Mounted Rotor Modal Deflection for Critical Speed at 6606 RPM.

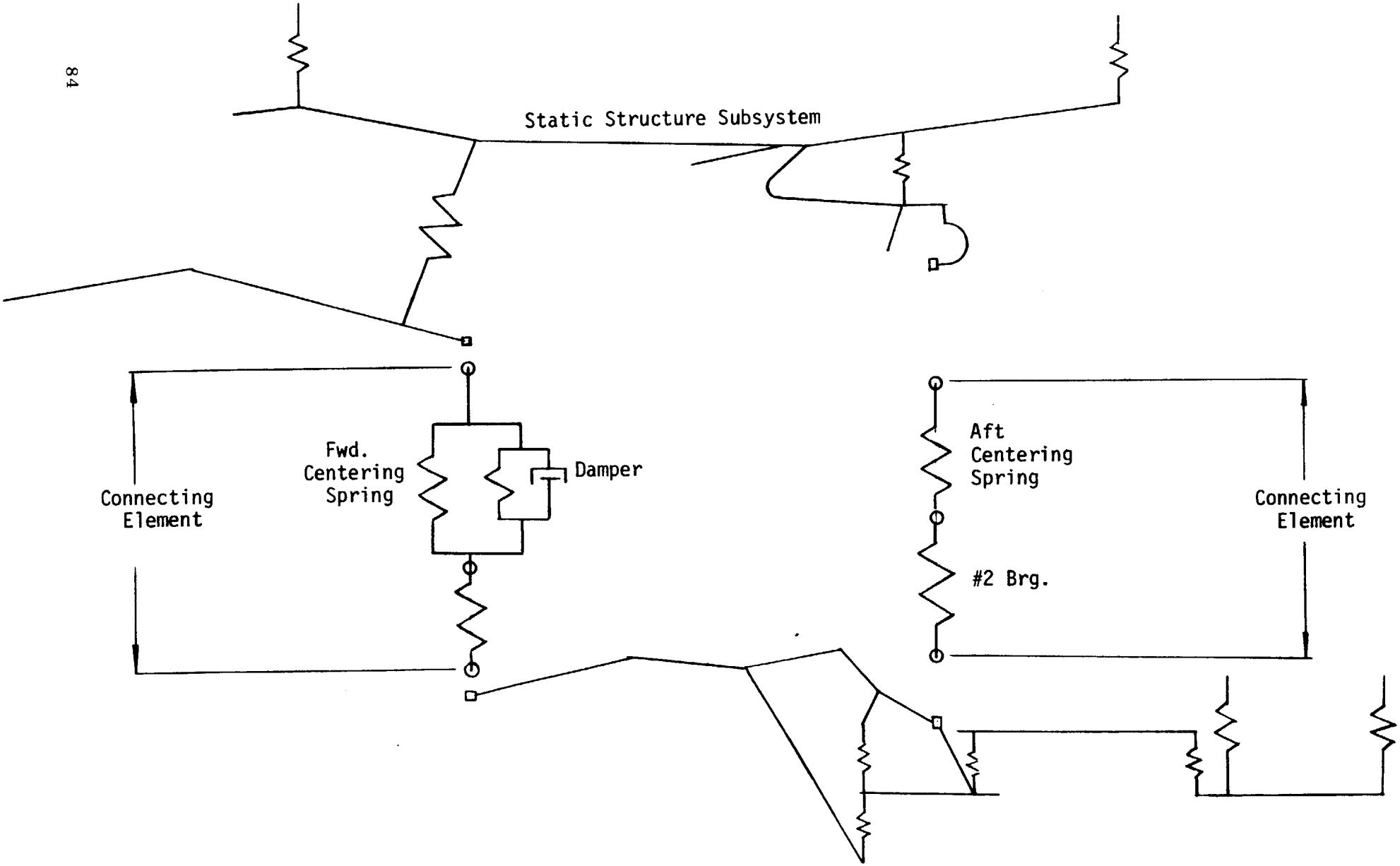

Figure 32. First 10-Stage Compressor Squeeze Film Damper Design Subsystems and Connecting Elements.

damper was designed to minimize bearing loads and rotor/stator clearance loss. The aft damper was added to provide additional damping capacity. Table IV describes the damper parameters.

Table IV. Ten-Stage Compressor Squeeze Film Damper Parameters.

Forward Damper

- Center hole feed - end flow damper
- Radial clearance 0.180 mm (7.1 mils)
- Overall length 3.04 cm (1.20 in.)
- Radius 12.34 cm (4.86 in.)

Aft Damper

- Center groove feed with end seals
- Radial clearance 0.178 mm (7 mils)
- Land length 0.635 cm (0.25 in.)
- Grove width 0.305 cm (0.12 in.)
- Radius 9.5 cm (3.74 in.)

The combined effect of the soft suspension system and squeeze film dampers resulted in a rotor with very low sensitivity to unbalance.

The soft mount rotor suspension system and squeeze film dampers performed as intended, resulting in synchronous vibration levels that were low and within the pretest established limits. Figure 33 illustrates the frequency response characteristics for the soft side of the No. 1 bearing support and compares the component mode analytical solution with the synchronous response recorded during a representative test run. Synchronous vibration levels recorded at all other accelerometer locations were less than 1.0 mil-DA at all speeds throughout the test program.

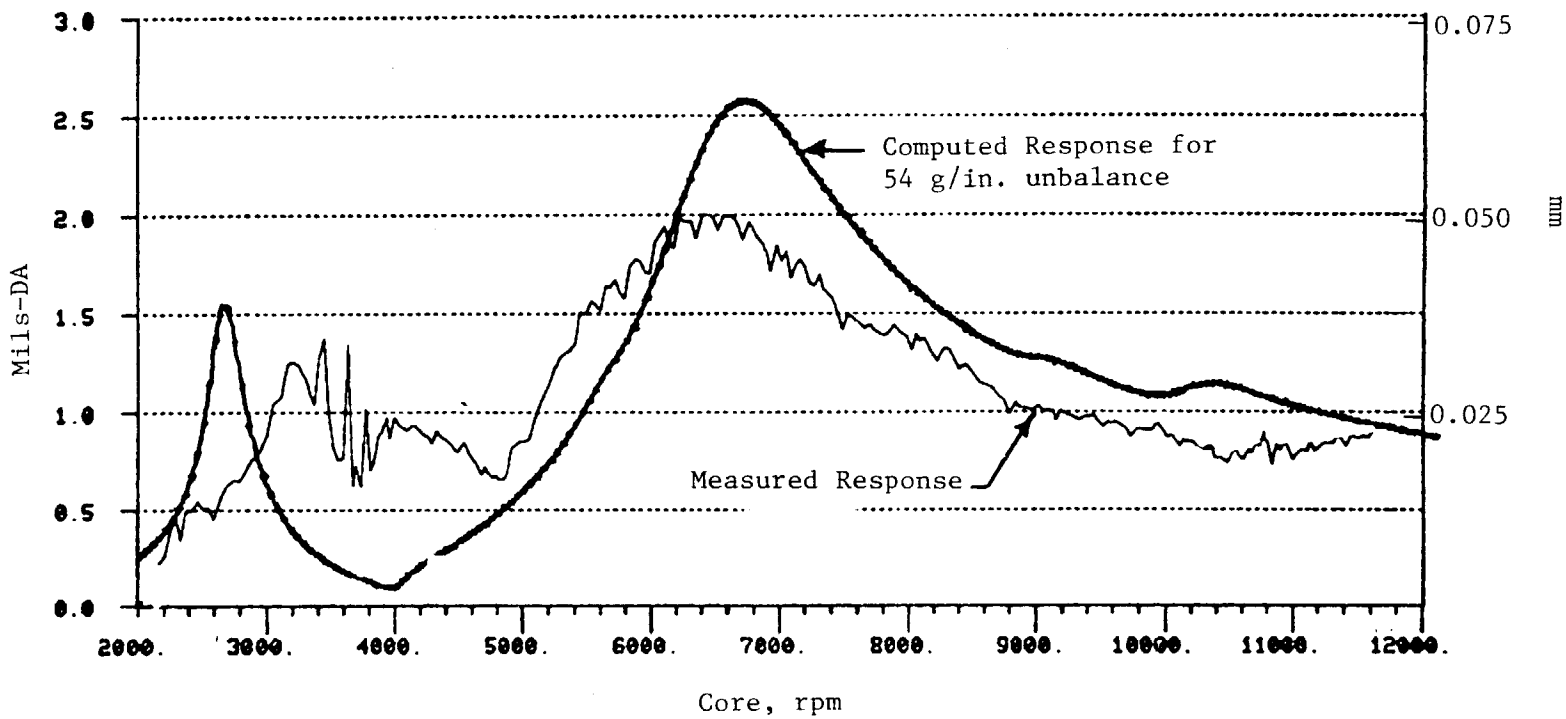

Figure 33. First 10-Stage Compressor Forward Bearing Damper Housing Synchronous Response Comparison.

A steady-state squeeze film damper performance investigation was conducted with the vehicle operating at 6200 rpm, the critical mode speed. The synchronous response of the soft side of the No. 1 bearing support increased by 43% when the oil supply to both dampers was turned off. This test further verified the effectiveness of the soft-mounted rotor and squeeze film damper system to reduce imbalance sensitivity.

No synchronous vibration problems were encountered during the extended stall which occurred during the final test run. The rotor remained stable and posttest FFT analysis of the associated decel indicated that the peak synchronous response was 0.0406 cm (1.6 mils-DA) at 6200 rpm at the soft side of the No. 1 bearing support.

5.3 TEN-STAGE COMPRESSOR TEST RESULTS, SECOND BUILD

The second test of the 10-stage compressor was completed without encountering any system vibration problems. All synchronous vibration levels were low and within limits throughout the test program up to and including the maximum physical speed of 12,000 rpm. The frequency response characteristics agreed with pretest analytical projections throughout the speed range.

The second build of the 10-stage compressor vehicle employed the same soft suspension system for the rotor and the same squeeze film damper configuration that was used in the first build. The rotor was rebuilt and rebalanced for the second test. Vibration characteristics during the second test were very similar to the first test. Synchronous vibration levels were lower during the second test indicating an improved rotor balance condition.

A squeeze film damper performance investigation was conducted during the mechanical checkout. A slow accel to top speed was made with the No. 2 damper supply oil turned off, leaving only the No. 1 damper active. The Campbell diagram in Figure 34 compares the frequency response characteristics for accels with both dampers active, and with only the No. 1 active. The accelerometer was located on the forward damper housing which corresponds to the soft side or rotor side of the forward centering spring. Maximum one per rev response with only the No. 1 damper active was 0.0558 cm (2.2 mils-DA) at

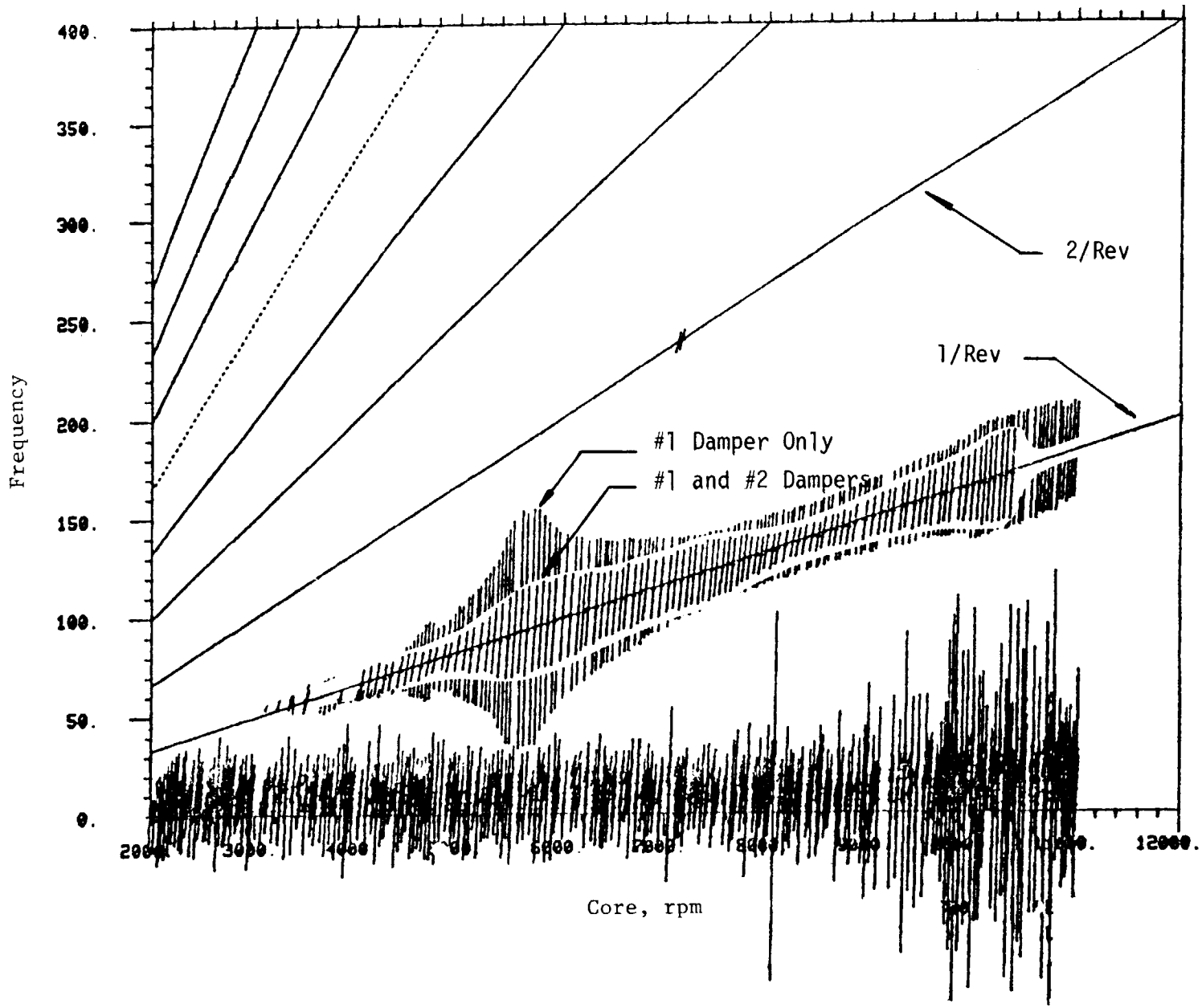

Figure 34. Ten-Stage Compressor Test, Build 2, Frequency Response at Forward Damper Housing.

ORIGINAL PAGE IS
OF POOR QUALITY

C-2

5750 rpm. Maximum one per rev response during normal operation (both dampers active) was 0.0254 cm (1.0 mil-DA) at 5750 rpm. The vibration limit at this accelerometer location was 0.102 cm (4.0 mils-DA).

The damped soft-mount concept has also been designed into the core, ICLS, and FPS engines. The low vibration response of both 10-stage compressor vehicles served to further demonstrate the validity of this design approach.

6.0 MECHANICAL/AEROMECHANICAL SUMMARY

6.1 SIX-STAGE COMPRESSOR TEST

6.1.1 Mechanical Results

The following observations were made upon posttest review of the compressor hardware. All blades and vanes were dirty. The forwardmost parts of the compressor (struts, IGV, Rotor 1 and Stator 1) were coated with a substance later identified as melted varnish sealer from the front frame wood panels. Several Rotor 1 and 2 blades had minor FOD nicks in the leading edge which were satisfactorily benched out later. All rotor blades exhibited an erosion or grit blast effect on the concave side of the trailing edge. The titanium rotor blades (1 through 4) had local discoloration on the trailing edge, most likely a result of high temperature stall pulses emanating from Plane 3. All stages of rotor blades rubbed into the casing liners, presumably during the stall events. The depths of the rubs varied from 0.0127 cm (0.005 in.) to 0.0381 cm (0.015 in.). The interstage honeycomb seals also experienced rubs which varied in depth from 0.0734 cm (0.029 in.) to 0.131 cm (0.052 in.).

One Stage 3 rotor blade was found to have a 0.635 cm (0.25 in.) long crack in the trailing edge 1.65 cm (0.65 in.) from the platform, which probably occurred during a 3.8-second sustained stall event at 100% speed. To summarize the previously submitted failure report, metallurgical examinations disclosed that the blade failed in fatigue and that the blade material (titanium 6-4) had experienced temperatures in excess of 1000° F at the failure location. Such temperatures would cause a significant reduction in blade fatigue life. Subsequent fatigue tests of Stage 3 blades from the rig denoted only a slight reduction in fatigue life of the unfailed blades. The remaining blades from the six-stage compressor were reshotpeened and deemed usable for the 10-stage compressor.

6.1.2 Aeromechanical Results

The two objectives of the six-stage compessor test, from a compressor mechanical design standpoint, were to assure safe operation during the testing

and to obtain test data to verify predicted operational characteristics. Assurance of safe operation was accomplished by monitoring selected strain gages and thermocouples and by periodic visual inspection of critical hardware.

Blade and vane vibratory stress levels observed during normal steady-state operations were less than 38% of high cycle fatigue limits. However, during one of the early tests in which the acoustic resonance was observed, stress levels went as high as 178% limits (Stage 4 rotor blade). These runs were made with an open IGV setting that generated a stall-like response in both rotor and stator airfoils. The blade and vane predicted and observed natural frequencies are shown in the Campbell diagrams, Figures 35 through 47. As is evidenced from the Campbell diagrams, the predicted frequencies correlated closely with the observed frequency.

The compressor was intentionally stalled 44 times. With the exception of Rotors 3 and 4, stall stress responses were unusually low. Maximum stall stress levels are noted below as a percentage of allowable vibratory limits.

Rotor Blade Stress	% Vibratory Limit	Stator Stress	% Vibratory Limit
Rotor 1	71	IGV	94
Rotor 2	69	Stator 1	71
Rotor 3	277	Stator 2	57
Rotor 4	170	Stator 3	70
Rotor 5	85	Stator 4	41
Rotor 6	97	Stator 5	27
		Stator 6	19

6.2 TEN-STAGE COMPRESSOR TEST, FIRST BUILD

6.2.1 Rotor Mechanical Results

The two objectives of the 10-stage compressor test, from a compressor mechanical design standpoint, were to assure safe operation during the testing and to obtain test data to verify predicted operational characteristics. Assurance of safe operation was accomplished by monitoring selected instrumen- strain gages and thermocouples and by periodic visual inspection of critical

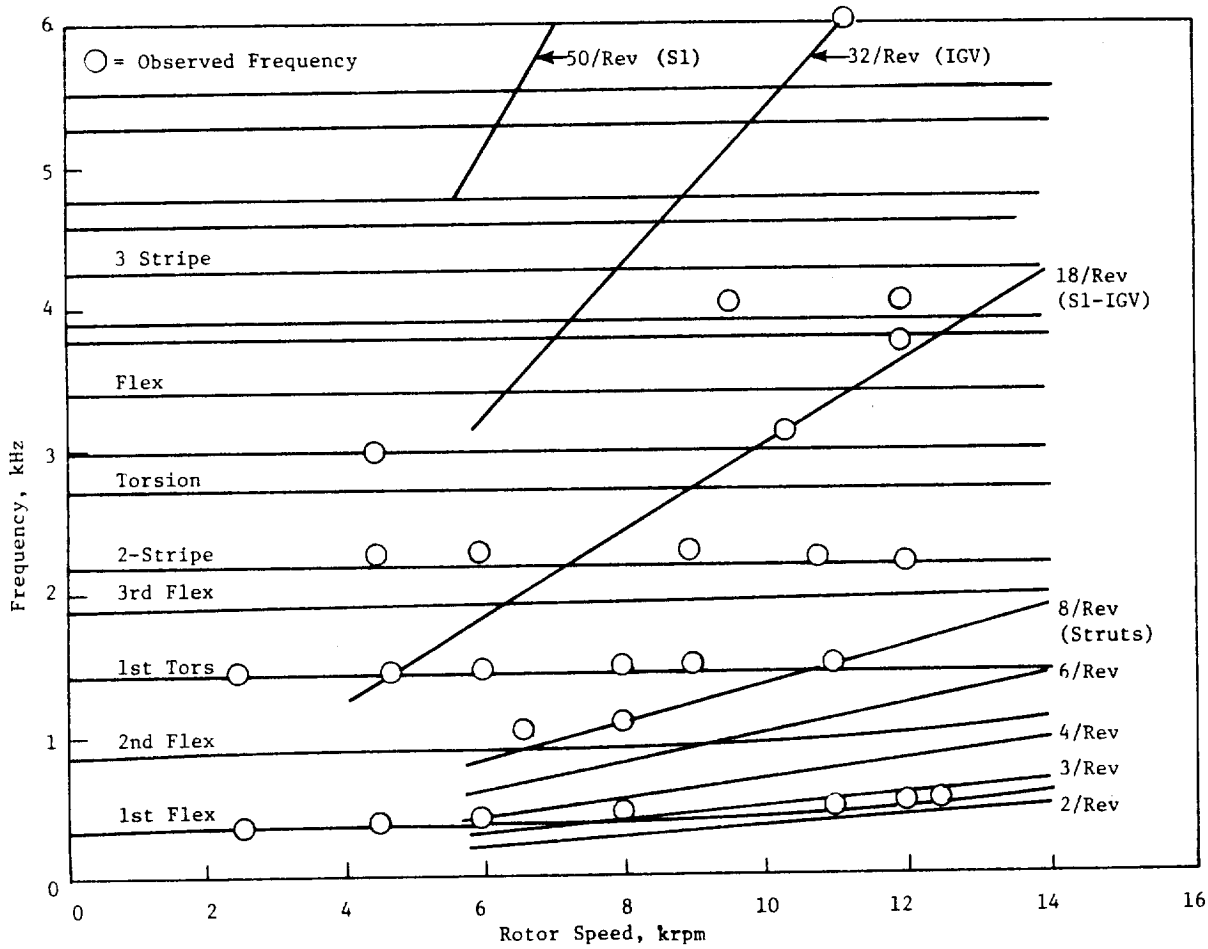

Figure 35. Compressor Rotor Stage 1 Blade Campbell Diagram.

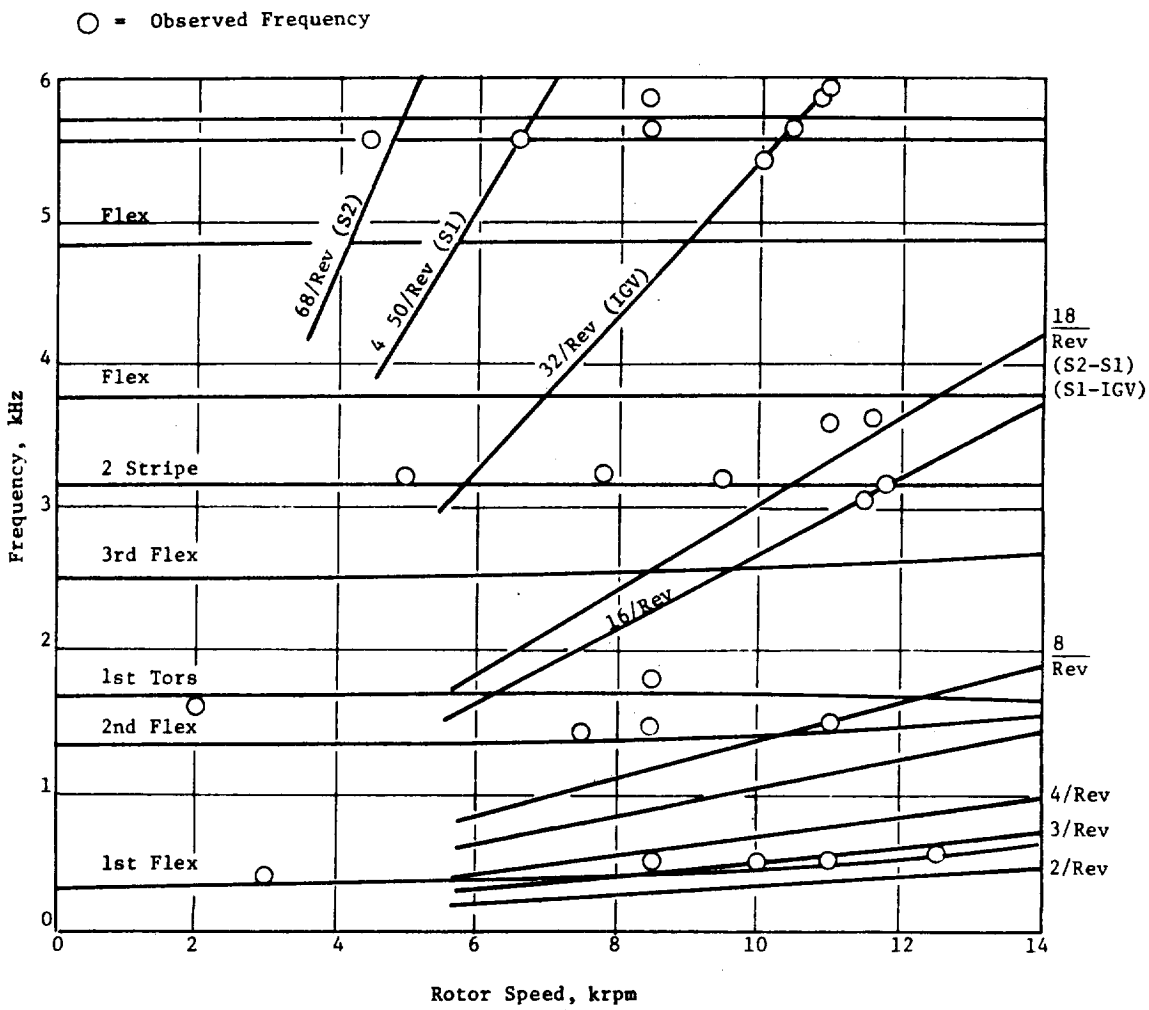

Figure 36. Compressor Rotor Stage 2 Blade Campbell Diagram.

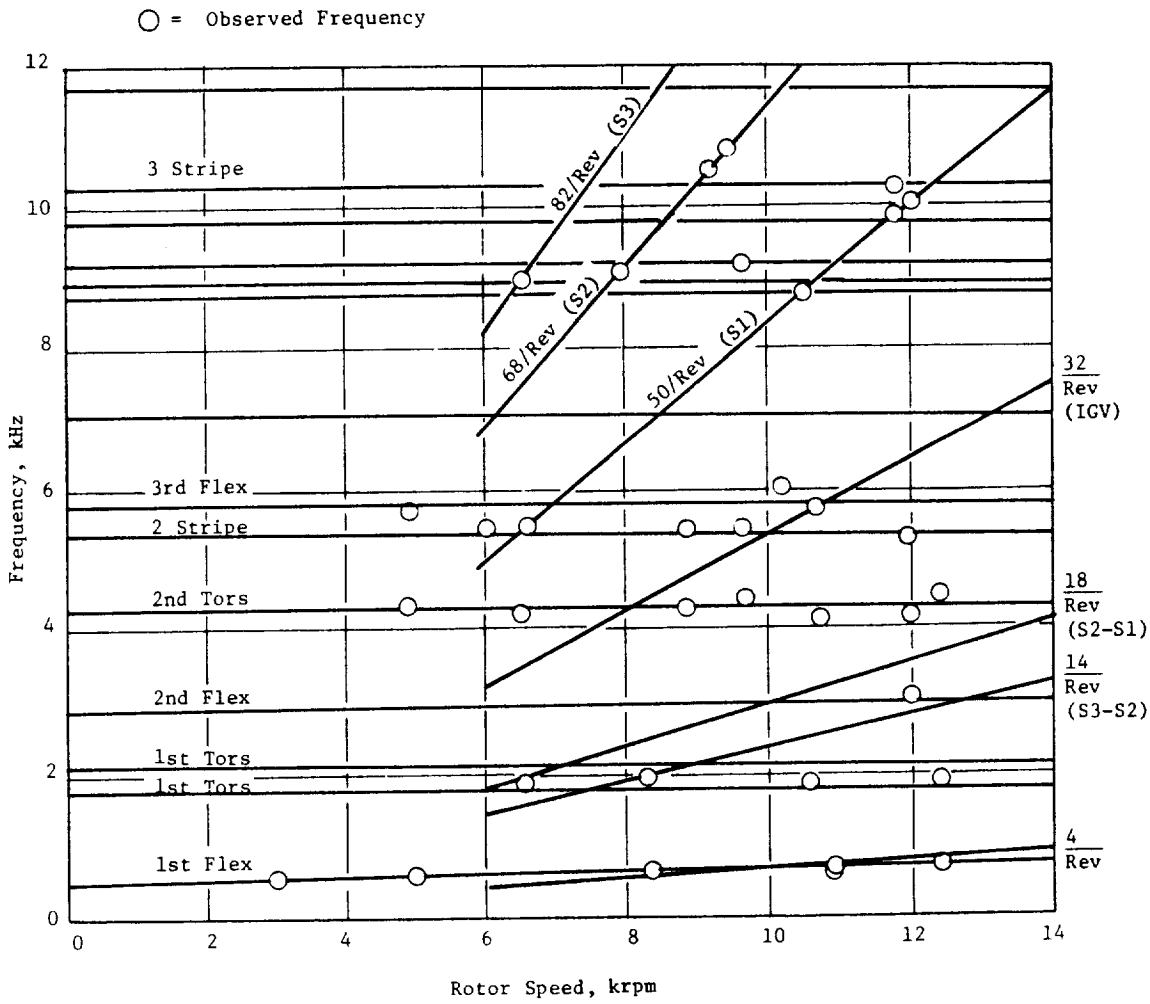

Figure 37. Compressor Rotor Stage 3 Blade Campbell Diagram.

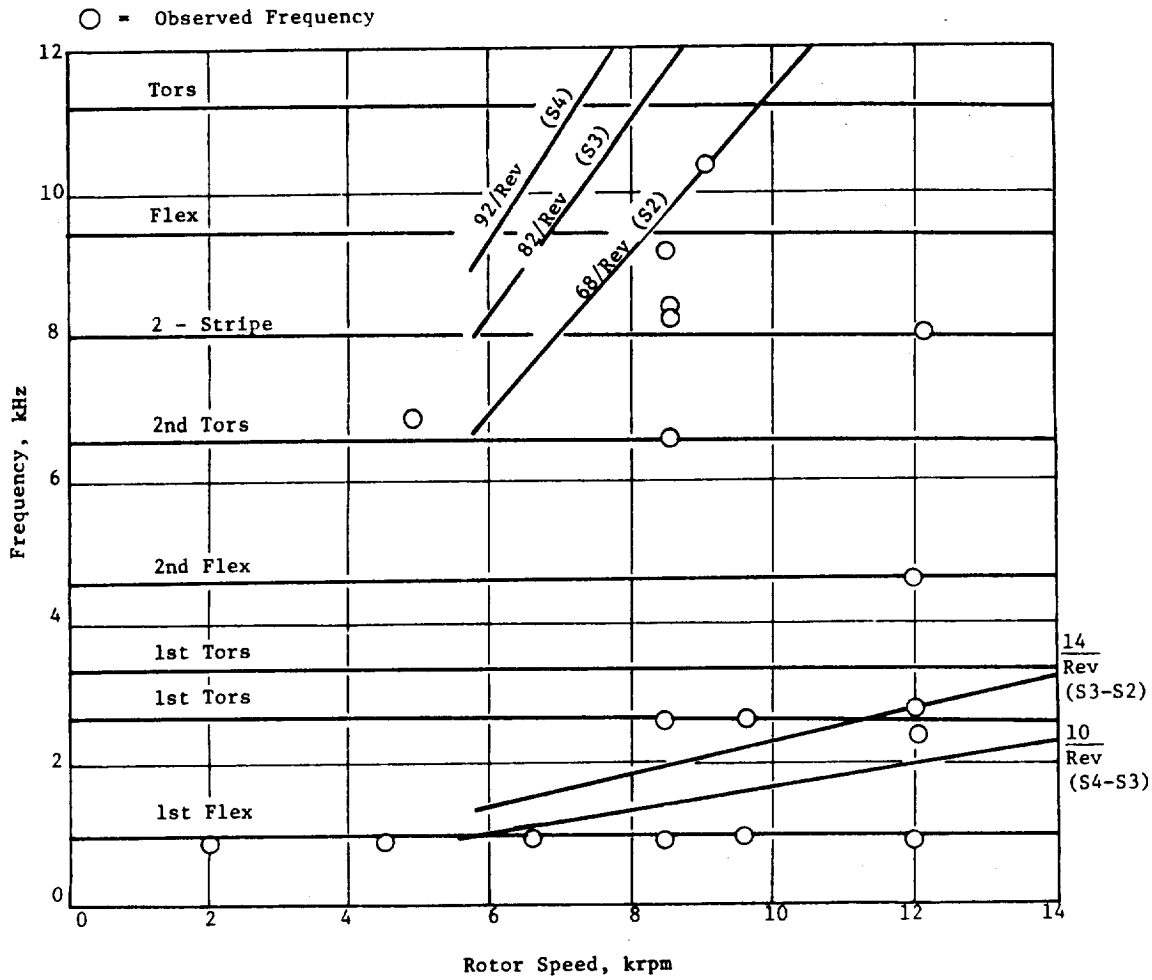

Figure 38. Compressor Rotor Stage 4 Blade Campbell Diagram.

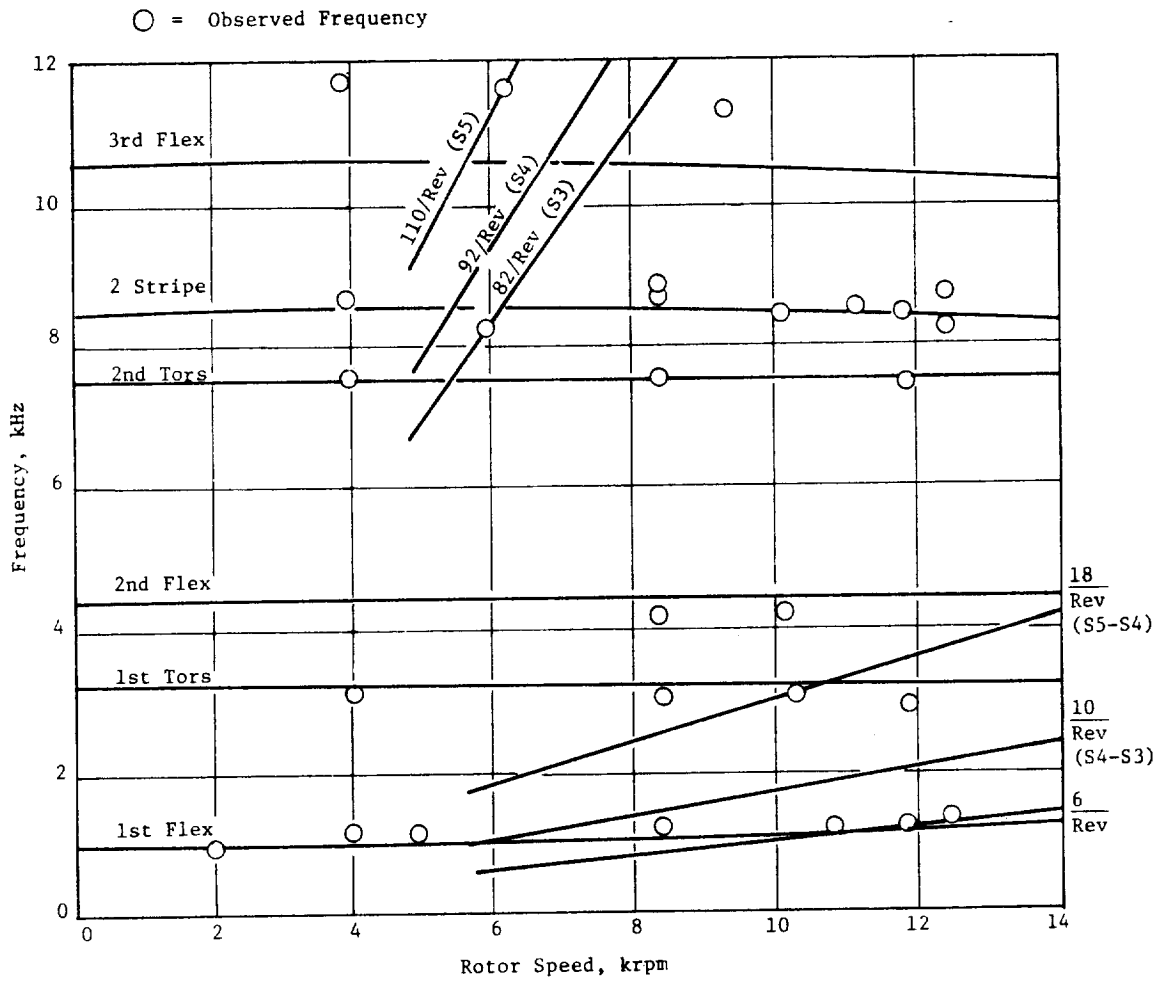

Figure 39. Compressor Rotor Stage 5 Blade Campbell Diagram.

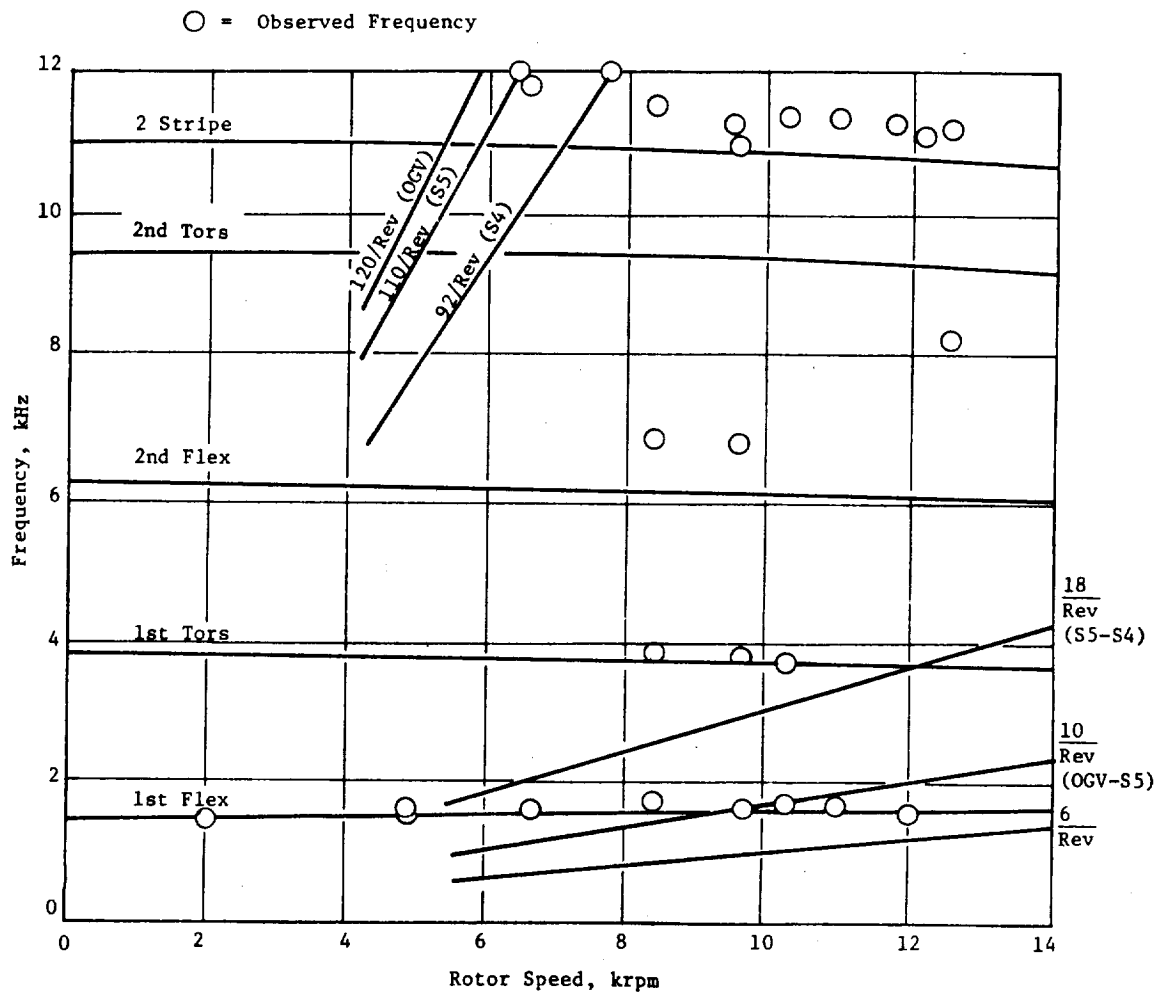

Figure 40. Compressor Rotor Stage 6 Blade Campbell Diagram.

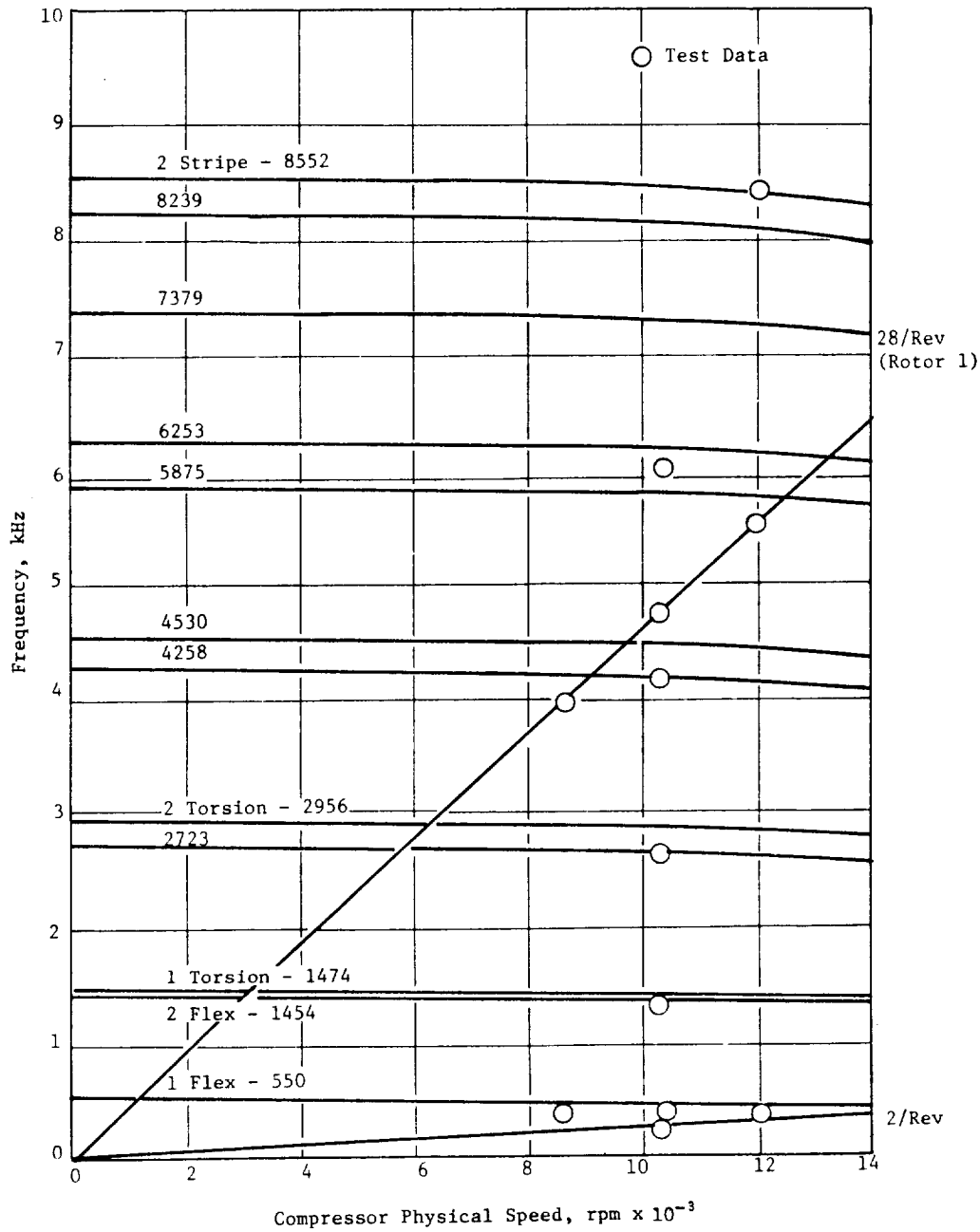

Figure 41. Compressor Stator IGV Campbell Diagram.

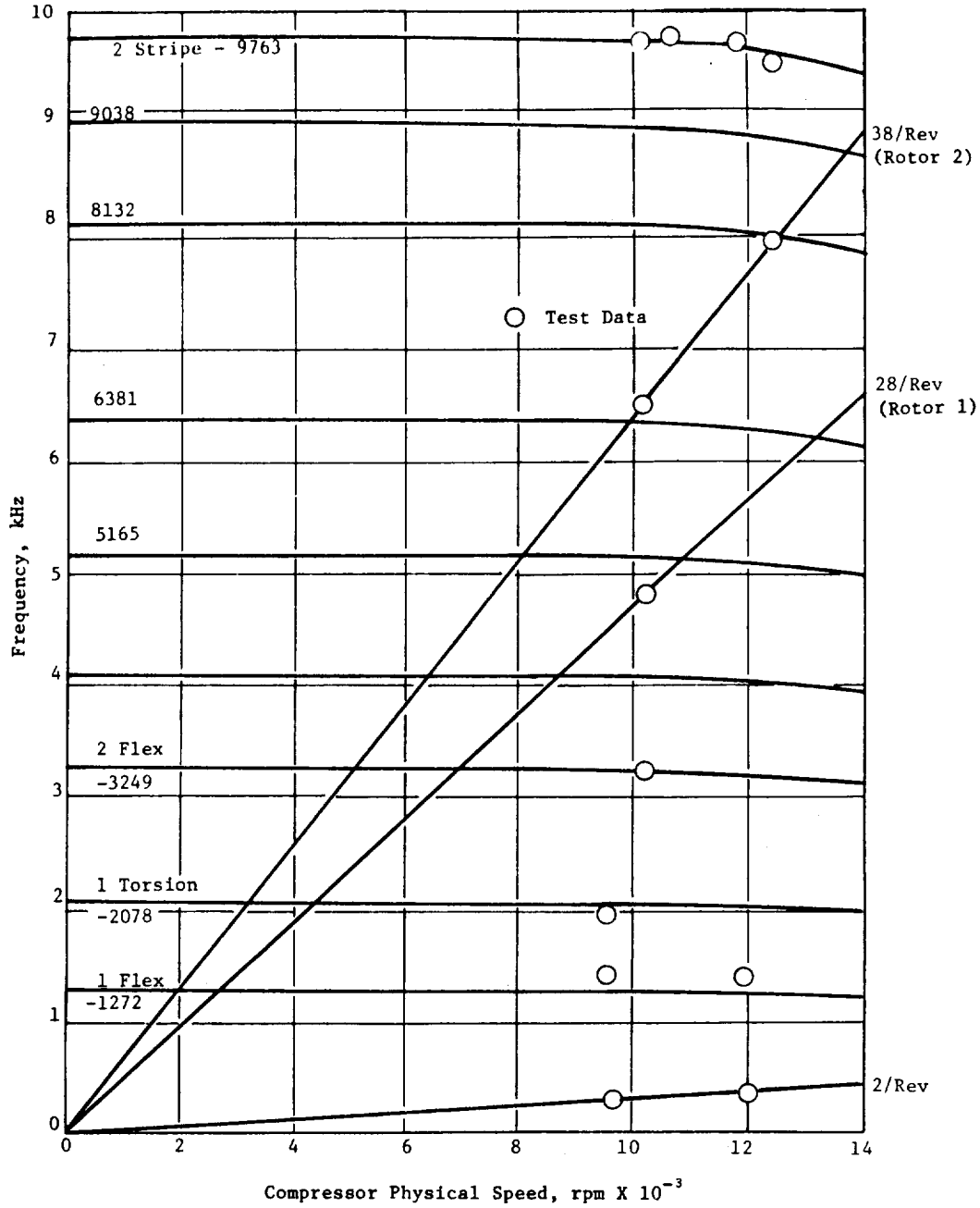

Figure 42. Compressor Stator 1 Campbell Diagram.

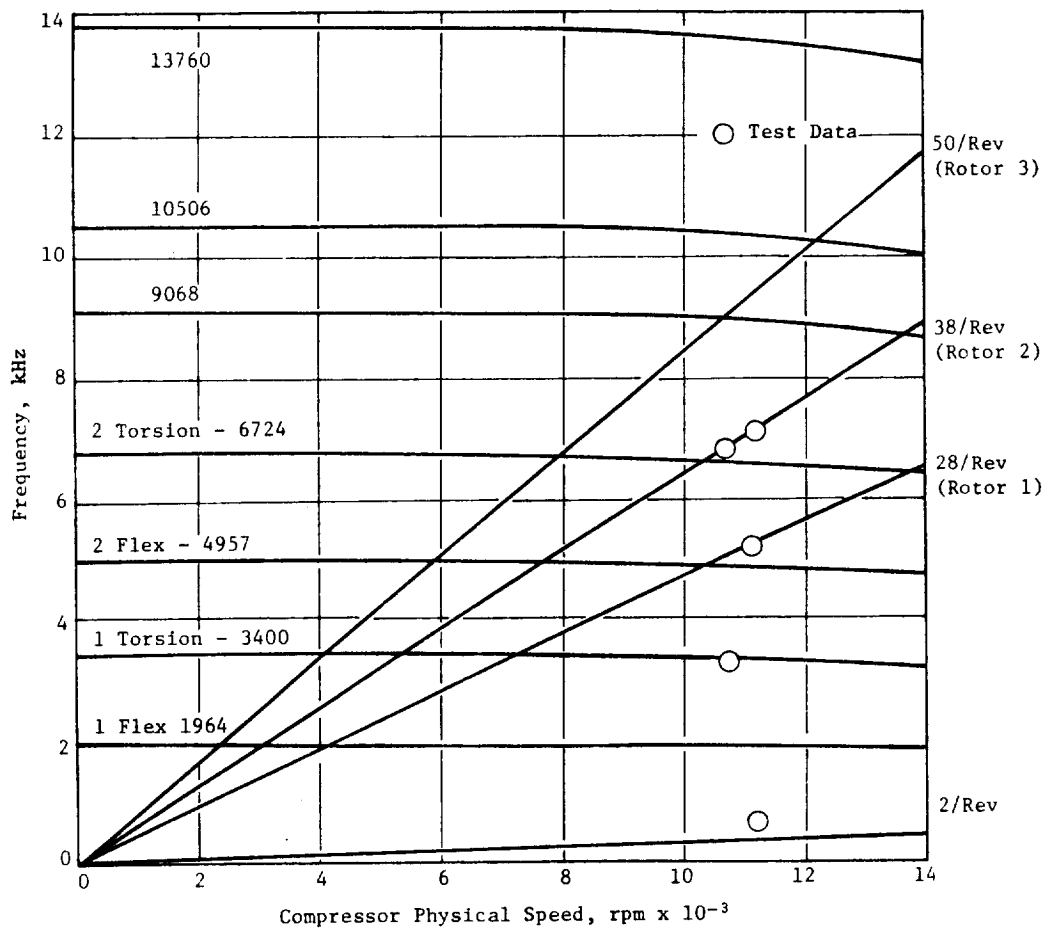

Figure 43. Compressor Stator 2 Campbell Diagram.

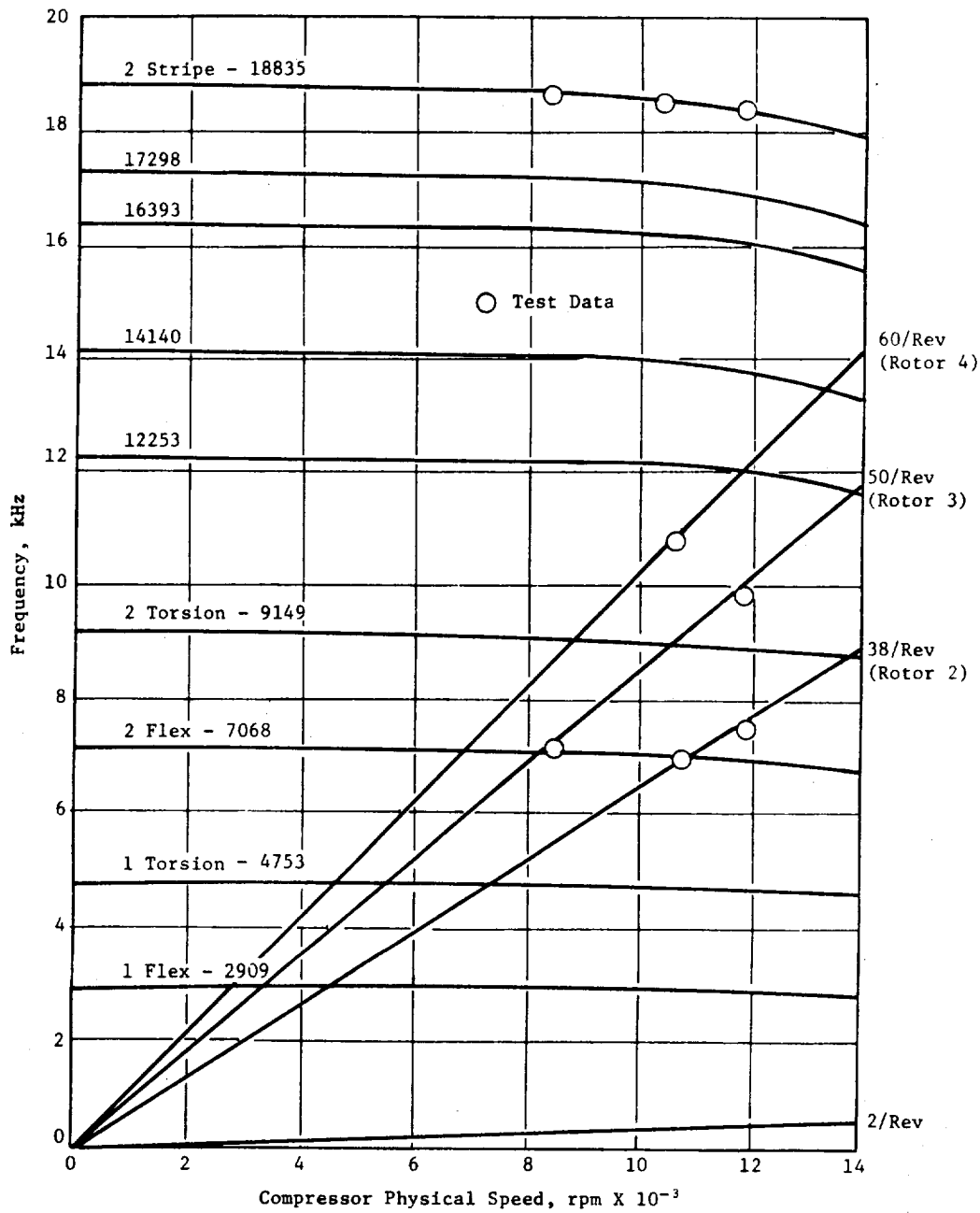

Figure 44. Compressor Stator 3 Campbell Diagram.

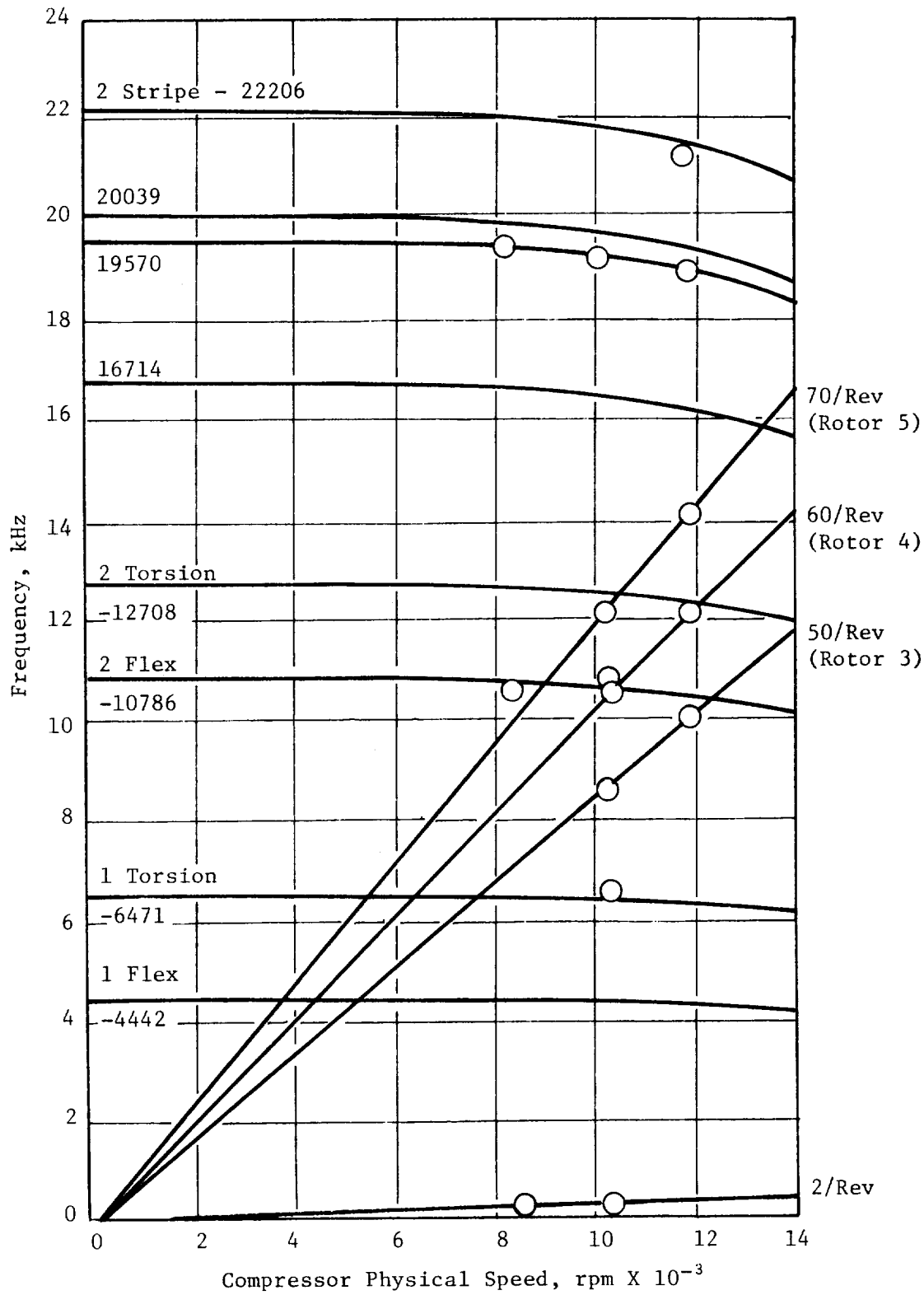

Figure 45. Compressor Stator 4 Campbell Diagram.

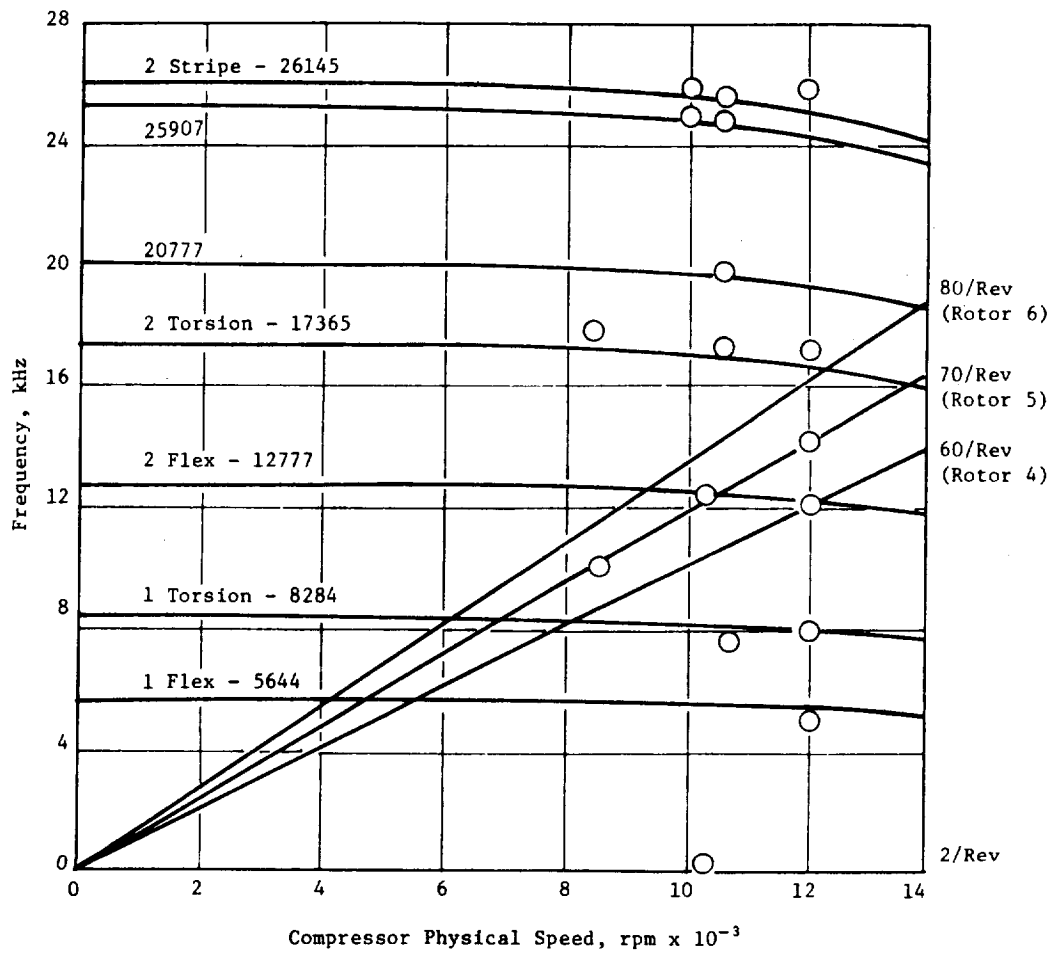

Figure 46. Compressor Stator 5 Campbell Diagram.

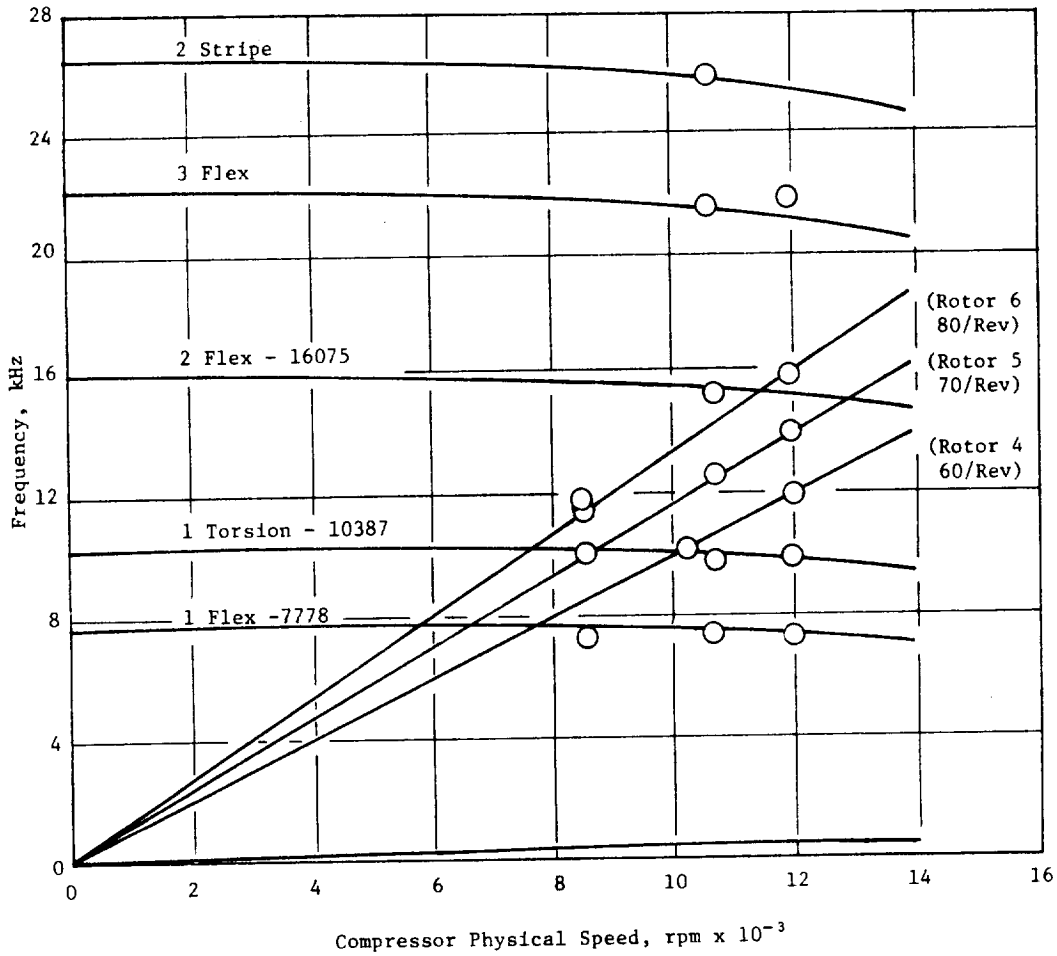

Figure 47. Compressor Stator 6 Campbell Diagram.

hardware. This visual inspection, specifically borescope inspections, will be discussed later in more detail. Also included are some particular observations made during the test and during compressor teardown.

Rotor structure temperatures were monitored in selected locations to provide correlation with stress and deflection analyses. At most locations, the data correlated closely with the predicted, as seen for a representative reading in Figure 48. Where data were not in reasonable agreement, the prediction models were updated and the results were factored into the 10B compressor and core engine builds.

During the test, a study was conducted to determine the effect of varying rotor bore cooling air on rotor structure temperatures and blade tip clearances. At a compressor physical speed of 10,385 rpm [12,047 rpm corrected (N_c)] with inlet conditions (Plane 25) of 214 K (75° F) (T25), 22.06 kPa (3.2 psia) (P25) and exhaust conditions (plane 3) of 578 K (580° F) T3 and 468.9 kPa (68 psia) (P3); 288 K (58° F) air was injected into the rotor bore at flows varying 0.154 kg/s (0.34 lbm/s) (0.29% W25C) to 0.385 kg/s (0.85 lbm/s) (0.72% W25C). The effects on bore temperatures and blade tip clearances were as anticipated and are shown for Stages 3 and 10 in Figure 49.

During the course of the testing, the rotor was borescoped two times. The first time was on April 2, 1981, after the first battery of high speed stall testing. At that time, the following blade FOD was noted:

Stage	No. Blades	Description
1	None	
2	None	
3	None	
4	None	
5	None	
6	None	
7	8	Leading Edge Nicks
8	2	Leading Edge Nicks
9	3	Leading Edge Nicks
10	2	Leading Edge Nicks

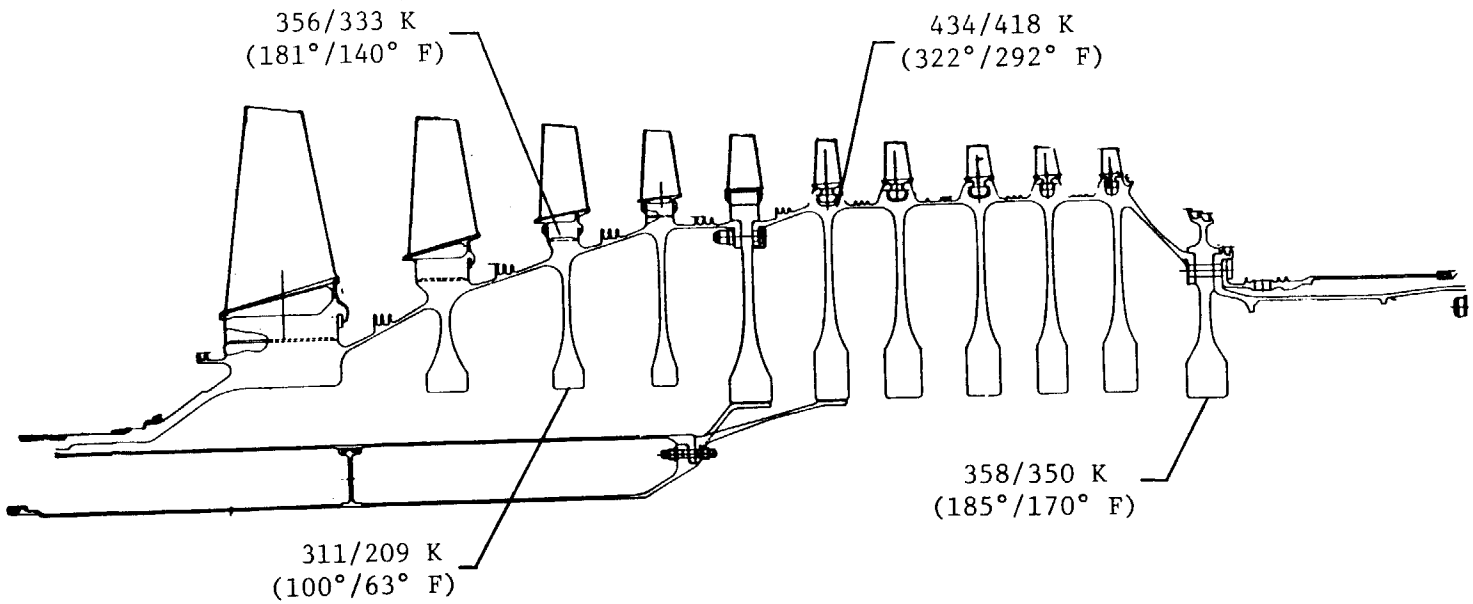

ORIGINAL PAGE IS
OF POOR QUALITY

Measured Temperature/Predicted Temperature

	T25 K (° F)	P25 kPa (psia)	T3 K (° F)	N_{Phys}	$\%N_{Corr}$	$T_{Bore\ Cool}$ K (° F)	$W_{Bore\ Cool}$ kg/s (lbm/s)
Test Point Conditions	255 (-67)	26.27 (3.81)	595 (611)	10,610	99	287 (57)	0.3896 (0.86)
Prediction Point Conditions	220 (-63)	29.5 (4.28)	592 (606)	10,764	100	289 (60)	0.3896 (0.86)

Figure 48. Compressor Rotor 10A Temperature Comparison.

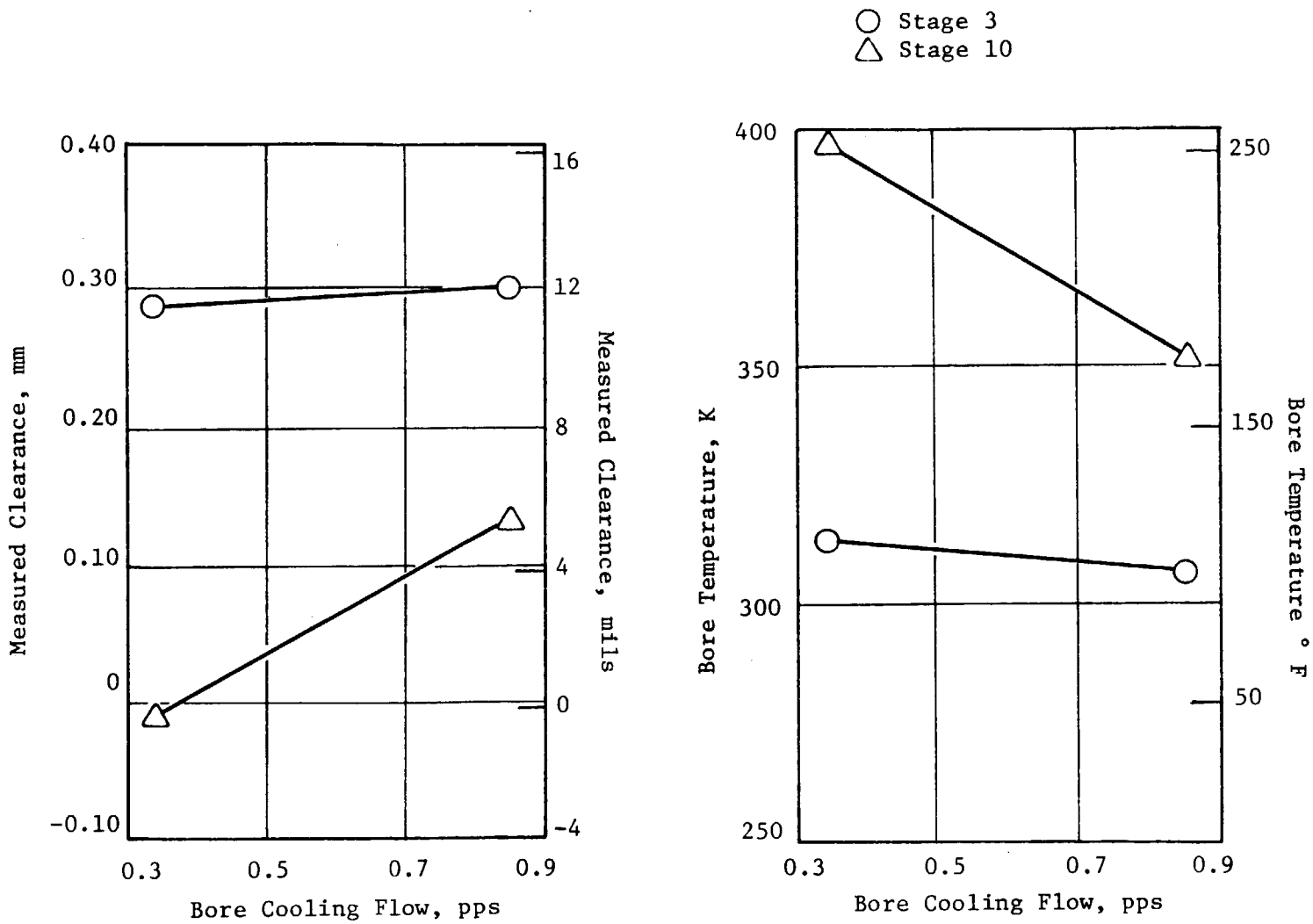

Figure 49. First 10-Stage Compressor Bore Cooling Flow Effects

The second borescope inspection was done April 10, 1981, after the compressor sustained an unexpected, long-duration stall that resulted in noticeable performance deterioration. At that time, the following FOD was noted:

Stage	No. Blades	Description
1	Not Inspected	
2	Not Inspected	
3	None	OK
4	Trailing Edge Only	OK
5	None	OK
6	6	Leading Edge Nicks
7	22	Leading Edge Nicks
8	15	Leading Edge Nicks
9	19	Leading Edge Nicks
10	12	Leading Edge Nicks

The FOD observed was severe enough to raise concerns that other unseen damage, possibly to the vanes, had occurred. Rather than risk additional and potentially catastrophic damage to the compressor, the vehicle was returned to Evendale for further teardown inspection.

Upon teardown, the following blade damage was found:

Stage	No. Blades	Description
1	9	Leading Edge Nicks + Tip Tears
2	3	Leading Edge Nicks
3	3	Leading Edge Nicks
4	8	Leading Edge Nicks
5	3	Leading Edge Nicks
6	16	Leading Edge Nicks
7	26	Leading Edge Nicks
8	17	Leading Edge Nicks
9	20	Leading Edge Nicks
10	21	Leading Edge Nicks

The most logical explanation for the cause of the damage was that ice formed on the IGV's during refrigerated inlet testing, and that during a stall (most likely on April 8, 1981) it broke loose and impacted the R1 blades. This caused leading edge distortion and fragmentation on three blade leading edge tips. These pieces of blade tips then passed through the compressor causing FOD in the remaining stages.

As a result of this incident, the FOD tolerance of the compressor was unexpectedly demonstrated to be excellent. This incident also prompted improvements to the dryer system, the installation of an ice detector at the IGV plane, and a revision of the operating procedures and limits.

Upon teardown, another unexpected distress area was discovered. The single tooth discourager seal on the aft side of the Stage 10 disk was severely worn. An approximation of the extent of the wear is shown in the 5X sketch in Figure 50. René 95 aft spool material was found in the stationary honeycomb rub seal, and the seal showed signs of wear in approximately a 90° to 120° segment of the lower case. Apparently, tighter than desired buildup clearances caused the abrasive tooth seal coating to be scraped away during buildup, leaving unprotected metal which was rubbed off during testing. Studies disclosed that the added seal clearance was no detriment to compressor operation, so the seal tooth was not refurbished for the 10B build.

All Stage 3 through 10 rotor blades, except instrumented blades, passed fluorescent-penetrant inspection (FPI) after disassembly. Sometime later, as the instrumented blades were being visually reviewed, a strain-gaged Stage 3 blade was found to have a crack in the trailing edge 2.032 cm (0.80 in.) above the platform. Although this failure was similar to the cracked blade from the six-stage compressor (Section 6.1.2), it differed in that the fatigue striations indicated only one initiation point and one stop. The crack occurred during a single event, probably during the sustained stall on April 10, 1981. Unfortunately, the strain gage had ceased functioning properly prior to this event, so no meaningful stress data could be discerned.

6.2.2 Rotor Aeromechanical Results

The quality and quantity of the aeromechanical data obtained from the test were less than desired for two reasons: (1) the strain gage signals were very noisy, and (2) a strong per-rev excitation was present in the Stage 5 through 10 blade signals.

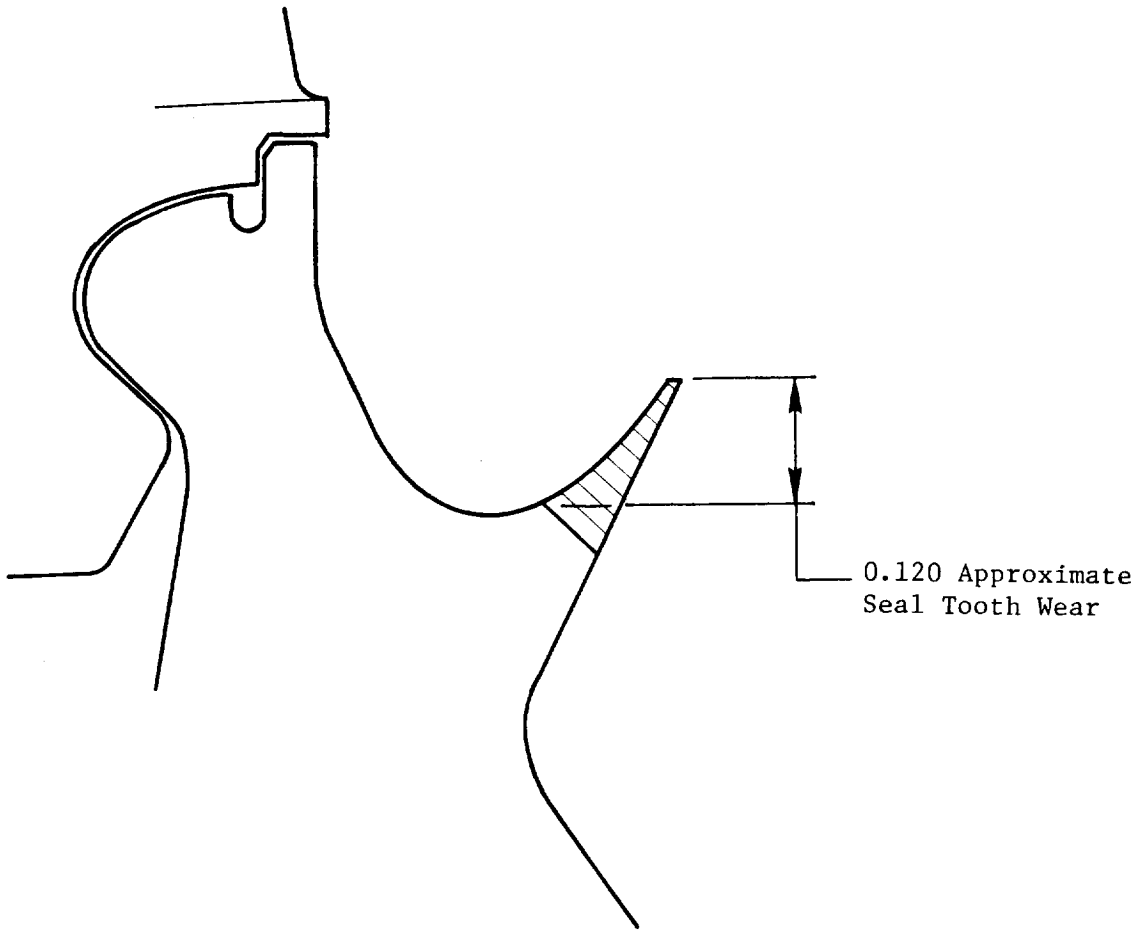

Figure 50. Wear on Single Tooth Discourager Seal.

The strain gage noise problem was investigated and was most likely a slipring operational/procedural quality problem. All relevant recommendations were assembled into a procedure to follow for future testing.

The extent and strength of the per rev signals are illustrated in Figures 51 and 52 which are Fast Fourier Transform (FFT)-produced Campbell diagrams for Stages 5 and 6 blade root gages during a decel on March 26, 1981. This condition persisted throughout the test as did attempts to isolate the cause. Based on past experience, the obvious cause was a disturbance in the flowpath caused by a stationary source. The most likely candidate was a misrigged stator vane in one of the mid-stages, 4 through 6. Exhaustive external and internal inspections of the compressor were made with no success. Upon teardown, visual inspection revealed that a Stage 6 instrumentated vane at 126° CW Aft looking forward (ALF) had been damaged during instrumentation or assembly such that its trailing edge (TE) metal angle was closed up to 60° at the hub. The damage was considered sufficient to cause the per rev disturbance. Subsequent visual inpsections during teardown failed to reveal any other candidate sources.

Airfoil vibratory frequencies and stresses were monitored and recorded during the test. The frequencies observed are shown in Figures 53 through 62, and exhibit close correlation to the predicted values.

Maximum normal operation vibratory stresses observed on the rotor blades are presented below as a percentage of limits:

Stage	Limits, %
1	12
2	11
3	29
4	24
5	120
6	92
7	42
8	33
9	15
10	17

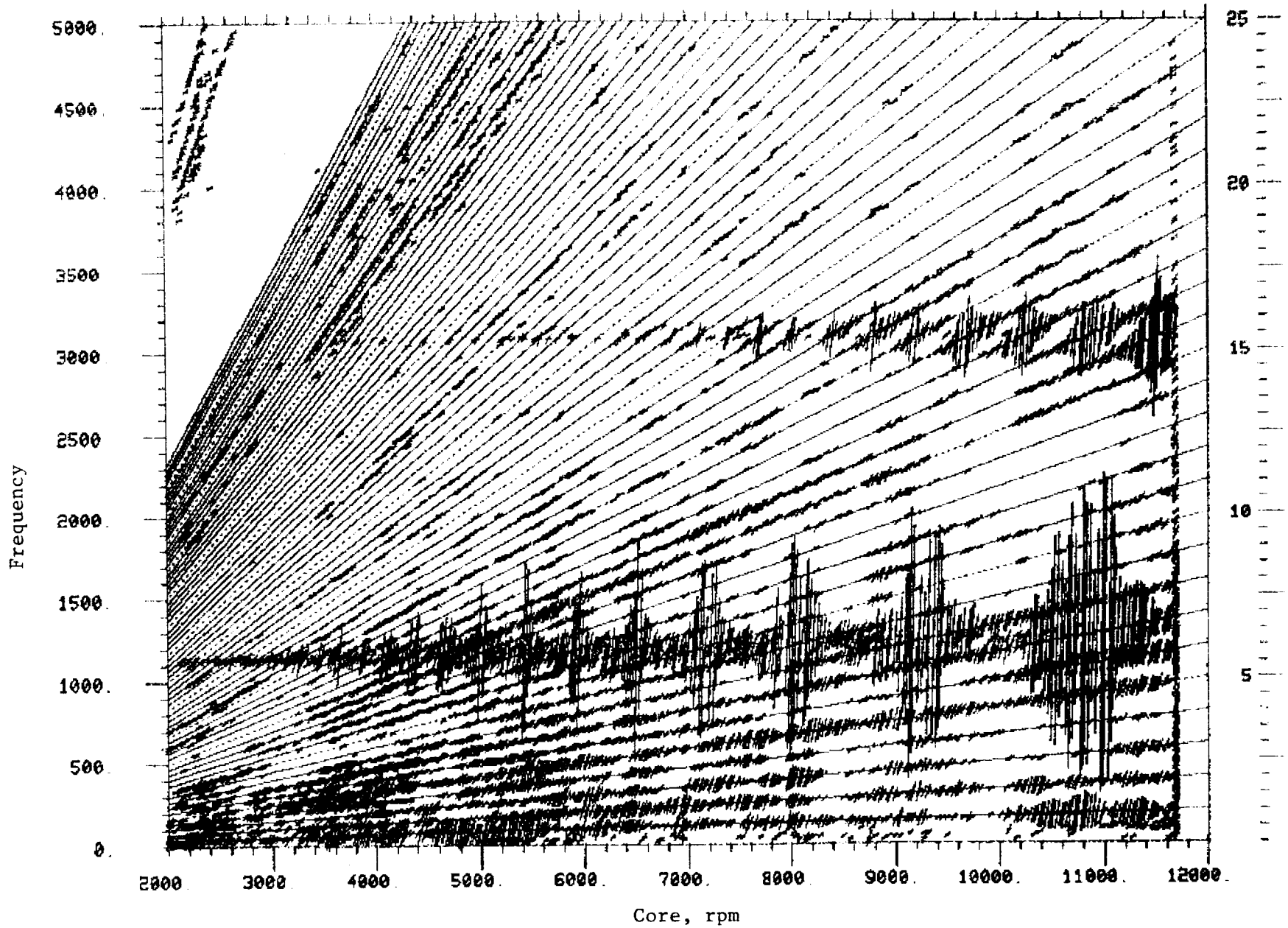

Figure 51. Campbell Diagram, Stage 5 Blade Root Gages.

ORIGINAL PAGE IS
OF POOR QUALITY

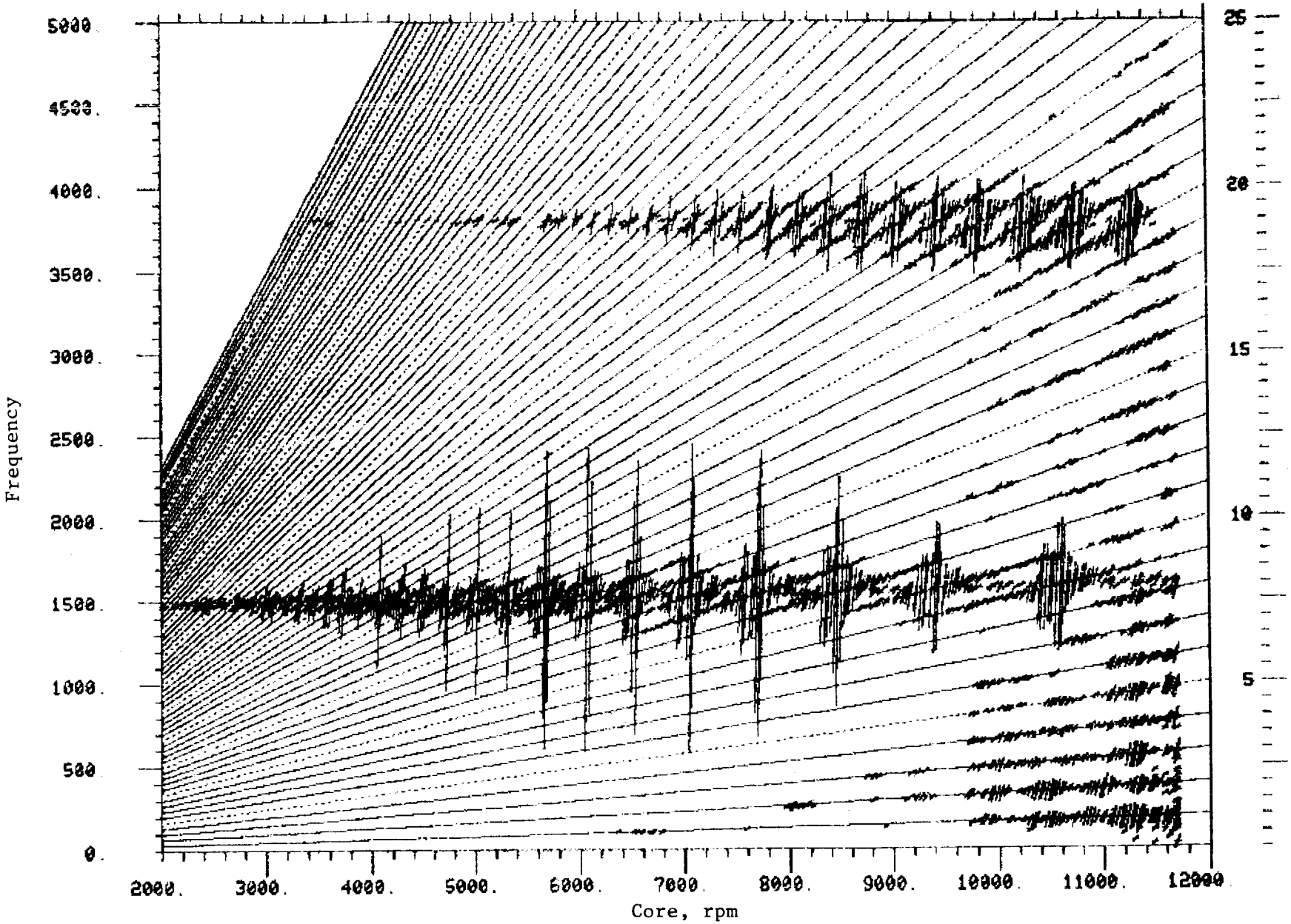

Figure 52. Campbell Diagram, Stage 6 Blade Root Gages.

ORIGINAL PAGE IS
OF POOR QUALITY

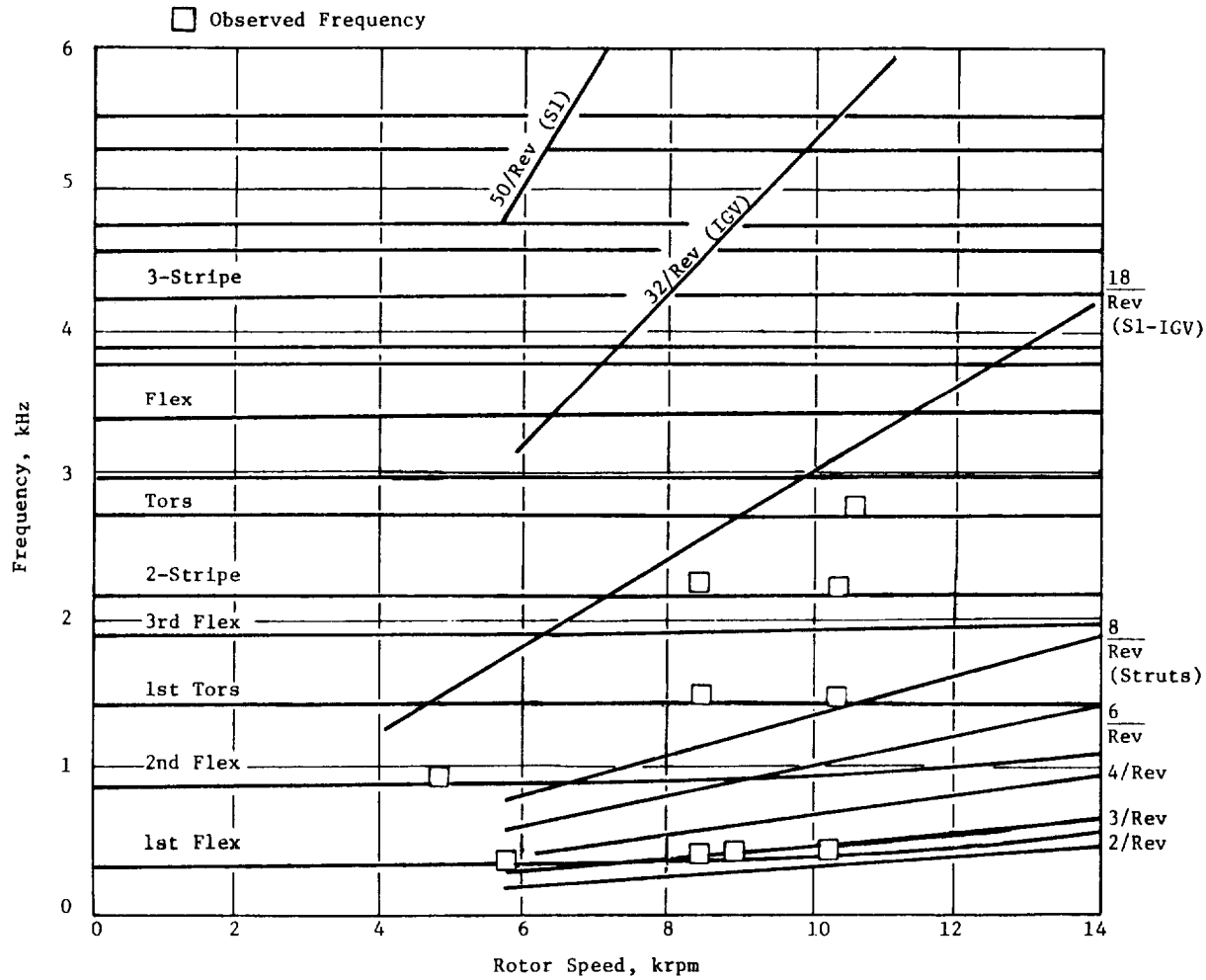

Figure 53. Ten-Stage Compressor Rotor Stage 1 Blade Campbell Diagram.

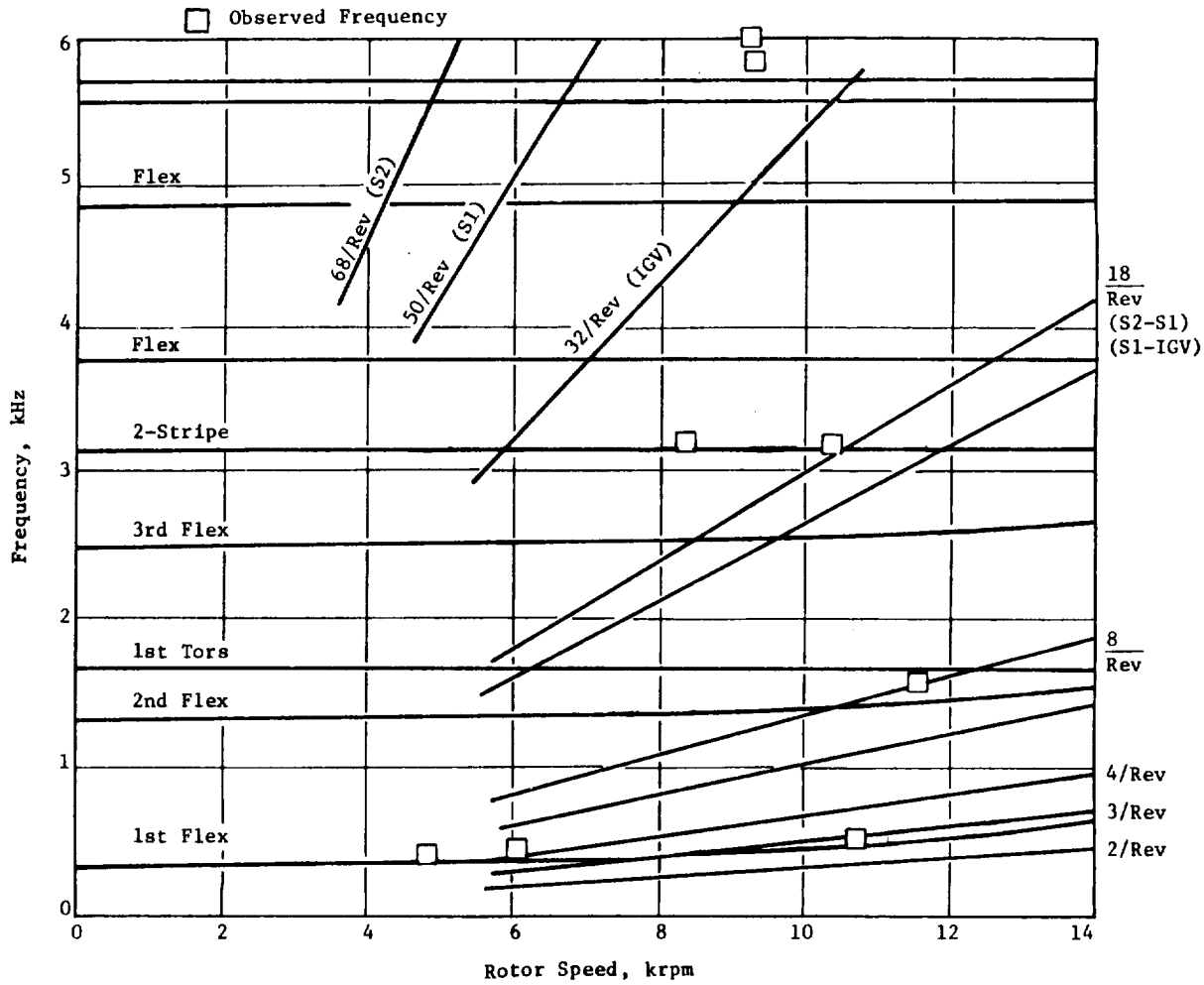

Figure 54. Ten-Stage Compressor Rotor Stage 2 Blade Campbell Diagram.

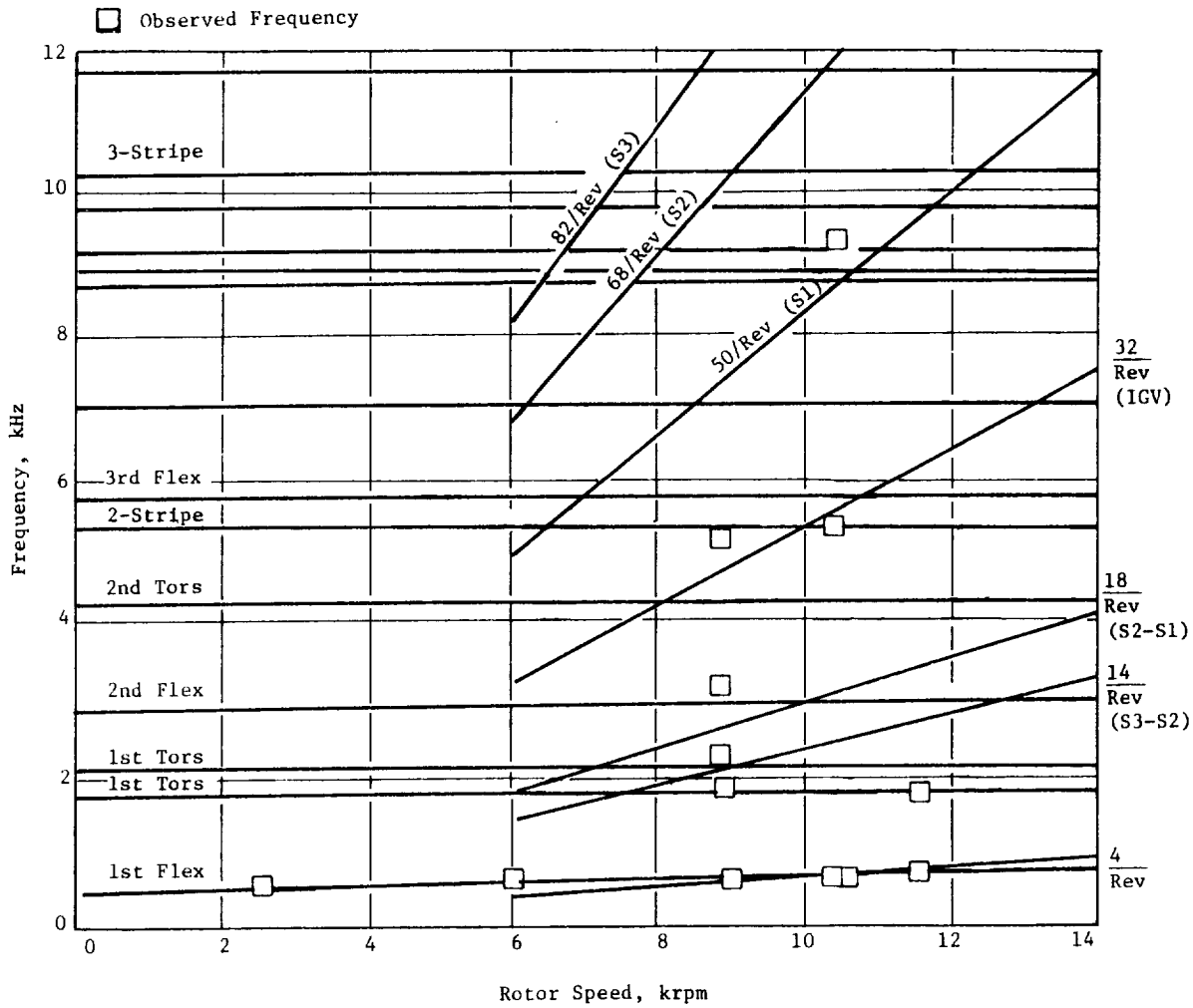

Figure 55. Ten-Stage Compressor Rotor Stage 3 Blade Campbell Diagram.

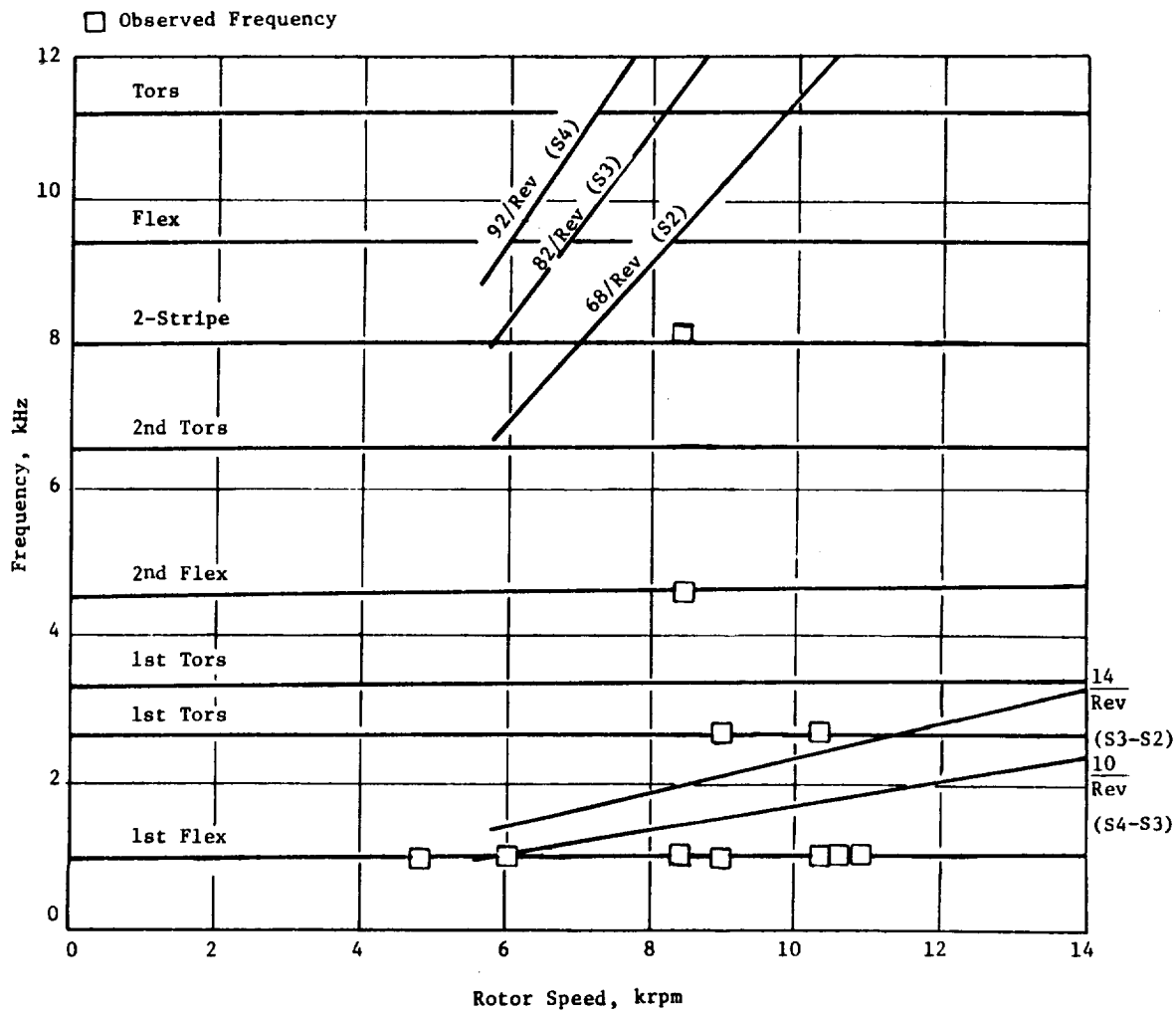

Figure 56. Ten-Stage Compressor Rotor Stage 4 Blade Campbell Diagram.

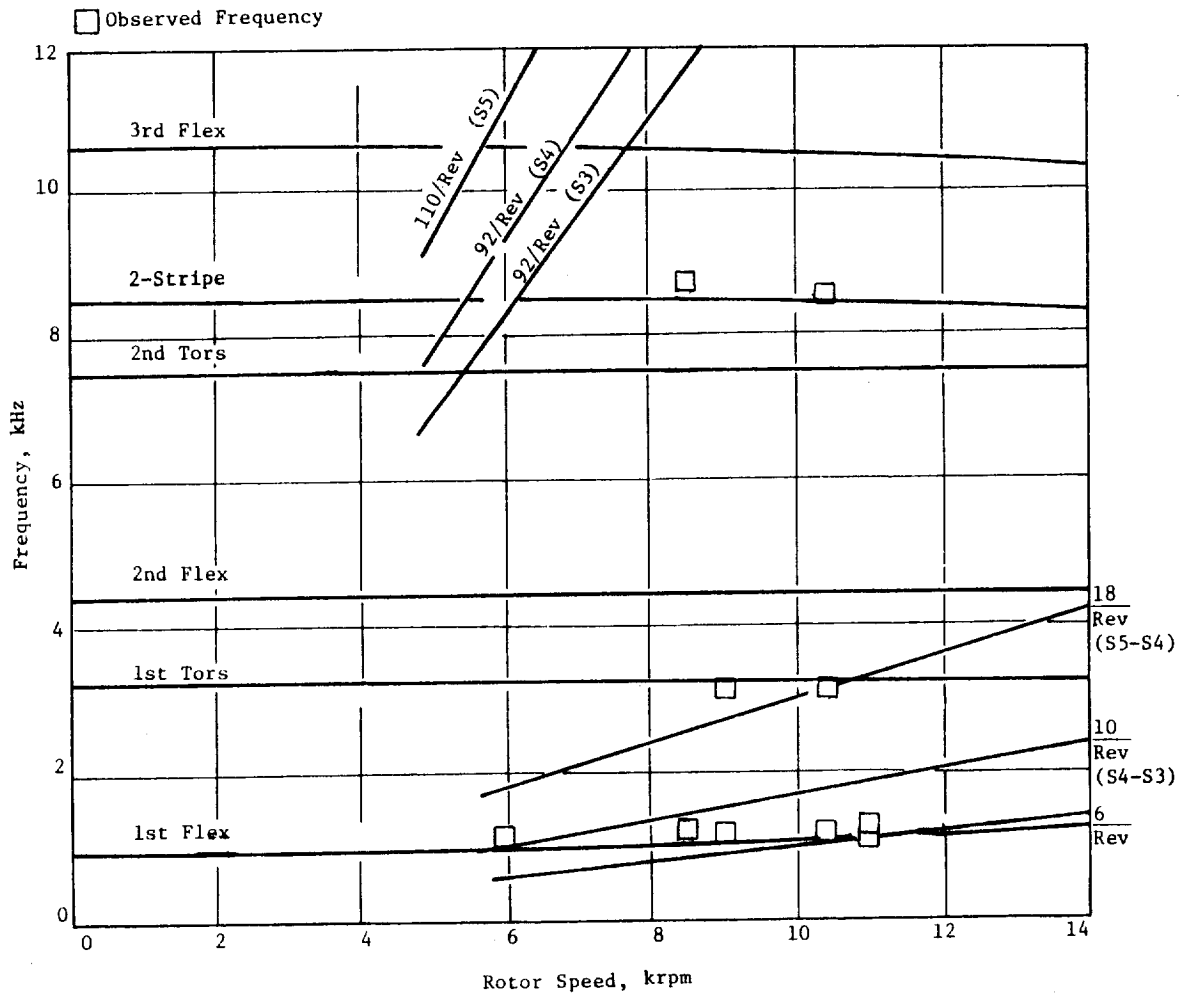

Figure 57. Ten-Stage Compressor Rotor Stage 5 Blade Campbell Diagram.

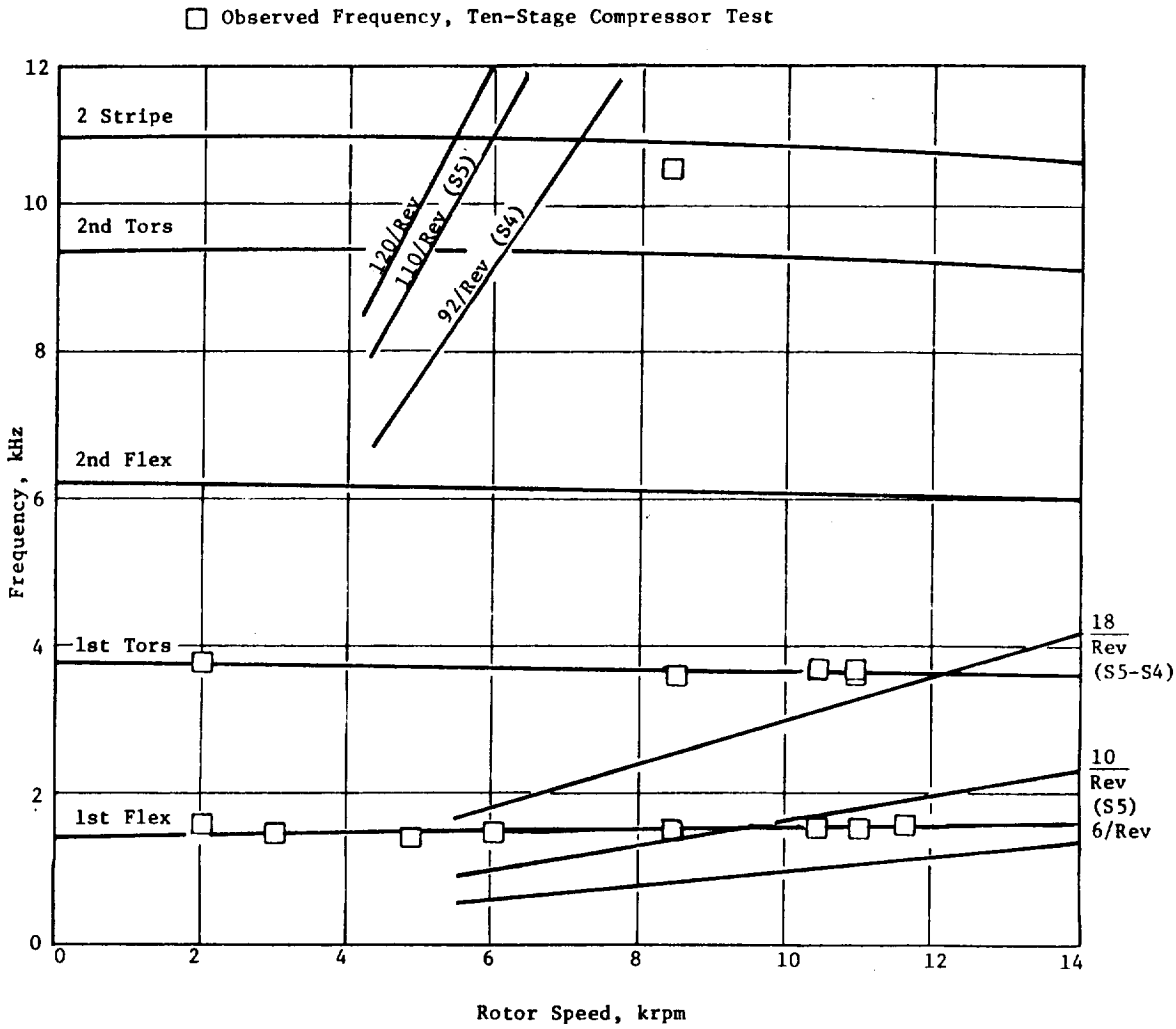

Figure 58. Ten-Stage Compressor Rotor Stage 6 Blade Campbell Diagram.

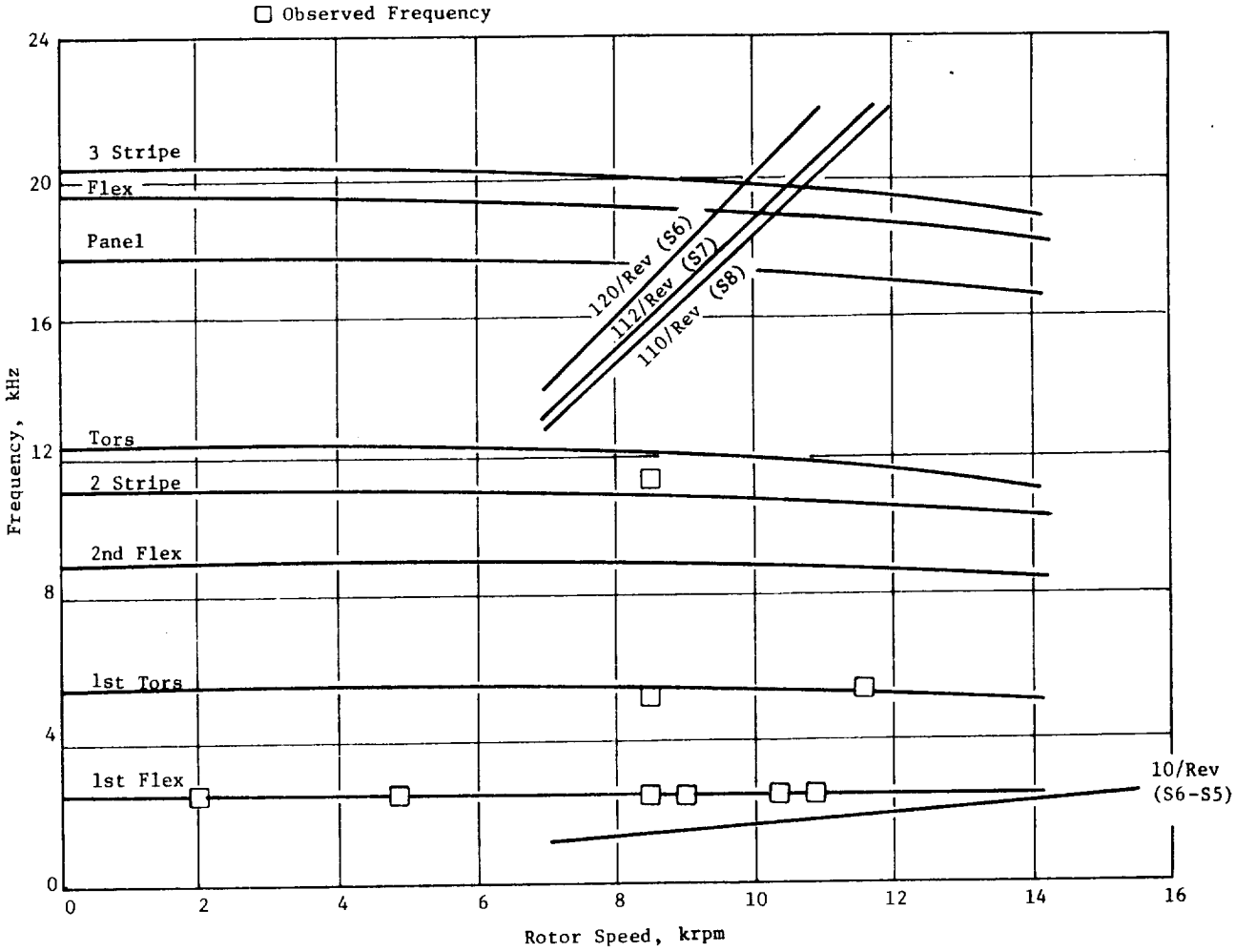

Figure 59. Ten-Stage Compressor Rotor Stage 7 Blade Campbell Diagram.

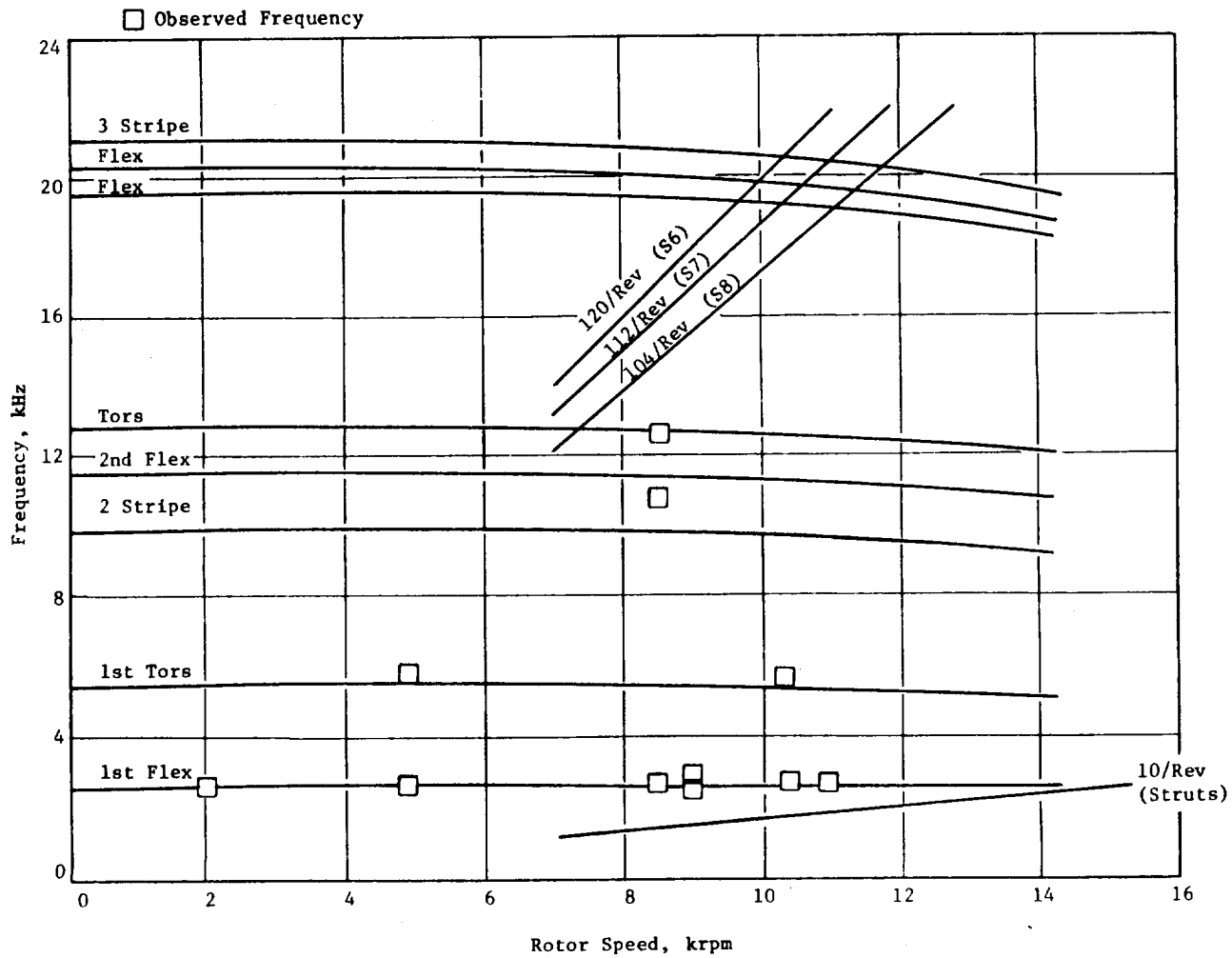

Figure 60. Ten-Stage Compressor Rotor Stage 8 Blade Campbell Diagram.

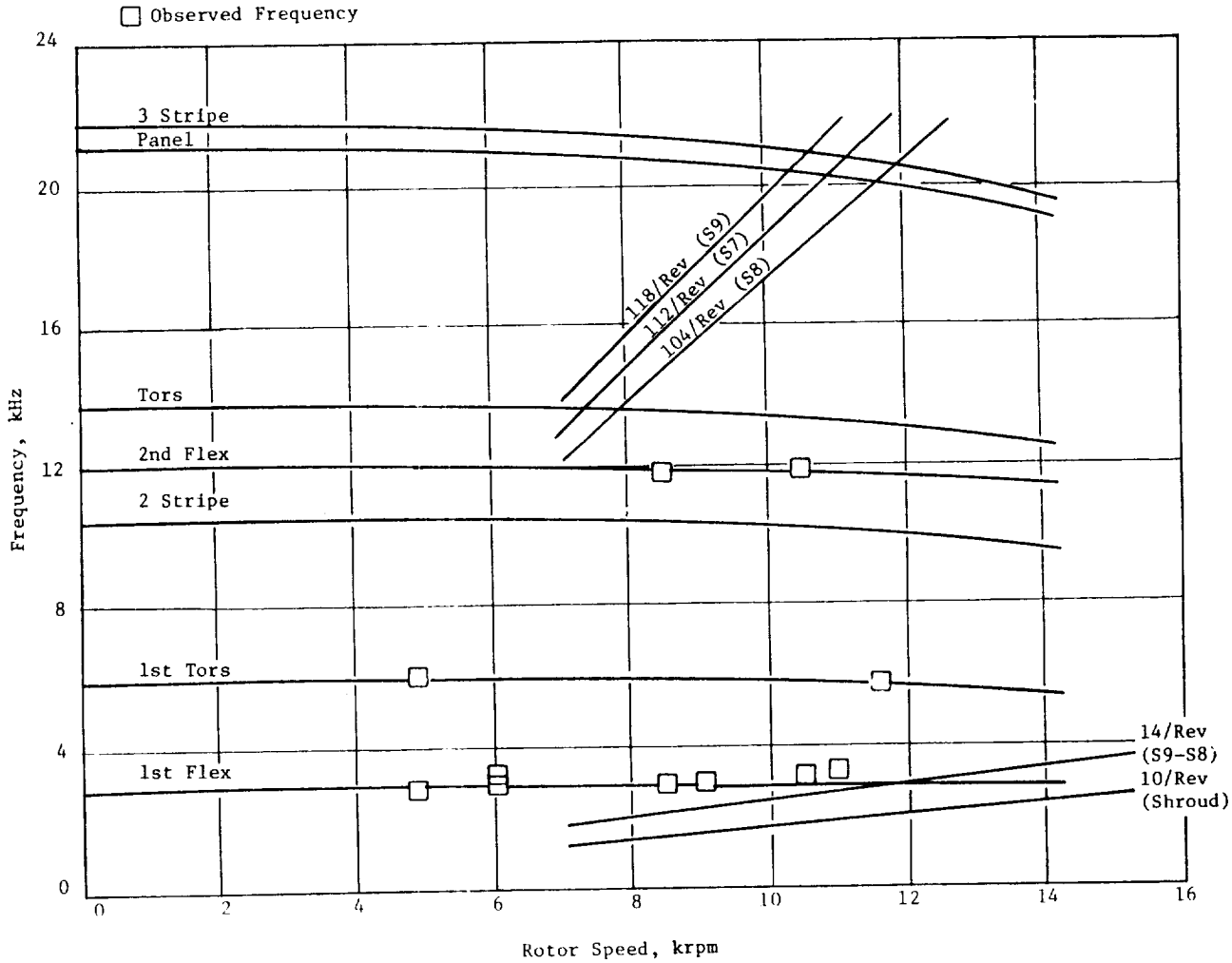

Figure 61. Ten-Stage Compressor Rotor Stage 9 Blade Campbell Diagram.

ORIGINAL PAGE IS
OF POOR QUALITY

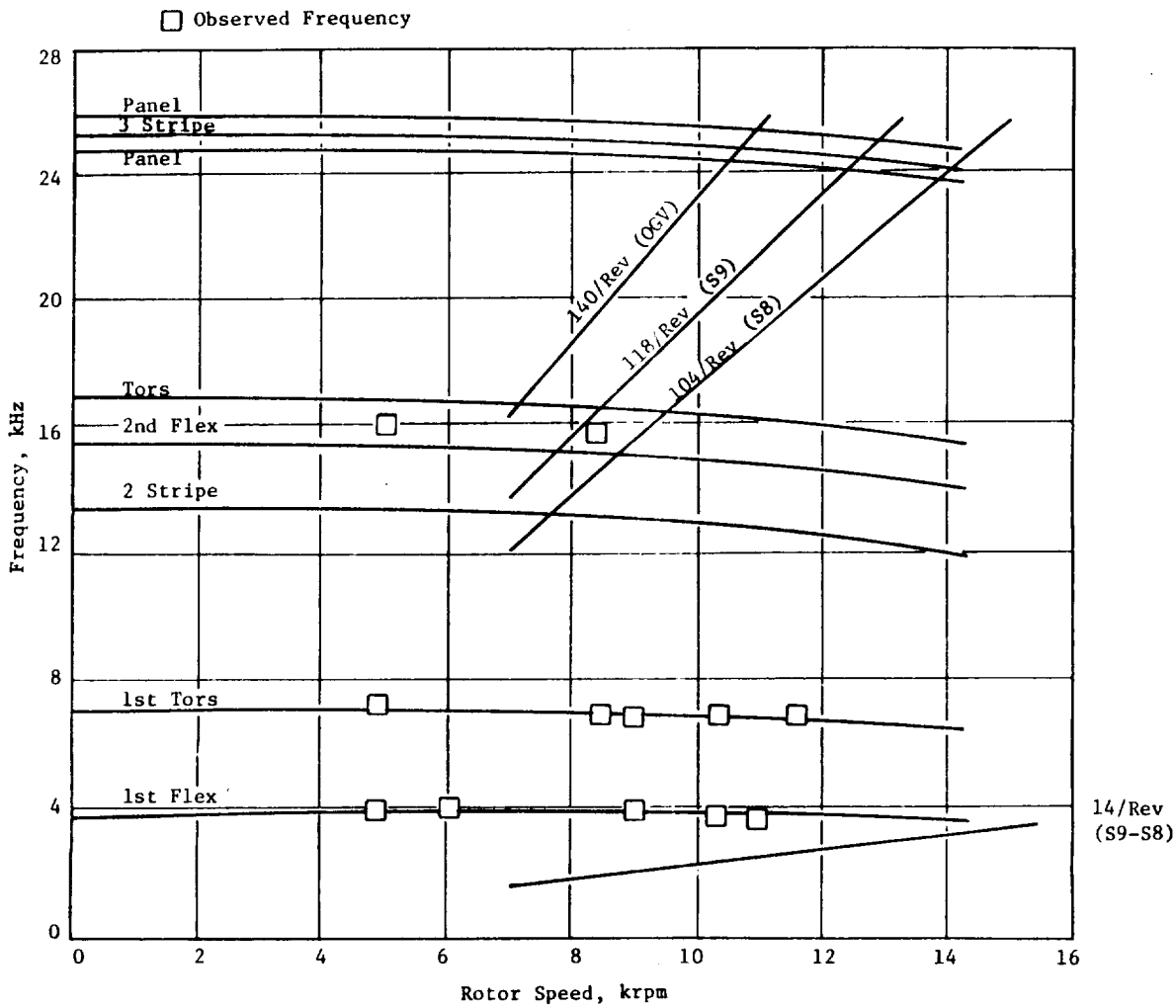

Figure 62. Ten-Stage Compressor Rotor Stage 10 Blade Campbell Diagram.

The values shown for Stages 5, 6, 7, and 8 are a result of the maverick per rev excitation and are not representative of normal operation. Stress levels on Rotors 5 and 6 did not exceed 18% of limits during the six-stage test. Similar levels were expected during normal operation of the 10-stage compressor.

The blade peak stall responses, as a percent of limits, are shown below:

Stage	Limits, %
1	30
2	100
3	250
4	175
5	168
6	118
7	70
8	30
9	30
10	30

With the exception of Rotor 3, the stall stresses are reasonable relative to previous engine experiences. Rotor 3 airfoil was redesigned to alleviate the high stress condition.

6.2.3 Stator Mechanical Results

Postest teardown inspections of the stator hardware disclosed vane airfoil damage as a result of ingesting the aforementioned Rotor 1 blade tips. The damage and available spares are listed below:

Stage	No. of Vanes/ Sector	No. of Damaged Vanes/Sector	No. of Spares
IGV	32	1	3
1	50	2	3
2	68	1	5
3	82	4	10
4	92	3	5
5	110	11	10
6	120	9	16
7	112/10	3/2	2
8	104/10	10/6	4
9	118/10	2/2	3

In most cases, the damage was minimal. For Build 2 testing, the damaged variable vanes were hand benched or replaced with spares, as required. Damaged cast vanes were also hand-benched. All other stator hardware was in good condition and required no rework prior to the Build 2 test. All rotor tip lands exhibited evidence of mild rubs, with the deepest rubs (approximately 10 mils maximum) occurring in the lower half. It was impossible to evaluate the extent of interstage seal rubs because of previous six-stage running on the front stages and assembly rub-in on the aft stages. The discourager seal exhibited a rub pattern on the lower half only. The unvarnished wooden inlet panels did not display the charring experienced by the varnished panels during the six-stage test.

After much scrutinization of the hardware, the source of the unusual 1/rev observed on Rotors 5 and 6 during the test was traced to a Stage 6 vane with a bent hub trailing edge, shown in Figure 63. The trailing edge was bent closed 40° to 60° over approximately 30% of the span. The damage appeared to be caused by improper handling prior to installation in the vehicle and unrelated to the FOD.

A portion of the test was devoted to investigating the affect of the casing active clearance control (ACC) on rotor/stator tip clearances. Data were taken at a vehicle operating point of 97.5% Nc with T25 = 215 K (72° F) and P25 = 24.13 kPa (3.5 psia). With rotor cooling air set at its maximum flow of 0.385 kg/s (0.85 lbm/s), rotor tip clearances were measured at Stages 3, 5, and 10, with ACC flows of 0, 0.037 kg/s (0.0819 lbm/s), 0.072 kg/s (0.1578 lbm/s), and 0.107 kg/s (0.2363 lbm/s). Measurements were also taken with rotor cooling flow set at 50% and with ACC flows of 0 and 0.087 kg/s (0.1916 lbm/s). The maximum clearance closure attained with the ACC was 0.2032 mm (8 mils) at Rotor 10, which was somewhat lower than expected. However, measured temperatures at growth-controlling rings on the casing were lower than predicted by the heat transfer model. The model was updated with thermocouple data recorded during the test and the revised results were input into the casing deflection prior to Build 2.

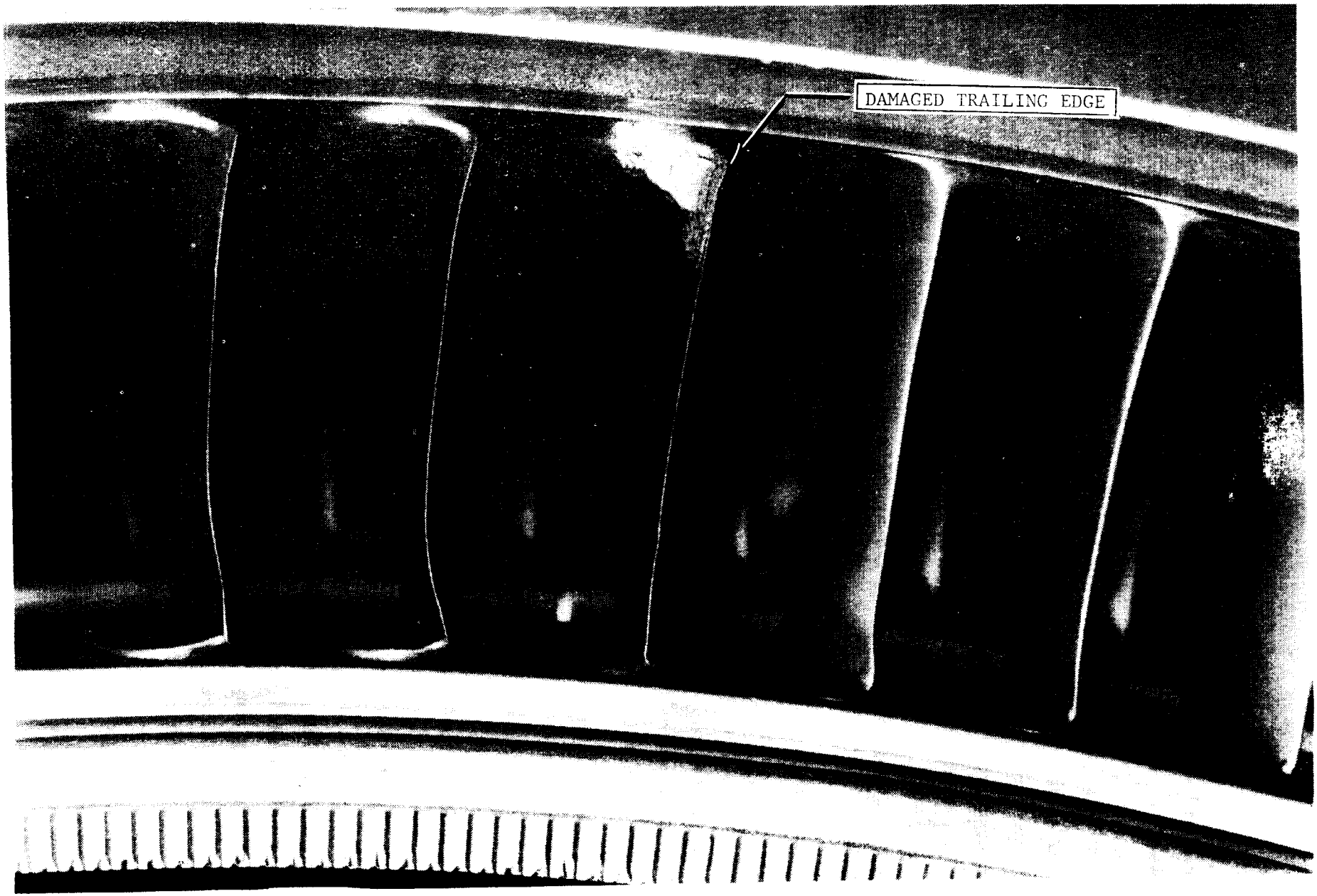

Figure 63. Stage 6 Stator Vanes, 10-Stage Compressor.

ORIGINAL PAGE IS
OF POOR QUALITY

6.2.4 Stator Aeromechanical Results

Stator vane stress responses during normal vehicle operation remained low over the entire speed range to 11,600 rpm as evidenced below:

Stage	Limits, %
IGV	3
1	7
2	11
3	4
4	24
5	30
6	30
7	30
8	40
9	56
10	1st Flex (1F) and 1st Tortion (1T)

Modal frequencies correlated closely with those predicted by bench testing, as can be seen on the accompanying Campbell diagrams, Figures 64 through 74. Predominantly, the modes observed were the fundamental flexural and torsional modes excited by the neighboring rotor passing frequencies. Stall stress responses were below 40% limits for all stator stages.

6.3 TEN-STAGE COMPRESSOR TEST, SECOND BUILD

The two mechanical objectives of the second build of the 10-stage (10B) compressor test were to assure safe operation during the testing and to obtain test data to verify predicted operational characteristics. Assurance of safe operation was accomplished by monitoring selected strain gages and thermocouples and by periodic visual inspection of critical hardware. This visual inspection, specifically borescope inspections, will be discussed later in more detail. Inspections of flowpath hardware made after partial teardown of the vehicle are reported herein.

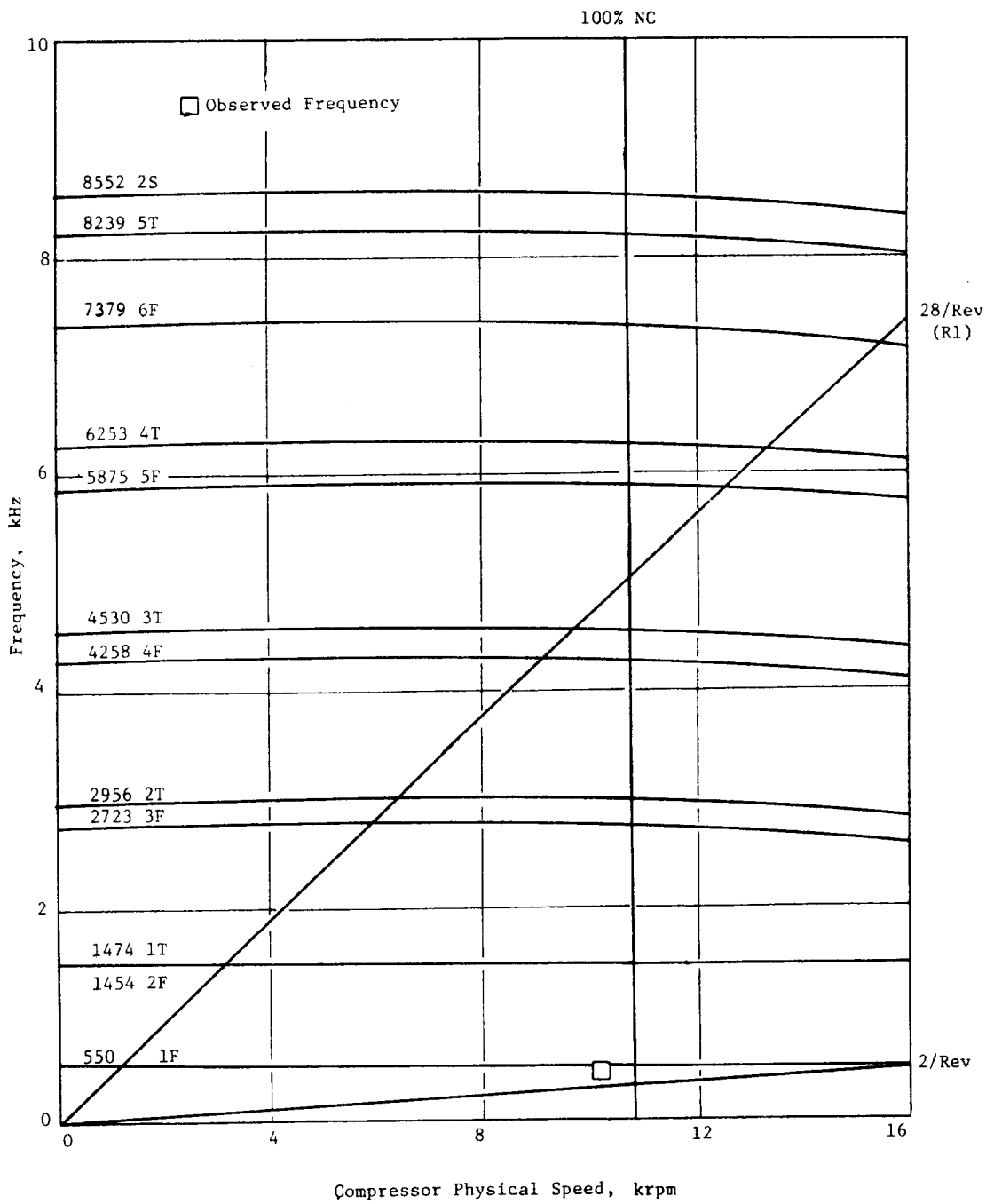

Figure 64. Ten-Stage Compressor IGV Campbell Diagram.

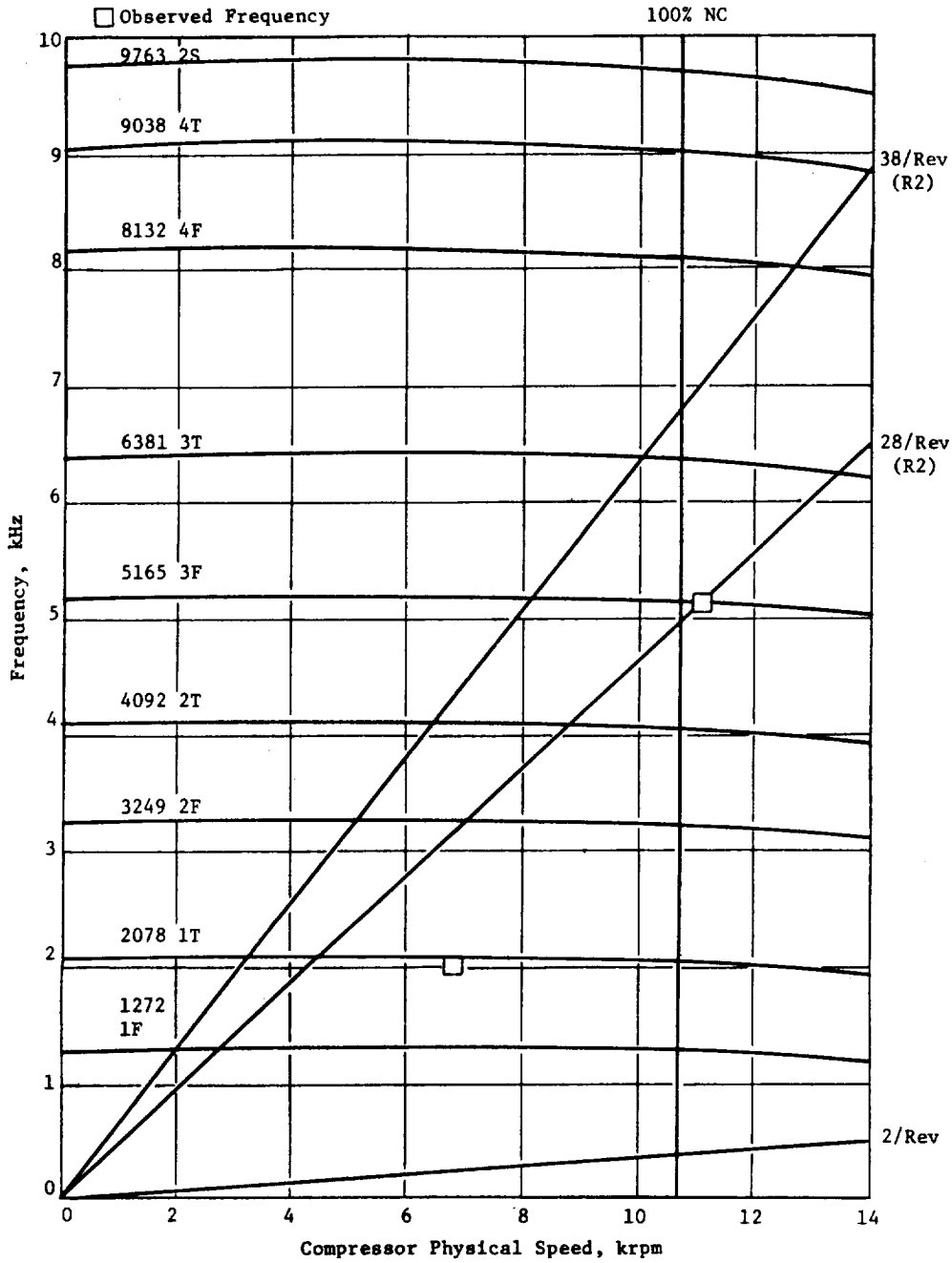

Figure 65. Ten-Stage Compressor Stator 1 Campbell Diagram.

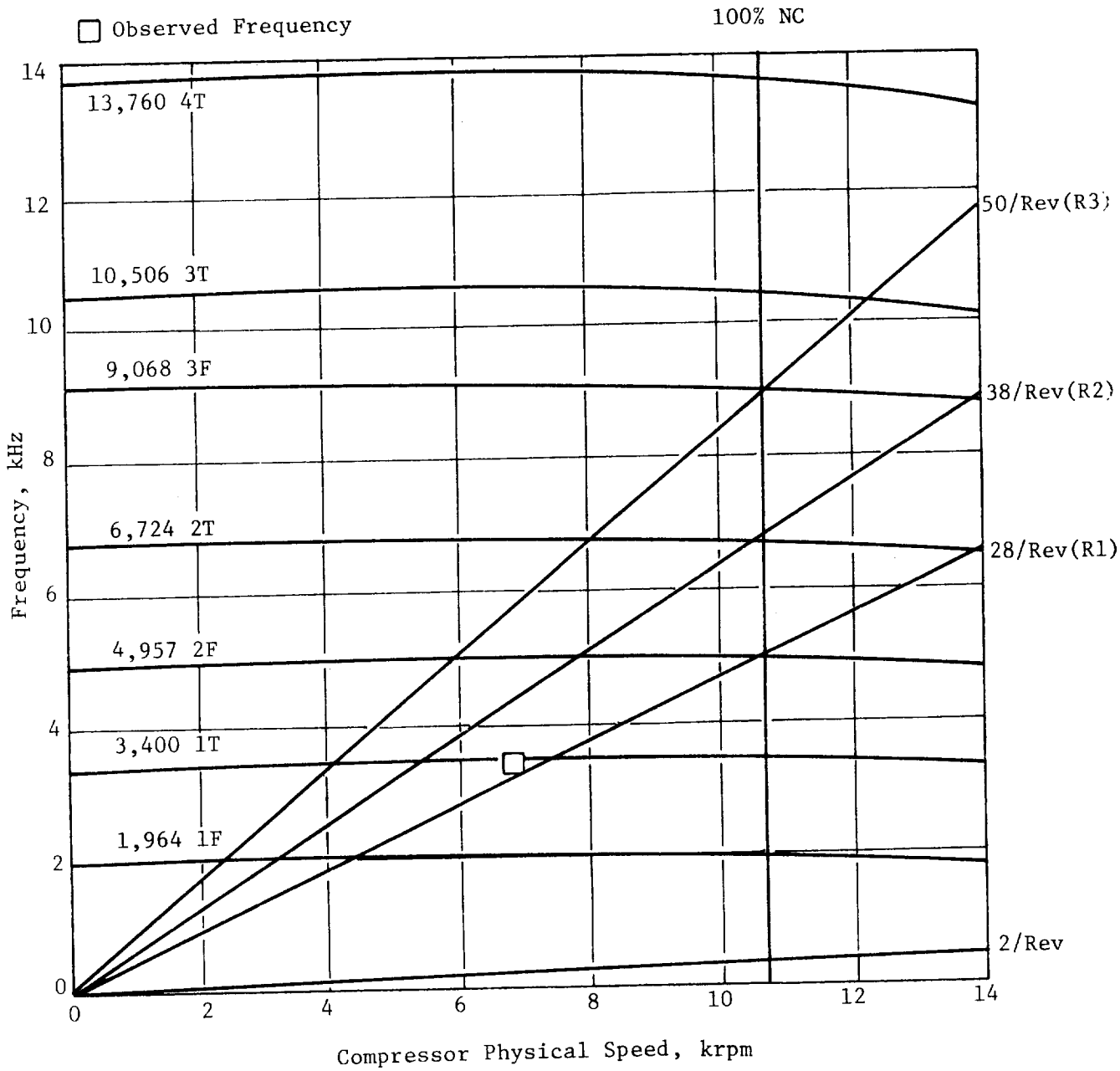

Figure 66. Ten-Stage Compressor Stator 2 Campbell Diagram.

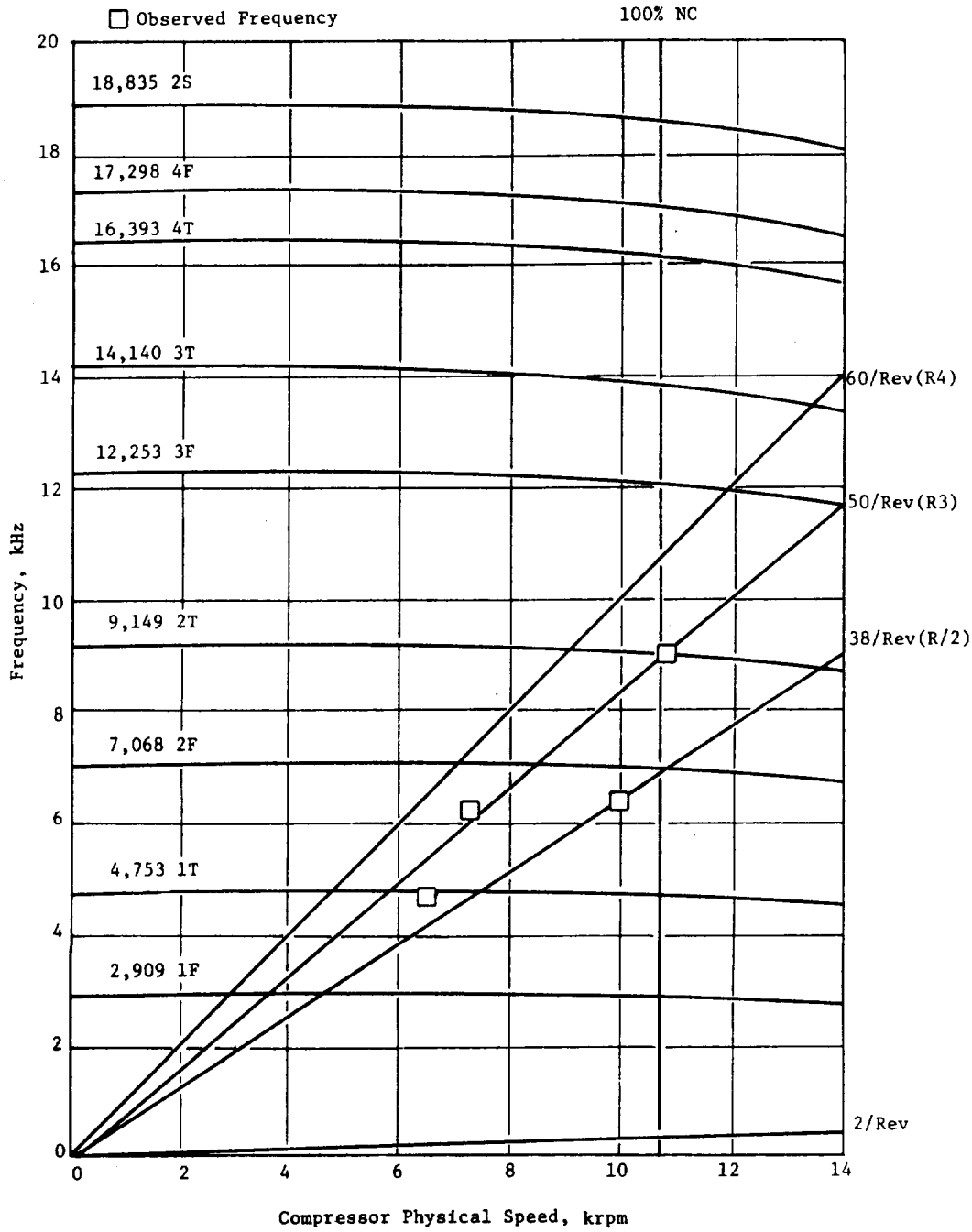

Figure 67. Ten-Stage Compressor Stator 3 Campbell Diagram.

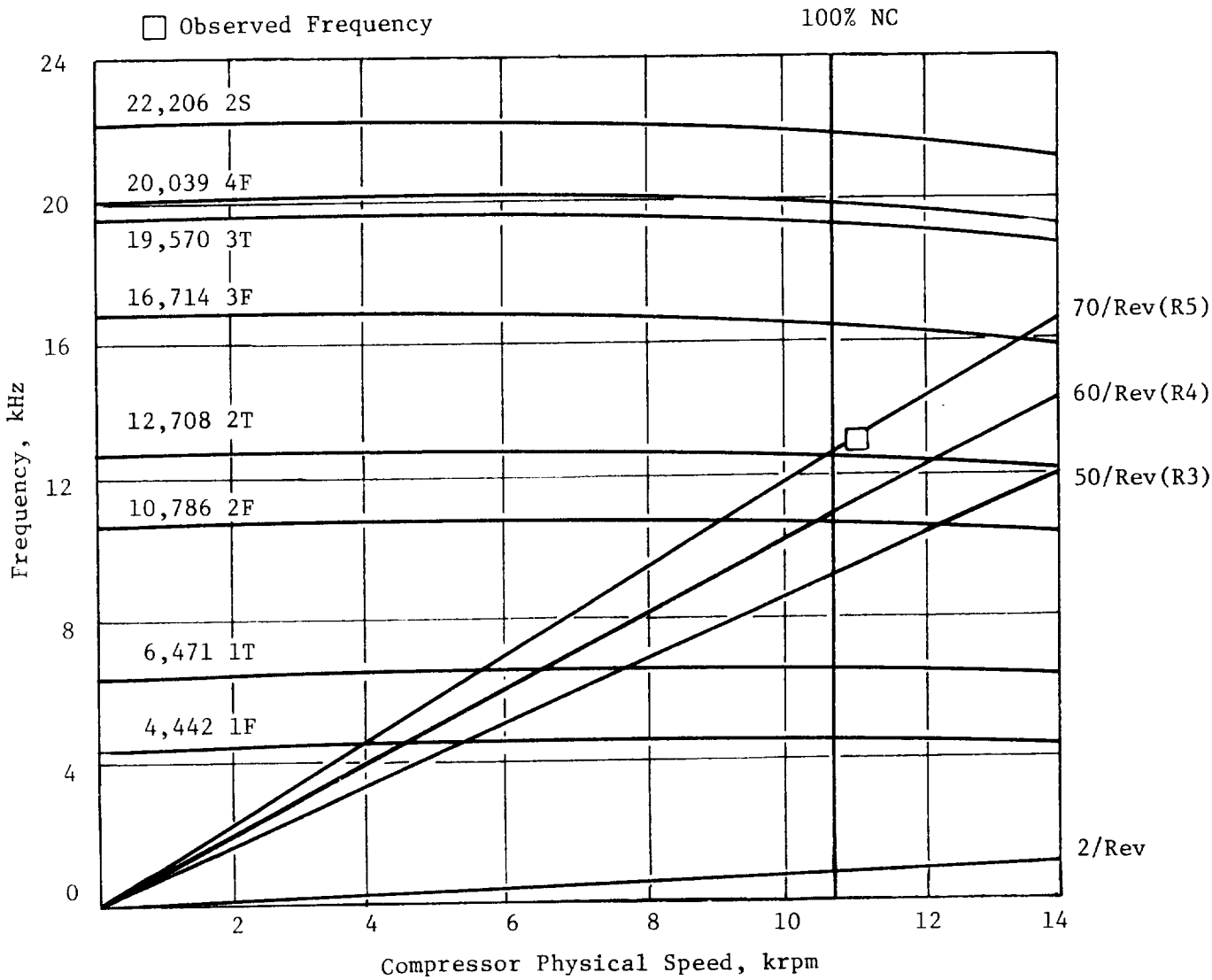

Figure 68. Ten-Stage Compressor Stator 4 Campbell Diagram.

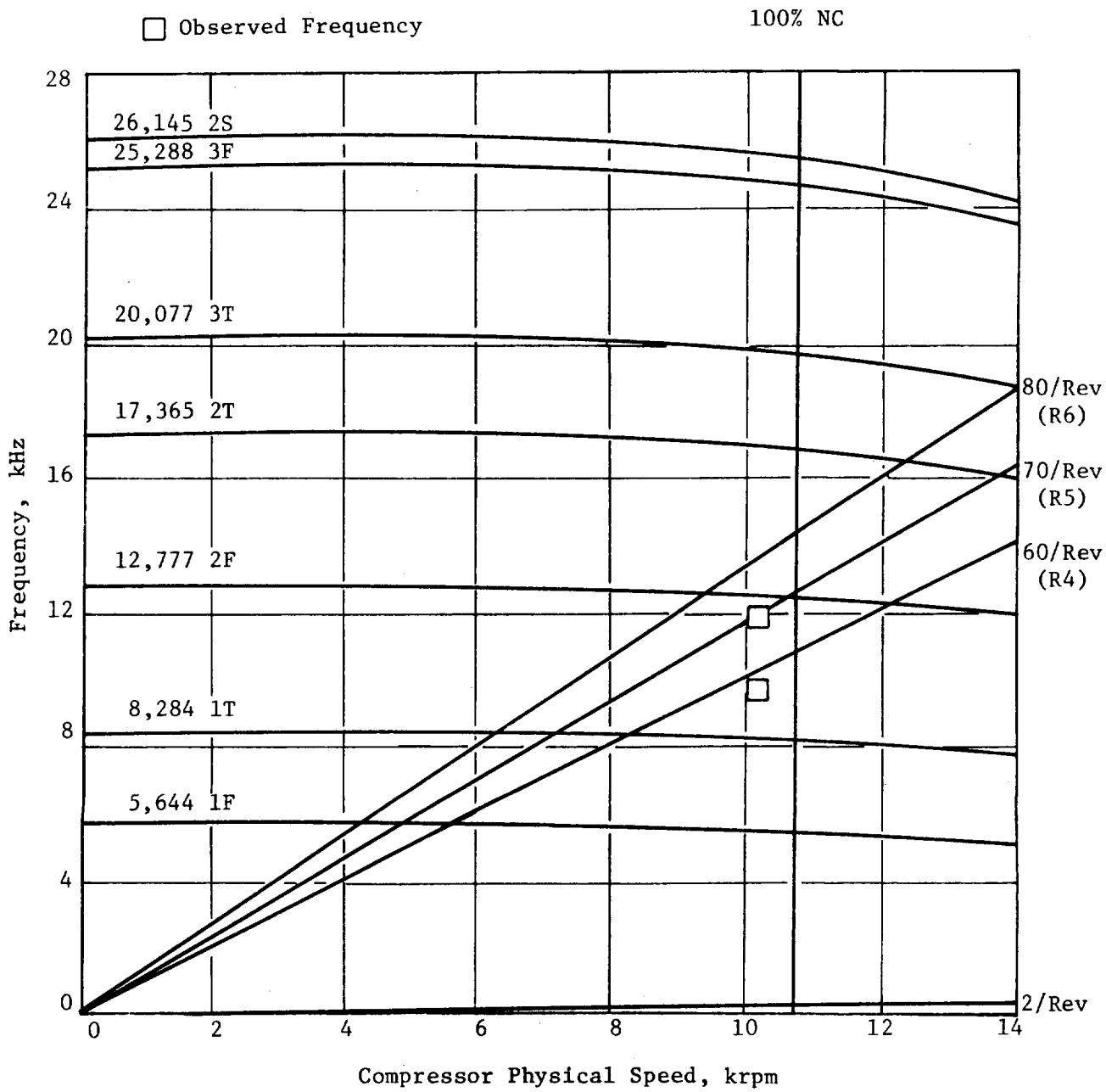

Figure 69. Ten-Stage Compressor Stator 5 Campbell Diagram.

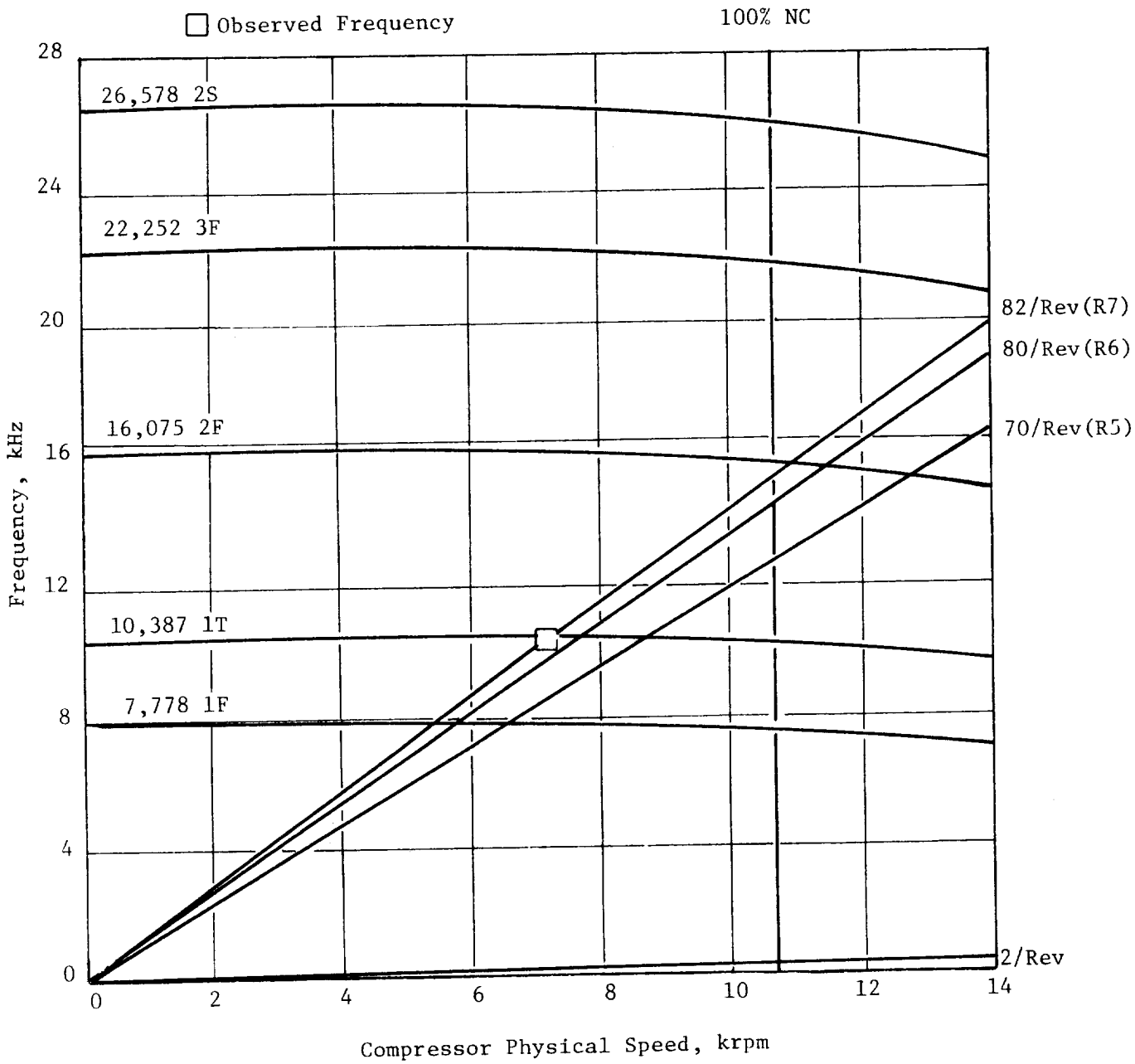

Figure 70. Ten-Stage Compressor Stator 6 Campbell Diagram.

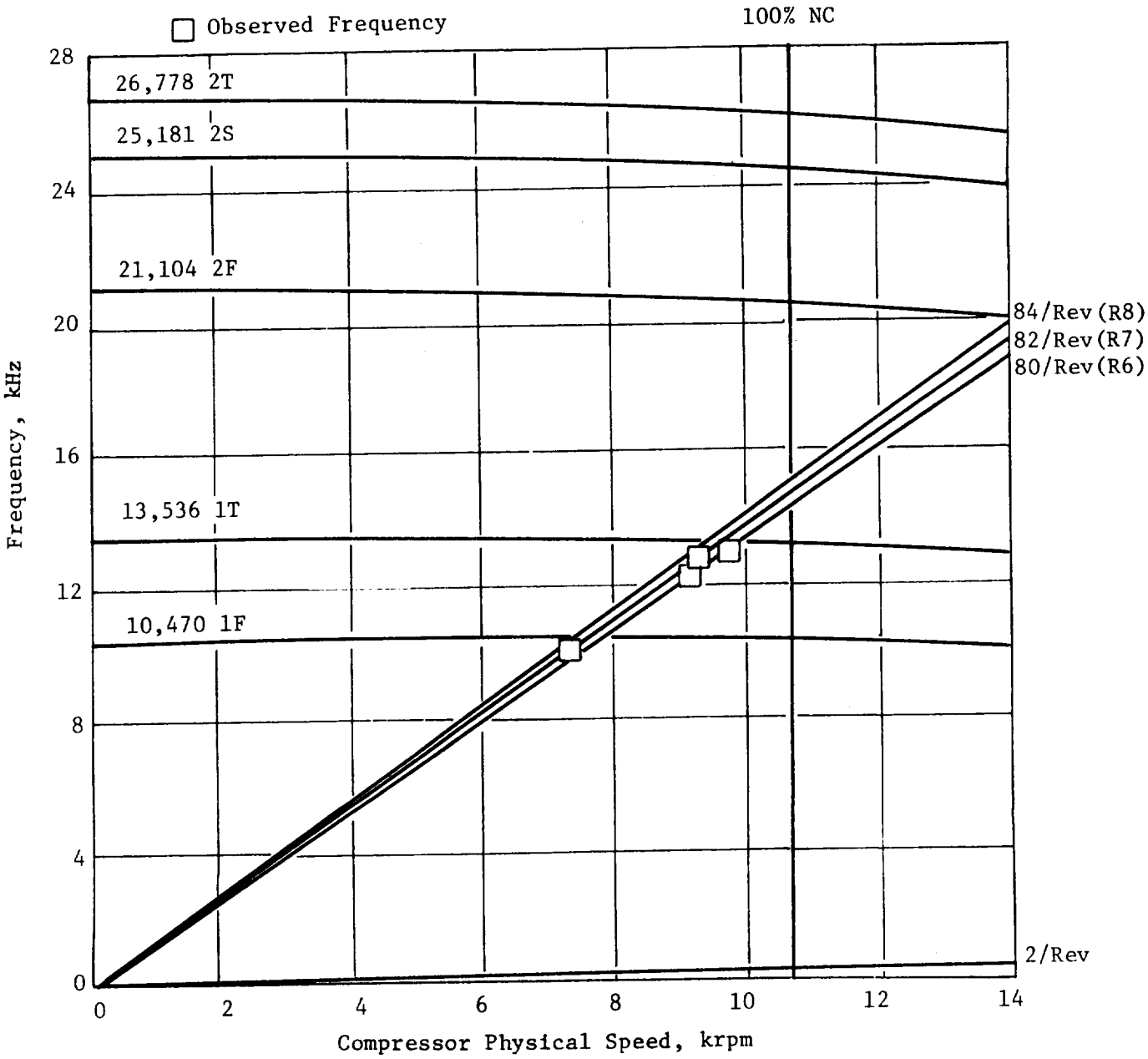

Figure 71. Ten-Stage Compressor Stator 7 Campbell Diagram.

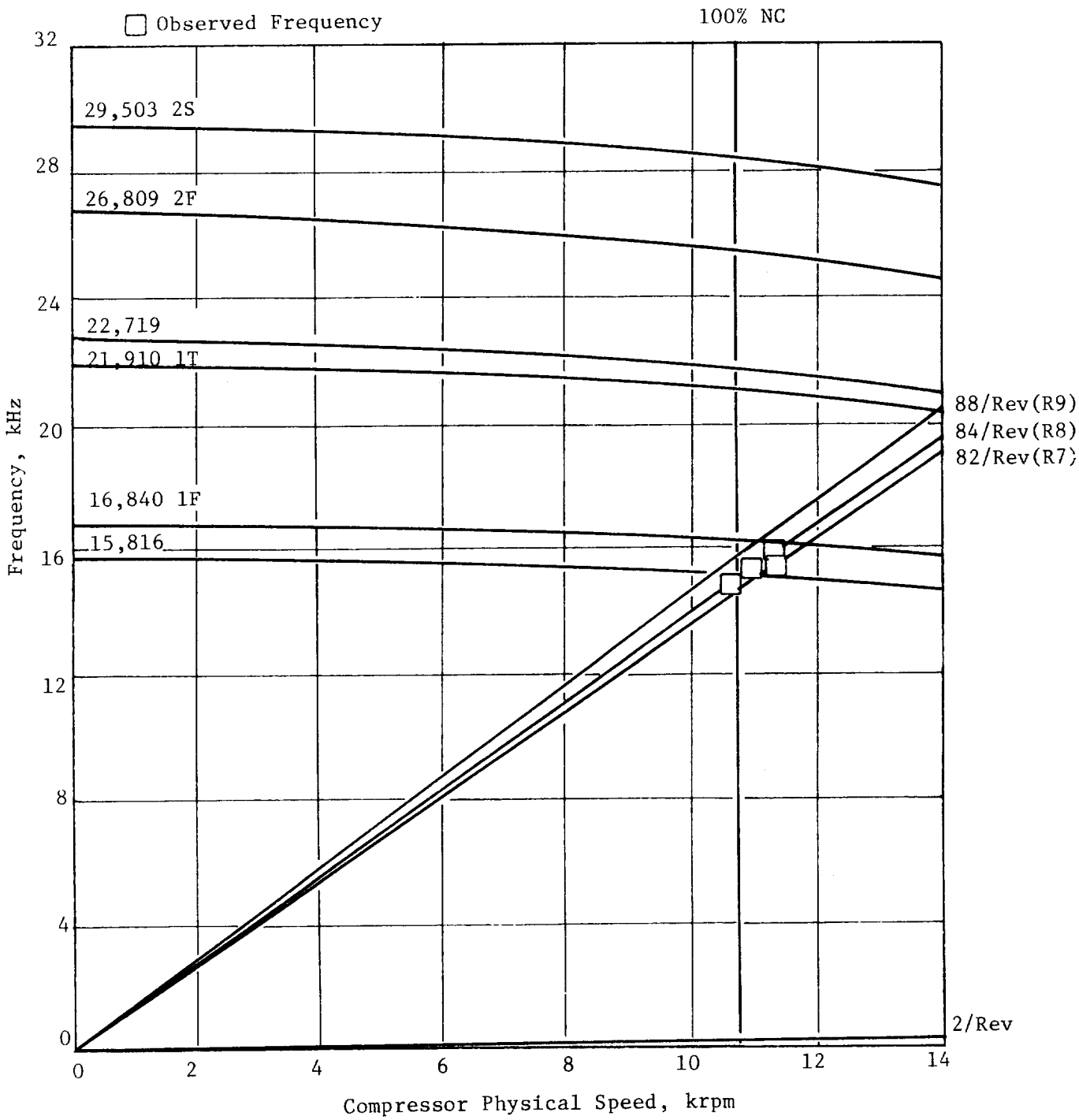

Figure 72. Ten-Stage Compressor Stator 8 Campbell Diagram.

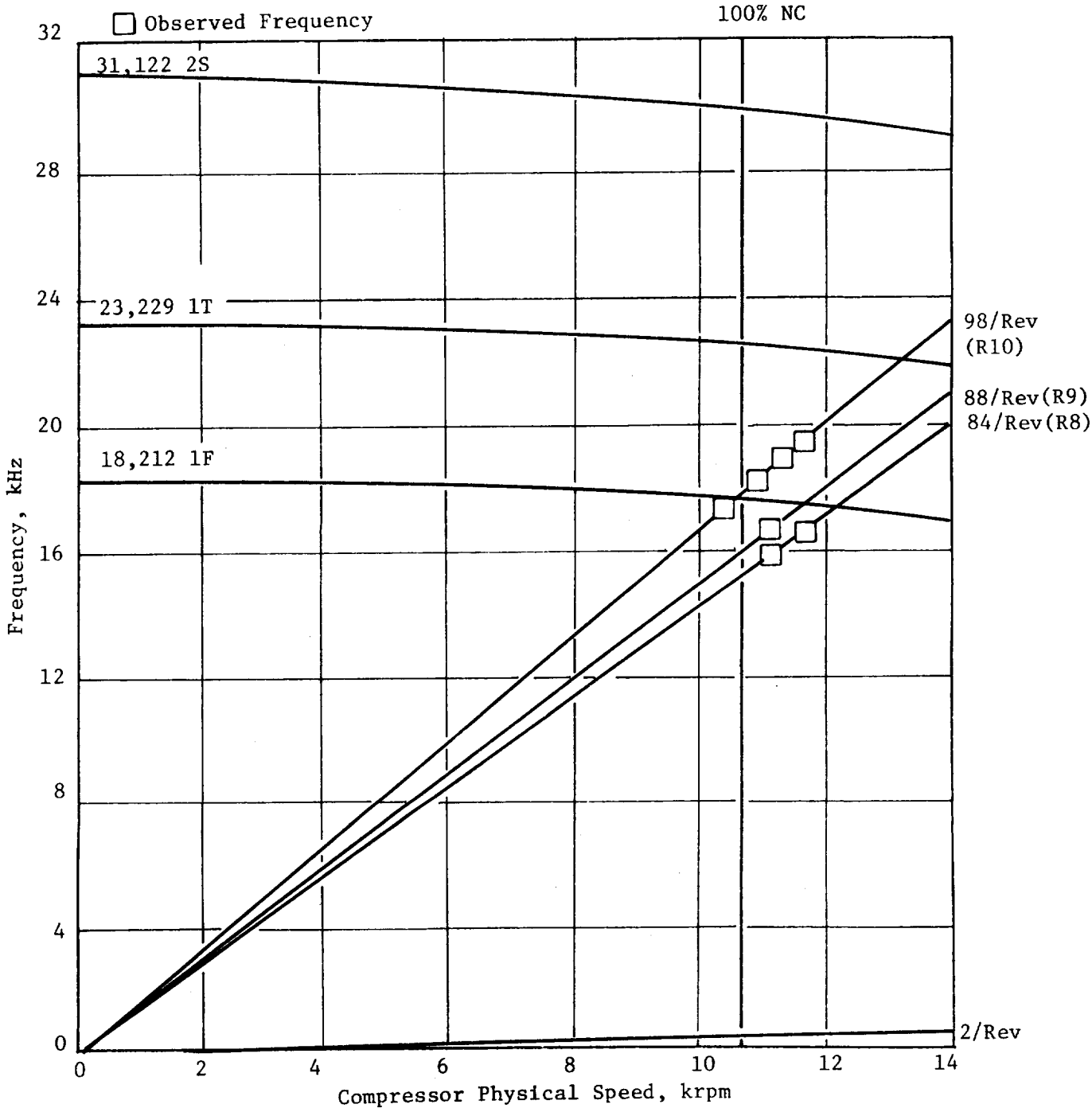

Figure 73. Ten-Stage Compressor Stator 9 Campbell Diagram.

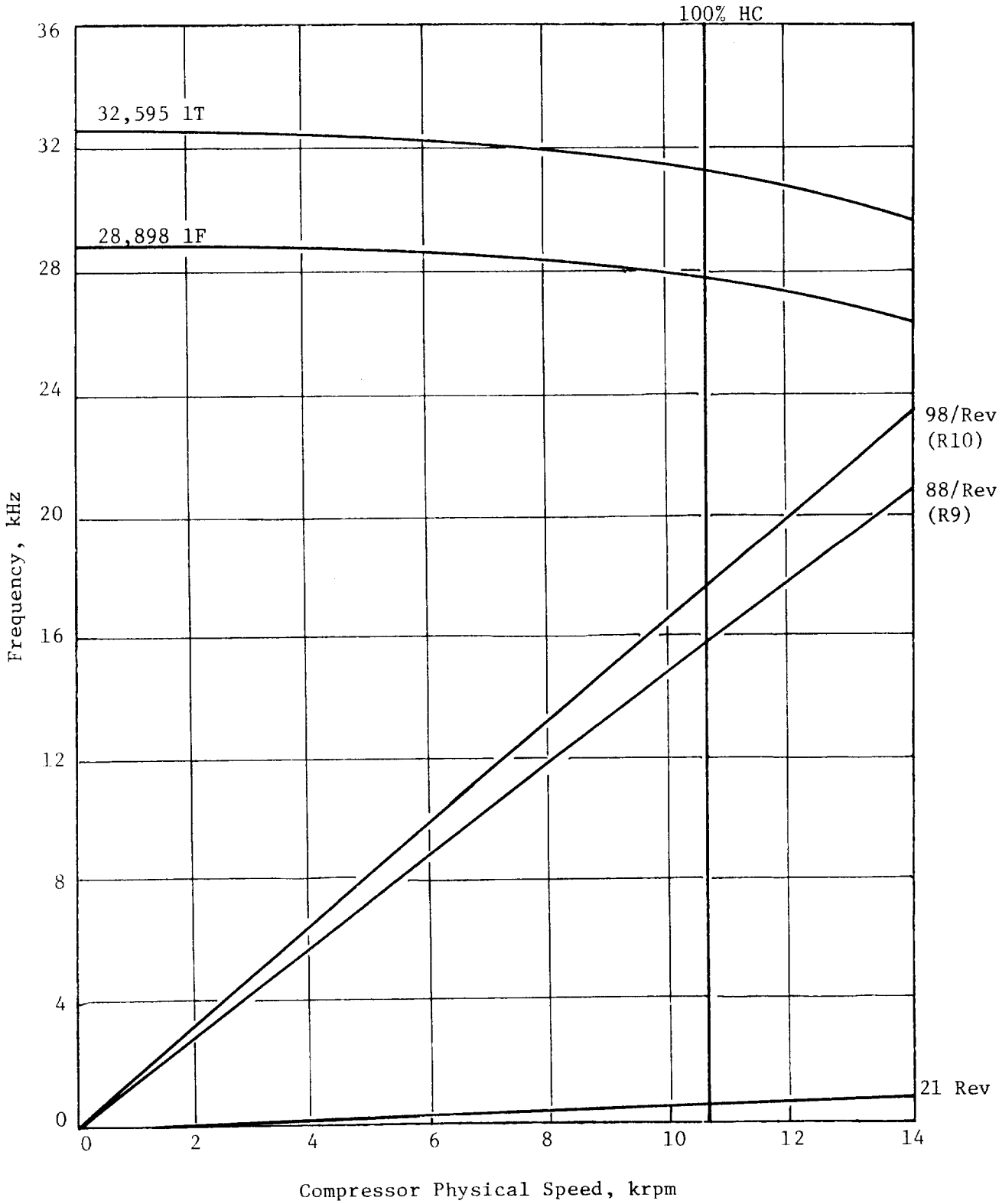

Figure 74. Ten-Stage Compressor OGV Campbell Diagram.

6.3.1 Rotor Mechanical Results

The compressor rotor consisted of the same spools and Stage 1 and 2 blades that were used in the first 10-stage compressor except for four damaged Stage 1 and three damaged Stage 2 blades that were replaced. The Stage 3 through 7 blades were new with redesigned airfoils that had added camber and lower stagger in the root. In addition, the Stage 3 blade was stiffened to raise the frequency of the first flexural mode above 4/rev to correct the high stall stress response observed during the previous two tests. The Stages 8, 9, and 10 blades were new, built to the original design which had less camber than those used in the first 10-stage compressor.

Rotor structure temperatures were measured with thermocouples located on disk bores and rims. As shown in Figure 75, the steady-state measured data compared well with that predicted.

The rotor was borescope inspected eight times during the test. The first inspection, after the December 18, 1981 test, revealed light tip rubs on the Stage 3 and 7 blades, but no material was missing, and no other distress was noted. Inspection after the January 12, 1982, test (compressor stalled when Stator 1 went off-schedule due to a facility fault) revealed severe tip damage on the Stage 3 and 4 blades, particularly at the trailing edge corner. The blade material had the appearance of being eroded or burned away, rather than being mechanically removed. Inspection after the March 4 test showed no further damage.

Teardown inspections were made with the forward and aft casing halves removed. One Stage 1 rotor blade experienced FOD which curled back about 1.27 cm (0.5 in.) of the leading edge tip. No other airfoil FOD was noted. The damage noted on Rotors 3 and 4 after the January 12 test was caused by titanium ignition. The trailing edge tips on both stages were burned away. Two leading edge squealer tips on Rotor 3 were also burned away; 70% of the squealer tips on Rotor 4 were burned away from 30% chord to the trailing edge. Stage 5 through 10 blades experienced light tip rubs.

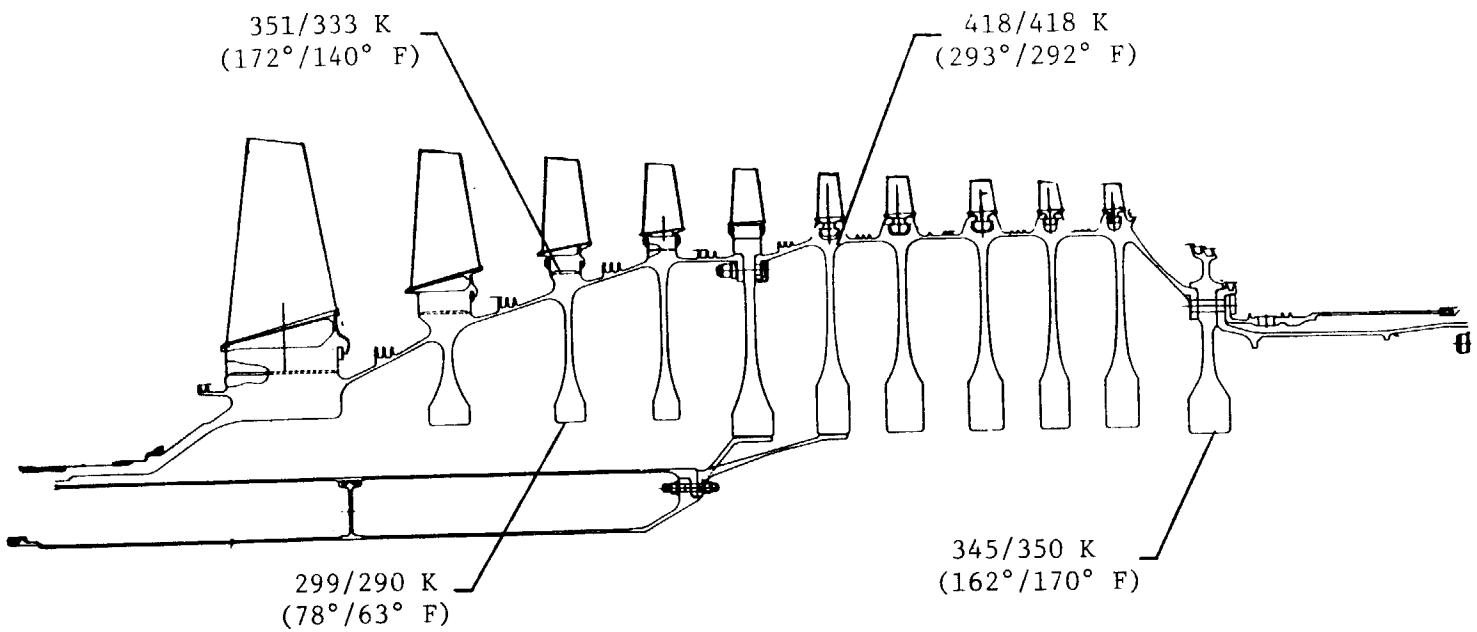

Measured Temperature/Predicted Temperature

	T25 K (° F)	P25 kPa (psia)	T3 K (° F)	N_{Phys}	$\%N_{Corr}$	$T_{Bore\ Cool}$ K (° F)	$W_{Bore\ Cool}$ kg/s (lbm/s)
Test Point Conditions Read. 98	211 (-80)	31.4 (4.56)	582 (588)	10,525	100	294 (69)	0.404 (0.89)
Prediction Point Conditions	220 (-63)	29.5 (4.28)	592 (606)	10,764	100	289 (60)	0.390 (0.86)

Figure 75. 10B Compressor Rotor Temperature Comparison.

6.3.2 Rotor Aeromechanical Results

The rotor blade dynamic strain signals were very good during the testing and a vast amount of data was obtained. Gage attrition was 50% which was an improvement over previous builds of this compressor when considering the test duration and number of stalls.

A strong per-rev disturbance, similar to that seen during the first 10-stage test, was again evident in this rig test. However, the source seemed to have moved aft, exciting Stages 6 through 10 instead of Stages 5 through 8 as in the previous build. The extent of this disturbance is noted in the FFT-produced Campbell diagrams for Stages 6 and 7; Figures 76 and 77. This event occurred during the accel to 11,350 rpm on January 12, 1982. The source of this disturbance was investigated in a diagnostic run and was determined to be located in a region near bottom vertical. Extensive in-cell inspections of the vehicle failed to reveal a source. A detailed Fourier analysis of the vane-mounted instrumentation groups was inconclusive in predicting this as a potential source (found to be the cause of a similar disturbance on another GE engine test). During vehicle teardown, it appeared that a Stage 6 vane could have been free to rotate during the test. This vane was located 7.5° from bottom vertical and was concluded to be the source of the disturbance. This will be discussed in greater detail in Section 6.3.3.

Airfoil frequencies and vibration stress levels were recorded during these tests. Frequencies observed are noted in Campbell diagrams (Figures 78 through 85) and compare favorably with the predicted frequencies. Campbell diagrams are not presented for Stage 1 and 2 blades as they are the same as the first test.

Maximum vibratory stresses observed during normal vehicle operation are listed below as a percentage of limits:

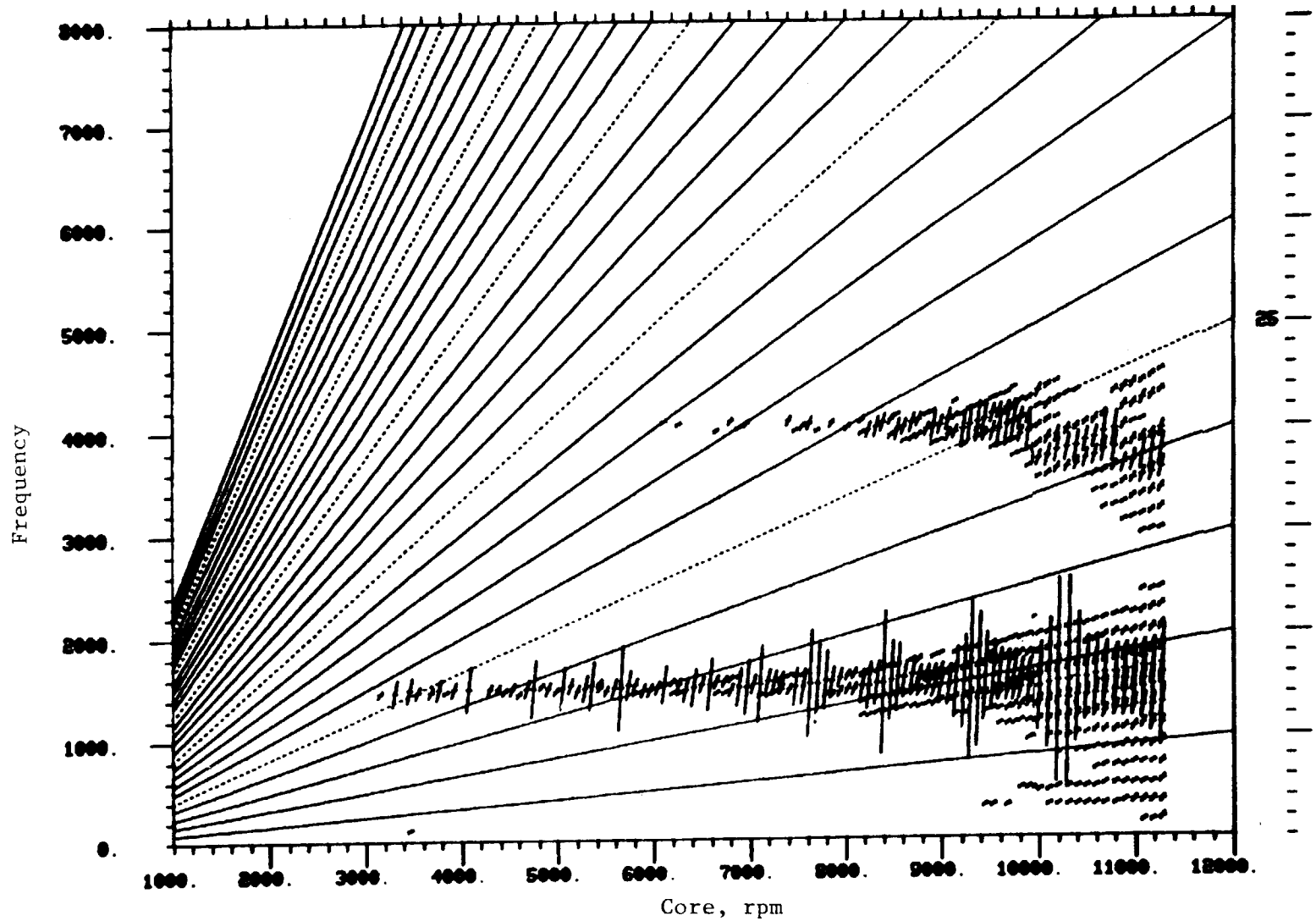

Figure 76. Compressor 10B, Stage 6 Campbell Diagram.

ORIGINAL PAGE IS
OF POOR QUALITY

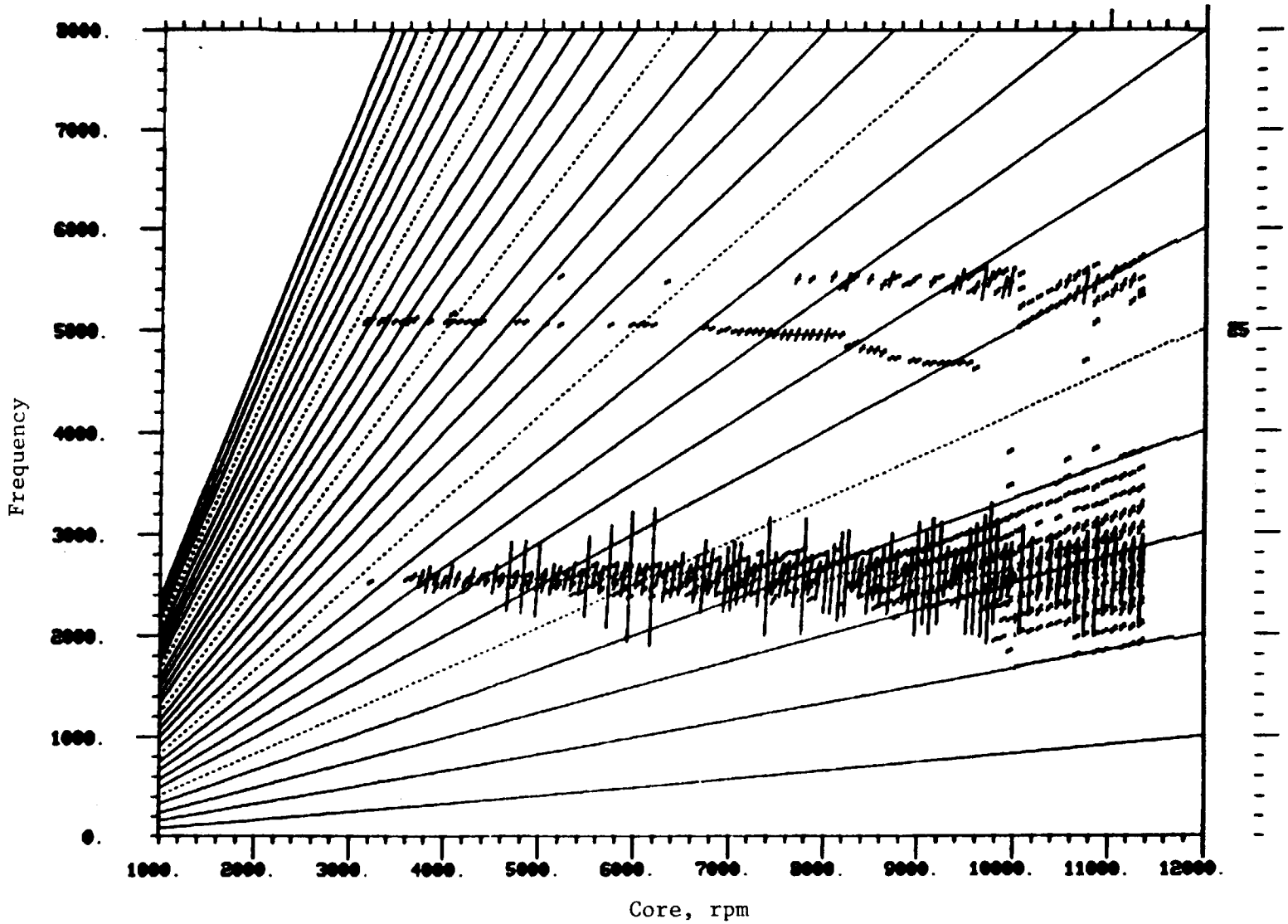

Figure 77. Compressor 10B, Stage 7 Campbell Diagram.

ORIGINAL PAGE IS
OF POOR QUALITY

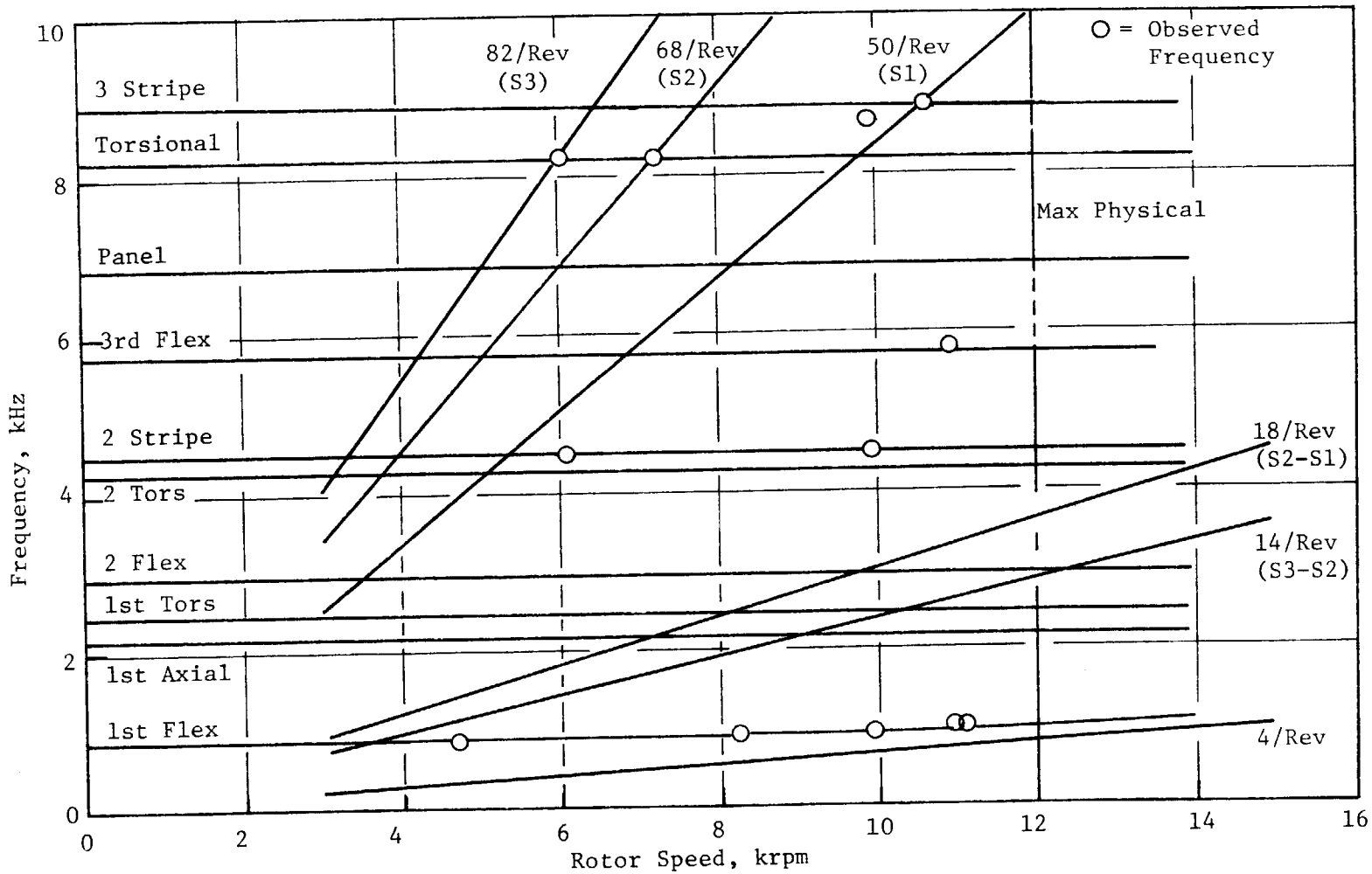

Figure 78. 10B Compressor Rotor Stage 3 Blade Campbell Diagram.

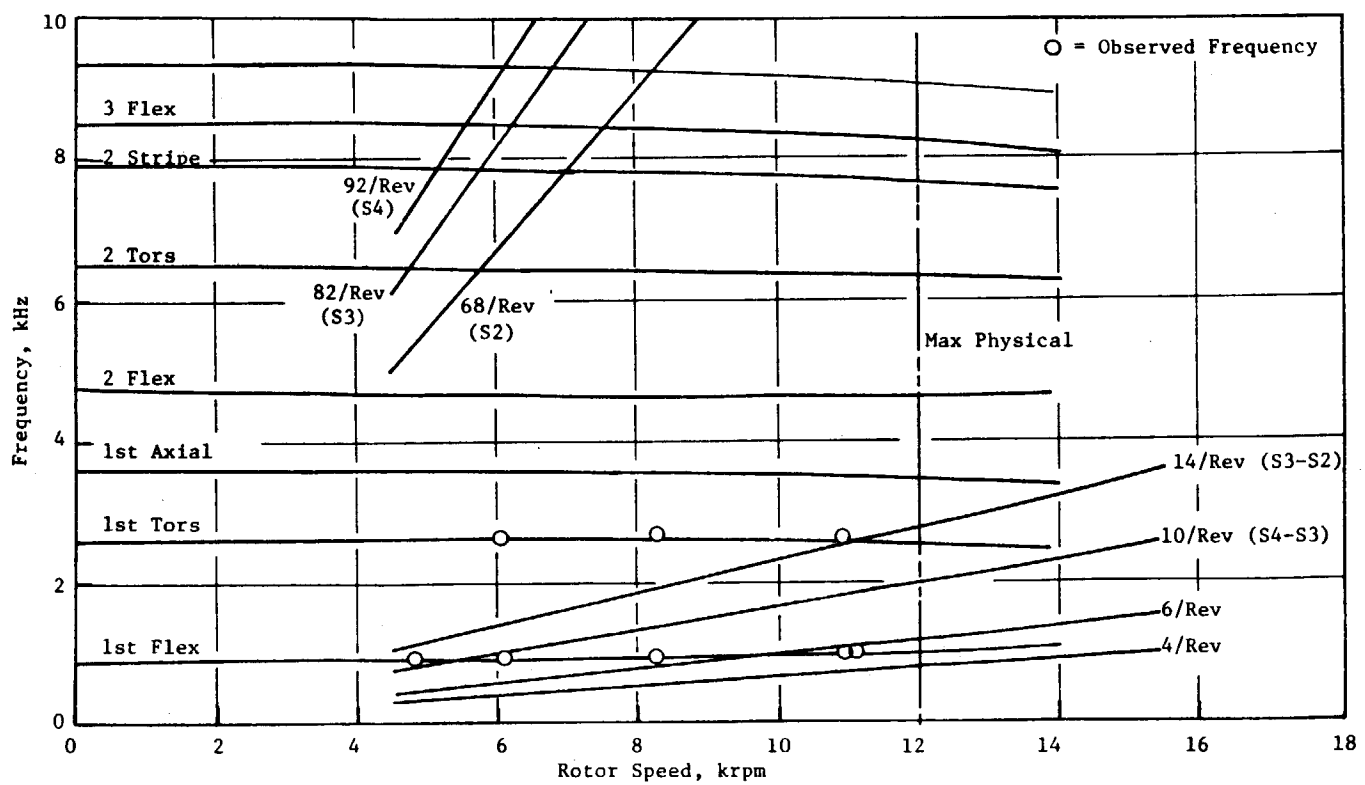

Figure 79. 10B Compressor Rotor Stage 4 Blade Campbell Diagram.

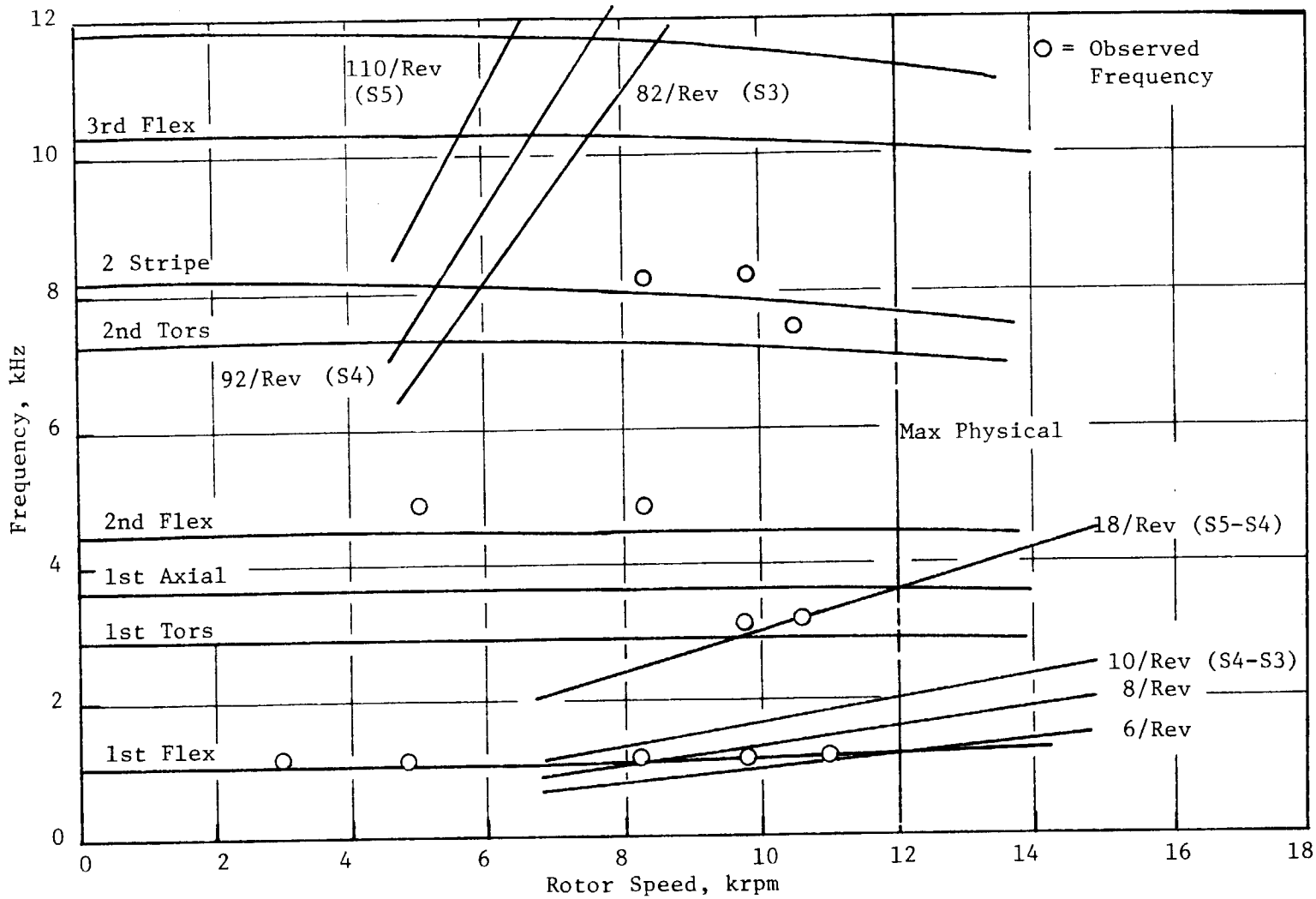

Figure 80. 10B Compressor Rotor Stage 5 Blade Campbell Diagram.

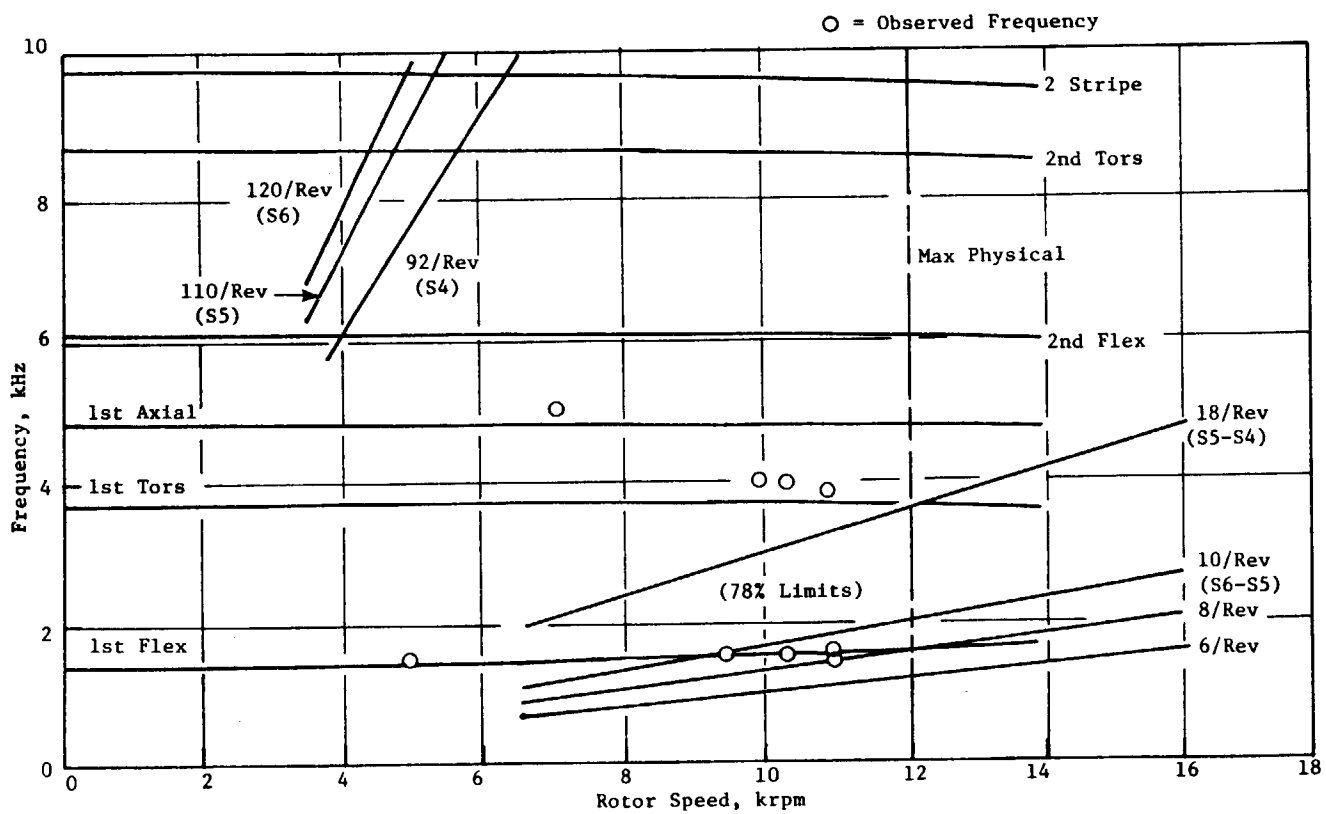

Figure 81. 10B Compressor Rotor Stage 6 Blade Campbell Diagram.

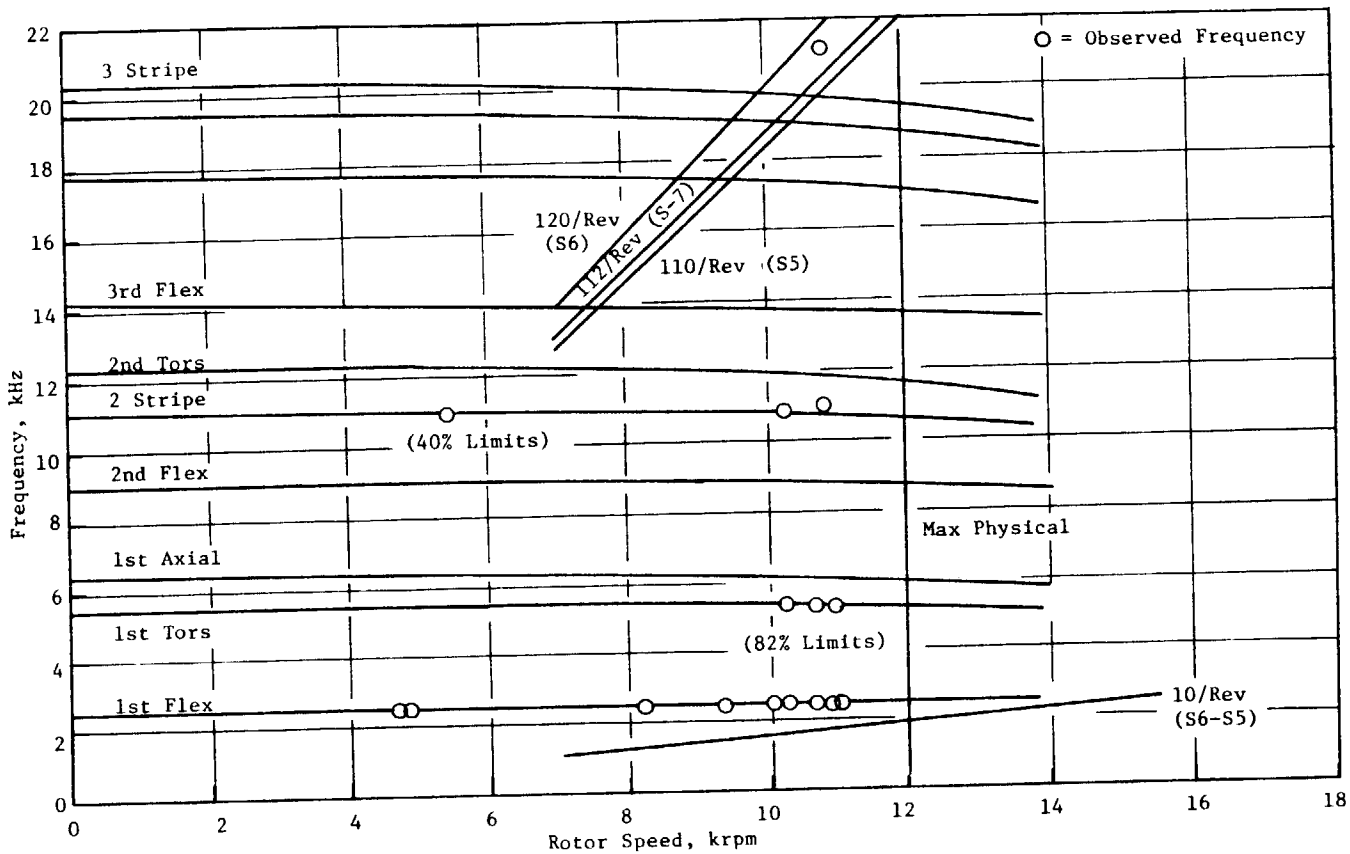

Figure 82. 10B Compressor Rotor Stage 7 Blade Campbell Diagram.

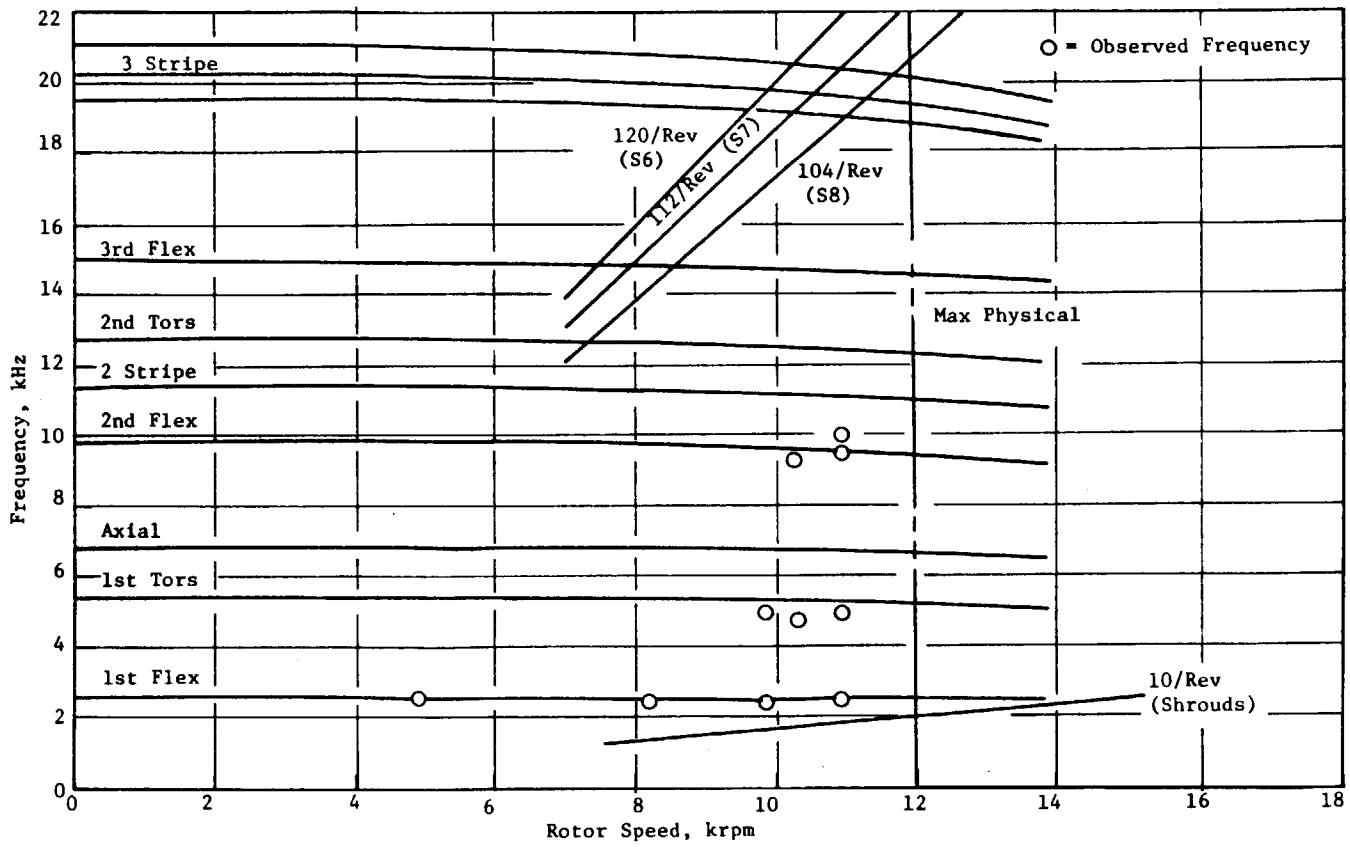

Figure 83. 10B Compressor Rotor Stage 8 Blade Campbell Diagram.

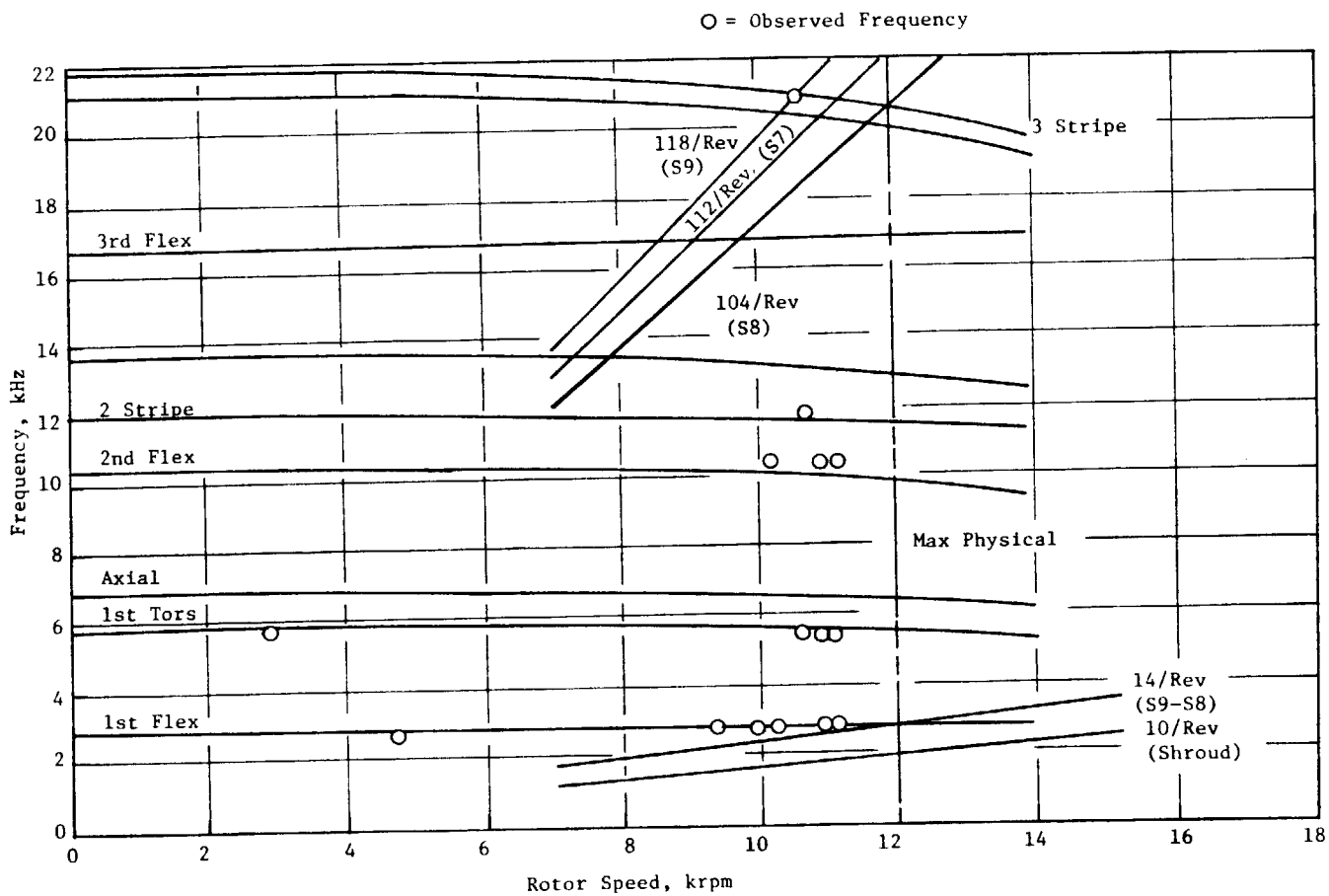

Figure 84. 10B Compressor Rotor Stage 9 Blade Campbell Diagram.

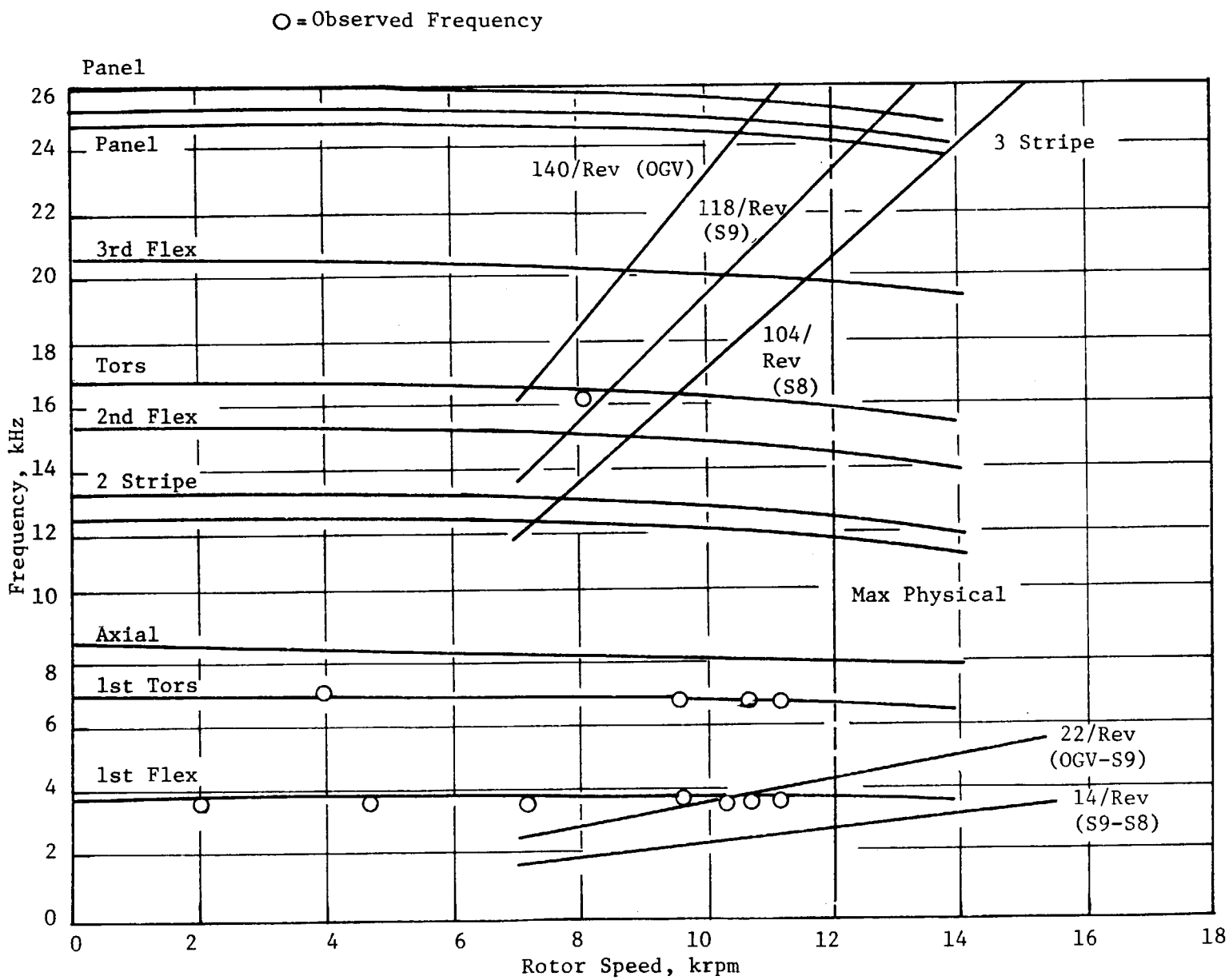

Figure 85. 10B Compressor Rotor Stage 10 Blade Campbell Diagram.

Stage	Limits, %
1	17
2	14
3	27
4	15
5	12
6	78
7	83
8	50
9	38
10	37

The levels shown for Stages 6 through 10 are a result of the abnormal per rev disturbance and are not considered representative of normal operating stress levels.

The maximum blade stall stresses, as a percent of limits, are shown below. The predominate frequency during stall was first flex unless noted.

Stage	Limits, %
1	30
2	233
3	112
4	166
5	121
6	127
7	89
8	64
9	200 (Torsional)
10	36

The high stress level noted on Stage 2 occurred during the unexpected stall of January 12, 1982, when a control malfunction caused Stage 1 stator to actuate to full open. This level was not representative of a normal stall. The strain gages on this stage became inoperative after this event and no other data are available. The improvement in the stall tolerance on the modified Stage 3 blade was significant. The high stall stress noted on Stage 9 may be the result of a faulty strain gage. Another instrumented Stage 9 blade with a strain gage in the same location responded at 1/3 the stress level during the same stall.

6.3.3 Stator Mechanical Results

Compressor stator hardware from the 10A compressor was utilized in the 10B compressor with the exception of a minimum number of variable vanes that were replaced due to nonreworkable FOD. As discussed previously, the airfoils of Stage 2 through 5 vanes were reworked back to the original six-stage design.

The 10B rotors experienced a per rev excitation similar to that observed during the 10A test. A potential source of that disturbance surfaced during vehicle teardown when it appeared that a Stator 6 spline adapter, which connect each individual vane to mating lever arm shafts, had been omitted during vehicle assembly, leaving that vane free to rotate during test. This vane was located within the calculated region of the per-rev disturbance. Subsequent examination of the flow patterns on the casing at Stator 6 discharge indicated that this vane had been 30° to 40° open during the test. Great care had been taken during assembly to prevent such an occurrence. Additional steps are being taken to prevent such an omission on later builds.

With the exception of the missing Stator 6 spline adapter, no other stator distress or damage was noted during teardown inspections.

A portion of the test was devoted to investigating the effect of the casing active clearance control on rotor/stator tip clearances. Data were taken at a vehicle speed of 100% N_c with T25 = 211 K (-80° F) and P25 = 31.7 kPa (4.6 psia). With rotor cooling air set at its maximum flow 0.404 kg/s (0.89 lbm/s), Rotor 3, 5 and 10 tip clearances were measured with ACC flows of 0, 0.6% WC, and 1.32% WC. The maximum clearance closure attained with the ACC was 0.076 mm (3 mils) as measured by the touchprobe and 0.152 mm (6 mils) as measured by the clearanceometer over rotor 10 in comparison to a predicted closure of 0.127 mm (5 mils).

Presented in Figure 86 are measured casing temperatures compared to those predicted by the updated thermal model. The close correlation between the measured and predicted temperatures verifies the accuracy of the analysis.

6.3.4 Stator Aeromechanical Results

Modal frequencies and scope limits remained unchanged from the 10A compressor even though Stators 2 through 5 were recambered. Frequency checks of

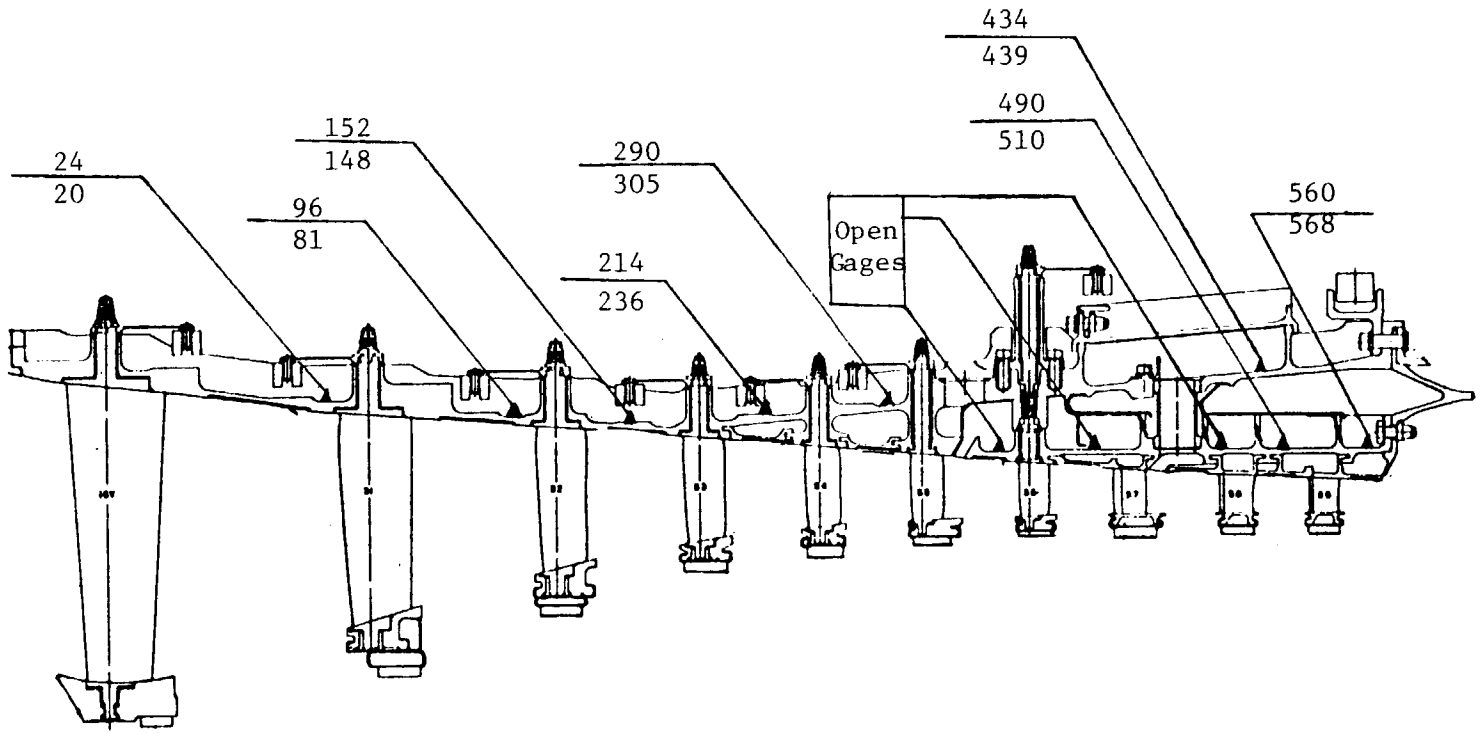

Measured Temperature/Predicted Temperature

	T25 K (° F)	P25 kPa (psia)	T3 K (° F)	$N_{Phys.}$	% $N_{Corr.}$	W kg/s (lbm/s) Bleed Air Cooling
Test Point Conditions RDG 298	220 (-64)	32.48 (4.71)	596 (613)	10,737	99.86	0.1134 (0.250)
Prediction Point Conditions	220 (-63)	29.50 (4.28)	600 (620)	10,764	100	0.134 (0.296)

Figure 86. 10B Compressor Casing Temperature Comparison.

the recambered vanes verified this. Campbell diagrams for the 10B vanes are the same as those presented for the 10A vanes (Section 6.2.4). Stator vane stresses remained relatively low during normal vehicle operation and compared closely with those recorded during the 10A test as evidenced by the following:

Stage	Limits, %	Limits (10A), %
IGV	3	3
1	7	7
2-6	Not Strain Gaged for 10B Test	
7	33	30
8	67	40
9	43	56
10	1F & 1T not excited	

Stator 8 and 9 stresses reached 140% and 200% limits, respectively, during testing on a low operating line with an off-design stator schedule. This occurred on January 12, 1982, just prior to the unintentional stall that was caused by Stator 1 opening up. Since stresses did not approach those levels during subsequent testing, it was theorized that Stator 1 had opened when those stresses were observed. Modal frequencies repeated those observed during the 10A test. They were predominately the fundamental flexural and torsional modes excited by the neighboring rotor passing frequencies.

Maximum recorded stall stresses are presented below and are compared with 10A results:

Stage	Limits, %	Limits (10A), %
IGV	2	> 40
1	40	> 40
2-6	Not Strain Gaged For 10B Test	> 40
7	22	> 40
8	120	> 40
9	143	> 40
10	1F & 1T not excited	

6.4 SUMMARY

With very few exceptions, the compressor hardware performed is predicted during the three rig tests. Observed airfoil vibratory frequencies verified

the pretest frequencies predicted by analysis and bench checks. Airfoil stresses were reasonably low throughout the tests, demonstrating the structural integrity of the hardware. Thermal and clearance measurements correlated closely with predicted values. The overall success of the compressor development program can be contributed, in part, to the quality and durability of the hardware.

APPENDIX

COMPRESSOR PERFORMANCE SUMMARY OF THE SECOND TEN-STAGE TEST

APPENDIX 1

PERFORMANCE DATA SUMMARY OF THE SECOND FULL 10-STAGE COMPRESSOR TEST (10B)

READING NUMBER	* * * * * * * * OVERALL * * * * * * * * CORRECTED SPEED	CORRECTED FLOW	PRESSURE RATIO	ADIABATIC EFFICIENCY	* * FRONT BLOCK * * PRESSURE RATIO	ADIABATIC EFFICIENCY	* * * * * * * REAR BLOCK * * * * * * * CORRECTED FLOW	PRESSURE RATIO	ADIABATIC EFFICIENCY	CORRECTED SPEED
229	102.52	128.14	24.284	0.704	10.182	0.798	18.337	2.385	0.852	99.01
230	102.45	128.36	25.131	0.786	10.433	0.803	17.960	2.409	0.848	98.72
231	102.46	127.91	26.648	0.783	10.904	0.804	17.228	2.444	0.839	98.07
415	84.84	55.13	8.317	0.794	3.856	0.789	17.788	2.157	0.869	95.76
416	84.90	52.89	9.870	0.775	4.275	0.775	15.672	2.309	0.850	93.89
419	80.10	43.96	6.447	0.764	3.122	0.750	17.050	2.065	0.854	92.84
420	80.11	41.78	7.616	0.745	3.476	0.735	14.831	2.191	0.837	90.84
421	60.07	20.08	3.061	0.671	1.841	0.579	12.322	1.663	0.894	74.25
431	99.84	121.92	22.591	0.814	9.696	0.838	17.933	2.330	0.846	98.44
432	99.91	122.26	23.201	0.814	9.855	0.836	17.748	2.354	0.851	98.18
433	99.74	120.89	25.878	0.799	10.848	0.820	16.231	2.385	0.845	96.10
434	99.01	117.61	21.588	0.823	9.285	0.850	17.885	2.325	0.844	98.62
435	98.96	117.30	22.158	0.822	9.395	0.846	17.675	2.359	0.849	98.29
436	98.95	117.05	23.454	0.817	9.798	0.840	17.043	2.394	0.850	97.47
437	98.93	115.23	24.533	0.803	10.260	0.828	16.192	2.391	0.837	96.40
440	97.50	109.25	19.783	0.826	8.526	0.848	17.877	2.320	0.856	98.32
441	97.43	108.83	20.273	0.824	8.635	0.847	17.617	2.348	0.851	98.05
442	97.25	105.76	21.939	0.803	9.232	0.826	16.255	2.376	0.843	96.24
443	94.93	95.26	16.830	0.823	7.292	0.847	17.795	2.308	0.848	98.06
444	94.96	94.67	17.258	0.821	7.377	0.837	17.555	2.339	0.864	97.64
445	94.91	92.47	18.715	0.801	7.903	0.820	16.229	2.368	0.847	96.07
446	40.15	9.97	1.770	0.632	1.361	0.509	7.779	1.300	0.926	52.63
447	40.20	10.75	1.695	0.636	1.330	0.524	8.545	1.274	0.889	53.12
448	40.18	11.23	1.609	0.619	1.298	0.508	9.125	1.240	0.882	53.31
451	50.21	13.50	2.337	0.631	1.505	0.532	9.376	1.474	0.870	63.59

ORIGINAL PAGE IS OF POOR QUALITY

PERFORMANCE DATA SUMMARY OF THE SECOND FULL 10-STAGE COMPRESSOR TEST (10B)

READING NUMBER	* * * * * * * * OVERALL * * * * * * * * CORRECTED SPEED	CORRECTED FLOW	PRESSURE RATIO	ADIABATIC EFFICIENCY	* * FRONT BLOCK * * PRESSURE RATIO	ADIABATIC EFFICIENCY	* * * * * * * REAR BLOCK * * * * * * * CORRECTED FLOW	PRESSURE RATIO	ADIABATIC EFFICIENCY	CORRECTED SPEED
452	50.21	14.19	2.253	0.643	1.539	0.535	10.096	1.464	0.887	64.10
453	50.25	14.98	2.060	0.624	1.462	0.511	11.152	1.409	0.878	64.68
454	60.18	19.95	2.806	0.647	1.722	0.558	13.015	1.630	0.851	75.14
455	89.96	70.47	11.185	0.806	4.945	0.812	18.428	2.262	0.865	97.88
456	90.03	68.94	13.076	0.794	5.509	0.803	16.470	2.374	0.854	96.05
457	89.97	67.61	13.253	0.784	5.603	0.788	15.982	2.366	0.858	95.32
460	90.03	70.07	10.550	0.802	4.056	0.815	18.595	2.172	0.847	98.32
462	92.47	81.82	12.578	0.812	5.751	0.832	18.755	2.187	0.843	98.72
463	92.47	81.23	13.248	0.816	5.836	0.830	18.396	2.270	0.858	98.44
464	92.42	81.55	14.116	0 816	6.035	0.830	17.949	2.339	0.862	97.86
465	92.51	78.23	14.792	0.799	6.155	0.810	17.017	2.403	0.858	97.10
466	92.54	77 14	15.289	0.789	6.388	0.803	16.282	2.393	0.845	96.40
474	100.02	121.61	20.141	0.803	9.217	0.831	18.733	2.185	0.826	99.15
475	99.96	121.31	21.237	0.806	9.350	0.829	18.469	2.271	0.841	98.80
476	99.96	120.91	24.743	0.801	10.370	0.824	16.866	2.386	0.843	97.08
477	97.54	107.84	19.423	0.819	8.269	0.843	18.138	2.349	0.845	98.70
478	97.55	108.67	17.569	0 816	7.939	0.846	18.915	2.213	0.830	99.39
479	97.53	107.99	18.528	0.819	8.086	0.846	18.498	2.291	0.840	99.10
480	97.41	106.98	21.438	0.810	8.918	0.836	16.889	2.404	0.838	97.23
481	97.48	110.81	20.859	0.828	8.754	0.856	17.685	2.383	0.845	98.12
483	60.15	20.19	2.527	0 619	1.636	0.533	13.783	1.544	0.824	75.62
484	60.19	19.94	2.827	0.647	1.733	0.559	12.935	1.631	0.852	75.06
485	60.18	18.58	3.212	0.644	1.919	0.572	11.057	1.674	0.836	73.58
486	60.13	19.40	3.078	0.656	1.847	0.570	11.924	1.667	0.869	74.10
487	70.05	28.06	3.710	0.670	2.090	0.622	15.543	1.776	0.814	85.05

ORIGINAL PAGE IS OF POOR QUALITY

PERFORMANCE DATA SUMMARY OF THE SECOND FULL 10-STAGE COMPRESSOR TEST (10B)

READING NUMBER	* * * * * * * * OVERALL * * * * * * * * CORRECTED SPEED	CORRECTED FLOW	PRESSURE RATIO	ADIABATIC EFFICIENCY	* * FRONT BLOCK * * PRESSURE RATIO	ADIABATIC EFFICIENCY	* * * * * * * REAR BLOCK * * * * * * * CORRECTED FLOW	PRESSURE RATIO	ADIABATIC EFFICIENCY	CORRECTED SPEED
488	69.94	27.93	3.918	0.683	2.141	0.630	15.142	1.830	0.835	84.63
489	70.07	27.71	4.175	0.688	2.224	0.631	14.557	1.877	0.849	84.18
490	70.02	27.28	4.489	0.690	2.347	0.644	13.665	1.912	0.837	83.45
491	69.94	26.22	4.706	0.675	2.468	0.632	12.625	1.907	0.825	82.31
492	74.97	34.46	4.707	0.708	2.487	0.679	16.399	1.893	0.824	89.08
493	75.03	34.36	4.966	0.716	2.547	0.685	16.009	1.950	0.833	88.86
494	75.05	34.05	5.267	0.722	2.634	0.694	15.398	2.000	0.836	88.52
495	75.03	33.38	5.665	0.716	2.776	0.689	14.458	2.041	0.834	87.53
496	75.17	32.73	5.834	0.706	2.863	0.682	13.833	2.038	0.824	87.05
497	20.08	5.49	1.113	0.568	1.076	0.464	5.142	1.034	1.120	27.96
498	20.11	5.32	1.132	0.610	1.082	0.441	4.937	1.046	1.814	27.94
499	20.11	4.94	1.151	0.634	1.087	0.440	4.570	1.059	1.728	27.89
501	30.06	8.46	1.269	0.580	1.162	0.479	7.474	1.092	0.925	40.99
502	30.10	8.22	1.318	0.623	1.179	0.510	7.151	1.117	0.950	40.97
503	30.10	7.75	1.369	0.643	1.196	0.514	6.656	1.145	0.983	40.83
504	30.09	7.36	1.389	0.638	1.199	0.491	6.305	1.158	1.041	40.70
523	85.13	55.39	7.920	0.782	3.823	0.793	18.033	2.072	0.831	96.27
524	85.07	54.64	8.827	0.788	3.980	0.789	17.202	2.218	0.854	95.48
525	85.03	53.91	9.428	0.784	4.139	0.787	16.423	2.278	0.849	94.79
526	85.02	54.87	8.305	0.787	3.876	0.789	17.674	2.143	0.850	95.85

ORIGINAL PAGE IS
OF POOR QUALITY

DISTRIBUTION

NASA Headquarters
600 Independence Avenue, SW
Washington, DC 20546
Attention: RTP-6/R.S. Colladay
RTP-6/C.C. Rosen
RTP-6/J. Facey
RTM-6/L. Harris

NASA-Lewis Research Center
21000 Brookpark Road
Cleveland, OH 44135

Attention:	D.L. Nored	MS 301-2
	C.C. Ciepluch	MS 301-4 (18 copies)
	J.W. Schaefer	MS 301-4
	P.G. Batterton	MS 301-4
	G.K. Sievers	MS 301-2
	M.A. Beheim	MS 3-5
	M.J. Hartmann	MS 3-7
	R.A. Rudey	MS 86-5
	W.C. Strack	MS 501-10
	T.P. Moffitt	MS 77-2
	R.E. Jones	MS 86-6
	L.J. Kiraly	MS 23-2
	D.C. Mikkelson	MS 86-1
	A. Long	MS 500-305
	J.F. Groeneweg	MS 54-3
	W.M. Braithwaite	MS 500-208
	J.C. Williams	MS 500-211
	R.L. Davies	MS 106-1
	R.H. Johns	MS 49-6
	L.J. Kaszubinski	MS 86-2
	J.F. Sellers	MS 100-1
	J.R. Mihaloew	MS 100-1
	L. Reid	MS 5-9
	D.W. Drier	MS 86-2
	R.W. Niedzwiecki	MS 86-6
	AFSC Liaison Office	MS 501-3
	ARMY R&T Propulsion Lab	MS 302-2

NASA Ames Research Center
Moffett Field, CA 94035
Attention: 202-7/M.H. Waters

NASA Langley Research Center
Langley Field, VA 23365
Attention: R. Leonard
D. Maiden
L.J. Williams

NASA Dryden Flight Research Center
P.O. Box 273
Edwards, CA 93523
Attention: J.A. Albers

Department of Defense
Washington, DC 20301
Attention: R. Standahar 3D1089 Pentagon

Wright-Patterson Air Force Base
Dayton, OH 45433
Attention: APL Chief Scientist
E.E. Abell
H.I. Bush
E.E. Bailey (NASA Liaison)
R.P. Carmichael
R. Ellis
W.H. Austin, Jr.

AFWAL/PS
ASD/YZE
AFWAL/POT
AFWAL/NASA
ASD/XRHI
ASD/YZN
ASD/ENF

Eustis Directorate
U.S. Army Air Mobility
R&D Laboratory
Fort Eustis, VA 23604
Attention: J. Lane, SAVDL-EU-Tapp

NAVY Department
Naval Air Systems Command
Washington, DC 20361
Attention: W. Koven AIR-03E
J.L. Byers AIR-53602
E.A. Lichtman AIR-330E
G. Derderian AIR-5362C

NAVAL Air Propulsion Test Center
Trenton, NJ 08628
Attention: J.J. Curry
A.A. Martino

U.S. Naval Air Test Center
Code SY-53
Patuxent River, MD 20670
Attention: E.A. Lynch

USAVRAD Command
P.O. Box 209
St. Louis, MO 63166
Attention: Robert M. Titus

Detroit Diesel Allison Div. G.M.C.
333 West First St.
Dayton, OH 45202
Attention: F.H. Walters

Department of Transportation
NASA/DOT Joint Office of
Noise Abatement
Washington, D.C. 20590
Attention: C. Foster

Federal Aviation Administration
Noise Abatement Division
Washington, DC 20590
Attention: E. Sellman AEE-120

Rohr Corporation
P.O. Box 1516
Chuyla Vista, CA 92012
Attention: James C. Fuscoe

TRW Equipment
TRW Inc.
23555 Euclid Ave.
Cleveland, Ohio 44117
Attention: I. Toth

Federal Aviation Administration
12 New England Executive Park
Burlington, MA 18083
Attention: Jack A. Sain, ANE-200

Curtiss Wright Corporation
Woodridge, NJ 07075
Attention: S. Lombardo
S. Moskowitz

AVCO/Lycoming
550 S. Main Street
Stratford, CN 06497
Attention: H. Moellmann

Williams Research Co.
2280 W. Maple Road
Walled Lake, MI 48088
Attention: R. VanNimwegen
R. Horn

Teledyne CAE, Turbine Engines
1330 Laskey Road
Toledo, OH 43612
Attention: R.H. Gaylord

Pratt & Whitney Aircraft Group/UTC
Government Products Division
P.O. Box 2691
West Palm Beach, FL 33402
Attention: B.A. Jones

Boeing Commercial Airplane Co.
P.O. Box 3707
Seattle, WA 98124
Attention: P.E. Johnson MS 9H-46
D.C. Nordstrom MS-73-01

Brunswick Corporation
2000 Brunswick Lane
Deland, FL 32720
Attention: A. Erickson

Delta Airlines, Inc.
Hartsfield-Atlanta International Airport
Atlanta, GA 30320
Attention: C.C. Davis

FluiDyne Engineering Corp.
5900 Olson Memorial Highway
Minneapolis, MN 55422
Attention: J.S. Holdhusen

Massachusetts Inst. of Technology
Dept. of Astronautics & Aeronautics
Cambridge, MA 02139
Attention: Mames Mar

Detroit Diesel Allison Div. G.M.C.
P.O. Box 894
Indianapolis, IN 46202
Attention: W.L. McIntire

The Garrett Corporation
AIResearch Manufacturing Co.
Torrance, CA 90509
Attention: F.E. Faulkner

The Garrett Corporation
AIResearch Manufacturing Co.
402 S. 36 Street
Phoenix, AZ 85034
Attention: Library

General Electric Co./AEG
1000 Western Avenue
Lynn, MA 01910
Attention: R.E. Nietzel

Pratt & Whitney Aircraft Group/UTC
Commercial Products Division
East Hartford, CT 06108
Attention: W. Gardner (3 copies)
I. Mendelson

Douglas Aircraft Co.
McDonnell Douglas Corp.
3855 Lakewood Boulevard
Long Beach, CA 90846
Attention: R.T. Kawai Code 36-41
M. Klotzsche 36-41

AIResearch Manufacturing Co.
111 South 34th Street
P.O. Box 5217
Phoenix, AZ 85010
Attention: C.E. Corrigan
(930120/503-4F)

American Airlines
Maint. & Engrg. Center
Tulsa, OK 74151
Attention: W.R. Neeley

Lockheed California Co.
Burbank, CA 91502
Attention: J.F. Stroud, Dept. 75-42
R. Tullis, Dept. 74-21

Grumman Aerospace Corp.
South Oyster Bay Road
Bethpage, NY 11714
Attention: C. Hoeltzer